GEOLOGICA ULTRAIECTINA

Mededelingen van de
Faculteit Aardwetenschappen
Universiteit Utrecht

No. 215

Early diagenesis of Manganese, Iron and Phosphorus in European continental margin sediments

Claar van der Zee

GEOLOGICA ULTRAIECTINA

Mededelingen van de
Faculteit Aardwetenschappen
Universiteit Utrecht

No. 215

Early diagenesis of Manganese, Iron and Phosphorus in European continental margin sediments

Claar van der Zee

ISBN 90-5744-071-7

Early diagenesis of Manganese, Iron and Phosphorus in European continental margin sediments

Vroege diagenese van Mangaan, IJzer en Fosfor in sedimenten van de Europese continentale helling

(met een samenvatting in het Nederlands)

Proefschrift

ter verkrijging van de graad van doctor
aan de Universiteit Utrecht
op gezag van de Rector Magnificus Prof. Dr. W.H. Gispen
ingevolge het besluit van het College voor Promoties
in het openbaar te verdedigen
op vrijdag 22 februari 2002 des middags te 2.30 uur

door

Clara van der Zee

geboren op 19 juni 1974 te Amstelveen

Promotor: Prof. Dr. P. Van Cappellen
Department of Geochemistry
Utrecht University
Utrecht, The Netherlands

Co-promotor: Dr. Ir. W. van Raaphorst
Department of Marine Chemistry and Geology
Royal Netherlands Institute for Sea Research
Texel, The Netherlands

The research described in this thesis was carried out at the Department of Marine Chemistry and Geology, Royal Netherlands Institute for Sea Research, P.O. Box 59, 1780 AB Den Burg, The Netherlands. This study was supported by The Netherlands Organisation for Scientific Research (NWO) within the framework of the Sedimentary Manganese and Iron cycLEs (SMILE) program.

TO SEE WHICH WAY IT GOES
YOU JUST HAVE TO BOUNCE IT
(Stereo MC's)

CONTENTS

CHAPTER ONE

Introduction

GENERAL BACKGROUND

Although ocean margins comprise less than 20% of the surface area of the global ocean, they play an important role in the biogeochemical cycles of the major elements (Walsh, 1991). High primary production over the shelf is sustained through the input of nutrients from rivers and coastal upwelling. In these shallow areas, between 18 and 33% of the total oceanic primary production takes place (Wollast, 1991). Whereas primary production in deep-sea regions is largely regenerated in the water column, up to 50% reaches the seafloor at continental margins (Müller and Suess, 1979; Suess, 1980; Jørgensen, 1983). Middelburg *et al.* (1997) calculated from empirical relationships that ~85% of the global organic matter mineralisation in marine sediments occurs along the margins between 0-2000 m depth. In addition to primary production, ocean margins receive organic and lithogenic particles from rivers, coast erosion and by aeolian input. The Iberian margin is a narrow shelf with the 200-m isobath situated 15 to 30 km offshore and it is interspersed with many canyons. The complex water circulation is dominated by a wind driven surface current in southward direction during summer and a density driven poleward current during winter (Van Aken, 2000). Filaments of cold upwelled water are formed during spring and summer and support high primary production. Suspended matter is transported from the shelf in benthic nepheloid layers, which form intermediate nepheloid layers at the shelf break. The majority of the particles is deposited within 50 km offshore (Van Weering *et al.*, 2002). Submarine canyons can focus suspended matter from the shelf and act as preferential conduits for particulate material transport from the shelf to the deep-sea (Carson *et al.*, 1986; Durrieu de Madron *et al.*, 1999). The Nazaré Canyon is one of the largest canyons of the Iberian Margin. Epping *et al.* (2002) showed that it is of quantitative importance for the concentration, oxidation and burial of organic matter.

"Diagenesis refers to the sum total of processes that bring about changes in a sediment or sedimentary rock subsequent to deposition in water. The processes may be physical, chemical, and/or biological in nature and may occur at any time subsequent to the arrival of a particle at the sediment-water interface. Early diagenesis refers to changes occurring during burial to a few hundred meters where elevated temperatures are not encountered and where uplift above sea level (or lake level) does not occur, so that the pore spaces of the sediment are continually filled with water" (Berner, 1980). The key early diagenetic process is the microbial degradation of organic matter, which is often called mineralisation, but should not be confused with the actual formation of minerals *per se*. Coupled to the oxidative degradation of organic matter is the reduction of a suite of dissolved oxidants, such as oxygen, nitrate and sulphate and solid phase oxidants such as manganese (III, IV) and iron (III)

(hydr-)oxides. The concept of redox zonation during organic matter mineralisation is usually explained by the Gibbs free energy yield of the different electron acceptors, i.e. the oxidants (Table 1; Fig. 1).

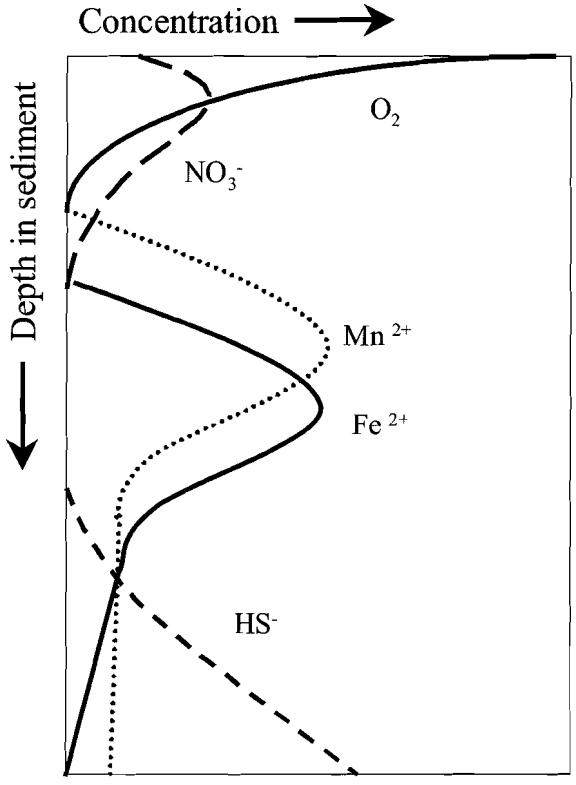

Figure 1. Redox zonation in marine sediments. Note the sequence from top to bottom of oxygen and nitrate depletion, followed by the increase in the products of Mn, Fe and sulphate reduction. Below the depth of oxygen penetration Mn^{2+} appears in the pore water. At the depth of nitrate depletion, Fe^{2+} appears in the pore water.

Table 1. Organic matter mineralisation. Sequence of electron acceptors after Froelich *et al.* (1979). Organic matter is represented by the simple CH_2O.

Reaction	Equation	Standard Gibbs free energy (KJ $mole^{-1}$)
Oxic respiration	$CH_2O + O_2 \rightarrow CO_2 + H_2O$	-3190
Denitrification	$5CH_2O + 4NO_3^- \rightarrow 2N_2 + 4HCO_3^- + CO_2 + 3H_2O$	-3030
Mn reduction	$CH_2O + 2\ MnO_2 + 3CO_2 + H_2O \rightarrow 2Mn^{2+} + 4HCO_3^-$	-2900
Fe reduction	$CH_2O + 4FeOOH + 7CO_2 + H_2O \rightarrow 4Fe^{2+} + 8HCO_3^-$	-1410
SO_4^{2-} reduction	$2CH_2O + SO_4^{2-} \rightarrow H_2S + 2HCO_3$	-380
Methane production	$2CH_2O \rightarrow CH_4 + CO_2$	-350

In addition to the mineralisation processes, inorganic reactions occur between some electron acceptors and their products, e.g. between iron oxides and sulphide (Pyzik and Sommer, 1981) and between manganese oxides and ferrous iron (Postma, 1985). Furthermore, in natural sediments a wide range of iron oxide reactivities is likely to cause considerable overlap between Fe (III) and SO_4^{2-} reduction (Postma and Jakobsen, 1996). Mn (III, IV) reduction and denitrification zones may overlap as well, depending on the Mn oxide reactivity (Froelich *et al.*, 1979).

The sedimentary Mn and Fe cycles involve the two-way redox transformations of the reduced soluble Mn^{2+} and Fe^{2+} to the oxidised particulate Mn (III, IV) oxides and Fe (III) oxyhydroxides, (Tables 2 and 3). Through their redox cycles Mn and Fe are coupled to the biogeochemical cycles of other elements such as C, N, S and P.

THE SEDIMENTARY MANGANESE CYCLE

Manganese oxides are the principle carriers of Mn to the sediment and they mainly occur in association with other sediment particles as aggregates or coatings (Burns and Burns, 1979). A number of manganese oxides may exist in marine sediments with varying Mn(III) and Mn(IV) contents (Burdige, 1993). Mn oxides are stable in oxidised sediment, whereas dissolved phase Mn^{2+} is stable in the reduced sediment layer. Therefore, solid Mn (III,IV) is reduced and subsequently dissolved as Mn^{2+} upon burial below the depth of oxygen penetration in the sediment. Reduction can be chemically or microbiologically mediated and both pathways are controlled by reactions occurring at the oxide surface. Thus, the overall rates are highest in case of high surface areas, for example due to poor crystalinity of the oxides (Burdige *et al.*, 1992). Through reduction, the Mn cycle is coupled to the biogeochemical cycles of C, N, S and Fe (Table 2).

Table 2. Mn redox reactions in marine sediments (modified after Aller, 1994)

Reaction	Equation
Mn oxidation	$2Mn^{2+} + O_2 + 2H_2O \rightarrow 2MnO_2 + 4H^+$
Dissimilatory Mn reduction	$CH_2O + 2MnO_2 + 3CO_2 + H_2O \rightarrow 2Mn^{2+} + 4HCO_3^-$
Anoxic nitrification	$4MnO_2 + NH_4^+ + 6H^+ \rightarrow 4Mn^{2+} + NO_3^- + 5H_2O$
N_2 generation	$3MnO_2 + 2NH_4^+ + 4H^+ \rightarrow 3Mn^{2+} + N_2 + 6H_2O$
Iron oxidation	$MnO_2 + 2Fe^{2+} + H_2O \rightarrow Mn^{2+} + 2FeOOH + 2H^+$
Sulphide oxidation I	$4MnO_2 + FeS + 8H^+ \rightarrow 4Mn^{2+} + SO_4^{2-} + Fe^{2+} + 4H_2O$
Sulphide oxidation II	$MnO_2 + SH^- + 3H^+ \rightarrow Mn^{2+} + S^0 + 2H_2O$
Anoxic precipitation	$xMn^{2+} + (1\text{-}x)Ca^{2+} + 2HCO_3^- \rightarrow Mn_xCa_{(1-x)}CO_3 + CO_2 + H_2O$

A variety of bacteria are capable of coupling Mn reduction to organic matter mineralisation to gain their energy for growth (Myers and Nealson, 1988; Lovley, 1991; Nealson and Myers, 1992; Nealson and Saffarini, 1994). Humic substances, phenols and microbial metabolites such as oxalate and pyruvate chemically reduce Mn oxides (Stone and Morgan, 1984; Stone 1987; Sunda and Kieber, 1994).

Furthermore, Mn oxide can be reduced with sulphide and FeS to Mn^{2+}, SO_4^{2-} and S^0 (Burdige and Nealson, 1986; Schippers and Jørgensen, 2001) and microbiologically with acid volatile sulphides to Mn^{2+} and SO_4^{2-} (Aller and Rude, 1988). Sørensen *et al.* (1987) were the first to suggest an interaction between the Mn and N cycles, chemo-denitrification with Mn^{2+}. Other interactions between Mn and N were proposed later, e.g. Mn oxide reduction with ammonia or organic nitrogen thereby producing N_2 (Luther *et al.*, 1997), and anoxic nitrification of NH_4^+ to NO_3^- during Mn reduction (Hulth *et al.*, 1999).

In the pore water, Mn^{2+} diffuses either upward into the oxic layer or downward to deeper layers where it ultimately precipitates as a reduced particulate phase (Ca,Mn)-CO_3 that is buried (Middelburg *et al.*, 1987; Böttcher, 1998). Mn^{2+} oxidation with oxygen can proceed both abiotically and by microbial catalysis. In aqueous systems oxidation of Mn^{2+} by molecular oxygen is auto-catalytic, but becomes pseudo first-order with respect to the concentration of dissolved Mn^{2+} when the amount of unreacted Mn^{2+} is small compared to the surface of the manganese oxides (Kessick and Morgan, 1975; Hem, 1981). The presence of mineral surfaces enhances Mn^{2+} oxidation by binding Mn^{2+} in a manner that facilitates the electron transfer for the oxidation reaction (Wilson, 1980; Davies and Morgan, 1988). Microbial catalysis of Mn^{2+} oxidation was first reported in the water column of Saanich Inlet (Emerson *et al.*, 1982). Mn^{2+} oxidation rates more than 1000 times higher than those reported for abiotic Mn oxidation provided evidence that Mn^{2+} oxidation was microbial mediated in Aarhus Bay sediments as well (Thamdrup *et al.*, 1994).

THE SEDIMENTARY IRON CYCLE

Fe (III) oxides account for only ~28% of total Fe in oxidised marine sediments, as most Fe is bound in aluminium-silicates (Raiswell and Canfield, 1998). Fe oxides are present in a continuum from amorphous to very crystalline forms (Murray, 1979). Fe (III) is reduced at more reducing conditions than Mn oxides, e.g. deeper in the anoxic layer of the sediment. When pore water Fe^{2+} diffuses upward away from the zone of Fe reduction, it can be oxidised by oxygen, nitrate or Mn oxide. The reaction between Fe^{2+} and molecular oxygen is fast under sedimentary conditions and strongly depends on pH, increasing in rate with increasing pH (Millero *et al.*, 1987). The reaction may be microbiologically catalysed by iron oxidising bacteria growing at the oxic-anoxic interface where the opposite gradients of O_2 and Fe^{2+} meet (Emerson and Moyer, 1997). Microbial Fe^{2+} oxidation in the absence of oxygen is possible when coupled to dissimilatory nitrate reduction (Straub *et al.*, 1996). Chemical oxidation of Fe^{2+} by nitrate does not proceed in the absence of a catalyst like Cu^{2+} (Buresh and Moraghan, 1976; Ottley *et al.*, 1997), but Mn oxide readily oxidises Fe^{2+} (Postma, 1985). The type of oxide formed depends on the conditions during oxidation and the duration. Solutes like silicate or phosphate present in the pore water influence the Fe oxidation product, e.g. silicate surface species inhibit the crystallisation of iron (III) hydroxides, whereas phosphate may be incorporated into the particles (Deng, 1997).

Table 3. Fe redox reactions in marine sediments (see text for references)

Reaction	Equation
Fe oxidation	$2\ Fe^{2+} + O_2 + 2\ H_2O \rightarrow 2\ FeOOH + 4\ H^+$
Oxidation – denitrification	$10\ FeCO_3 + 2\ NO_3^- + 24\ H_2O \rightarrow 10\ Fe(OH)_3 + N_2 + 10HCO_3^- + 8\ H^+$
Oxidation – Mn reduction	$2Fe^{2+} + MnO_2 + H_2O \rightarrow 2FeOOH + Mn^{2+} + 2H^+$
Dissimilatory Fe reduction	$CH_2O + 4FeOOH + 7CO_2 + H_2O \rightarrow 4Fe^{2+} + 8HCO_3^-$
Chemical Fe reduction	$FeOOH + SH^- + 3H^+ \rightarrow Fe^{2+} + S^0 + 2H_2O$
Precipitation	$Fe^{2+} + SH^- \rightarrow FeS + H^+$
Pyrite formation I	$FeS + S^0 \rightarrow FeS_2$
Pyrite formation II	$FeS + S_x^{2-} \rightarrow FeS_2 + S_{(x-1)}^{2-}$

The first organism found to couple its growth to Fe (III) reduction was an isolate from freshwater sediment, *Geobacter metallireducens* (Lovley and Phillips, 1988). In addition to Fe oxides, Fe (III) bound in clay minerals (smectite) is subject to reduction as well. The tan-green colour transition in pelagic sediments is indicative for clay-bound Fe reduction (Lyle, 1983; König *et al.*, 1997; König *et al.*, 1999). Bacteria can even directly couple the reduction of Fe^{3+} bound in smectites to organic matter oxidation (Kostka *et al.*, 1999). Sulphate reducing bacteria may also reduce Fe (III), producing siderite ($FeCO_3$), which is, however, anomalous in marine sediments as it is unstable in the presence of H_2S (Coleman *et al.*, 1993). More importantly sulphate-reducing bacteria indirectly reduce iron as they produce sulphide, which reduces Fe oxyhydroxides to form iron (II) sulphides and elemental sulphur (Pyzik and Sommer, 1981). Iron (II) sulphides react with elemental sulphur or polysulphides to produce pyrite (FeS_2) (Berner, 1970; Luther, 1991). Pyrite formation appears almost never limited by the amount of total iron deposited, except in highly calcareous environments, instead it is controlled by the reactivity of iron minerals (Berner, 1984). Pyrite burial in the main sink for reduced iron in the marine environment.

THE SEDIMENTARY PHOSPHORUS CYCLE

Phosphorus (P) is an essential nutrient for phytoplankton growth. Because cyanobacteria are capable to fix N_2 from the atmosphere, it is believed that P is the limiting nutrient for global marine productivity on geological time scales (Holland, 1978; Broecker and Peng, 1982; Howarth *et al.*, 1995). Recycling and removal of P in marine systems are therefore important controls on marine productivity, both over geological and shorter time-scales (Van Cappellen and Ingall, 1996). In this way, changes in the oceanic P burial flux can affect the organic carbon burial and atmospheric CO_2 and O_2 concentrations (Holland, 1978; Broecker and Peng, 1982; Van Cappellen and Ingall, 1994 and 1996). Most removal of P from the water column takes place through sedimentation of organic material on continental margins (Berner, 1993). Thus, it is important to know the fate of P in the sediment. P burial is a function of the input flux to the sediment and its retention, which is influenced by: (1) input quality, (2) sedimentation rate, i.e. burial of P below the depth of no return, (3) pore water irrigation and sediment reworking, and (4) formation of secondary authigenic phases due to precipitation and sorption (Ruttenberg and Berner, 1993).

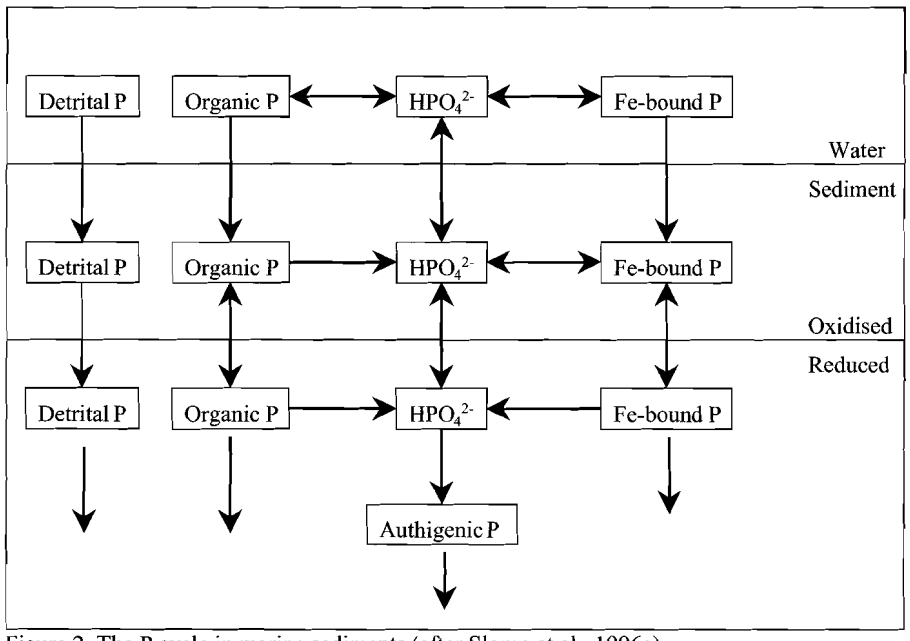

Figure 2. The P cycle in marine sediments (after Slomp et al., 1996a).

The three sedimentary forms of reactive P, and thus potentially bio-available P, are organic P, Fe-bound P and authigenic P minerals. Organic matter is the principle carrier of reactive P to the sediment (Froelich *et al.*, 1982; Berner *et al.*, 1993). Upon organic matter degradation, phosphate is released into the pore water and subsequently adsorbed onto Fe oxides in the oxic layer of the sediment (Krom and Berner, 1980; Sundby *et al.*, 1992; Van Raaphorst and Kloosterhuis, 1994). When the oxic layer is thin or absent phosphate released from organic matter and Fe oxides escapes to the water column (Sundby *et al.*, 1986; Ingall and Jahnke, 1994). Fe oxides do not always act as a 100% efficient trap due to phosphate release very close to the sediment-water interface (Martens *et al.*, 1978) and non-local transport of phosphate from deeper layers to the water column, i.e. irrigation by benthic organisms (Aller and Yingst, 1985). Also, phosphate desorption from Fe oxides close to the sediment-water interface may sustain an efflux even when phosphate concentrations are low (Schink and Guinasso, 1978; Van Raaphorst *et al.*, 1988; Slomp *et al.*, 1998). In the anoxic layer, organic matter degradation continues to deliver phosphate to the pore water, but additionally the previously adsorbed P is released upon the reduction of Fe oxides. There, the phosphate concentration in the pore water may become sufficiently high for the precipitation of authigenic carbonate fluorapatite (CFA) (Van Cappellen and Berner, 1988). CFA is the dominant mineral phase in phosphorite deposits. Authigenic P can form at the expense of organic P (Ruttenberg and Berner, 1993) and Fe-bound P (Lucotte *et al.*, 1994; Slomp *et al.*, 1996a). CFA formation in marine sediments is important because it is a permanent sink of reactive P, in addition to CFA, Fe-bound P and organic P can act as permanent or temporal sinks (Ingall and Van Cappellen, 1990; Slomp *et al.*, 1996b).

SMILE AND OMEX PROJECTS

This thesis describes the results of a project that was carried out as a part of the Sedimentary Manganese and Iron cycLEs (SMILE) research program funded by the Netherlands Organisation of Scientific Research (NWO/ALW). SMILE aimed at studying the biogeochemistry of iron and manganese cycles in sedimentary environments along a carbon-loading gradient, i.e. from estuarine, via shelf and slope sediments to deep-sea sediments. SMILE consists of three components, each focussing on separate sedimentary environments; Mn and Fe cycling in estuarine sediments (Netherlands Institute for Ecology, NIOO-CEMO), Atlantic shelf and slope sediments (Netherlands Institute for Sea Research, NIOZ) and the Mediterranean (Utrecht University- Institute for Earth Sciences, UU-IES). The SMILE objectives include:

(1) to establish the role of Mn and Fe in the oxidation of organic matter,
(2) to examine the metal reduction rates as a function of organic carbon loading and bioturbation,
(3) to investigate the interaction between Mn and Fe cycles and the phosphorus cycle, and
(4) to study the formation and preservation of metal-rich layers and their geological information.

The work presented here concentrated on Mn and Fe cycling as driven by the input of organic matter and the recycling and burial of phosphorus in sediments of the European continental margin. The problems were addressed by a combination of fieldwork, laboratory work and modelling studies.

Laboratory and fieldwork were done within the framework of two other projects. Investigations described in chapters 4, 5 and 6 of this thesis were carried out during two Ocean Margin EXchange (OMEX-II) cruises. The aim of the OMEX project, supported by the European Commission, was to gain a better understanding of the physical, chemical and biological processes occurring at the ocean margins in order to quantify fluxes of energy and matter across this boundary. The project characterises the flux of carbon, nutrients and trace elements between the open ocean and the coastal seas. Data from four cruises with the RV Pelagia across the North Sea are presented in chapter two and three. The North Sea stations were sampled in the framework of the VvA project ("Verstoring van Aardsystemen") funded by NWO/ALW.

OUTLINE OF THIS THESIS

In this thesis the cycles of manganese, iron and phosphorus in marine sediments of the North Sea (chapters 2 and 3) and Iberian continental margin (chapters 4, 5 and 6) are discussed. In dynamic shelf systems such as the North Sea, the sedimentary depth distributions of Mn and Fe (hydr-) oxides do not only depend on their redox reactions, the disturbance by hydrodynamic forces and the benthic community also exert a great influence on their distributions. Three contrasting sites were visited in February, May, August and November. The stable environment of the Skagerrak served as a base-line

for the moderately dynamic Frisian Front and the highly energetic German Bight. In **chapter 2**, the implications of highly dynamic conditions in temporal deposition areas for Mn and Fe diagenesis are discussed. In **chapter 3**, the assemblage of sedimentary Mn oxides is described as a reactive continuum with a gamma distribution of Mn oxide reactivities. Conventional sediment extractions are compared with the reactive continuum approach. The importance of heterogeneity of Mn oxides on the Mn cycle and the redox zonation is discussed. In **chapter 4**, the role of Mn^{2+} sorption in the Mn redox cycle at the Iberian continental margin is described. Mn reaction rates (oxidation, reduction, sorption and precipitation) are estimated by application of a diagenetic Mn model. The Mn cycling intensity is discussed as a function of organic carbon mineralisation gradient going from the shelf across the slope to the deep-sea and a comparison is made between the stations on the margin and in the canyon. **Chapter 5** investigates the role of adsorbed Fe^{2+} in the Fe cycle at the Iberian continental margin. A diagenetic model was developed and applied to the Fe data. Fe redox cycling as a function of organic carbon mineralisation rate is discussed. Mn and Fe cycling at the Iberian margin are compared; their rate limiting factors and the roles of the adsorbed species in the redox cycle. Canyons can be major transport routes and/or sinks for shelf derived particulate matter. In **chapter 6**, a sequential leaching technique was applied to two contrasting shelf sites and a slope site on the Iberian margin and one site in the Nazaré canyon to investigate sedimentary P cycling. The reactive P burial efficiency for the contrasting depositional sites is discussed.

REFERENCES

Aller, R.C. and P.D. Rude. 1988. Complete oxidation of solid phase sulfides by manganese and bacteria in anoxic marine sediments. Geochim. Cosmochim. Acta, 52, 751-765.

Aller, R.C. and Y. Yingst. 1985. Effects of the marine deposit feeders *Heteromastus filiformis* (Polychaeta), *Macoma Baltica* (Bivalvia) and *Tellina texana* (Bivalvia) on averaged sedimentary solute transport, reaction rates and microbial distributions. J. Mar. Res., 43, 615-645.

Berner, R.A. 1970. Sedimentary pyrite formation. Am. J. Sci., 268, 1-23.

Berner, R.A. 1980. Early diagenesis. A theoretical approach. Princeton Univ. Press.

Berner, R.A. 1984. Sedimentary pyrite formation: an update. Geochim. Cosmochim. Acta, 48, 605-615.

Berner, R.A., K.C. Ruttenberg, E.D. Ingall and J.-L. Rao. 1993. The nature of phosphorus burial in modern marine sediments. In R. Wollast, F.T. Mackenzie and L. Chou, eds. Interactions of C,N,P and S Biogeochemical Cycles and Global Change, Springer-Verlag, NATO ASI Series, Vol. 14, 521p.

Böttcher, M.E. 1998. Manganese(II) partitioning during experimental precipitation of rhodochrosite-calcite solid solutions from aqueous solutions. Mar. Chem., 62, 287-297.

Broecker, W.S. and T.-H. Peng. 1982. Tracers in the sea. Eldigo Press, Palisades. 690p.

Burdige, D.J. 1993. The biogeochemistry of manganese and iron reduction in marine sediments. Earth Sci. Rev., 35, 249-284.

Burdige, D.J. and K.H. Nealson. 1986. Chemical and Microbiological studies of sulfide-mediated manganese reduction. Geomicrobiol. J., 4, 361-387.

Burdige, D.J., S.P. Dhakar and K.H. Nealson. 1992. Effects of manganese oxide mineralogy on microbial and chemical manganese reduction. Geomicrobiol. J., 10, 27-48.

Buresh, R.J. and J.T. Moraghan. 1976. Chemical reduction of nitrate by ferrous iron. J. Environ. Qual., 5, 320-325.

Burns, R.G. and V.M. Burns. 1979. Manganese oxides. In Marine Minerals. R.G. Burns (ed.) Reviews in Mineralogy Vol. 6. Mineralogy Society of America, Washington DC, p 1-46.

Carson, B., E. T. Baker, B.M. Hickey, C.A. Nittrouer, D.J. DeMaster, K.W. Thorbjarnarson, and G.W. Snyder. 1986. Modern sediment dispersal and accumulation in Quinault submarine canyon – A summary. Mar. Geol., 71, 1-13.

Coleman, M.L., D.B. Hedrick, D.R. Lovley, D.C. White and K. Pye. 1993. Reduction of Fe(III) in sediments by sulphate reducing bacteria. Nature, 361, 436-438.

Davies, S.H.R. and J.J. Morgan. 1988. Manganese(II) oxidation kinetics on metal oxide surfaces. J. Coll. Interface Sci., 129, 63-77.

Deng, Y. 1997. Formation of iron(III) hydroxides from homogeneous solutions. Wat. Res., 31, 1347-1354.

Durrieu de Madron, X., P. Castaing, F. Nyffeler and T. Courp. 1999. Slope transport of suspended particulate matter on the Aquitanian margin of the bay of Biscay. Deep-sea Res. I, 46, 2003-2027.

Emerson, D. and C. Moyer. 1997. Isolation and characterization of novel iron-oxidising bacteria that grow at cirumneutral pH. Appl. Environ. Microbiol., 63, 4784-4792.

Emerson, S., S. Kalhorn, L. Jacobs, B.M. Tebo, K.H. Nealson, and R.A. Rosson. 1982. Environmental oxidation rate of manganese(II): bacterial catalysis. Geochim. Cosmochim. Acta., 46, 1073-1079.

Epping, E., C. van der Zee, K. Soetaert and W. Helder. 2002. On the oxidation and burial of organic carbon in sediments of the Iberian margin and Nazaré canyon (NE Atlantic). Progr. Oceanogr. Accepted.

Froelich, P.N., G.P. Klinkhammer, M.L. Bender, N.A. Luedtke, G.R. Heath, D. Cullen, P. Dauphin, D. Hammond, B. Hartman and V. Maynard. 1979. Early oxidation of organic matter in pelagic sediments of the eastern equatorial Atlantic: suboxic diagenesis. Geochim. Cosmochim. Acta, 43, 1075-1090.

Froelich, P.N., M.L. Bender, N. A. Luedtke, G.R. Heath and T. DeVries. 1982. The marine phosphorus cycle. Am. J. Sci., 282, 474-511.

Hem, J.D. 1981. Rates of manganese oxidation in aqueous systems. Geochim. Cosmochim. Acta, 45, 1369-1374.

Holland, H.D. 1978. The chemistry of atmosphere and oceans Wiley Interscience, NY.

Howarth, R.W., H.S. Jensen, R. Marino and H. Postma. 1995. Transport to and processes of phosphorus in near-shore and oceanic waters. In H. Tiesen (ed.) Phosphorus in the global environment, Wiley NY, SCOPE 54, 323-346.

Hulth, S., R.C. Aller, F. Gilbert, 1999. Coupled anoxic nitrification/manganese reduction in marine sediments. Geochim. Cosmochim. Acta, 63, 49-66.

Ingall, E.D. and P. Van Cappellen. 1990. Relation between sedimentation rate and burial of organic phosphorus and organic carbon in marine sediments. Geochim. Cosmochim. Acta, 54, 373-386.

Ingall, E.D. and R. Jahnke. 1994. Evidence for enhanced phosphorus regeneration from sediments overlain by oxygen depleted waters. Geochim. Cosmochim. Acta, 58, 2571-2575.

Jørgensen. B.B. 1983. Processes at the sediment-water interface. In The major biogeochemical cycles and their interactions. B. Bolin and R.B. Cook, eds, John Wiley ,Chichester. p 477-515.

Kessick, M.A. and J.J. Morgan. 1975. Mechanism of autoxidation of manganese in aqueous solution. Environ. Sci. Technol., 9, 157-159.

König, I., M. Drodt, E. Suess and A.X. Trautwein. 1997. Iron reduction through the tan-green color transition in deep-sea sediments. Geochim. Cosmochim. Acta, 61, 1679-1683.

König, I., M. Haeckel, M. Drodt, E. Suess and A.X. Trautwein. 1999. Reactive Fe(II) layers in deep-sea sediments. Geochim. Cosmochim. Acta, 63, 1517-1526.

Kostka, J.E., E. Haefele, R. Viehweger and J.W. Stucki. 1999. Respiration and dissolution of iron(III)-containing clay minerals by bacteria. Environ. Sci Technol., 33, 3127-3133.

Krom, M. D. and R.A. Berner. 1980. Adsorption of phosphate in anoxic marine sediments. Limnol. Oceanogr., 25, 797-806.

Lovley, D.R. 1991. Dissimilatory Fe(III) and Mn(IV) reduction. Microbial. Rev., 55, 259-287.

Lovley, D.R. and E.J.P. Phillips. 1988. Novel mode of microbial energy metabolism: Organic carbon oxidation coupled to dissimilatory reduction of iron or manganese. Appl. Environ. Microbiol., 54, 1472-1480.

Lucotte, M., A. Mucci, C. Hillaire-Marcel and S. Tran. 1994. Early diagenetic processes in deep Labrador Sea sediments: reactive and non-reactive iron and phosphorus. Can. J. Earth Sci., 31, 14-27.

Luther III, G.W., 1991. Pyrite synthesis via polysulphide compounds. Geochim. Cosmochim. Acta, 55, 2839-2849.

Luther III, G.W., B. Sundby, B.L. Lewis, P.J. Brendel and N. Silverberg. 1997. Interactions of manganese with the nitrogen cycle: Alternative pathways to dinitrogen. Geochim. Cosmochim. Acta, 61, 4043-4052.

Lyle, M. 1983. The brown-green color transition in marine sediments: A marker of the Fe(III)-Fe(II) redox boundary. Limnol. Oceanogr., 28, 1026-1033.

Martens, C.S., R.A. Berner and J.K. Rosenfeld. 1978. Interstitial water chemistry of anoxic Long Island Sound sediments. 2. Nutrient regeneration and phosphate removal. Limnol. Oceanogr., 23, 605-617.

Middelburg, J.J., G.J. de Lange and C.H. van der Weijden. 1987. Manganese solubility control in marine pore waters. Geochim. Cosmochim. Acta, 51, 759-763.

Middelburg, J.J., K. Soetaert, and P.M.J. Herman. 1997. Empirical relationships for use in global diagenetic models. Deep-Sea Res., 44, 327-344.

Millero, F.J., S. Sotolongo and M. Izaguirre. 1987. The oxidation kinetics of Fe(II) in seawater. Geochim. Cosmochim. Acta, 51, 793-801.

Müller, P.J. and E. Suess. 1979. Productivity, sedimentation rate and sedimentary organic matter in the oceans. I. Organic carbon preservation. Deep-sea Res., 26A, 1347-1362.

Murray, J.W. 1979. Iron oxides. In Marine Minerals R.G. Burns (ed) Reviews in Mineralogy, Vol. 6, Mineralogical Society of America, Washington DC, pp 47-97.

Myers, C. R and K. H. Nealson. 1988. Bacterial manganese reduction and growth with manganese oxide as the sole electron acceptor. Science, 240, 1319-1321.

Nealson, K.H. and C.R. Myers. 1992. Microbial reduction of manganese and iron: New approaches to carbon cycling. Appl. Environ. Microbiol., 58, 439-443.

Nealson, K.H. and D. Saffarini. 1994. Iron and manganese in anaerobic respiration: Environmental significance, physiology and regulation. Annu. Rev. Microbiol., 48, 311-343.

Ottley, C.J., W. Davison, and W.M. Edmunds. 1997. Chemical catalysis of nitrate reduction by iron(II). Geochim. Cosmochim. Acta, 61, 1819-1828.

Postma, D. 1985. Concentration of Mn and separation from Fe in sediments. Kinetics and stoiciometry of the reaction between birnessite and dissolved Fe(II) at 10°C. Geochim. Cosmochim. Acta, 49, 1023-1033.

Postma, D. and R. Jakobsen. 1996. Redox zonation: Equilibrium constraints on the Fe(III)/SO_4-reduction interface. Geochim. Cosmochim. Acta, 60, 3169-3175.

Pyzik, A.J. and S.E. Sommer. 1981. Sedimentary iron monosulphides: kinetics and mechanism of formation. Geochim. Cosmochim. Acta, 45, 687-698.

Raiswell, R. and Canfield, D.E., 1998. Sources of iron for pyrite formation in marine sediments. Am. J. Sci., 298, 219-245.

Ruttenberg, K.C. and R.A. Berner. 1993. Authigenic apatite formation and burial in sediments from non-upwelling, continental margin environments. Geochim. Cosmochim. Acta, 57, 991-1007.

Schink, D.R. and N.L. Guinasso Jr. 1978. Redistribution of dissolved and adsorbed materials in abyssal marine sediments undergoing biological stirring. Am. J. Sci., 278, 687-702.

Schippers, A. and B.B. Jørgensen. 2001. Oxidation of pyrite and iron sulfide by manganese dioxide in marine sediments. Geochim. Cosmochim. Acta, 65, 915-922.

Slomp, C.P., E.H.G. Epping, W. Helder and W. van Raaphorst. 1996a. A key role for iron-bound phosphorus in authigenic apatite formation in North Atlantic continental platform sediments. J. Mar. Res., 54, 1179-1205.

Slomp, C.P., J.F.P. Malschaert and W. van Raaphorst. 1998. The role of sorption in sediment-water exchange of phosphate in North Sea continental margin sediments. Limnol. Oceanogr., 43, 832-846.

Slomp, C.P., S.J. Van der Gaast and W. Van Raaphorst. 1996b. Phosphorus binding by poorly crystalline iron oxides in North Sea sediments. Mar. Chem., 52, 55-73.

Sørensen, J., K.S. Jørgensen, S. Colley, D.J. Hydes, J. Thomson and T.R.S. Wilson. 1987. Depth localization of denitrification in a deep-sea sediment form the Madeira Abyssal Plain. Limnol. Oceanogr., 32, 758-762.

Stone, A.T. 1987. Microbial metabolites and the reductive dissolution of manganese oxides: Oxalate and pyruvate. Geochim. Cosmochim. Acta, 51, 919-925.

Stone, A.T. and J.J. Morgan. 1984. Reduction and dissolution of Manganese(III) and Manganese(IV) oxides by organics: 2. Survey of the reactivity of organics. Environ. Sci. Technol., 18, 617-624.

Straub, K.L., Benz, M., Schink,B., Widdel, F., 1996. Anaerobic, nitrate-dependent microbial oxidation of ferrous iron. Appl. Environ. Microbiol., 62, 1458-1460.

Suess, E. 1980. Particulate organic carbon flux in the oceans: Surface productivity and oxygen utilization. Nature, 288, 260-263.

Sunda, W.G. and D.J. Kieber. 1994. Oxidation of humic substances by manganese oxides yields low-molecular-weight organic substrates. Nature, 367, 62-64.

Sundby, B., C. Gobeil, N. Silverberg and A. Mucci. 1992. The phosphorus cycle in coastal marine sediments. Limnol. Oceangr., 37, 1129-1145.

Sundby, B., L.G. Anderson, P.O.J. Hall, A. Iverfeldt, M.M. Rutgers van der Loeff, S.F.G. Westerlund. 1986. The effect of oxygen on release and uptake of cobalt, manganese, iron and phosphate at the sediment-water interface. Geochim. Cosmochim. Acta, 50, 1281-1288.

Thamdrup, B., R.N. Glud and J.W. Hansen. 1994. Manganese oxidation and in situ manganese fluxes from a coastal sediment. Geochim. Cosmochim. Acta, 58, 2563-2570.

Van Aken, H. 2000. The hydrography of the mid-latitude Northeast Atlantic Ocean II: The intermediate water masses. Deep Sea Res. I., 47, 789-824.

Van Cappellen, P. and E.D. Ingall. 1994. Benthic phosphorus regeneration, net primary production, and ocean anoxia: a model of the coupled marine biogeochemical cycles of carbon and phosphorus. Paleoceanography, 9, 677-692.

Van Cappellen, P. and E.D. Ingall. 1996. Redox stabilisation of the atmosphere and oceans by phosphorus-limited marine productivity. Science, 271, 493-496.

Van Cappellen, P. and R.A. Berner. 1988. A mathematical model for the early diagenesis of phosphorus and fluorine in marine sediments: apatite precipitation. Am. J. Sci. 288, 289-333.

Van Raaphorst, W. and H.T. Kloosterhuis. 1994. Phosphate sorption in superficial intertidal sediments. Mar. Chem., 48, 1-16.

Van Raaphorst, W., P. Ruardij and A.G. Brinkman. 1988. The assessment of benthic phosphorus regeneration in an estuarine ecosystem model. Neth. J. Sea Res., 22, 23-36.

Van Weering, T.C.E., H.C. De Stigter, W. Boer and H. De Haas. 2002. Recent sediment transport and accumulation at the western Iberian margin. Progr. Oceanogr., Accepted.

Walsh, J.J. 1991. Importance of continental margins in the marine biogeochemical cycles of carbon and nitrogen. Nature, 350, 53-55.

Wilson, D.E. 1980. Surface and complexation effects on the rate of Mn(II) oxidation in natural waters. Geochim. Cosmochim. Acta., 44, 1311-1317

Wollast, R. 1991. The coastal organic carbon cycle: Fluxes, sources and sinks. p 365-382. In, Mantoura, R.F.C., J.M. Martin, R. Wollast, eds. Ocean margin processes in global change, Dahlem Workshop reports. Wiley Interscience, Chichester.

CHAPTER TWO

Manganese and Iron diagenesis in temporal and permanent depositional areas of the North Sea[1]

ABSTRACT

In hydrodynamically active systems such as the North Sea, Mn and Fe (hydr-) oxide distributions in the sediment depend on (1) redox reactions, (2) sediment reworking by biota, and also (3) on the hydrodynamic regime through episodic sorting of particles. After a perturbation, pore water distributions adjust rapidly to new conditions, whereas the solid phase may exhibit transient concentration profiles for a longer period. The aim of this study was to investigate Mn and Fe diagenesis in such dynamic shelf sediments. We sampled three silty stations in the North Sea (Frisian Front, German Bight and Skagerrak) during February, May, August 1994 and November 1995. The Skagerrak is a very stable environment that served as base-line for the moderately energetic Frisian Front and highly energetic German Bight. Profiles of solid phase Mn and Fe were transient at the Frisian Front and the German Bight, although the pore water profiles appeared at steady state. Association of the Mn-and Fe oxides with organic matter that is preferentially reworked by biota was one reason of non-steady state depth distributions. The second reason was the hydrodynamic regime at the shallow sites which affected the vertical layering of particle size distribution and thus of the Mn and Fe associated with specific grain sizes. Mn and Fe diagenesis is stimulated in dynamic temporal deposition areas due to burial of reactive Mn and Fe oxides and organic material below the depth of oxygen penetration, thereby providing the prerequisites for suboxic diagenesis. These "disturbed" sediments, that occupy a major part of shelf seas, are important, yet often overlooked areas for suboxic diagenesis.

INTRODUCTION

Degradation of organic matter occurs in the water column and in the sediment after deposition (Nedwell, 1984). Depending on their free energy yield and availability, a suite of electron acceptors is used in the oxidation of organic matter, i.e. first oxygen in the oxic layer, then NO_3^-, Mn^{4+} and Fe^{3+} (as solid phase oxides) in the suboxic layer, and finally SO_4^{2-} in the anoxic layer of the sediment (Froelich *et al.*, 1979). In addition, Mn oxide reduction can be coupled to the oxidation of solid phase sulphides by bacteria (Aller and Rude, 1988), or to the chemical oxidation of Fe^{2+}

[1] This Chapter by Claar van der Zee, Wim van Raaphorst, Willem Helder and Hans de Heij has been submitted to Continental Shelf Research.

(Postma, 1985). Mn^{2+} is usually oxidised by dissolved oxygen, whereas Fe^{2+} oxidation can be coupled to the microbial reduction of nitrate (Straub *et al.*, 1996). Fe oxyhydroxides are reduced chemically by hydrogen sulphide produced during bacterial sulphate reduction (Pyzik and Sommer, 1981). The chemical depth zonation that results from these redox reactions is well developed in undisturbed marine sediments (Froelich *et al.*, 1979) and can be reproduced by early diagenetic models (Rabouille and Gaillard, 1991;Van Cappellen and Wang, 1996).

In highly energetic environments, the oxidised and reduced layers are mixed or turned over occasionally due to bioturbation (Aller 1994a), wave action (Aller*et al.*, 1986) and other perturbations such as trawling (Churchill, 1989). Aller (1994a) argued that disturbed sediments should be conceptualised as a spatially and temporally changing mosaic of redox environments. Recently, Anschutz*et al.* (2000) supported this concept showing pore water profiles of Mn^{2+}, Fe^{2+}, N and I species in bioturbated shelf sediments. Bioturbation can be regarded as a succession of local and non-local mixing events that disrupt the distributions of pore water and solid phase species, which afterwards evolve toward a steady state. Consequently, such distributions reflect a transient state. Sediment reworking, be it biological or physical, enhances suboxic diagenesis. In Panama Basin and Long Island Sound sediments, the rapid reworking by the benthic community enhances the intensity of Mn cycling (Aller 1994b; Aller *et al.*, 1998). In Amazon shelf sediments, physical reworking enhances Fe cycling and suboxic organic matter decomposition (Aller*et al.*, 1986).

Both biological and physical reworking of the sediment is important in shelf seas like the North Sea. Jenness and Duineveld (1985) demonstrated that phytodetritus was mixed into the sediment under influence of ripple formation and breakdown. Van Raaphorst *et al.* (1998) showed the occurrence of tidal erosion and deposition in the Oyster grounds of the North Sea, with major erosion events during storms and enhanced deposition thereafter. Mixing of recent fine-grained sediment with relic deposits due to bioturbation, physical processes and beam trawl fishery resulted in phantom ^{210}Pb activity profiles in North Sea sediments (De Haas *et al.*, 1997). In this contribution, we focus on the solid phase distributions of manganese and iron. As diffusive transport of pore water species is typically faster than mixing of particles in the sediment, we expect pore water profiles to readjust more rapidly to new conditions after a perturbation than the solid phases. Therefore, transient features are expected most pronounced in solid Mn and Fe profiles.

Three stations representative for different erosion-deposition regimes were sampled in the North Sea. The relatively deep and sheltered Skagerrak is selected as a reference site characterised by a steady sedimentation regime, where the well-established redox sequence is reflected in a vertical chemical zonation (Bakker and Helder, 1993). In contrast with the Skagerrak, two shallow and highly dynamic areas were sampled. These sites in the Frisian Front and the German Bight are characterised by periods of deposition alternated by erosion (Lohse *et al.*, 1995). The Skagerrak, Frisian Front and German Bight stations were sampled in February, May and August 1994 and November 1995. In North Sea surface sediments, the sediment grain size fraction < 20 μm correlates positively with organic carbon content (Wiesner *et al.*, 1990). Both metals and C_{org} are expected to be associated with the finer fraction, although not necessarily with each other. Mn and Fe (hydr-) oxides are believed to be present as coatings on particles (Burns and Burns, 1979), and because finer particles

have a higher specific surface area their Mn and Fe contents will be higher also. Mn and Fe oxides precipitated *in situ* from solution are fine-grained as well (Murray *et al.*, 1985; Buffle *et al.*, 1989; Deng, 1997). Therefore, we measured Mn, Fe, C_{org} and the grain size distribution of the solid phase. In this contribution, we attempt to explain non-steady state situations and to estimate Mn and Fe reduction rates in these dynamic North Sea sediments. Several examples of biological and physical reworking are discussed as well as the correlation of solid Mn and Fe with C_{org} at our stations. Metal oxide reduction rates are estimated and discussed and we conclude with a section on the implications of highly dynamic conditions in temporal deposition areas for Mn and Fe diagenesis.

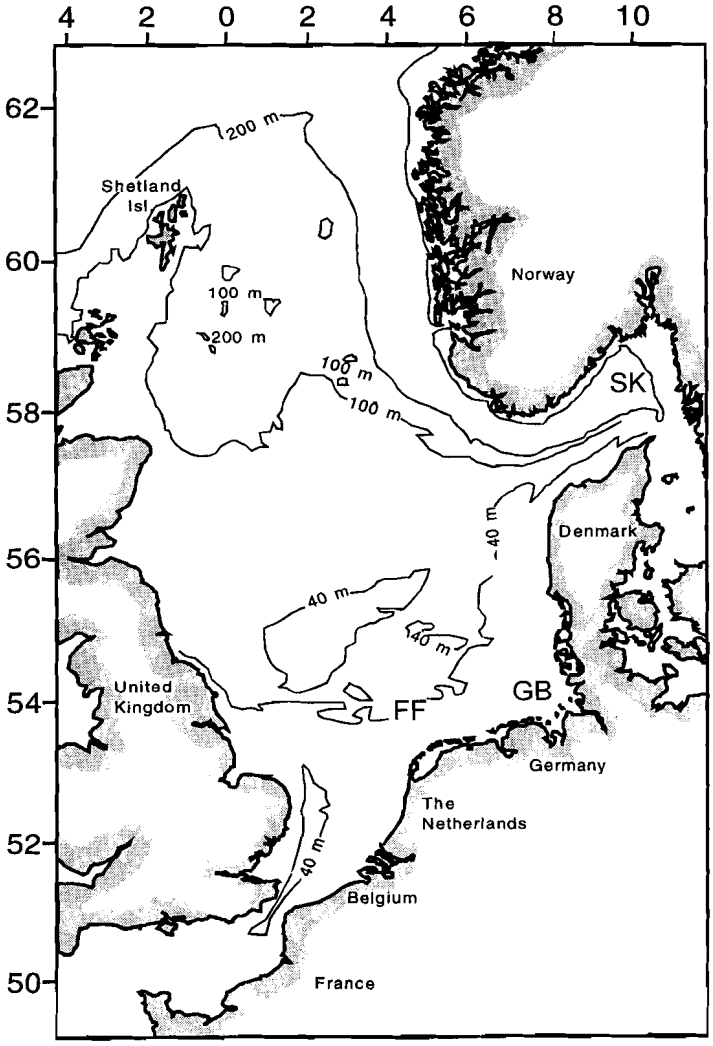

Figure 1. Map of the North Sea indicating the visited stations (FF, GB and Sk).

MATERIALS AND METHODS

Study Area

The North Sea is a semi-enclosed shelf sea, connected with the North East Atlantic Ocean through the Strait of Dover between the United Kingdom and France in the south, and through the large open boundary between Norway and Scotland in the north (Fig. 1). Thermal stratification develops during the summer in areas with a water depth > 30 m, while at shallower depth the water column is well mixed throughout the year due to tidal stirring (Otto *et al.*, 1990). The main water circulation pattern and suspended matter transport is counter-clockwise. Along its transport route, the organic matter becomes progressively more refractory due to ageing following upon a series of deposition-resuspension events (Lohse *et al.*, 1995; Dauwe and Middelburg, 1998). Consequently, organic matter in the sediments of the Frisian Front and German Bight are less aged and more labile than in the Skagerrak (Lohse *et al.*, 1995; Dauwe and Middelburg, 1998). Anaerobic carbon oxidation is important at all three stations visited (Canfield *et al.*, 1993; Jørgensen, 1989; Osinga *et al.*, 1996; Slomp *et al.*, 1997; Upton *et al.*, 1993). The Skagerrak/Norwegian Trench (~700 m) is the major deposition area for North Sea sediments (sedimentation rate up to 1.1 cm yr^{-1}, Erlenkeuser and Pederstad, 1984; Van Weering *et al.*, 1987; Van Weering *et al.*, 1993; De Haas and Van Weering, 1997). Input of organic material in the Skagerrak is dominated by relatively refractory organic matter from the Scandinavian mainland, the Baltic and particularly from the North Sea shelf (Van Weering *et al.*, 1987; Anton *et al.*, 1993).

Particles from the East Anglian turbidity plume and the south-western North Sea can settle in the Frisian Front area in spring and summer (Puls and Sündermann, 1990; Sündermann, 1993; Van Raaphorst et al., 1998), however, these particles are eroded again during autumn and winter storms (Kempe et al., 1988; Puls and Sündermann, 1990). As a result, net deposition of sediment at the Frisian Front is probably minor (Eisma, 1981; Nedwell et al., 1993). The sediment consists of old reworked deposits partly mixed with recent sediments (De Haas et al., 1997). Data obtained during our August cruise indicate that the brittle star *Amphiura filiformis* and the subsurface deposit feeding shrimp Callianassa subterranea are important members of the macrofaunal community (Dauwe et al., 1998). Echinoderms (particularly *Amphiura*) are the dominant group (in terms of biomass) and most abundant in the 2-5 cm depth interval (Dauwe et al., 1998).

In the German Bight, residence times of the water are relatively long due to a counter clockwise circulation pattern. The main sources of nutrient input are the rivers Elbe and Weser, which directly discharge into the German Bight (Bauerfeind et al., 1990). As a result, large amounts of locally produced organic material are deposited in summer (Joint and Pomroy, 1993). Interface feeders dominate the macrofaunal community in the German Bight (Dauwe *et al.*, 1998). They are more adapted to the strongly variable tidal currents that frequently resuspend surficial organic matter (Boon and Duineveld, 1996) than the subsurface deposit feeders as found at the Frisian Front. The German Bight (~20 m water depth) is a deposition area for which sedimentation rates ranging between 0.16-0.50 cm yr^{-1} have been reported (Reineck, 1960 and 1963; Reineck *et al.*, 1967; Gadow, 1969; McCave, 1970; Dominik *et al.*, 1978). These sedimentation rates should, however, be considered on the appropriate

timescale and used with caution, because the German Bight is a relict depression that was filled up during the Holocene. At present, fine-grained suspended material from the Wadden Sea is temporarily deposited in the German Bight (Dellwig *et al.*, 2000), before it is eroded again by wave action and transported further to the Skagerak/ Norwegian Trench area. Oxygen deficiency may develop in the bottom water during calm weather conditions in summer (Von Westernhagen *et al.*, 1986).

Table 1. Name, geographical position, water depth and bottom water temperature in February, May, August and November.

Station	N	E	Depth (m)	Bottom water Temperature (°C)			
				Feb	May	Aug	Nov
Frisian Front	53°42'	04°30'	39	4.5	11.2	17.6	13.0
German Bight	54°05'	08°09'	20	3.8	10.3	19.1	10
Skagerrak	58°12'	10°15'	270	6.8	5.9	6.5	7.2

Sampling, pore water and sediment characteristics

The three stations were visited during four cruises with RV Pelagia in February, May and August 1994 and November 1995 (Table 1). Sediment cores were obtained either with a cylindrical corer (31 cm i.d.), which was sub-sampled with acrylic liners (5.4 cm i.d.) closed with rubber stoppers, or directly with a multi-corer (tubes 6.3 cm i.d.). Only cores without visible surface disturbance were used. All subsequent sediment handling took place at *in situ* temperature. Cores were sliced in four 2.5-mm intervals (0-2.5, 2.5-5, 5-7.5 and 7.5-10 mm), four 5-mm intervals (10-15, 15-20, 20-25 and 25-30 mm), four 10-mm intervals (30-40, 40-50, 50-60 and 60-70 mm) and two 15-mm intervals (70-85, 85-100 mm). Sediment of 4 cores was pooled and centrifuged (10 min, 3000 rpm). Pore water was collected after centrifugation and filtered (0.45 µm, Acrodisc). Aliquots for nitrate and ammonia were measured on board on a TRAACS-800 auto-analyser according to the method of Strickland and Parsons (1972) and Helder and De Vries (1979), respectively. Aliquots for iron and manganese were acidified to pH ~ 1 and measured on a TRAACS-800 auto-analyser according to the methods of Stookey (1970) and Brewer and Spencer (1971), respectively. After pore water collection the sediment was stored frozen (-20 °C) until solid phase analysis in the NIOZ laboratory. Freeze-dried and ground (teflon mortar and pestle) sediment was extracted for reactive Fe and Mn with 1M HCl (20 °C, 24 hrs; Canfield, 1988; Slomp *et al.*, 1997). HCl (1M) is expected to extract Fe from poorly crystalline Fe oxides, acid volatile sulphides and some Fe from clay minerals (Canfield, 1988; Slomp *et al.*, 1996). We assume that FeS accounted for less than ~10% of the 1M HCl-extracted Fe based on results of other studies on Fe in North Sea sediments (e.g. Jorgensen, 1989; Canfield *et al.*, 1993). Organic carbon was measured on a Carlo-Erba N-1500 elemental analyser following the procedure of Verardo *et al.* (1990) and Lohse *et al.* (2000). Grain size distributions were measured by laser diffraction on a Coulter LS 230 after organic matter removal with peroxide (Konert and Vandenberghe, 1997). Porosity was determined by weight loss after drying at 60 °C for 48 h and assuming a specific weight of 2.65 g cm^{-3}.

Oxygen measurements and Sediment Oxygen Demand

Oxygen penetration depths were measured in subcores taken from the box-corer. A stirrer was placed in the overlying water at about 3 cm above the sediment surface and the core was left to equilibrate at *in situ* temperature for several hours before measuring the oxygen penetration depth with Clark-type micro electrodes (Diamond, type 737). Tidal currents may induce enhanced turbulent diffusion transport of oxygen in the upper millimetres of sandy sediments, thereby altering the oxygen penetration depth (Lohse *et al.*, 1996). Also coring may possibly cause artefacts. After equilibration, the core adjusts to molecular diffusion-dominated conditions and the oxygen penetration depths are comparable with pore water profiles of other dissolved constituents. The micro-electrodes were mounted on a automated profiler with a minimum step-size of 10 μm. In general a step-size of 100 μm was chosen.

The sediment community oxygen consumption was measured by on-deck incubation of whole cylindrical cores (31 cm i.d.) made of polyester. A detailed description is given in Boon *et al.* (1998). Briefly, the corer encloses a 30 to 50 cm sediment column and 15 to 25 l of overlying water. On deck the box was closed with an acrylic lid mounted with a sampling port, a stirring motor and an oxygen and temperature electrode (YSI, type 5739). Boxes were kept at *in situ* temperature by a thermostatic water bath and incubated for about 10 hours. The diffusive boundary layer was 390 μm thick. Oxygen electrodes were calibrated in aerated, oxygen saturated water (100% O_2) and in oxygen-depleted (sodium sulphite) water (0% O_2) by Winkler titration.

Models

The diagenetic model of Slomp *et al.* (1997) was applied to selected metal profiles for two purposes; (1) to estimate metal reduction rates, assuming steady state, e.g. at the Skagerrak, and (2) to asses the deviations from a steady state situation in the more energetic Frisian Front and German Bight. The model describes steady state pore water and solid phase metal profiles, for details see Slomp *et al.* (1997). Briefly, the sediment column is divided into an oxic layer and an anoxic layer, that is, the oxic-anoxic boundary depth is imposed. Transport of the solid phase in both layers is assumed to result from sediment accumulation and bioturbational/ physical mixing described as a biodiffusion process. Transport of dissolved constituents is assumed to occur by molecular diffusion in both layers. First-order reactions include dissolved Mn^{2+} and Fe^{2+} oxidation in the oxic layer and precipitation in the anoxic layer, and metal oxide reduction in the anoxic layer. In addition, instantaneous reversible sorption of dissolved Mn^{2+} and Fe^{2+} is assumed. The input parameters are sedimentation rate, molecular diffusion coefficients, biodiffusion coefficient, porosity, depth of redox boundary, first-order rate constants for oxidation, linear sorption coefficients, and the pore water and solid phase concentrations at each depth interval. Four parameters (the oxide deposition flux, the first-order rate constants for reduction and precipitation, and the concentration of unreactive oxide) were varied to fit the model to the data while variance-weighted sums of squares for the solute and oxide were minimised simultaneously. Values for input parameters (Table 2) for the Skagerrak and Frisian Front are the same as given in Slomp *et al.* (1997), except for the molecular diffusion coefficients. Those were calculated as described below in the paragraph on estimates of diffusive fluxes by application of Fick's first law. Because

data on the linear sorption coefficients, biodiffusion coefficient and sedimentation rate were not available for the German Bight, the values of the input parameters of the Frisian Front were also used for the German Bight (Table 2).

Table 2. Input parameters used for model calculations (Slomp *et al.*, 1997).

Station Season	(1) k_{ox} Mn^{2+} (d^{-1})	(2) k_{ox} Fe^{2+} (d^{-1})	(3) Db ($m^2\ d^{-1}$)	(4) $D_s Mn^{2+}$ ($m^2\ d^{-1}$)	(5) $D_s Fe^{2+}$ ($m^2\ d^{-1}$)	(6) Sed. rate ($m\ d^{-1}$)	(7) L Mn^{2+} (m)	(8) L Fe^{2+} (m)	(9) Ks Mn^{2+} (-)	(10) Ks Fe^{2+} (-)	(11) Por. (v/v)
					Skagerrak						
Feb	1	10	2.76E-6	2.61E-5	2.67E-5	1.37E-5	7.1E-3	2.8E-2	4	4	0.85
May	1	10	2.76E-6	2.52E-5	2.52E-5	1.37E-5	4.3E-3	1.3E-2	4	4	0.85
Aug	1	10	2.76E-6	2.61E-5	2.67E-5	1.37E-5	9.2E-3	2.3E-2	4	4	0.85
Nov	1	10	2.76E-6	2.61E-5	2.67E-5	1.37E-5	9.7E-3	1.8E-2	4	4	0.85
					Frisian Front						
May	1	10	1.4E-6	1.80E-5	1.83E-5	2.74E-8	2.2E-3	2.0E-2	1	1	0.55
Nov	1	10	1.4E-6	1.91E-5	1.93E-5	2.74E-8	3.9E-3	7.5E-3	1	1	0.55
					German Bight						
Aug	1	10	1.4E-6	2.44E-5	2.45E-5	2.74E-8	2.2E-3	1.3E-2	1	1	0.60
Nov	1	10	1.4E-6	1.89E-5	1.92E-5	2.74E-8	3.3E-3	5.0E-3	1	1	0.60

(1) and (2): the oxidation rate constants for Mn and Fe, (3) biodiffusion coefficient, (4) and (5) the molecular diffusion coefficients for Mn and Fe in sea water corrected for temperature (Li and Gregory, 1974) and tortuosity (Boudreau, 1997), (6) sedimentation rate, (7) and (8) depth of Mn and Fe redox boundary, (9) and (10) linear sorption coefficients for Mn and Fe, (11) porosity.

A second model was applied in cases where solid phase metal profiles were believed to be transient, but pore water profiles in pseudo-steady state. The inverse model for the analysis of pore water profiles of Berg *et al.* (1998) was used. This model calculates the net consumption or production of a solute species at discrete depth intervals, assuming steady state of the pore water profile. It was applied to the Mn^{2+} and Fe^{2+} pore water profiles of the Frisian Front and German Bight. Three kinds of transport can be included in the analysis, molecular diffusion, bioturbation and irrigation. Measured concentrations are used to approximate concentration gradients and with known values of porosity, molecular diffusion coefficient, biodiffusion coefficient and irrigation coefficient, the net rate of production can be estimated via an optimisation procedure. A series of possible fits are compared through statistical F-testing to select the simplest production-consumption profile that reproduces the concentration profile. The input parameters were the porosity and pore water depth distributions, the biodiffusion coefficient (Table 2) and the molecular diffusion coefficients calculated as described in the following paragraph. Irrigation was not included, as quantitative data on this process were not available.

Finally, diffusive fluxes (J) of Mn^{2+} and Fe^{2+} were estimated directly from the application of Fick's first law to the observed pore water gradients in the Frisian Front and German Bight. The diffusion coefficient in seawater corrected for temperature (D_{sw}; Li and Gregory, 1974) and tortuosity (Boudreau, 1997) gives the sedimentary diffusion coefficient (D_{sed}) in which ϕ represents porosity. The flux J is then determined as:

$$J = -\phi . D_{sed} \frac{\partial C}{\partial x} \quad \text{with } D_{sed} = \frac{D_{sw}}{1 - \ln(\phi^2)}$$

The steepest gradients in the pore water profiles were used to calculate the upward and downward dissolved metal fluxes and their sum gives the dissolved metal production, i.e. the metal reduction rate.

RESULTS

General sediment characteristics

In the Skagerrak, sediment porosity, bulk median grain size (Lohse *et al.*, 1995) and ^{210}Pb activity (De Haas *et al.*, 1997) are rather depth invariant (Fig. 2). Median grain size is 11 μm. Sediment porosity is ~0.9 (v/v) at the sediment-water interface (SWI) decreasing to ~0.8 (v/v) at depth. The porosity profiles are near exponential and little differences exist between the different times of sampling.

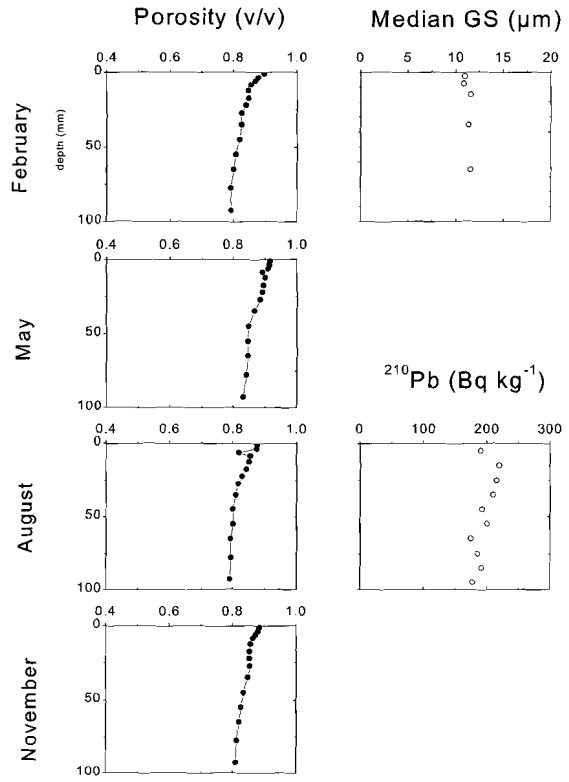

Figure 2. Depth distributions of porosity, median grain size and ^{210}Pb activity at the Skagerrak.

At the Frisian Front, porosity is ~0.6-0.7 at the SWI decreasing to ~0.5 (v/v) at depth (Fig. 3). Median grain size is around 100 µm with some major deviations. Several layers can be distinguished at the Frisian Front, which deviate from the trends observed at the reference station Skagerrak. Fine-particle or high-porosity layers are indicated with hatched bars in the figures. In May, a high-porosity layer is observed at depths of ~3 to 6 cm, with the same porosity as observed at the sediment-water interface. In November, a fine-particle layer is present in dept interval ~1.5-5 cm. Above and below this layer, the particles are coarser with similar median grain sizes as in the other seasons. In February and August, thin fine-particle layers with minor deviations in porosity and grain size occur close to the sediment-water interface. De Haas *et al.* (1997) interpret the ^{210}Pb activity profile as a representation of sediment consisting of old reworked deposits that are partly mixed with recent sediments, for example by the burrowing shrimp *Callianassa subterranea*.

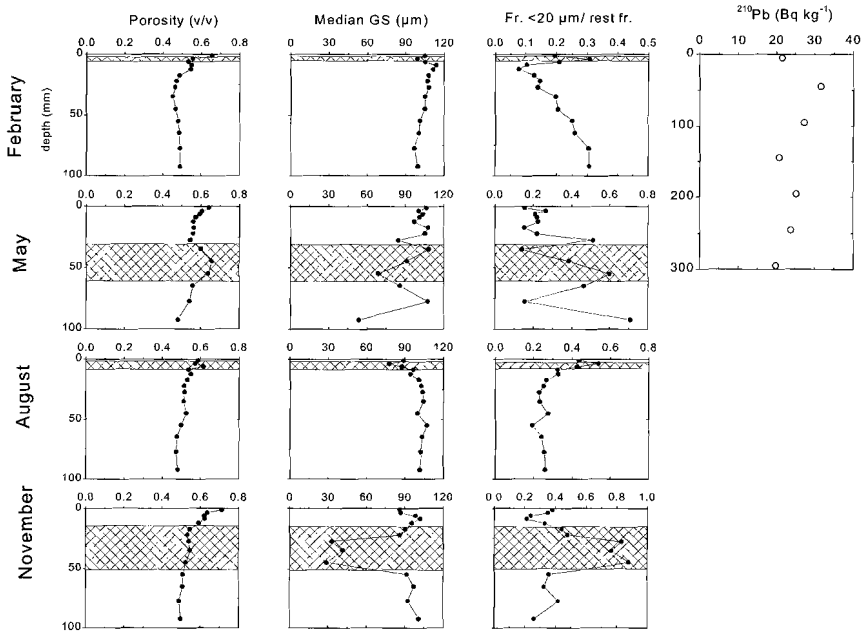

Figure 3. Depth distributions of porosity, median grain size, fraction < 20µm normalised to the fraction > 20µm and ^{210}Pb activity at the Frisian Front.

In the German Bight, sediment porosity varies between 0.4 and 0.9 (v/v), but roughly converges to 0.6 (v/v) at depth (Fig. 4). The median grain size is ~60 µm, however, it exhibits major variations (Fig. 4). In February and May, the normalised size fraction <20 µm increases from the sediment surface to 2 cm depth as indicated with the upper hatched bar. A coarser sediment layer is present from 2 to 6 cm, whereas the normalised fraction < 20 µm increases again from 6 to 10 cm. In general, high porosity is associated with fine material and low porosity with coarser sandier sediment. The porosity profiles show the same trend as the grain size data in February and May (Fig. 4). Thus, the sediment consists of three layers, fine – coarse – fine, in February and May. In February, a veneer of coarser particles appears on top of the sediment. In August, sediment porosity and grain size profiles indicate a high-porosity layer consisting of very fine material (~7 µm) in the upper 2 cm (hatched bar). The fine material appears to be deposited on top of "older" coarser German Bight sediment, below ~4 cm depth, with a porosity of ~0.6 and median GS of ~60 µm like the 7-10-cm layer in May. The smaller particles are admixed with the "older" sediment in the transition layer between 2 and 4 cm depth. In November, sediment porosity and grain size show a coarse layer between 0.75 and 2.5 cm depth. The normalised fraction <20 µm shows a layers of finer material (hatched bars) between 0.25 and 0.75 cm, 2.5 and 6 cm and 8.5 and 10 cm depth, alternated with coarser layers. De Haas *et al.* (1997) measured a ^{210}Pb-activity profile with three peaks, which

coincide with thin light layers in the X-radiograph of the same core from a station near our German Bight station (Fig. 5).

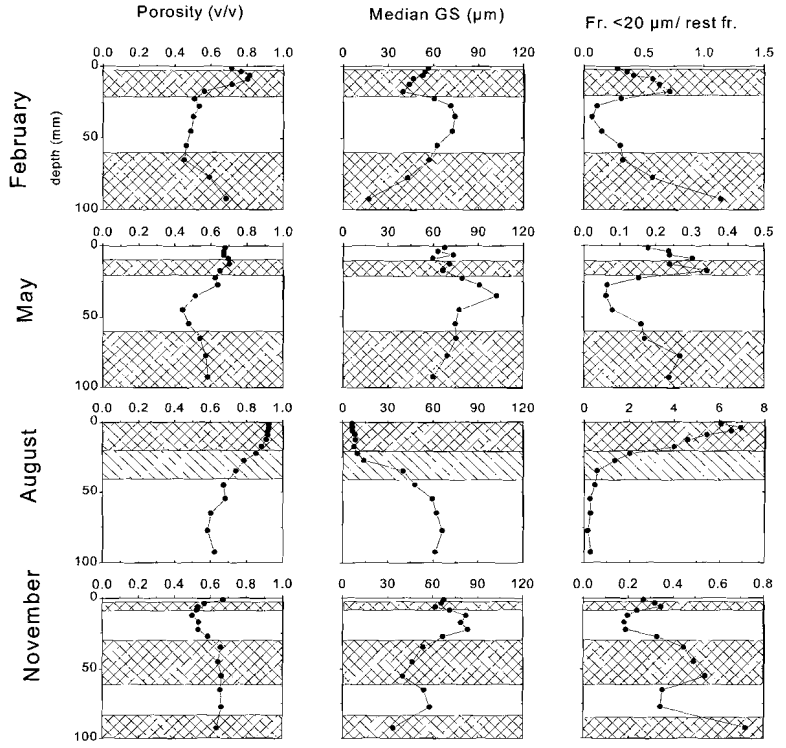

Figure 4. Depth distributions of porosity, median grain size, and fraction < 20µm normalised to the fraction > 20µm at the German Bight.

Organic matter mineralisation

Sediment community oxygen consumption (SCOC) shows seasonal variations (Table 3), but is generally highest in the German Bight and lowest in the Skagerrak. Frisian Front and Skagerrak sediment communities consumed most oxygen in May, whereas at the German Bight SCOC was highest in August, probably associated with the layer of fine particles on top of the sediment in that month. The SCOC values are comparable to the total mineralisation rates estimated by sediment incubations and subsequent headspace analysis of evolved CO_2 at the same stations (Dauwe *et al.*, 2001).

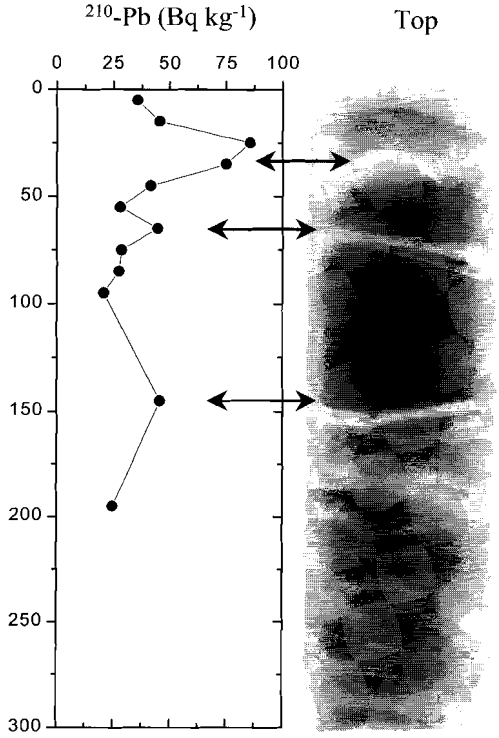

Figure 5. Vertical profile of the ^{210}Pb activity and X-radiograph a sediment core retrieved close to our German Bight station (De Haas *et al.*, 1997).

Table 3. Sediment Community Oxygen Consumption (mmol O_2 m^{-2} d^{-1}).

Station	February	May	August	November
Frisian Front	5.5	42.2	23.2	18.0
German Bight	8.3	36.3	86.1	27.9
Skagerrak	5.8	15.8	11.5	8.5

In the Skagerrak, oxygen penetration depths range between ~4-10 mm (Table 4). The nitrate concentrations reach their maximum close to the sediment-water interface (Fig. 6). We do not have an explanation for the large sub-surface nitrate maximum in May. Irrigation is unlikely, since the bottom water has lower nitrate and ammonia concentrations and only nitrate has a large subsurface maximum. Anoxic oxidation of ammonia by Mn oxides (Hulth *et al.*, 1999; Anschutz *et al*, 2000) is also unlikely, because this is not apparent in the ammonia profile. Furthermore, Thamdrup *et al.* (2000) recently showed that the anoxic oxidation of ammonia by Mn oxides does not occur in Skagerrak sediments. We therefore regard the nitrate subsurface maximum as suspect. Ammonia concentrations increase with depth without reaching an asymptotic value within the sampled interval. The organic carbon profiles are rather uniformly distributed with depth, with some small deviations.

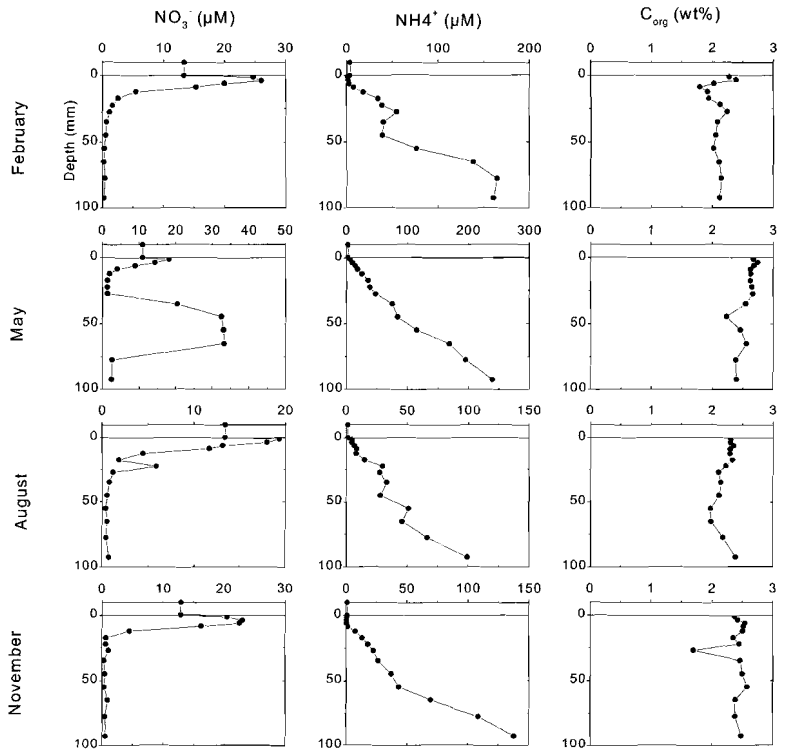

Figure 6. Pore water profiles of nitrate and ammonia, and organic carbon profiles at the Skagerrak.

Table 4. Oxygen penetration depth (mm) in the sediment of the Frisian Front, German Bight and Skagerrak.

Station	February	May	August	November
Frisian Front	4.4	2.2	3.7	3.9
German Bight	2.3	2.3	2.2	3.3
Skagerrak	7.1	4.3	9.2	9.7

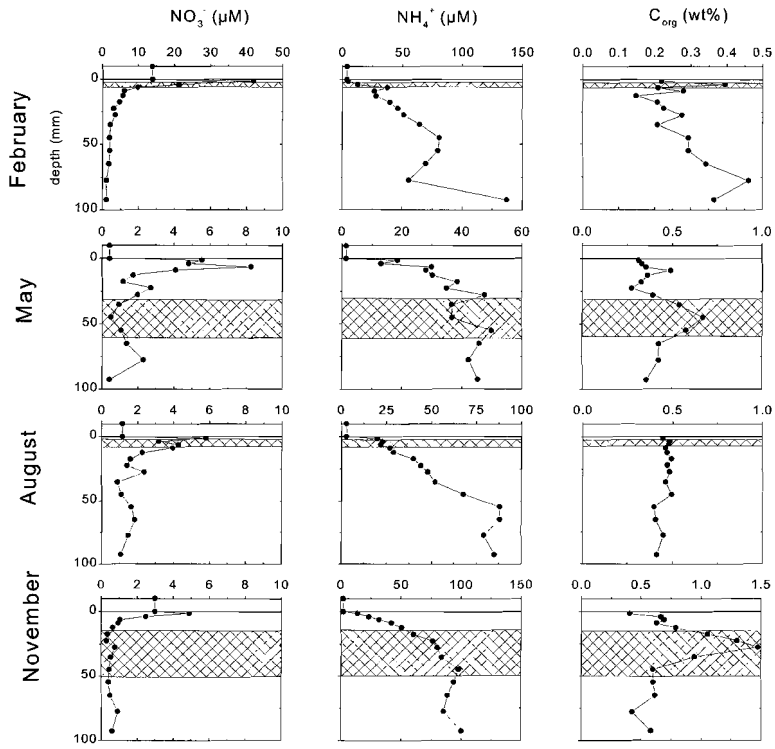

Figure 7. Pore water profiles of nitrate and ammonia, and organic carbon profiles at the Frisian Front.

At the Frisian Front, oxygen penetration depth ranges from ~2-4 mm into the sediment (Table 4). Nitrate 'background' concentrations of ~1-2 µM are reached between ~7.5-35 mm depth (Fig. 7). Ammonia concentrations increase with depth and reach their asymptotic values in May and November within the sampled interval. Sediment heterogeneity has a major effect on the organic carbon distributions and a minor effect on the pore water species. Elevated organic carbon concentrations are found in the high-porosity layer (3-6 cm) in May and in the fine-particles layer (1.5-5 cm) in November. In February, a relatively high C_{org} concentration is found in the fine-particle layer.

At the German Bight, oxygen penetration ranges between ~2-3 mm depth (Table 4). Nitrate concentrations rapidly decline with depth in the sediment, with the exception of a small subsurface peak at the top of the coarse-particle layer in August (Fig. 8). Ammonia concentrations increase with depth up to mM level indicating high metabolic activity and consequently reducing conditions. Elevated ammonia concentrations are found in the fine-particle layer in August. As at the Frisian Front,

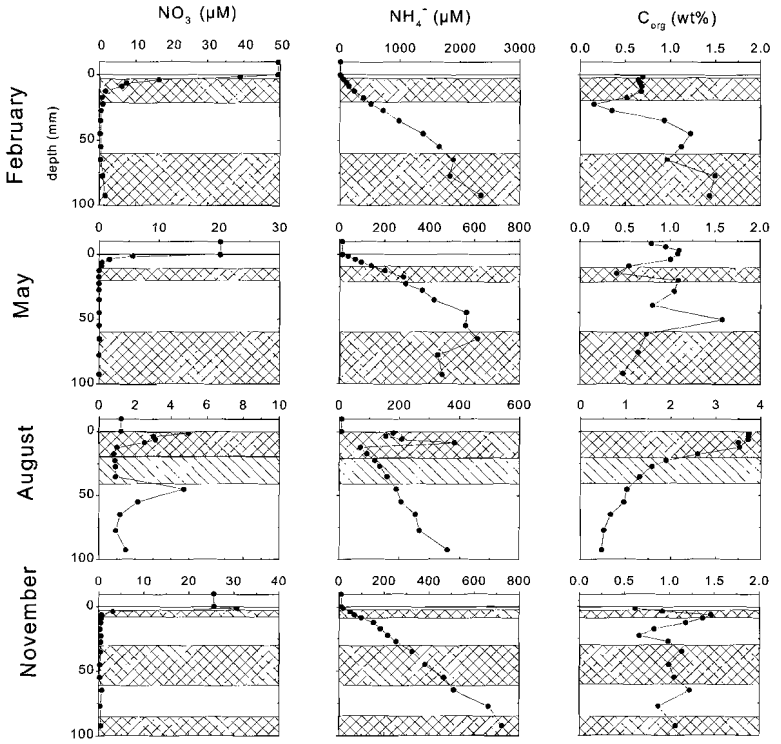

Figure 8. Pore water profiles of nitrate and ammonia, and organic carbon profiles at the German Bight.

the different sediment layers have a major impact on the C_{org} distributions. The organic carbon profiles of February and May show minima at the transition from the upper fine-particle layer to the coarse-particle layer below. In August, very high organic carbon concentrations are found in the upper 2-cm of the sediment, i.e. the fine-particle layer. In November, the organic carbon content is highest in the upper fine-particle layer and decrease with depth in the coarse-particle layers, from 0.75 to 3 cm and from 6 to 8.5 cm depth.

Manganese and Iron diagenesis

At the Skagerrak, Mn^{2+} appears in the pore water below the depth of oxygen penetration (Fig. 9). Upward diffusing Mn^{2+} is oxidised in the oxic layer and forms a solid phase Mn oxide enrichment near the sediment-water interface with contents ranging between ~2.7 and 11.7 µmol Mn g^{-1}. At the Skagerrak, solid iron oxides are rather uniformly distributed with depth, although a small surface enrichment is observed in all months. Fe contents range between 178-271 µmol Fe g^{-1}. Fe^{2+} appears

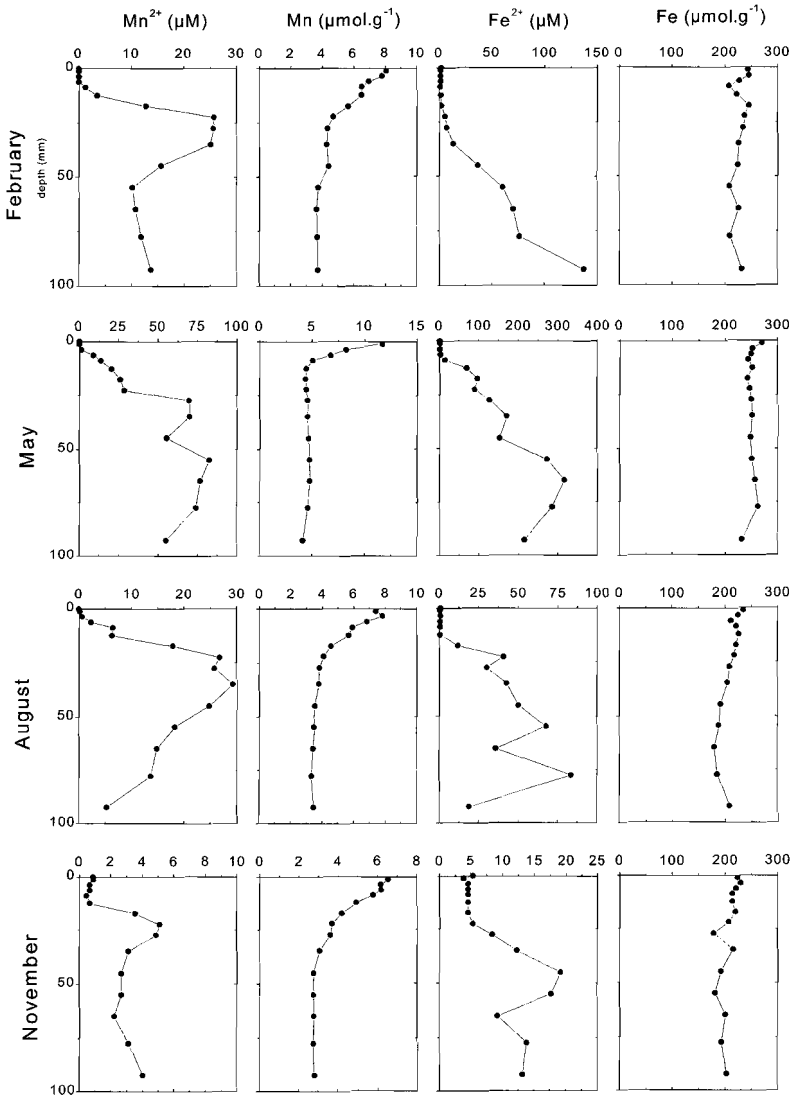

Figure 9. Profiles of dissolved Mn^{2+} and Fe^{2+}, and solid phase manganese and iron at the Skagerrak.

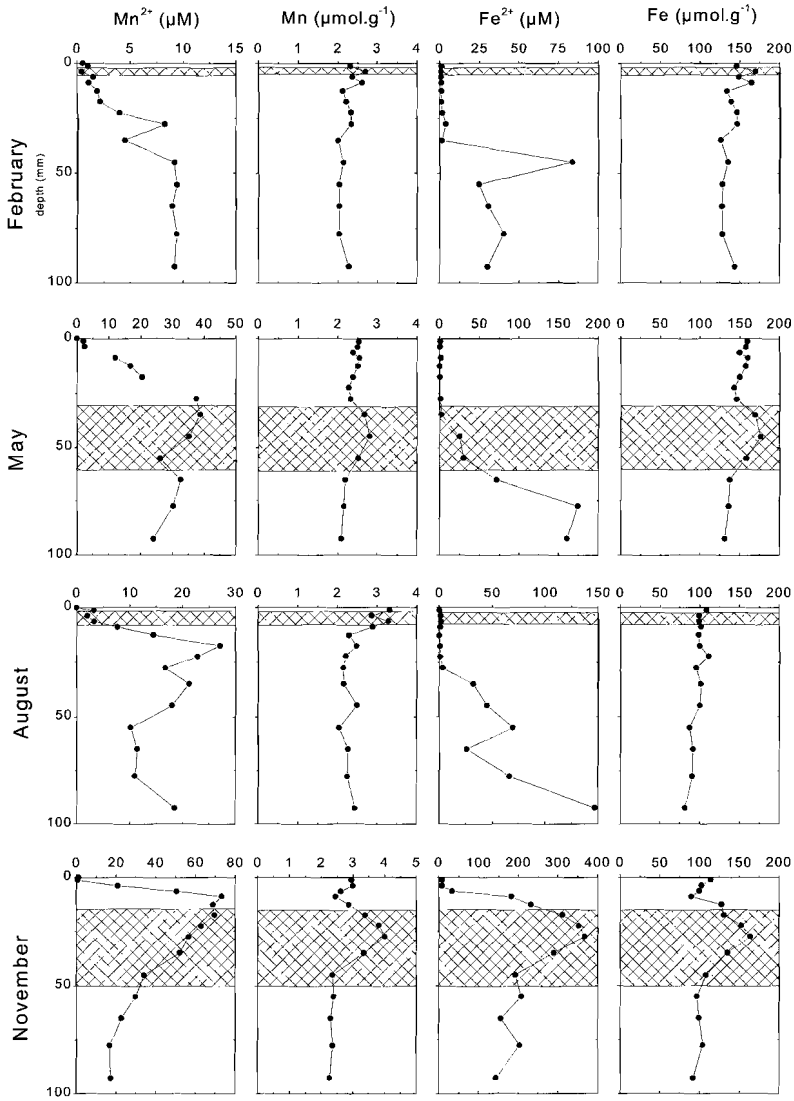

Figure 10. Profiles of dissolved Mn^{2+} and Fe^{2+}, and solid phase manganese and iron at the Frisian Front.

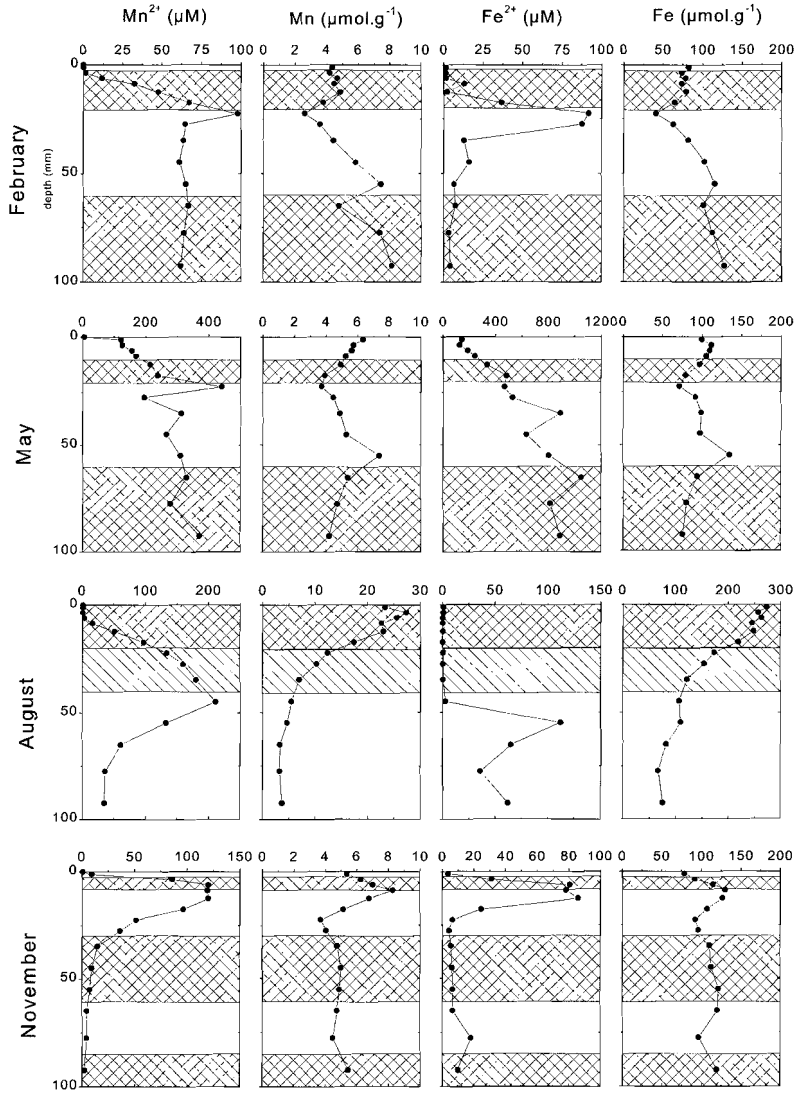

Figure 11. Profiles of dissolved Mn^{2+} and Fe^{2+}, and solid phase manganese and iron at the German Bight.

in the pore water at the depth where nitrate reaches its background value. Dissolved Fe^{2+} has its maximum always deeper than Mn^{2+}, consistent with the classical redox zonation (Froelich *et al.*, 1979).

At the Frisian Front, oxygen penetrates less deep in the sediment than at the Skagerrak allowing pore water Mn^{2+} to accumulate at shallower depth in the sediment (Fig.10). The solid phase Mn profiles have a surface enrichment indicating that pore water Mn^{2+} is oxidised in the oxic layer. The different sediment layers have a major impact on the solid Mn and Fe distributions in May and November. In addition to the surface enrichments, subsurface maxima of both solid Mn and Fe occur in May and November, corresponding with the high-porosity layer in May and the fine-particle layer in November. These maxima are located in the anoxic layer and thus are possibly dissolving at the time of sampling. The broad dissolved Mn^{2+} maximum in May is likely to be the result of the merging of two sources of Mn^{2+}, i.e. the Mn oxide enrichment at the sediment-water interface and the Mn oxide maximum associated with the high-porosity layer. The upward diffusing Mn^{2+} is oxidised near the sediment-water interface resulting in the observed surface enrichments, whereas the upward diffusing Fe^{2+} is oxidised well below the sediment-water interface except in November. At the Frisian Front pore water Fe^{2+} has its maximum deeper than Mn^{2+} as observed at the Skagerrak. The solid phase Mn and Fe contents of the Frisian Front sediment ranges from ~2-4 μmol Mn g^{-1} and ~80-180 μmol Fe g^{-1}, respectively.

At the German Bight, sediment community oxygen consumption is highest of the three stations and pore water Mn^{2+} and Fe^{2+} reach their highest concentrations at this station (Fig. 11). Again, the different sediment layers have similar effects on the solid Mn and Fe distribution as on the organic carbon profiles. Solid phase Mn and Fe contents range between ~2-28 μmol Mn g^{-1} and 40-273 μmol Fe g^{-1}. Surface enrichments of solid phase Mn and Fe are observed in February, May and August. The subsurface maxima in the solid phase in February, May and November are located in the anoxic layer, and thus should be dissolving. In August, exceptionally high solid phase contents of Mn and Fe coincide with the layer of very fine sediment on top of coarser sediment in August. The indicated transition layer shows the decline of Mn and Fe content with depth due to mixing of both end members. The subsurface metal peaks in November are located in the metal reduction zone and were likely dissolving at the time of sampling. Although, both Mn^{2+} and Fe^{2+} are oxidised at the sediment-water interface, no visible surface enrichment had formed, yet. The solid Mn and Fe contents decrease with depth in the coarse sediment layers and are roughly constant in between, similar to the organic carbon.

Table 5. Integrated metal reduction rate obtained by fitting the model of Slomp *et al.* (1997) to the metal profiles of the Skagerrak, values between brackets are estimated using the model of Berg *et al.* (1998).

Skagerrak Season	Mn reduction (μmol m^{-2} d^{-1})	Fe reduction (μmol m^{-2} d^{-1})
February	141 (82)	283 (56)
May	127 (89)	340 (265)
August	158 (50)	958 (74)
November	174 (13)	559 (39)

Model results

At the Skagerrak, it is reasonable to assume steady state, including constant deposition fluxes of Mn and Fe oxides, and perturbations can be described by biodiffusive mixing. Thus the model of Slomp *et al.* (1997) is applied in order to estimate metal reduction rates. The model fits the data fairly well, except for the solid Mn profile in May and the pore water Fe^{2+} in November (Fig. 12). These non-zero Fe^{2+} concentrations in the upper 2-cm are likely to be an artefact. Depth integrated Mn reduction rates are fairly constant throughout the season, whereas the depth integrated Fe reduction rates vary seasonally at the Skagerrak (Table 5). Reduction rates estimated using the model of Berg are always lower than those estimated using the model of Slomp (Table 5). The reason is that the mechanistic model of Slomp estimates the total reduction rate, whereas the inverse fit model of Berg estimates the net metal reduction rate. This is because the model of Slomp includes the recycling between the oxides and the solutes, i.e. dissolved metals are re-oxidised to oxide and subsequently reduced again.

The model of Slomp *et al.* (1997) was applied to profiles of the Frisian Front (May and November) and the German Bight (August and November) as well, to illustrate the deviation from "normal" steady state profiles and to assess the qualitative effect of the vertical sediment heterogeneity on metal reduction (Fig. 13). At the Frisian Front, the model can not reproduce the subsurface maxima in solid Mn and Fe associated with the high-porosity layer in May. Here, the dissolved Mn maximum is too broad to be modelled, because of the existence of two distinct Mn reduction sources: the subsurface and surface Mn oxide maxima. The surface enrichment, however, is also replenished by re-oxidation of upward diffusing Mn^{2+}. The modelled Fe reduction starts at the depth where nitrate is depleted, but pore water Fe^{2+} appears deeper in the sediment. In November, the subsurface maxima of solid phase Mn and Fe are not reproduced either. No broad Mn^{2+} maximum is observed like the one in May, because the subsurface maximum is closer to the sediment-water interface in November. At the German Bight in August, Fe reduction starts a few cm below the depth where nitrate is depleted like in May at the Frisian Front and the solid Mn gradient is larger than that of the pore water. At the German Bight in November, Mn and Fe reduction takes place in a relatively sharp confined layer, where pore water and solid Mn and Fe maxima coincide, which can not be reproduced by the model.

The numerical code of Berg *et al.* (1998) selects the simplest production-consumption profile that reproduces the measured data. Due to the relatively low resolution of the data, the numerical code does not resolve all maxima and minima typical for the disturbed sediments. (The fits are not shown in order to reduce the number of graphs in this paper). The relatively small production layers are lumped together excluding the possibility to discriminate between metal reduction close to the SWI and deeper in the sediment. Consequently, it is not possible to quantify the additional metal reduction due to perturbations.

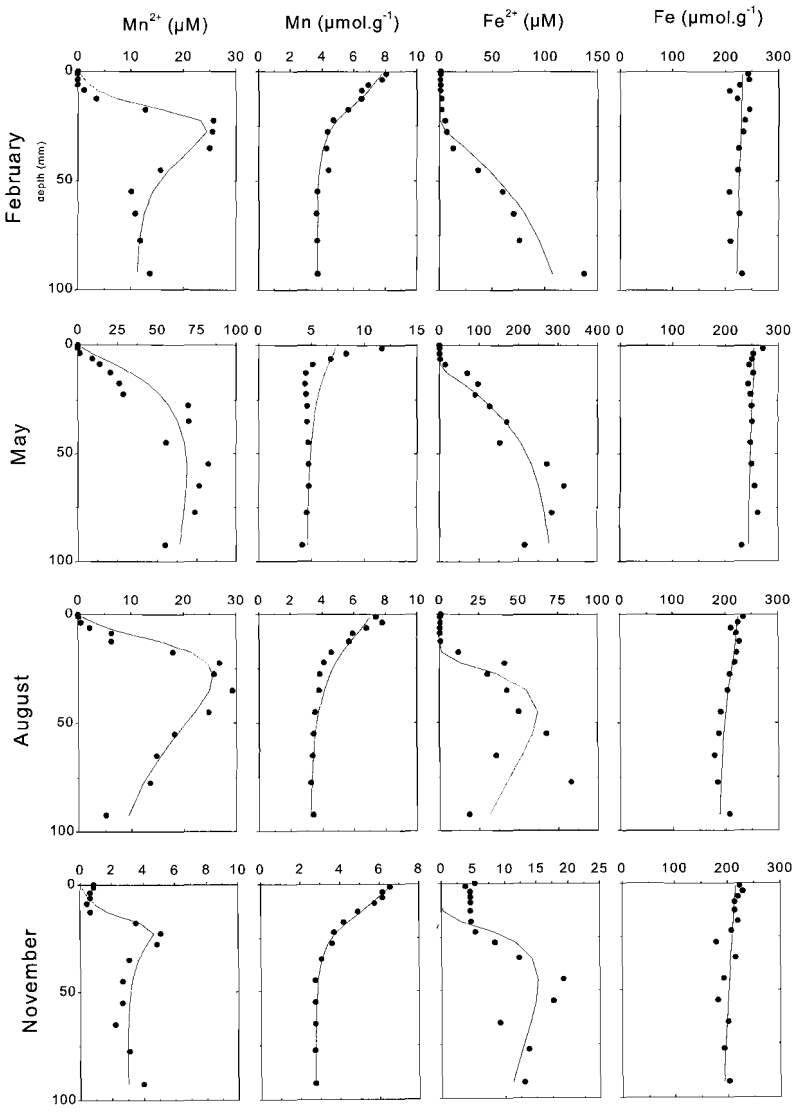

Figure 12. Model fits (lines) to the Mn and Fe data (dots) of the Skagerrak.

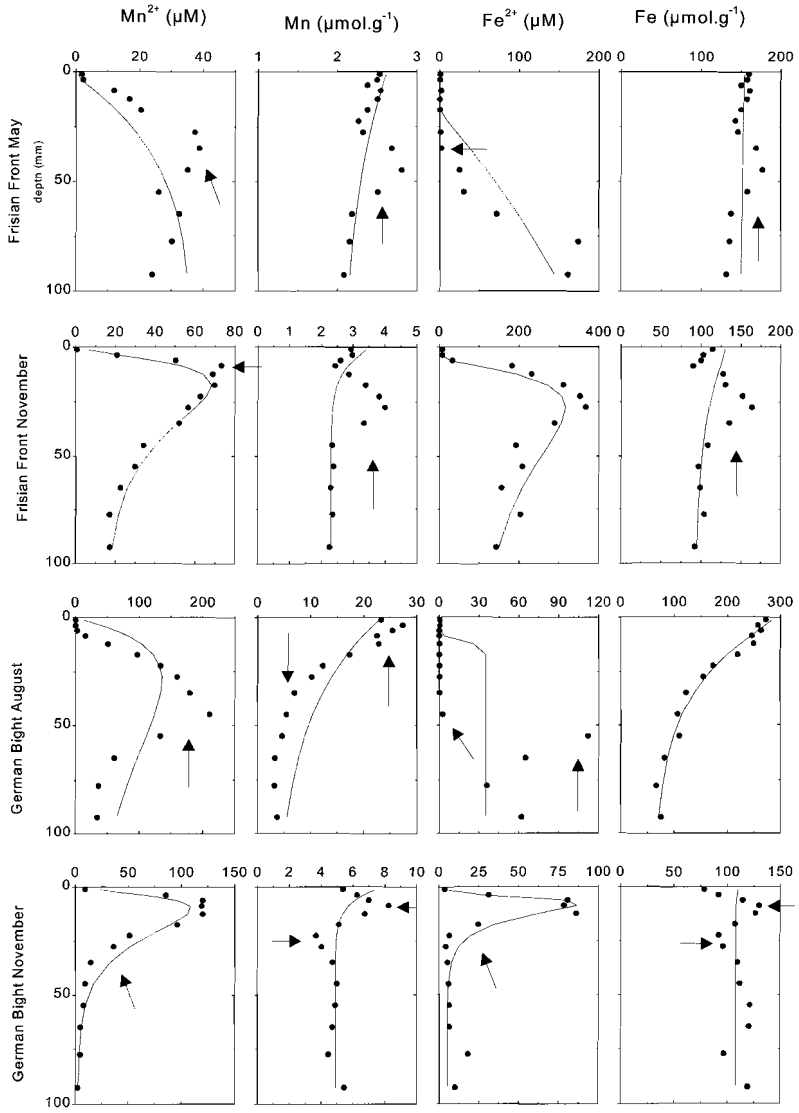

Figure 13. Model non-fits (lines) to the Mn and Fe data (dots) of the Frisian Front and German Bight.

The net metal reduction rates in sediments of the Frisian Front and German Bight calculated using Fick's first law are presented in Table 6. Metal reduction rates are higher at the German Bight than at the Frisian Front, except for Fe in November. At the Frisian Front, both Mn and Fe reduction rates are highest in November exceeding those in the other seasons by an order of magnitude. At the German Bight metal reduction rates are highest in May also exceeding those in other seasons by an order of magnitude.

Table 6. Metal reduction rate estimated using Fick's first law and Berg's numerical code in brackets

	Mn reduction $\mu mol\ m^{-2}\ d^{-1}$	Fe reduction $\mu mol\ m^{-2}\ d^{-1}$		Mn reduction $\mu mol\ m^{-2}\ d^{-1}$	Fe reduction $\mu mol\ m^{-2}\ d^{-1}$
FF feb	4 (1)	86 (55)	GB feb	194 (61)	157 (109)
FF may	18 (19)	90 (109)	GB may	1434 (323)	1719 (381)
FF aug	30 (14)	42 (29)	GB aug	405 (413)	287 (124)
FF nov	154 (106)	903 (691)	GB nov	451 (254)	300 (166)

DISCUSSION

Factors influencing Mn and Fe distributions

The pore water profiles are internally consistent and follow the well-known sequence of electron acceptor utilisation (Froelich *et al.*, 1979). Deviations from this pattern are, for example, the subsurface nitrate peaks and small peaks and dips in the metal pore water profiles. Solid phase Mn and Fe, however, seem to be in a transient state. The particular shapes of these metal profiles and of C_{org} were also found by Slomp *et al.* (1997) and Van Raaphorst *et al.* (1992) at the same stations in the same seasons, but in other years, suggesting that the underlying processes are not accidental and seasonally reoccurring. Factors of influence on the sedimentary distribution of Mn and Fe (hydr-) oxides are (1) redox reactions, (2) biological and physical reworking of the sediment, and (3) grain size distributions by different sedimentation patterns. All three factors influence to different extents each profile making it difficult to separate the influence of a single factor. Some examples of sediment disturbances will be discussed below, e.g. tidal or storm-induced sediment erosion and deposition, and the activity of a subsurface dwelling organism.

Grain size. De Haas *et al.* (1997) showed the importance of the hydrodynamic regime on the sedimentary structure and grain size of a core taken close to our German Bight station. The X-radiograph taken from this core showed an alternation of thick sandy layers, deposited under high-energy conditions, and thin light layers consisting of clayey-silty deposits, deposited under quiet conditions and coinciding with ^{210}Pb peaks (Fig. 5). This indicates that the core consists of a sequence of storm deposits (De Haas *et al.* 1997). Because fine-grained sediments have a larger specific surface area and ^{210}Pb is attached to the surface of sediment particles, the ^{210}Pb activity of fine particles is higher than that of coarse particles (Nittouer *et al.*, 1979). Organic matter in marine sediments is primarily associated with the mineral phase and the relation between organic matter concentration and sediment specific surface area suggests adsorption (Mayer, 1994). By this rationale, smaller particles, with larger specific

surface area contain more organic matter. Recently, organic matter was found to be associated with mineral grains in a localised patch-like fashion instead of a monolayer coating (Ransom *et al.*, 1997; Mayer 1999). Nevertheless, grain size and organic matter concentration are inversely correlated (Mayer et al., 1993; Mayer 1994; Keil et al., 1994), as is also observed in the North Sea sediments (Cadée, 1984; Creutzberg*et al.*, 1984; Wirth and Wiesner, 1988; Wiesner *et al.* 1990). At the Frisian Front, the fine-particle layer in November corresponds with peaks observed in the Mn, Fe and C_{org} profiles. The higher Mn, Fe and C_{org} concentrations in November are likely the result of a surface area effect. At the German Bight, the solid phase Mn and Fe profiles in February resemble the C_{org} and normalised <20 μm-fraction profiles suggesting a distribution predominantly dictated by grain size, although the minimum is shifted somewhat deeper for the fraction <20 μm. Trap samples collected during the February cruise at the German Bight point at a strong resuspension event (Boon and Duineveld, 1996). Thus, hydrodynamics appears dominating over redox reactions in determining the observed solid phase Mn and Fe profiles in February at the German Bight and in November at the Frisian Front. Layers of fine material with concomitant higher contents of Mn, Fe and C_{org} are buried below the depth of oxygen penetration, which may result in the reductive dissolution of the Mn and Fe oxides coupled to the oxidation of organic carbon by bacteria.

Sediment reworking by biota. The high-porosity layer at the Frisian Front in May contains higher amounts of C_{org}, Mn and Fe than the sediment above and below. The grain size distribution does not provide any evidence for storm deposits as possible explanation of the observed C_{org} maximum. Van Raaphorst *et al.* (1992) showed organic carbon data from the same location with distinct maxima at ~30 mm (January and April 1989 and April 1990) and at ~50 mm depth in August (1989). The observed maxima in the organic carbon profiles can be explained by the feeding behaviour of the brittle star *Amphiura* (Van Raaphorst *et al.*, 1992) which is very abundant at this station (Dauwe *et al.,* 1998). *Amphiura* transports food with its arms from the sediment surface to the place where it lives, which is usually around 30-mm depth (Ockelmann and Muus, 1978) and is known as an indicator of an enhanced supply of food to the benthos (Cramer 1991). The sediment oxygen demand increases dramatically in May, coinciding with the formation of a large subsurface enrichment in organic carbon due to *Amphiura* translocating organic material to depth. Apparently, solid phase Mn and Fe are associated with the organic material. This is not observed in August, possibly because the SCOC is already reduced considerably in August 1994. Alternatively, bioturbation may also play a role in smoothing the solid phase profiles. By transporting particles from the sediment surface to a few cm depth, *Amphiura* injects relatively fresh organic material together with Mn and Fe oxides into the reduced sediment layer providing the prerequisites for suboxic diagenesis. Also, it enhances the rate of particle transport from the oxic to the reduced layer, which has been found to be the rate limiting factor for Mn and Fe cycling in Iberian margin sediments (Van der Zee *et al.*, 2001; 200x).

Mass deposition of fine material. A clear example of the grain size effect is demonstrated at the German Bight in August. The very high organic carbon content of almost 4 wt % C at the sediment water interface compared with 1 wt % C in August 1991 (Lohse *et al.*, 1995) suggests that a major deposition event occurred just before

the sediment was sampled. The chlorophyll a inventory measured over the upper 10 cm shows a higher value in May than in August (Boon, 1998). Therefore, it is unlikely that settlement of a phytoplankton bloom caused the observed layer. Probably, the calm weather in August provided the conditions necessary for the deposition of this fine particulate material. Annual wind speed data show consistent weakening in summer, together with a decreased discharge of the Elbe (Bauerfeind, 1990; Radach *et al.*, 1990). Grain size analysis indicates that a thick layer of very fine material (7-8 μm median grain size) is deposited on top of the "old" sediment with a median grain size of 60-70 μm (Fig. 14). Intermixing of the upper fine-grained sediment with the older coarser sediment only occurs between 2 and 4 cm depth. Although the C_{org}, Mn and Fe profiles in this season appear to be the only "normal" distributed profiles at the German Bight, they are completely dictated by sediment grain size, reflecting the recent deposition history.

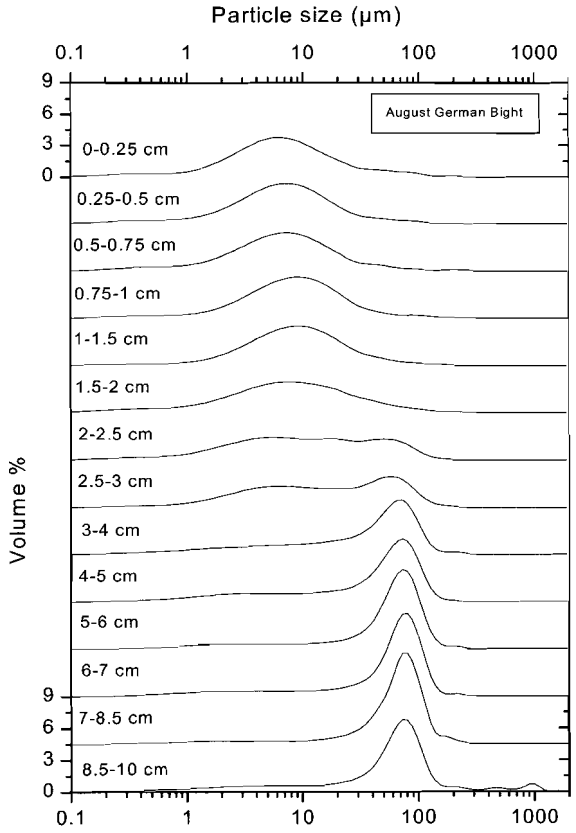

Figure 14. Grain size spectra for all sediment depth intervals at the German Bight in August.

Mn and Fe association with C_{org}

Although the extent to which different factors influence the Mn and Fe distribution varies per station and season, Mn and Fe are evidently associated with fine particles and C_{org}. Linear regression shows good correlations between Mn and Fe vs. C_{org} at the German Bight, reasonable correlations at the Frisian Front, but poor correlations in the Skagerrak (Table 7). Although the correlation between Mn and C_{org} is poor in the Skagerrak, the average ratio of Mn to C_{org} is identical to the one at the Frisian Front. The sediment is relatively enriched in manganese at the German Bight compared to the Frisian Front and the Skagerrak (Table 7) particularly in August. Mn and Fe coatings on suspended matter in the North Sea have been speculated to originate from epibenthic fluxes of dissolved Mn^{2+} and Fe^{2+} that oxidise on particulate matter in the water column (Dehairs *et al.*, 1989; Schoemann *et al.*, 1998). Thus, effluxes of Mn^{2+} and Fe^{2+} in May in the Wadden Sea (König 1996) may fuel the Mn and Fe enrichment on suspended matter, which settles during low energy conditions, like in August, at the German Bight (Dellwig *et al.*, 2000). This explains the higher sedimentary ratio of Mn to C_{org} in August at the German Bight. For Fe the same scenario could operate, but because the Fe concentration is much higher than the Mn concentration, the extra Fe is not as obvious in the ratio. The ratio of Fe to C_{org} is similar at the German Bight and the Frisian Front. Between February-May and August-November the intercept, B in Table 7, decreases. The higher value in February-May is similar to the Skagerrak value and the lower one in August-November is similar to that of the German Bight. The larger intercept may indicate a higher Fe background concentration associated with sediments containing refractory organic carbon. Possibly, the solid phase Fe is more crystalline after several resuspension-deposition cycles, while the labile organic carbon is degraded and the refractory carbon fraction remains.

Table 7. Results from linear regression,
1N HCl-extractable metal ($\mu mol\ g^{-1}$) = A x C_{org} (wt%) + B

Metal	A	B	r^2	n	Seasons	Station*
Mn	6.6	- 0.7	0.95	56	All	GB
Mn	2.8	+ 2.5	0.64	42	Nov, Feb, May	GB
Mn	7.0	- 1.0	0.99	14	Aug	GB
Mn	1.6	+ 1.8	0.60	56	All	FF
Mn	1.6	+ 1.4	0.05	56	All	SK
Fe	60	+ 43	0.97	56	All	GB
Fe	57	+44	0.81	42	Nov, Feb, May	GB
Fe	58	+50	0.99	14	Aug	GB
Fe	63	+ 68	0.97	28	Aug, Nov	FF
Fe	56	+ 128	0.24	28	Feb, May	FF
Fe	44	+ 122	0.22	56	All	SK

* GB represents German Bight, FF is Frisian Front and SK stands for Skagerrak

Mn and Fe reduction rates

At the Skagerrak, some seasonal variation is observed in the Fe reduction rates as well as in the sediment community oxygen consumption, and suggests minor temporal variation in organic matter input. Sediment trap studies in the western Skagerrak did show some variations in deposition fluxes associated with end of the spring and autumn bloom (Kempe and Jennerjahn, 1988). The seasonal variation at the Skagerrak is probably caused by a small contribution of local primary production, additive to a large and more stable background.

Due to their highly energetic nature, steady state conditions can not be assumed at the Frisian Front and German Bight, which complicates the estimation of actual metal reduction rates. Application of the Slomp model to the Frisian Front and German Bight metal profiles exemplifies the transient state of the solid phase profiles and the inability to simultaneously resolve pore water and solid phase data with a steady state model. As a consequence of sediment layers with different Mn and Fe contents, metal reduction zones may occur at "unusual" or multiple depth intervals, e.g. close to the SWI and in subsurface peaks associated with buried layers of fines. This results in merged broader pore water maxima (Mn^{2+} in May at FF; Fig. 13) or maxima located deeper in the sediment than expected based on redox zonation as indicated by nitrate penetration depth (Fe^{2+} in May at FF and in August at GB; Fig. 13). The dissolved metals are produced by reductive dissolution of oxides at both the SWI and the subsurface maxima. The re-oxidised Mn^{2+}, however, is only precipitated close to the SWI, where dissolved oxygen is present. Consequently, our profiles reflect conditions in which the subsurface solid Mn maxima are dissolving and the surface maxima are growing. In some cases, the re-oxidised Fe^{2+} does not precipitate near the depth of nitrate penetration, suggesting oxidation by Mn oxides relatively deep in the sediment (May at FF and August at GB). The downward diffusing Mn^{2+} and Fe^{2+} may precipitate with carbonates and sulphides or the profiles may still be relaxing from a non-steady state.

The net Mn^{2+} and Fe^{2+} production rates estimated with the numerical code of Berg *et al.* are very similar to the metal reduction rates obtained from the sum of fluxes as calculated by applying Fick's law directly to the observed gradients, except for both Mn^{2+} and Fe^{2+} in May at the German Bight (Table 5). The Berg model averages the gradients over the upper 2 to 3 cm of the sediment, which results in smaller fluxes than when the steepest slope is used, i.e. from the SWI to the first data point in the sediment. One could argue that a point-to-point gradient is less reliable than averaged over more data points. The seasonal trends in the Mn and Fe reduction rates at the Frisian Front and the Fe reduction rates at the German Bight are the same using either method. Metal reduction rates are highest in November at the Frisian Front and the Fe reduction rate is highest in May at the German Bight. The Mn reduction rate is higher in August than in May using Berg's model, but the difference is small.

The metal reduction rates at the Skagerrak obtained from the model of Slomp *et al.* (1997) are estimates for the total metal reduction rate. For the Frisian Front and German Bight, however, the estimated metal reduction rates are net rates and can not directly be compared to those obtained for the Skagerrak using the model of Slomp. The highest metal reduction rates of the three stations estimated with Berg's model occur at the German Bight.

In order to quantify the effect of perturbations on the suboxic decomposition we compare the metal reduction rates of the different seasons with each other at the moderately energetic Frisian Front. Here, February and August represent months with little disturbance in contrast to May and especially November. The fine-particle layer in November provides elevated concentrations of organic material, solid Mn and Fe below the depth of oxygen penetration. Manganese and iron reduction rates are one order of magnitude higher in November than in the other months. It is likely that the fine particle layer stimulated suboxic diagenesis. The high porosity layer in May represents a much smaller disturbance in terms of elevated organic carbon content compared to the fine particle layer in November. Although it does effect the metal reduction, i.e. the Mn reduction zone is broadened and the Fe reduction zone is located deeper in the sediment, the metal reduction rates are not as high as in November.

At the highly energetic German Bight, major sedimentary disturbances are observed during all seasons, hence making a comparison like at the Frisian Front impossible. Metal reduction rates are one order of magnitude higher in May than in the other seasons. Boon (1998) found a higher chlorophyll-a inventory in May than in August at the German Bight suggesting that organic matter from the spring bloom had settled, which can not be inferred from the organic carbon profile due to the highly perturbed C_{org} distribution. Metal reduction rates are higher at the German Bight than at the Frisian Front, except for the Fe reduction rate in November.

We speculate that the highly energetic German Bight has higher metal reduction rates than the moderately energetic Frisian Front due to the larger perturbations, although differences also exist in sedimentary properties between the two stations. An important factor for Mn and Fe cycling in Iberian Margin sediments is transport of Mn- and Fe-oxides from the oxic to the anoxic layer (Van der Zee *et al.*, 2001; submitted). Sediment mixing stimulates Mn and Fe cycling in several ways. First of all, mixing increases the transport rate of the oxides from the oxic into the anoxic layer where they can be reduced. Secondly, mixing facilitates the upward transport of especially solid but also dissolved reduced species into the oxic layer where they can be re-oxidised again instead of being buried in the anoxic layer and thereby removed from the redox cycle. Thirdly, sediment reworking causes organic material to experience alternatively oxic and anoxic conditions which results in the enhanced overall mineralisation rate (e.g. Aller, 1994; Hulthe *et al.*, 1998; Kristensen and Holmer, 2001) which may additionally drive the Mn and Fe cycles. The perturbations as described here can be regarded as pulsed mixing events and therefore also likely to stimulate the Mn and Fe cycling.

Implications for Mn and Fe cycling

Sediment reworking, be it biological or physical, enhances suboxic diagenesis (Aller *et al.*, 1986; 1998, Ingalls *et al.*, 2000). The balance between aerobic and anaerobic decomposition pathways is drastically altered by sediment reworking due to the utilisation of oxygen in the re-oxidation of reduced species instead of direct oxidation of organic carbon (Aller, 1990). The benthic community in the Skagerrak is characterised by a homogeneous depth distribution, relatively low macrofaunal biomass and very small mean individual weight, which is probably due to the low food quality of the organic matter (Dauwe *et al.*, 1998). The bioturbation mode is

diffusive and does not greatly effect the C_{org} depth distribution, because diffusive mixing flattens an already homogeneous profile (Dauwe *et al.*, 1998). The bioturbation potential, estimated from fauna data, is higher at the Frisian Front and German Bight than at the Skagerrak (Dauwe *et al.*, 1998). Furthermore, wave action and tidal currents mix sediments of the German Bight and Frisian Front in contrast to those of the Skagerrak (Boon and Duineveld, 1996). Due to the association of solid Mn and Fe with organic carbon at these North Sea stations, sedimentary reworking results in an elevated concentration of metal oxides and organic matter below the depth of oxygen penetration. Thus, it provides both oxidants and reductant in an environment favourable for suboxic diagenesis. Physical reworking stimulates suboxic diagenesis at the Frisian Front, i.e. Mn and Fe cycling. Biological and physical reworking of the sediment is likely to enhance suboxic diagenesis at the German Bight as well, although due to frequent perturbations quantification of their effect of on the Mn and Fe reduction rates proved difficult. Hulthe *et al* (1998) found that bioturbation by exposing "old" material to oxygen may enhance integrated organic carbon oxidation in marine sediments (the Skagerrak). They argued that the oxic-anoxic-oxic transitions promoted degradation. These transitions need not only be governed by diffusive mixing, but non-local mixing can be important as well. Together with the organic carbon oxidation, Mn and Fe cycling are stimulated during these redox transitions. Mn and Fe reduction are the only organic matter degradation pathways that depend on solid phase oxidants and consequently transport processes involving the solid phase, including intermittent perturbations, are decisive for Mn and Fe cycling.

Acknowledgements We thank the captain, crew and scientific party of R.V. Pelagia for their help during the cruises. Pore water analyses were performed by Karel Bakker, Jan van Ooijen and Evaline van Weerlee (NIOZ, department of Marine Chemistry and Geology). We thank Henk de Haas and Philippe van Cappellen for their helpful critical comments on the manuscript. This study is part of the VvA-4 studies on disturbed earth systems supported by the Research Council for Earth and Life Science (ALW) with financial aid from the Netherlands Organisation for Scientific Research (NWO) (no. 770.91.187). CvdZ is supported through a grant to WvR from the Netherlands Organisation for Scientific Research (NWO) SMILE programme (no. 750.297.01). This is publication no. 3586 of the Netherlands Institute for Sea Research.

REFERENCES

Aller, R.C., Mackin, J.E., Cox Jr., R.T., 1986. Diagenesis of Fe and S in Amazon inner shelf muds: apparent dominance of Fe reduction and implications for the genesis of ironstones. Cont. Shelf Res., 6, 63-289.

Aller, R.C., Rude, P.D., 1988. Complete oxidation of solid phase sulfides by manganese and bacteria in anoxic marine sediments. Geochim. Cosmochim. Acta, 52, 751-765.

Aller, R.C., 1990. Bioturbation and manganese cycling in hemipelagic sediments. Phil. Trans. Royal Soc., London A, 331, 51-68.

Aller, R.C., 1994a. Bioturbation and remineralization of sedimentary organic matter: effects of redox oscillation. Chem. Geol., 114, 331-346.

Aller, R.C., 1994b. The sedimentary Mn cycle in Long Island Sound: Its role as intermediate oxidant and the influence of bioturbation, O_2 and C_{org} flux on diagenetic reaction balances. J. Mar. Res., 52, 259-295.

Aller, R.C., Hall, P.O.J., Rude, P.D., Aller, J.Y., 1998. Biogeochemical heterogeneity and suboxic diagenesis in hemipelagic sediments of the Panama Basin. Deep-Sea Res. I, 45, 133-165.

Anschutz, P., Sundby, B., Lefrançois, L., Luther III, G.W., Mucci, A., 2000. Interactions between metal oxides and species of nitrogen and iodine in bioturbated marine sediments. Geochim. Cosmochim. Acta, 64, 2751-2763.

Anton, K.K., Leibezeit, G., Rudolph, C., Wirth, H., 1993. Origin, distribution and accumulation of organic carbon in the Skagerrak. Mar. Geol., 111, 287-297.

Bakker, J.F., Helder, W., 1993. Skagerrak (northeastern North Sea) oxygen microprofiles and porewater chemistry in sediments. Mar. Geol., 111, 299-321.

Bauerfeind, E., Hickel, W., Niermann, U., Westernhagen, H.V., 1990. Phytoplankton biomass and potential nutrient limitation of phytoplankton development in the southeastern North Sea in spring 1985 and 1986. Neth. J. Sea Res., 25, 131-142.

Boon, A.R. 1998. Benthic-pelagic coupling: the nature and fate of labile organic matter in the benthic environment of the North Sea. Ph. D. Thesis, University of Groningen, pp. 1-117.

Boon, A.R., Duineveld, G.C.A., 1996. Phytopigments and fatty acids as molecular markers for the quality of near bottom particulate organic matter in the North Sea. J. Sea Res., 35, 279-291.

Boon, A.R., Duineveld, G.C.A., Berghuis, E.M., van der Weele, J.A., 1998. Relationships between benthic activity and the annual phytopigment cycle in near-bottom water and sediments in the southern North Sea. Est. Coast. Shelf Sci., 46, 1-13.

Boudreau, B.P., 1997. Diagenetic models and their implementation, Springer Verlag, Heidelberg, pp. 414.

Brewer, P.G., Spencer, D.W., 1971. Colorimetric determination of manganese in anoxic waters. Limnol, Oceanogr., 16, 107-110.

Buffle, J., De Vitre, R.R., Perret, D., Leppard, G.G., 1989. Pysico-chemical characteristics of a colloidal iron phosphate species formed at the oxic-anoxic interface of a eutrophic lake. Geochim. Cosmochim. Acta, 53, 399-408.

Burns, R.G., Burns, V.M., 1979. Manganese oxides. In: Burns, R.G. (Ed.), Marine Minerals. Reviews in Mineralogy 6, Mineralogy Society of America, Washington DC, pp. 1-46.

Cadée, G.C., 1984. Macrobenthos and macrobenthic remains on the Oyster Ground, North Sea. Neth. J. Sea Res., 18, 160-178.

Canfield, D.E., 1988. Sulfate reduction and the diagenesis of iron in anoxic marine sediments. Ph.D. thesis. Yale University.

Canfield, D.E., Thamdrup, B., Hansen, J.W., 1993. The anaerobic degradation of organic matter in Danish coastal sediments: iron reduction, manganese reduction and sulfate reduction. Geochim. Cosmochim. Acta, 57, 3867-3883.

Churchill, J.H., 1989. The effect of commercial trawling on sediment resuspension and transport over the Middle Atlantic Bight continental shelf. Cont. Shelf Res., 9, 841-864.

Cramer, A., 1991. Benthic metabolic activity at frontal systems in the North Sea. Ph.D. thesis, University of Amsterdam, Amsterdam, pp. 1-93.

Creutzberg, F., Wapenaar, P., Duineveld, G., Lopez Lopez, N., 1984. Distribution and density of the benthic fauna in the southern North Sea in relation to bottom characteristics and hydrographic conditions. Rapp. P.-v. Réun. Cons. Int. Explor. Mer, 18: 101-110.

Dauwe, B., Middelburg, J.J., 1998. Amino acids and hexosamines as indicators of organic matter degradation state in North Sea sediments. Limnol. Oceanogr., 43, 782-798.

Dauwe, B., Herman, P.M.J., Heip, C.H.R., 1998. Community structure and bioturbation potential of macrofauna at four North Sea stations with contrasting food supply. Mar. Ecol. Progr. Ser., 173, 67-83.

Dauwe, B., Middelburg, J.J., Herman, P.M.J., 2001. The effect of oxygen on the degradability of organic matter in subtidal and intertidal sediments of the North Sea area. Mar. Ecol. Progr. Ser., 215, 13-22.

De Haas, H., van Weering, T.C.E., 1997. Recent sediment accumulation, organic carbon burial and transport in the northeastern North Sea. Marine Geology 136, 173-187.

De Haas, H., Boer, W., van Weering, T.C.E., 1997. Recent sediment and organic carbon burial in a shelf sea; the North Sea. Mar. Geol., 144, 131-146.

Dehairs, F., Baeyens, W., Van Gansbeke, D., 1989. Tight coupling between enrichment of iron and manganese in North Sea suspended matter and sedimentary redox processes: Evidence for seasonal variability. Est. Coast. Shelf Sci., 29, 457-471.

Dellwig, O., Hinrichs, J., Hild, A., Brumsack., H.-J., 2000. Changing sedimentation in tidal flat sediments of the southern North Sea from the Holocene to the present: a geochemical approach. J. Sea Res., 44, 195-208.

Dominik, J. Förstner, U., Mangini, A., Reineck, H.-E., 1978. ^{210}Pb and ^{137}Cs chronology of heavy metal pollution in a sediment core from the German Bight (North Sea). Senckenberg. Mar., 10, 213-228.

Deng, Y., 1997. Formation of iron(III) hydroxides from homogeneous solutions. Wat. Res., 31, 1347-1354.

Eisma, D., 1981. Supply and deposition of suspended matter in the North Sea. Spec. Publs. Int. Ass. Sed., 5, 415-428.

Erlenkeuser, H., Pederstad, K., 1984. Recent sediment accumulation in Skagerrak as depicted by ^{210}Pb-dating. Norsk Geol. Tids., 64, 135-152.

Froelich, P.N., Klinkhammer, G.P., Bender, M.L., Luedtke, N.A., Heath, G.R., Cullen, D., Dauphin, P., Hammond, D., Hartman, B., Maynard, V., 1979. Early oxidation of organic matter in pelagic sediments of the eastern equatorial Atlantic: suboxic diagenesis. Geochim. Cosmochim. Acta, 43, 1075-1090.

Gadow, S., 1969. Gips als Leitmineral für das Liefergebiet Helgoland und für den Transport bei Sturmfluten. Natur Mus., 99, 537-540.

Helder, W., De Vries, R.P.T., 1979. An automatic phenol-hypochlorite method for the determination of ammonia in sea- and brackish waters. Neth. J. Sea Res., 13, 154-160.

Hulth, S., Aller, R.C. ,Gilbert, F., 1999. Coupled anoxic nitrification/manganese reduction in marine sediments. Geochim. Cosmochim. Acta, 63, 49-66.

Hulthe, G., Hulth, S., Hall, P.O.J., 1998. Effect of oxygen on degradation rate of refractory and labile organic matter in continental margin sediments. Geochim. Cosmochim. Acta, 62, 1319-1328.

Ingalls, A.E., Aller, R.C., Lee, C., Sun, M.-Y., 2000. The influence of deposit-feeding on chlorophyll-a degradation in coastal marine sediments. J. Mar. Res., 58, 631-651.

Jenness, M. I., Duineveld, G.C.A., 1985. Effects of tidal currents on chlorophyll a content of sandy sediments in the southern North Sea. Marine Ecology Progress Series 21, 283-287.

Joint, I., Pomroy, A. 1993. Phytoplankton biomass and production in the southern North Sea. Mar. Ecol. Progr. Ser., 99, 169-182.

Jørgensen, B.B., 1989. Sulfate reduction in marine sediments from the Baltic Sea-North Sea transition. Ophelia 31, 1-15.

Kempe, S., Liebezeit, G., Dethlefsen, V., Harms, U., 1988. Biogeochemistry and distribution of suspended matter in the North Sea and implications to fisheries biology. Synopsis. Mitt. Geol. Pal. Inst. Univ. Hamburg, SCOPE/UNEP, Sonderband 65, XI-XXIV.

Konert, M., Vandenberghe, J., 1997. Comparison of laser grain size analysis with pipette and sieve analysis: a solution for the underestimation of the clay fraction. Sedimentology 44, 523-535.

König, R., 1996. Black spots blot German coastal flats. Science, 273, 25.

Kristensen, E., Holmer, H., 2001. Decomposition of plant materials in marine sediment exposed to different electron acceptors (O_2, NO_3 and SO^2_4), with emphasis on substrate origin, degradation kinetics, and the role of bioturbation. Geochim. Cosmochim. Acta, 65, 419-433.

Li, Y.H., Gregory, S., 1974. Diffusion of ions in seawater and in deep-sea sediments. Geochim. Cosmochim. Acta, 38, 703-714.

Lohse, L., Epping, E.H.G., Helder, W., van Raaphorst, W., 1996. Oxygen pore water profiles in continental shelf sediments of the North Sea: turbulent versus molecular diffusion. Mar. Ecol. Progr. Ser., 145, 63-75.

Lohse, L., Malschaert, J.F.P., Slomp, C.P., Helder W., van Raaphorst, W., 1995. Sediment-water fluxes of inorganic nitrogen compounds along the transport route of organic matter in the North Sea. Ophelia 41, 173-197.

Lohse. L., Kloosterhuis, R.T., de Stigter, H.C., Helder, W., van Raaphorst, W., van Weering, T.C.E., 2000. Carbonate removal by acidification causes loss of nitrogenous compounds in continental margin sediments. Mar. Chem., 69, 193-201.

Mayer, L.M., 1994. Surface area control of organic carbon accumulation in continental shelf sediments. Geochim. Cosmochim. Acta, 58, 1271-1284.

Mayer, L.M., 1999. Extent of coverage of mineral surfaces by organic matter in marine sediments. Geochim. Cosmochim. Acta, 63, 207-215.

McCave, I.N., 1970. Deposition of fine grained suspended sediment from tidal currents. J. Geophys. Res., 75, 4151-4159.

Murray, J.W., Dillard, J.G., Giovanoli, R., Moers, H., Stumm, W., 1985. Oxidation of Mn(II): Initial mineralogy, oxidation state and ageing. Geochim. Cosmochim. Acta, 49, 463-470.

Nedwell, D.B., 1984. The input and mineralisation of organic carbon in anaerobic aquatic sediments. Adv. Microb. Ecol., 7, 93-131.

Nedwell, D.B., Parkes, R.J., Upton, A.C., Assinder, D.J., 1993. Seasonal fluxes across the sediment-water interface, and processes within the sediments. Phil. Trans.Royal Soc., London A, 343, 519-529.

Nittouer, C.A., Sternberg, R.W., Carpenter, R., Bennet, J.T., 1979. The use of Pb-210 as a sedimentological tool: applications on the Washington continental shelf. Mar. Geol., 31, 297-316.

Ockelmann, K.W., Muus, K., 1978. The biology, ecology and behaviour of the bivalve Mysella bidentate (montagu). Ophelia 17, 1-93.

Osinga, R., Kop, A.J., Duineveld, G.C.A., Prins, R.A.,, van Duyl, F.C., 1996. Benthic mineralization rates at two locations in the southern North Sea. J. Sea Res., 36, 181-191.

Otto, L., Zimmerman, J.T.F., Furnes, G.K., Mork, M. Saetre, R., Becker, G., 1990. Review of the physical oceanography of the North Sea. Neth. J. Sea Res., 26, 161-238.

Postma, D., 1985. Concentration of Mn and separation from Fe in sediments – I. Kinetics and stoichiometry of the reaction between birnessite and dissolved Fe(II) at 10°C. Geochim. Cosmochim. Acta, 49, 1023-1033.

Puls, W., Sündermann, J., 1990. Simulation of suspended sediment dispersion in the North Sea. In: Cheng, R.T. (Ed.), Residual currents and long-term transport, Coastal and estuarine studies 38, Springer, New York, pp. 35-372.

Pyzik, A.J., Sommer, S.E., 1981. Sedimentary iron monosulphides: kinetics and mechanism of formation. Geochim. Cosmochim. Acta, 45, 687-698.

Rabouille, C., Gaillard, J.-F., 1991. Towards the EDGE: Early diagenetic global explanation. A model depicting the early diagenesis of organic matter, O_2, NO_3, Mn, and PO_4. Geochim. Cosmochim. Acta 55, 2511-2525.

Radach, G., Berg, J. Hagmeier, E., 1990. Long-term changes of the annual cycles of meteorological, hydrographic, nutrient and phytoplankton time series at Helgoland and at LV ELBE 1 in the German Bight. Cont. Shelf Res., 10, 305-328.

Ransom, B., Kim, D., Kastner, M., Wainwright, S., 1998. Organic matter preservation on continental slopes: Importance of mineralogy and surface area. Geochim. Cosmochim. Acta, 62, 1329-1345.

Ransom, B., Bennett, R.J. Baerwald, R., Shea, K., 1997. TEM study of in situ organic matter on continental shelf margins: occuence and the 'monolayer' hypothesis. Mar. Geol., 138, 1-9.

Reineck, H-E., 1963. Sedimentgefüge im Bereich der südlichen Nordsee. Abh. Senckenberg. Naturforsch. Ges., 505, 138.

Reineck, H-E., 1960. Über Zeitlücken in rezenter Flachseesedimenten. Geol.Rundschau, 49, 149-161.

Reineck, H-E., Gutman, W.F. Hertweck, G., 1967. Das Schlickgebiet südlich Helgoland als Beispiel rezenter Schelfablagerungen. Senckenberg. Leth., 48, 219-275.

Schoemann, V., de Baar, H.J.W., de Jong, J.T.M., Lancelot, C., 1998. Effects of phytoplankton blooms on the cycling of manganese and iron in coastal waters. Limnol. Oceanogr., 43, 1427-1441.

Slomp, C.P., Malschaert, J.F.P., Lohse, L., van Raaphorst, W., 1997. Iron and manganese cycling in different sedimentary environments on the North Sea continental margin. Cont. Shelf Res., 17, 1083-1117.

Stookey, L.L., 1970. A new spectrophotometric reagent for iron. Anal. Chem., 42, 779-781.

Straub, K.L., Benz, M., Schink,B., Widdel, F., 1996. Anaerobic, nitrate-dependent microbial oxidation of ferrous iron. Appl. Environ. Microbiol., 62, 1458-1460.

Strickland, J.D., Parsons, T.R., 1972. A practical handbook of seawater analysis. 2nd edn., Bull. Fish. Res. Board Can. 167, pp. 310.

Sündermann, J. 1993. Suspended particulate matter in the North Sea: field observations and modelling. Phil. Trans. Royal Soc., London A, 343, 45-52.

Thamdrup, B., Dalsgaard, T., 2000. The fate of ammonium in anoxic manganese oxide-rich marine sediment. Geochim. Cosmochim. Acta, 64, 4157-4164.

Upton, A.C., Nedwell, D.B., Parkes, R.J., Harvey, S.W., 1993. Seasonal benthic microbial activity in the southern North Sea; oxygen uptake and sulphate reduction. Mar. Ecol. Progr. Ser., 101, 273-281.

Van Cappellen, P., Wang, Y., 1996. Cycling of iron and manganese in surface sediments: a general theory for the coupled transport and reaction of carbon, oxygen, nitrogen, sulfur, iron, and manganese. Am. J. Sci., 296, 197-243.

Van der Zee, C., van Raaphorst, W., Epping, E., 2001. Adsorbed Mn^{2+} and Mn redox cycling in Iberian continental margin sediments (northeast Atlantic). J. Mar. Res., 59, 133-166.

Van der Zee, C., van Raaphorst, W., Helder, W., 200x. Adsorbed Fe^{2+} and Fe redox cycling in Iberian continental margin sediments (northeast Atlantic). J. Mar. Res., submitted.

Van Raaphorst, W., Malschaert, H., van Haren, H., 1998. Tidal resuspension and deposition of particulate matter in the Oyster grounds, North Sea. J. Mar. Res., 56, 257-291.

Van Raaphorst, W., Kloosterhuis, H.T., Berghuis, E.M., Gieles, A.J.M., Malschaert, J.F.P., van Noort, G.J., 1992. Nitrogen cycling in two types of sediments of the southern North Sea (Frisian Front, Broad Fourteens): field data and mesocosm results. Neth. J. Sea Res., 28, 293-316.

Van Weering, T.C.E., Berger, G.W., Okkels, E., 1993. Sediment transport, resuspension and accumulation rates in the northeastern Skagerrak. Mar. Geol. 111, 269-285.

Van Weering, T.C.E., Berger, G.W., Kalf, J., 1987. Recent sediment accumulation in the Skagerrak, northeastern North Sea. Neth. J. Sea Res., 21, 177-189.

Verardo, D.J., Froelich, P.N., McIntyre, A., 1990. Determination of organic carbon and nitrogen in sediments using the Carlo Erba NA-1500 analyzer. Deep-Sea Res., 37, 157-165.

Von Westernhagen, H., Hickel, W., Bauerfeind, E., Niermann, U., Kröncke, I., 1986. Sources and effects of oxygen deficiencies in the south-eastern North Sea. Ophelia 26, 457-473.

Wiesner, M.G., Haake, B., Wirth, H., 1990. Organic facies of surface sediments in the North Sea. Org. Geochem., 15, 419-432.

Wirth, H. and Wiesner, M.G., 1988. Sedimentary facies in the North Sea. Mitt. Geol. Pal. Inst. Univ. Hamburg, 65, 269-287.

CHAPTER THREE

Manganese oxide reactivity in North Sea sediments[2]

ABSTRACT

Bulk Mn oxide dissolution rates were determined in dilute acid (HCl, pH=3, proton assisted dissolution) and in saturating ascorbic acid (pH=3, proton assisted plus reductive dissolution) for North Sea sediments from three sites characterized by different intensities of sediment reworking. Profiles of extractable manganese (0.1N hydrochloric acid, 1N hydrochloric acid, citrate-dithionite-bicarbonate buffer and hydroxylamine hydrochloride in acetic acid) are presented for the three sites.

The assemblage of sedimentary Mn oxides was described as a reactive continuum with a gamma distribution of Mn oxide reactivities. Initial reduction rates were highest for the oxidized sediment samples. The reactivity of the Mn assemblages during reductive dissolution in ascorbic acid decreased by up to ~9 orders of magnitude. The largest heterogeneity in Mn reactivity of the oxidized sediment samples was found at the site experiencing most intense sediment reworking, while the most homogeneous Mn assemblage was found at the least intense reworked site. Due to sediment mixing, Mn^{2+} ions experience a variable chemical environment resulting in different oxidation products and thus, a large heterogeneity. The perturbations that mix the sediments of the Frisian Front and German Bight result in a layering of the sediment. Therefore these perturbations increase the sedimentary heterogeneity instead of homogenizing the sediments. The large range in sedimentary Mn oxide reactivity may explain the great variability in values for kinetic coefficients used to describe Mn reduction. Considering the broad spectrum of Mn oxide reactivities, extensive overlap of the Mn reduction zone with that of Fe oxides is expected.

INTRODUCTION

Manganese can be the most important intermediate oxidant between oxygen and organic carbon in marine sediments (Aller, 1990 and 1994; Canfield *et al.*, 1993; Thamdrup *et al.*, 1994). A number of manganese oxides and oxyhydroxides (hereafter called Mn oxides) may exist in marine sediments with variable Mn (III) and Mn (IV) contents (Burdige, 1993). Below the depth of oxygen penetration in the sediment, Mn oxides are reductively dissolved thereby releasing Mn^{2+} into the pore water (Froelich *et al.*, 1979; Burdige and Gieskes, 1983). Mn oxide reduction can be coupled to

[2] This chapter by Claar van der Zee and Wim van Raaphorst has been submitted to Geochimica et Cosmochimica Acta.

organic carbon oxidation (Myers and Nealson, 1988) and to the oxidation of reduced species such as dissolved ferrous iron (Postma, 1985) and sulfide (Burdige and Nealson, 1986). Microelectrode work showed field evidence consistent with the oxidation of Mn^{2+} by NO_3^- thereby producing N_2, whereas ammonium or organic nitrogen can reduce Mn oxides resulting in the production of N_2 as well (Luther *et al.*, 1997). The rate of Mn reduction is affected by the reductant involved, microbial catalysis, and the mineralogy of the Mn oxide (Burdige *et al.*, 1992). Mn reduction is a surface controlled process and consequently, amorphous manganese oxides with a larger specific surface area are reduced generally faster than highly crystalline oxides (Burdige *et al.*, 1992). Dollhopf *et al.* (2000) showed that micro-organisms reduce Fe(III) electron acceptor phases with different kinetics; soluble Fe(III)-citrate faster than amorphous Fe(OH)3 than solid α-FeOOH. These findings suggest that different Mn electron acceptor phases are also likely to be reduced with different kinetics by bacteria. Also, the microbial community structure and viable cell numbers of relevant bacteria are important factors that affect the kinetics of metal oxide reduction (Dollhoph *et al.*, 2000).

Natural marine Mn oxide phases are often intergrown with other materials and so poorly crystalline that their identification with x-ray diffraction techniques is very difficult (Burns and Burns, 1979). They deviate from pure minerals in their reactivity due to ionic substitution within the mineral and sorption of organic molecules and inorganic ions. Therefore, sediment extraction techniques are widely applied to marine sediments. Although these techniques are calibrated for iron phases (e.g. Canfield, 1988; Kostka and Luther, 1994; Haese *et al.*, 1997), and much less for Mn phases (e.g. Chester and Hughes, 1969; Schenau, 1999), they are applied to both Mn and Fe. The disadvantage of extraction methods is that they are empirically defined and not mineral specific. Postma (1993) introduced a more quantitative method for natural sediments, based on the measurement of the rate of reductive dissolution of Fe oxides in ascorbic acid and using a reactive continuum model to describe the intrinsic reactivity of the assemblages of Fe-oxides.

Similarly, the reactivity of an assemblage of natural Mn oxides can be modelled as a reactive continuum, as was originally elaborated for organic matter degradation (Boudreau and Ruddick, 1991; Tarutis, 1993). The model has also been applied to the alkaline dissolution of biogenic silica (Koning *et al.*, 1997). Based on the Gamma distribution of reactivities, the total amount of Mn oxides remaining, m (μmol g^{-1}), in a sample as a function of time, t (s), can be described by equation (1), where the mass at time zero is m_0. The parameter a (s) indicates the average lifetime of the reactive components in the mixture and υ is a dimensionless parameter solely related to the shape of the Gamma distribution curve.

$$\frac{m}{m_0} = \left(\frac{a}{a+t}\right)^{\upsilon} \tag{1}$$

The rate equation for Mn oxide dissolution is

$$J = k_m m^{1+\frac{1}{\upsilon}} \tag{2}$$

where J is the rate of dissolution (μmol g^{-1} s^{-1})

$$k_m = \frac{\upsilon}{a(m_0)^{1/\upsilon}} \tag{3}$$

Substitution of the rate constant k_m into (2) and rearranging gives

$$\frac{J}{m_0} = \frac{\upsilon}{a}\left(\frac{m}{m_0}\right)^{1+\frac{1}{\upsilon}} \tag{4}$$

Equation (4) is similar to the general dissolution kinetics of a polydisperse sample of crystals (eq. 5; Christoffersen and Christoffersen, 1976), in case of constant solution composition (i.e. constant concentration of reductant used). The parameter $k' = \upsilon/a$ (s^{-1}) represents the apparent rate constant.

$$\frac{J}{m_0} = k'\left(\frac{m}{m_0}\right)^{\gamma} \tag{5}$$

In this study, we present results on classical extraction methods and a reactive continuum approach applied to assemblages of natural Mn oxides in North Sea sediments. Three sites were selected on the basis of differences in their sediment reworking intensity. The objective was to investigate the effect of sediment reworking on the reactivity of natural marine Mn oxide assemblages. Sediment reworking affects the manganese redox cycling in sediments (Aller, 1990) and, thus, may affect the degree of ageing and reactivity of the sedimentary Mn oxides. Second objective was to quantify the range of Mn oxide reactivities encountered in one assemblage. This may at least partly explain the large variability found in kinetic coefficients of Mn reduction (Burdige and Gieskes, 1983; Van Cappellen and Wang, 1996; Slomp *et al.*, 1997; Boudreau *et al.*, 1998; Van der Zee *et al.*, 2001). Insight in the Mn reactive continuum provides constraints on the kinetic coefficients and thus improves modelling of the Mn cycle. Also, because the stability of Mn oxides in natural sediments is roughly paralleled by their reactivity, a heterogeneous assemblage of Mn oxides may cause an extensive overlap between the Mn reduction zone with that of Fe oxides.

METHODS

Research Area

Three sites in the North Sea representing different energy regimes were visited with the RV Pelagia in November 1995 (Fig.1; Table 1). The relatively deep and sheltered Skagerrak is selected as a low energy site characterised by a steady sedimentation of relatively refractory organic matter from the Scandinavian mainland, the Baltic and particularly from the North Sea shelf (Van Weering *et al.*, 1987). The

low food quality of the organic matter (Dauwe *et al.* 1999) is reflected in the relatively low biomass and the very small mean individual weight of the macrofauna (Dauwe *et al.* 1998).

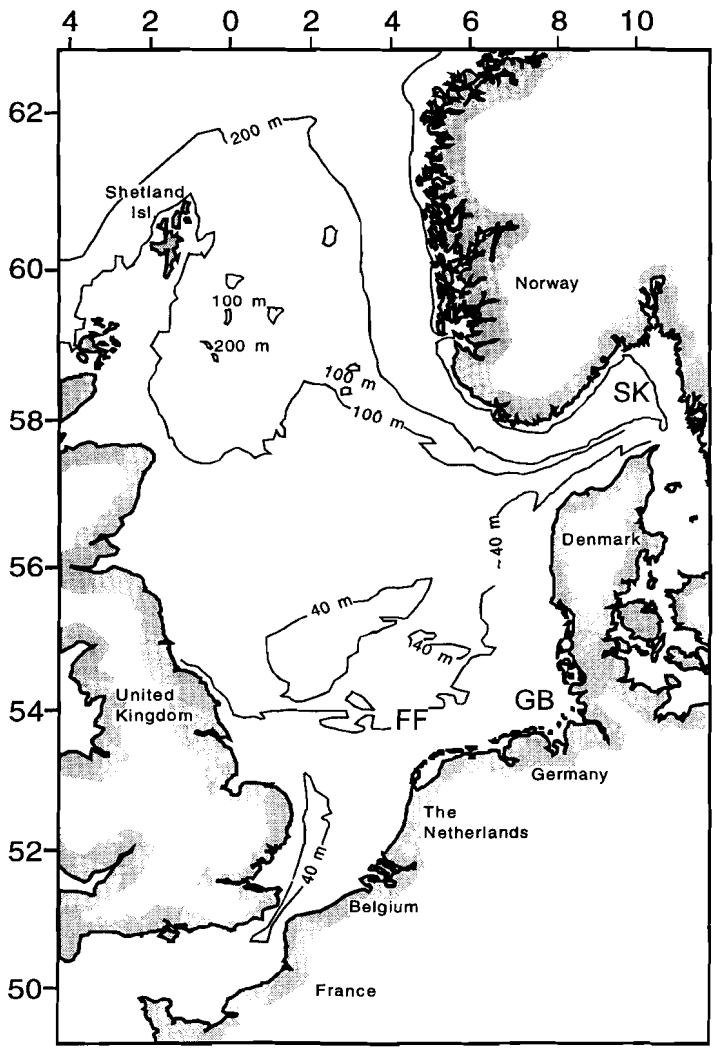

Figure 1. Map of the North Sea indicating the visited stations (FF, GB and Sk).

Table 1. Name, geographical position, water depth, bottom water temperature of visited stations.

Station	N	E	Depth (m)	BW Temp (°C)
Frisian Front	53° 42'	04° 30'	39	13
German Bight	54° 05'	08° 09'	20	10
Skagerrak	58° 12'	10° 15'	270	7.2

In contrast with the Skagerrak, two shallow and highly dynamic areas were sampled, the moderately energetic site in the Frisian Front and the highly energetic site in the German Bight. Particles from the East Anglian turbidity plume and the south-western North Sea settle at the Frisian Front area in spring and summer (Puls and Sündermann, 1990; Sündermann, 1993; Van Raaphorst *et al.*, 1998), however, these particles are eroded again during autumn and winter storms (Kempe*et al.*, 1988; Puls and Sündermann, 1990). The sediment consists of old reworked deposits, which are partly mixed with recent sediments (De Haas *et al.*, 1997). In contrast to the vertically homogenous sediment column of the Skagerrak, a distinct layer with fine particles, median grain size ~30 μm, was present between ~1.5 to 5 cm depth at the Frisian Front. Above and below this layer the particles were coarser with a median grain size of ~100 μm (Van der Zee *et al.*, subm.). The upper 10 cm of the sediment at the German Bight consisted of 6 alternating fine- and coarse-particle layers with median grain sizes varying between ~30 and 90 μm (Van der Zee *et al.*, subm.). Strongly variable tidal currents resuspend the surface sediment at the German Bight regularly (Boon and Duineveld, 1996). Physical and biological sediment reworking stimulates Mn cycling in these dynamic areas (Van der Zee et al., subm.).

Sediment Handling

Sediment was sampled with a multi-corer and processed immediately upon retrieval onboard. All subsequent sediment handling took place at *in situ* temperature. Cores were sliced in four 2.5-mm intervals (0-2.5, 2.5-5, 5-7.5 and 7.5-10 mm), four 5-mm intervals (10-15, 15-20, 20-25 and 25-30 mm), four 10-mm intervals (30-40, 40-50, 50-60 and 60-70 mm) and two 15-mm intervals (70-85, 85-100 mm). Sediment slices of 4 cores were pooled and centrifuged (10 min, 3000 rpm). Pore water was collected after centrifugation and filtered (0.45 μm, Acrodisc). Aliquots for manganese were acidified to pH ~ 1 and measured on a TRAACS-800 auto-analyser according to the method Brewer and Spencer (1971). After pore water collection the sediment was stored frozen (-20 °C) until solid phase analysis in the NIOZ laboratory. Freeze-dried and ground (Teflon mortar and pestle) sediment was extracted for reactive Mn at room temperature with 1N HCl for 24 h (Slomp et al., 1997), 0.1N HCl for 18 h (Duinker et al., 1974), 1M Hydroxylamine hydrochloride in 25% (v/v) acetic acid for 1 h (HA.AA, Chester and Hughes, 1967), and Citrate-Dithionite-Bicarbonate for 8 h at pH 7.3 (CDB, Ruttenberg, 1992). Both 1N and 0.1N HCl should dissolve Mn in carbonate phases and "reactive" Mn oxides, where 0.1N HCl is assumed to extract the same phases as 1N HCl but with less attack on clay minerals (Duinker et al., 1974; Slomp et al., 1997). CDB is expected to be selective for Mn oxides. CDB reduces Fe oxides without dissolution of carbonate phases (Ruttenberg, 1992). HA.AA extracts all Mn in oxides and carbonates (Chester and Hughes, 1967).

Dissolution Experiments

The top (0-0.25 cm) and bottom (8.5-10 cm) layers of the three stations and the Mn oxide maximum (0.75-1cm) layer of the German Bight were used in proton-assisted and reductive dissolution experiments. Postma (1993) used ascorbic acid as reductant in his Fe oxide dissolution experiments and it is a suitable reductant for Mn oxides as well. It dissolved Mn (III) and (IV) oxides at pH 7.2 as quickly as any of the 27 aromatic and non-aromatic compounds tested by Stone and Morgan (1984). The Mn oxide dissolution experiments were carried out with excess ascorbic acid, following Postma (1993), so that the rate is independent of the reductant concentration, which does not change appreciably over time. The reductive dissolution experiment started by adding sediment (~1 g) to 250 ml freshly prepared 10 mM ascorbic acid solution (pH 3). The suspension was stirred continuously preventing the particles to settle and kept at constant pH 3.0 ± 0.1 by adding 1N HCl. Aliquots of the suspension were filtered (0.2 μm), acidified to pH ~1 and measured for Mn^{2+} by flame AAS. Postma (1993) found that in the presence of only HCl at pH 3 less than 1% of ferrihydrite dissolved in ~ 5 hours. In order to test proton-assisted manganese dissolution at pH 3, an additional experiment was carried out in a HCl solution at pH 3.0 ± 0.1. Aliquots of the suspension were filtered (0.2 μm), acidified to pH ~1 and measured on a TRAACS-800 auto-analyser according to the method Brewer and Spencer (1971).

The released Mn^{2+} (μM) normalised to the added amount of sediment (g) and volume of ascorbic acid or HCl solution (L) results in a dissolution curve of released Mn^{2+} in μmol g^{-1} versus time. The amount of released Mn^{2+} is equal to the m_0 (μmol g^{-1}), when no further dissolution occurs. The amount of Mn oxides remaining, m, is the difference between m_0 and the amount of released Mn^{2+} at time t. Sums of squares were minimised while the parameters a, v and m_0 were varied to fit equation (1) to the dissolution data using the Excel solver routine.

RESULTS

Pore Water and Classical Extractions

For Frisian Front sediments, Mn profiles from the 0.1N HCl, 1N HCl and HA.AA extractions are almost identical, whereas CDB-extractable Mn shows a similar depth distribution but with a lower offset of ~1μmol Mn g^{-1} (Fig. 2). The pore water profile indicates Mn oxide reduction between ~1 to 2 cm depth and oxidation of dissolved Mn^{2+} upon diffusion into the upper cm of the sediment. For German Bight sediments, the HA.AA, 0.1N and 1N HCl solutions dissolve similar amounts of Mn, except in the subsurface maximum (~1cm depth), where more Mn is dissolved with HA.AA (Fig. 3). As for Frisian Front, CDB extracts the least amount of Mn. The pore water profile of Mn^{2+} shows that Mn reduction takes place around 1 cm depth and that dissolved Mn^{2+} is re-oxidised in the upper half cm of the sediment. Mn^{2+} is precipitated as a reduced Mn phase below 1.5 cm depth, unless the decrease with depth of Mn^{2+} is due to intense pore water irrigation. At the Skagerrak, 1N HCl extracts most and CDB least Mn (Fig. 4). Again, the vertical distribution is the same for all extractions. Mn oxide is reduced between 2-3 cm depth and Mn^{2+} is re-oxidised at the sediment-water interface, which is visible as an enrichment of extractable Mn in surface sediments.

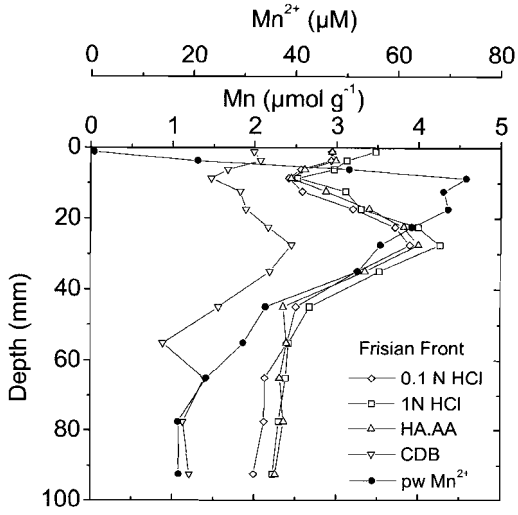

Figure 2. Vertical profile of pore water Mn^{2+} (solid circles) and Mn extracted with 0.1N HCl (square), 1N HCl (open circle), HA.AA (up triangle) and CDB (down triangle) at the Frisian Front.

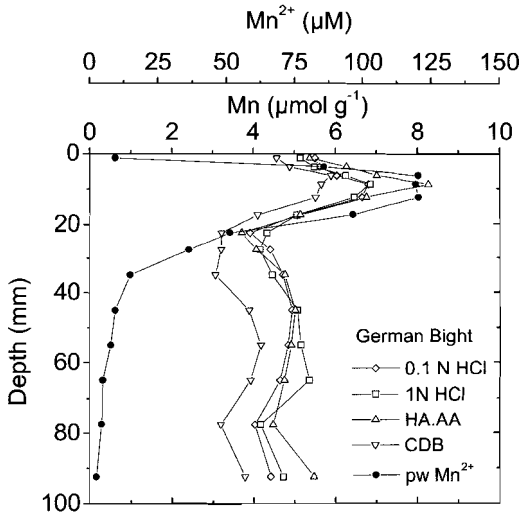

Figure 3. Vertical profile of pore water Mn^{2+} (solid circles) and Mn extracted with 0.1N HCl (square), 1N HCl (open circle), HA.AA (up triangle) and CDB (down triangle) at the German Bight.

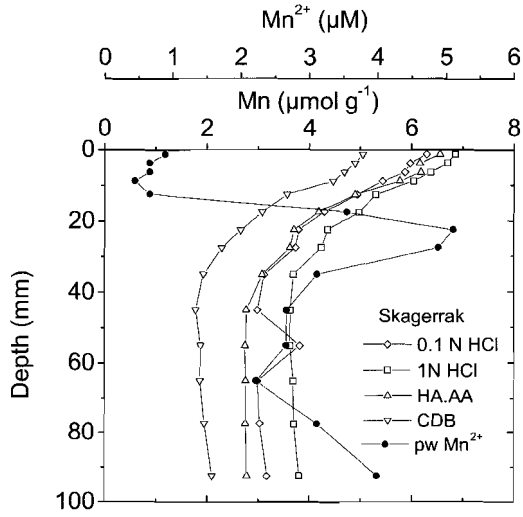

Figure 4. Vertical profile of pore water Mn^{2+} (solid circles) and Mn extracted with 0.1N HCl (square), 1N HCl (open circle), HA.AA (up triangle) and CDB (down triangle) at the Skagerrak.

Reactive Continuum Approach

During the dissolution experiments, a fast initial release of Mn^{2+} was observed that strongly decelerated when the major part of the Mn oxide assemblage was dissolved (Fig. 6). The fraction of Mn oxide remaining during the reduction by ascorbic acid and proton-assisted dissolution can be well described by the reactive continuum as shown by the model fit to the dissolution curves (Fig. 6). Fitted values (a, υ and m_0) are given as υ/a and $1+1/\upsilon$ in Table 2 and m_0 in Table 3. The fitted m_0 values are thus ascorbic acid-extractable and HCl pH 3 m_0 values, respectively, and are comparable to the ones obtained by the classical extraction methods (Table 3) suggesting that the model parameter estimates are realistic. The HCl (pH 3)m_0 values in the top layers are comparatively low, however. Comparison with the Mn values from the classical extractants is complicated by differences is extraction time, pH, extracted Mn phases and dissolution mechanism, e.g. proton assisted or reductive dissolution or a combination of both.

The constant term υ/a in equation 4 can be regarded as an apparent rate constant (k') for the reductive dissolution of a natural Mn oxide mixture with 10mM ascorbic acid or proton-assisted dissolution in HCl at pH 3.0 and room temperature. For an ideal dissolving cube or sphere γ is 0.67 predicted by the relation between volume and surface area. In natural samples, the exponential term $1+1/\upsilon$ can not be interpreted in physical terms, but it is characteristic for the reactivity of the oxides present (Postma, 1993). The reactivity is not only related to the mineralogy, but also to the crystal

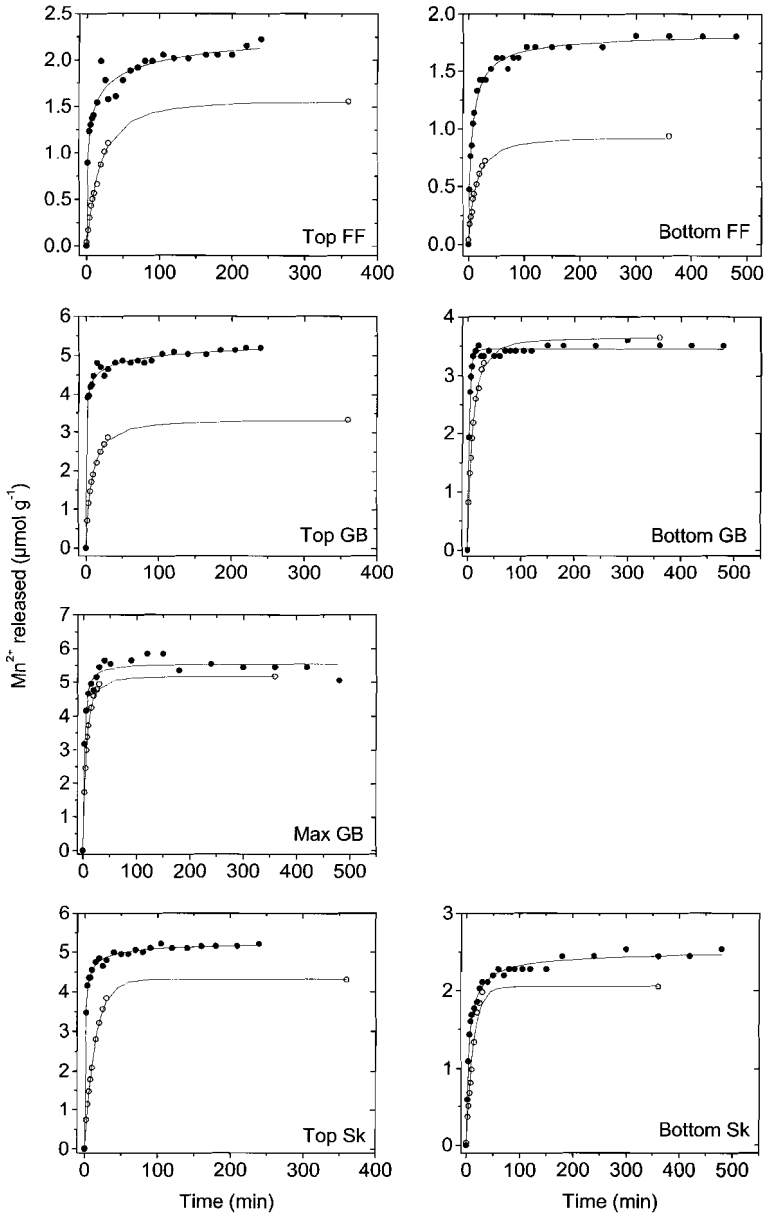

Figure 6. The Mn^{2+} release per gram sediment during the dissolution of natural Mn oxides in 10mM ascorbic acid (solid circles) and HCl solution (open circles) at pH 3. The line represents the fit of equation 1 to the data.

Table 2. Values obtained by fitting equation (1) to the dissolution curves of Mn^{2+} in ascorbic acid and HCl (pH=3).

Sample	constant (υ/a) (s^{-1}) Ascorbic acid	exponent ($1+1/\upsilon$) (-) Ascorbic acid	constant (υ/a) (s^{-1}) HCl	exponent ($1+1/\upsilon$) (-) HCl
FF – 0-0.25 cm	9.9 E-3	5.8	8.7 E-4	1.4
FF – 8.5-10 cm	3.3 E-3	2.4	1.3 E-3	1.7
GB – 0-0.25 cm	8.9 E-1	8.9	2.0 E-3	1.7
GB – 0.75-1 cm	8.0 E-3	1.8	3.2 E-3	1.5
GB – 8.5-10 cm	7.7 E-3	1.3	2.0 E-3	1.5
Sk – 0-0.25 cm	2.9 E-2	2.8	1.2 E-3	1.0
Sk – 8.5-10 cm	3.8 E-3	2.4	1.3 E-3	1.0

geometry, particle size distribution and reactive site density (Burdige *et al.*, 1992; Postma, 1993; Larsen and Postma, 2001). The estimated rate constants and exponential terms are both higher in the top sediments than in the bottom sediments for ascorbic acid (Table 2). The higher rate constant indicates a higher initial reduction rate and the higher exponential term indicates a larger range of Mn oxide reactivity in the oxic top layer of the sediment. The estimated rate constants in the HCl (pH 3) dissolution experiments are always lower than the corresponding rate constants found in the dissolution experiments with ascorbic acid. The differences are most pronounced in the top layers, whereas only small differences are found in the subsurface and bottom layers. The estimated exponents in the HCl (pH 3) experiment are low and very similar between top and bottom sediments from each station.

Table 3. Mn (μmol g^{-1}) values obtained by fitting equation (1) to the dissolution curves and the amount of Mn extracted with 0.1N HCl, 1N HCl, CDB and HA.AA.

Sample	m_0 Ascorbic acid	m_0 HCl (pH 3)	0.1N HCl	1N HCl	CDB	HA.AA
FF – 0-0.25 cm	2.4	1.6	2.9	3.5	2.0	2.9
FF – 8.5-10 cm	1.8	0.9	2.0	2.2	1.2	2.3
GB – 0-0.25 cm	5.6	3.3	5.5	5.1	4.6	5.4
GB – 0.75-1 cm	5.5	5.2	5.6	5.5	4.9	6.3
GB – 8.5-10 cm	3.5	3.6	4.4	4.7	3.8	5.5
Sk – 0-0.25 cm	5.3	4.3	6.3	6.9	5.1	6.6
Sk – 8.5-10 cm	2.6	2.1	3.2	3.8	2.1	2.8

DISCUSSION

Classical Extractions

The CDB extraction did leach less Mn from the sediments than HCl and HA.AA, probably because Mn in carbonates is not dissolved in the ~neutral CDB solution. The 0.1N HCl solution always extracts less Mn than 1N HCl suggesting that Mn is leached preferentially from clay minerals in HCl. For the Skagerrak, a Mn oxide enrichment at the sediment surface is visible, in contrast to the Frisian Front and German Bight. The vertical distribution of solid phase and pore water Mn is governed by physical and biological mixing events at the Frisian Front and German Bight (Van der Zee *et al*,

subm.). After a perturbation the pore water distributions adjust rapidly, whereas the solid phase exhibits a transient profile for a longer period. As a result, depth distributions of 1N HCl-extractable Mn in sediments of the Frisian Front and especially the German Bight measured in different months (February, May, August and November) are very different (Van der Zee *et al.*, subm.). Features of several solid phase depth distributions (Mn, Fe, C_{org}) are also encountered in the same seasons but in other years for these sites (Van Raaphorst *et al*, 1992; Slomp *et al.*, 1997) suggesting that the underlying processes are not accidental and seasonally reoccurring. Thus, the cores are representative for the sites in these particular seasons.

The pore water Mn^{2+} profiles suggest the formation of a reduced authigenic Mn mineral. Precipitation of Mn in calcium carbonates is not visible, however, in the solid Mn profiles as the difference between HA.AA, 0.1N HCl or 1N HCl and CDB extractable Mn does not increase at depth, where the dissolved Mn^{2+} starts to decrease. Alternatively, the profiles may still be relaxing from a non-steady state in case of the Frisian Front and German Bight or we may see the effect of irrigation. The difference between Mn extractable in CDB and the other extractants may point at a constant "background" concentration of Mn in calcium carbonates or silicates. Few differences are observed between the various extractions and their depth distributions.

Reactive Continuum Approach: the initial rates

The ascorbic acid dissolution is used to quantify the Mn oxide reactivity, because it combines proton assisted and reductive dissolution. Therefore this experiment will be discussed in more detail than the HCl experiment, which only serves as a comparison to the ascorbic acid dissolution. For iron oxides proton assisted dissolution is usually the slowest of the oxide dissolution pathways, while the presence of a ligand increases the rate, but dissolution is fastest in the presence of a reductant like ascorbic acid (e.g. Schulzberger *et al.*, 1989; Stumm and Schulzberger, 1992). This is consistent with the observation of Postma (1993), that no more than 1% of the ferrihydrite dissolved in HCl solution (pH 3). The substantial dissolution of Mn in dilute HCl (pH 3), however, suggests that proton assisted dissolution is of importance for Mn, which was also suggested by the classical extractions discussed earlier. Mn dissolution in dilute HCl may not be true proton assisted dissolution, because the acid can liberate Fe^{2+} and organics that reductively dissolve Mn. Nevertheless, the difference between the two experiments is due to the reductive power of ascorbate and therefore solely represents Mn(III) and Mn(IV). Dissolution of Mn from carbonates or silicates due to the solution pH (3.0) is the same for both ascorbate and dilute HCl.

The dissolution rates of the different samples are plotted in Figure 6a as $-\log (J/m_0)$ versus $-\log (m/m_0)$ to compare their Mn oxide reactivities. At time zero, the reaction rate J normalised to m_0 equals υ/a, which is the apparent rate constant, k' (Fig. 6a). On the x-axis, increasing values indicate decreasing amounts of Mn oxides remaining as dissolution proceeds. In the sediment, reduction rates also depend on factors such as the specific reductant involved and pH, bacterial community structure and number of viable cells (Dollhopf *et al.*, 2000), but the dissolution rates estimated in the experiments are a function of the Mn oxide reactivity only in this case. The rate is independent of the ascorbic acid concentration, because it does not change appreciably over time. The initial dissolution rates ($J\ m_0^{-1}$) roughly range between 10^{-3}

and 10^{0} (s^{-1}) in ascorbic acid and between 10^{-6} and 10^{-3} (s^{-1}) in HCl, showing the difference in reductive plus proton-assisted dissolution versus proton-assisted dissolution alone (Fig. 6a,b). At the same pH, Mn oxides will dissolve faster in the presence of a reductant such as ascorbic acid.

The three oxidised surface sediment samples have the highest initial dissolution rates in ascorbic acid (Fig. 6a). The variation of the initial rates over more than 2 orders of magnitude indicates that large differences in the most reactive Mn oxide phase exist between the different marine sediments. The variation is greatest among the top sediments (2 orders of magnitude) and much smaller among the bottom samples (half an order of magnitude). The German Bight is an area of intense cycling apparently containing very reactive Mn oxides as suggested by the very high initial dissolution rate in the top sample.

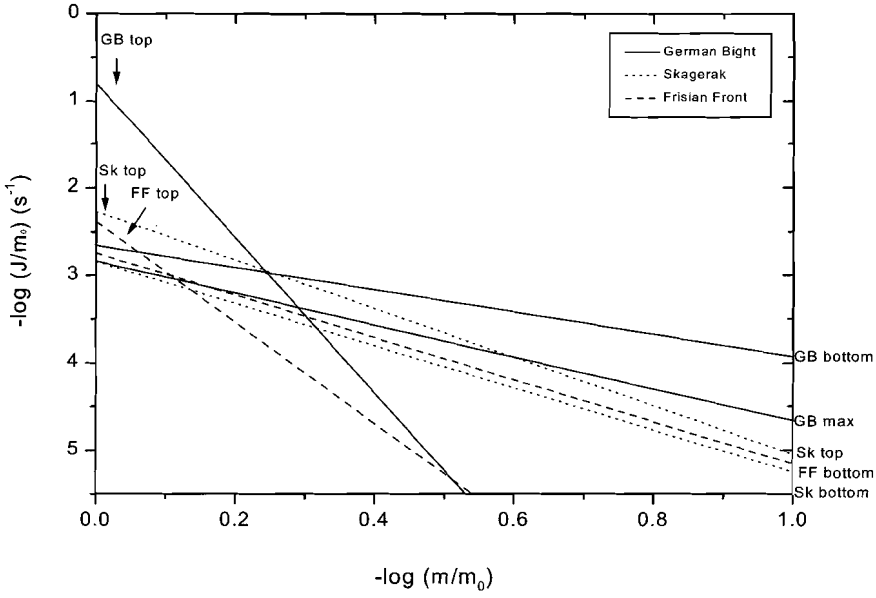

Figure 6a. Mn oxide reduction rates in ascorbic acid (pH 3) solution normalised to the initial mass (J/m_0) versus the fraction (m/m_0) remaining in the solid phase of the top and bottom samples of the Frisian Front (dashed lines), German Bight (solid lines), and Skagerrak (dotted lines).

Reactive Continuum Approach: the range of reactivities

The negative slopes of the lines in Fig. 6a reflect the decrease in dissolution rate. The three oxidised surface sediment samples have the largest range of reactivities. The bottom samples, from the reduced sediment layer, have much smaller ranges of reactivities, i.e. the lines are more horizontally oriented. Deeper in the sediment, the

Mn pool becomes more homogeneous probably leaving only the very resistant Mn oxides to be buried together with detrital Mn in clay minerals and reduced authigenic phases. The decrease in reactivity during dissolution in ascorbic acid can span several orders of magnitude suggesting an enormous heterogeneity in Mn oxide reactivity, especially for the top sediments of the highly energetic German Bight (~ 9 orders of magnitude) and the moderately energetic Frisian Front (~6 orders of magnitude). In contrast, the oxidised top sample from the Skagerrak is relatively homogeneous (~3 orders of magnitude variation). Thus, most heterogeneous Mn oxide assemblages are found in more intense reworked sediments. Postma (1993) found a change in reactivity of the ferric oxides of almost 5 orders of magnitude in Aarhus Bight sediment. The reactivity of the subsurface maximum at the German Bight is similar to that of the bottom sample, thus the most reactive Mn is already dissolved in the upper zone of Mn reduction.

The difference between dissolution by ascorbic acid and HCl (Table 2) is large in the top layers, where the Mn oxide heterogeneity is large. For the bottom layers, however, the difference is very small. The bottom layer sediment already has past the Mn reduction zone, therefore the major part of the "easily reducible" Mn oxides should be gone. This effect is reflected in the smaller difference between the reductive plus proton-assisted dissolution (ascorbic acid) and the proton-assisted only dissolution (HCl) in the deeper layers. Suppose that in the bottom layers Mn is associated with carbonates only and the difference between HCl and ascorbic acid in the top layers represents additional Mn oxides. The amount of Mn extracted in the bottom layers would then equal the difference between HA.AA and CDB extractable Mn, which is 1.1 μmol Mn g^{-1} at the Frisian Front, 1.7 μmol Mn g^{-1} at the German Bight and 0.7 μmol Mn g^{-1} at the Skagerrak. The fitted m_0 for Mn dissolution in HCl (pH 3) is 0.9 μmol Mn g^{-1} at the Frisian Front, 3.6 μmol Mn g^{-1} at the German Bight and 2.1 μmol Mn g^{-1} at the Skagerrak. Thus, at the Frisian Front it is possible that HCl at pH 3 only extracted Mn associated with carbonates. At the German Bight and Skagerrak, however, twice that amount was extracted with HCl at pH 3. Thus, the differences between top and bottom layers more likely reflect the differences between the Mn oxide assemblage before and after Mn reduction.

Mn oxidation products/ heterogeneity

Hem and Lind (1983) argued that in aerated aqueous systems the initial Mn^{2+} oxidation product would be a metastable solid species with the Mn oxidation number no greater than +3.0. Depending on the ionic medium and the reaction temperature several Mn oxidation products may form (Hem and Lind, 1983). Conditions favourable for the development of Mn (IV) oxides (MnO_2) are most likely to occur when the initial precipitate is β-MnOOH (feithknechtite). However, if the initial product is Mn_3O_4 (hausmannite), it will transform into γ-MnOOH (manganite), which is more stable than β-MnOOH and is not altered to more oxidised forms within a period of several months (Hem and Lind, 1983; Murray et al., 1985). Microbial Mn^{2+} oxidation can result in various oxidation products as well. Bacterial spores of the marine *Bacillus* strain SG-1 can directly oxidise Mn (II) to Mn (IV) without the formation of Mn (III) intermediates (Mandernack et al., 1995). The biogenic Mn oxides produced by the bacterium *Leptothrix discophora* SS-1, however, were shown to be mixed Mn (III, IV) oxides with an average oxidation state of 3.6 and a rather

high surface area of 224 m^2 g^{-1} implying a high reactivity (Nelson et al., 1999; Adams and Ghiorse, 1988). Based on these experiments, a large range of Mn reactivity can be expected in the oxic layer of the sediment. Both freshly precipitated Mn (III) oxides with a high reactivity and more aged crystalline Mn (IV) oxides with a lower reactivity are likely to occur. This is consistent with the large heterogeneity found in the oxidised surface samples. Some field investigations do not suggest a large mineralogical diversity in marine and lake sediments (e.g. Canfield*et al.,* 1993; Friedl *et al.*, 1997). Nevertheless a range of reactivities is likely in natural sediments, because the reactivity of a single mineral depends greatly on its particle size distribution, crystal morphology and reactive site density (Larsen and Postma, 2001).

The Mn oxide heterogeneity in the top layer increases with physical sediment mixing intensity. The Mn^{2+} ions experience a variable chemical environment (e.g. Luther *et al.,* 1997; Huettel *et al.*, 1998), which results in different oxidation products and thus, a large heterogeneity. In contrast to biodiffusional mixing, which tends to flatten concentration profiles, the physical perturbations that mix the sediments of the Frisian Front and German Bight result in a layering of the sediment. Therefore these perturbations increase the sedimentary heterogeneity instead of homogenising the sediments.

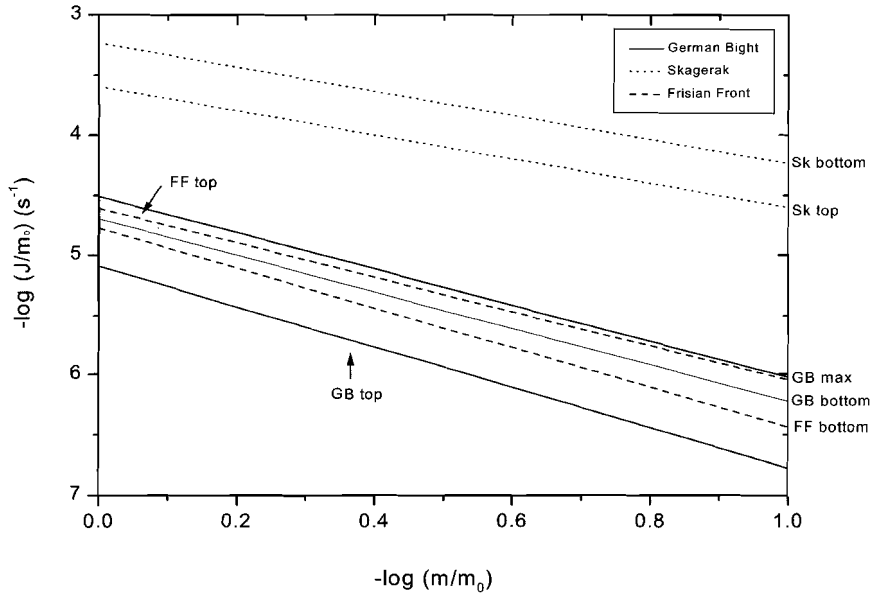

Figure 6b. Mn oxide reduction rates in HCl (pH 3) solution normalised to the initial mass (J/m_0) versus the fraction (m/m_0) remaining in the solid phase of the top and bottom samples of the Frisian Front (dashed lines), German Bight (solid lines), and Skagerrak (dotted lines).

Manganese cycling

Diagenetic models generally describe sediment profiles of Mn oxides and dissolved Mn^{2+} rather well (e.g. Burdige and Gieskes, 1983; Van Cappellen and Wang, 1996; Slomp *et al.*, 1997; Boudreau *et al.*, 1998; Van der Zee *et al.*, 2001). Large variations in kinetic coefficients are found in these studies, however, because a number of processes are lumped into one single rate constant. The Mn reduction rate depends on several factors, e.g. Mn oxide reactivity, temperature, bacterial versus inorganic catalysis, organic matter reactivity, and the type of reductant involved (e.g. Burdige and Gieskes, 1983; Slomp *et al.*, 1997). Considering the large variation in Mn reactivity found in this study, this could be one of the major factors determining these large variations in kinetic coefficients. In the sediment, the most reactive Mn oxides will be reduced preferentially leaving more resistant Mn oxides behind. The Mn reduction rate will decrease upon removal of the most reactive Mn oxides. Therefore Mn cycling is most intense close to the Mn redox boundary, where Mn reactivity is largest.

The reactive continuum approach offers the possibility to compare the intrinsic Mn reactivity in a standardised way, which can be used to assess the rate limiting factors for Mn reduction and its contribution to total carbon mineralisation. Previously, the relatively low concentration of sedimentary Mn oxides was suggested to limit the contribution of Mn reduction to overall carbon mineralisation (Bender and Heggie, 1984). However, the Mn oxide concentration is not per se rate limiting for the Mn reduction rate, due to rapid recycling. Manganese is an efficient electron shuttle between oxygen and organic matter, through re-oxidation of Mn^{2+} by molecular oxygen (Aller, 1994). The Mn oxide reactivity likely affects the microbial Mn reduction rate as has been shown for Fe (Dollhopf *et al.*, 2000) and thus Mn cycling in aquatic sediments.

Redox Zonation

Depending on their free energy yield and availability, a suite of electron acceptors is used in the degradation of organic matter, oxygen, nitrate, Mn oxides, Fe oxides and sulphate (Froelich *et al.*, 1979). The reactivity of Fe oxides in natural sediments vary over orders of magnitude (Postma, 1993) and their reactivity is roughly paralleled by their instability (Dos Santos Afonso and Stumm, 1992). Postma and Jakobsen (1996) argued therefore that due to the large variability in Fe oxides present in marine sediments, Fe reduction is favored in the presence of amorphous Fe hydroxides, but as the stability of the Fe oxide increases, sulfate reduction becomes the favorite pathway for organic matter degradation. Similar to the Fe oxides, the bulk dissolution experiments show that natural Mn oxides are present in widely variable reactivities. Analogous to the iron-sulfate equilibrium, the nitrate-manganese redox equilibrium strongly depends on the stability of the Mn oxides present in the sediment. Although one may argue that synthetic Mn oxides, even the amorphous, are not the same as natural amorphous Mn oxides, nitrate reduction appears to be favored over amorphous Mn oxide reduction, because bacteria prefer a soluble electron acceptor to a solid form (Dollhopf *et al.*, 2000). Considering the enormous range of reactivities found for both Mn oxides and Fe oxides in natural sediments, extensive vertical overlap of the metal reduction zones can be expected. Some Mn oxides may

escape reduction and be buried, when the Fe oxides are more reactive. The solid Mn profiles do show that Mn oxides are present below the Mn reduction zone. At the Skagerrak, for example, ~40% of the CDB-extractable Mn of the top layer is preserved at 10cm depth.

CONCLUSIONS

The application of the reactive continuum approach provides more information on the Mn reactivity than conventional extraction methods do. It can be useful in the interpretation of Mn profiles from energetic environments like the German Bight and Frisian Front, which are difficult to interpret from the depth distributions only.

Comparison of the oxidised sediment samples shows that the heterogeneity of the natural assemblage of Mn oxides increases with physical sediment mixing intensity. The homogeneous assemblage of Mn oxides in the reduced sediment samples suggests that some Mn oxides escape reduction in the sediment. Considering the enormous variability in reactivity found for both Mn oxides and Fe oxides in natural sediments, extensive vertical overlap of metal reduction zones can be expected.

Acknowledgements We thank the captain, crew and scientific party of the RV Pelagia for their help. Karel Bakker and Jan van Ooyen performed the Mn^{2+} analyses (Dept. Marine Chemistry and Geology, NIOZ). Critical comments by Philippe van Cappellen and Eric Epping on earlier drafts of the manuscript were much appreciated. This study is part of the VvA-4 studies on disturbed earth systems supported by the Research Council for Earth and Life Science (ALW) with financial aid from the Netherlands Organisation for Scientific Research (NWO) (no. 770.91.187). CvdZ is supported through a grant to WvR from the Netherlands Organisation for Scientific Research (NWO) SMILE program (no. 750.297.01). This is publication no. 3634 of the Royal Netherlands Institute for Sea Research.

REFERENCES

Adams, L.F. and Ghiorse, W.C. 1988. Oxidation state of Mn in the Mn oxide produced by *Leptothrix discophora* SS-1. Geochim. Cosmochim. Acta, 52, 2073-2076.

Aller, R.C. 1990. Bioturbation and manganese cycling in hemipelagic sediments. Phil. Trans. Royal Soc. London A, 331, 51-68.

Aller, R.C. 1994. The sedimentary Mn cycle in Long Island Sound: Its role as intermediate oxidant and the influence of bioturbation, O2, and Corg flux on diagenetic reaction balances. J. Mar. Res., 52, 259-295.

Bender, M.L. and Heggie, D.T. 1984. Fate of organic carbon reaching the deep sea floor: a status report. Geochim. Cosmochim. Acta, 48, 977-986.

Boudreau, B.P., Mucci, A., Sundby, B., Luther, G.W., and Silverber, N. 1998. Comparative diagenesis at three sites on the Canadian continental margin. J. Mar. Res., 56, 1259-1284.

Boudreau, B.P. and Ruddick, B.R. 1991. On a reactive continuum representation of organic matter diagenesis. Am. J. Sci., 291, 507-538.

Boon, A.R., and Duineveld, G.C.A. 1996. Phytopigments and fatty acids as molecular markers for the quality of near bottom particulate organic matter in the North Sea. J. Sea Res., 35, 279-291.

Brewer, P. G. and D. W. Spencer. 1971. Colorimetric determination of manganese in anoxic waters. Limnol. Oceanogr., 16, 107-110.

Burdige, D.J. and Gieskes, J.M. 1983. A pore water/solid phase diagenetic model for manganese in marine sediments. Am. J. Sci., 283, 29-47.

Burdige, D.J., and Nealson, K.H. 1986. Chemical and microbial studies of sulfide-mediated manganese reduction. Geomicrobiol. J., 4, 361-387.

Burdige, D.J., Dhakar, S.P., and Nealson, K.H. 1992. Effects of manganese oxide mineralogy on microbial and chemical manganese reduction. Geomicrobiol. J., 10, 27-48.

Burdige, D.J. 1993. The biogeochemistry of manganese and iron reduction in marine sediments. Earth Sci. Rev., 35, 249-284.

Burns, R.G. and Burns, V.M. 1979. Manganese oxides. In Marine Minerals. R.G. Burns (ed.) Reviews in Mineralogy Vol. 6. Mineralogy Society of America, Washington DC, p 1-46.

Canfield, D.E. 1988. Sulfate reduction and the diagenesis of iron in anoxic marine sediments. Ph.D. thesis. Yale University.

Canfield, D.E., Thamdrup, B., and Hansen, J.W. 1993. The anaerobic degradation of organic matter in Danish coastal sediments: iron reduction, manganese reduction and sulfate reduction. Geochim. Cosmochim. Acta, 57, 3867-3883.

Chester, R. and Hughes, M.J. 1967. A chemical technique for the separation of ferro-manganese minerals, carbonate minerals and adsorbed trace elements from pelagic sediments. Chem. Geol., 2, 249-262.

Christoffersen, J. and Christoffersen, M.R. 1976. The kinetics of dissolution of calcium sulphate dihydrate in water. J. Crystal Growth, 35, 79-88.

Dauwe, B., Herman, P.M.J., and Heip, C.H.R. 1998 Community structure and bioturbation potential of macrofauna at four North Sea stations with contrasting food supply. Mar. Ecol. Progr. Ser., 173, 67-83.

Dauwe, B., Middelburg, J.J., van Rijswijk, P., Sinke, J., Herman, P.M.J. and Heip, C.H.R. 1999. Enzymatically hydrolyzable amino acids in North Sea sediments and their possible implication for sediment nutritional values. J. Mar. Res., 57, 109-134.

De Haas, H., Boer, W., and van Weering, T.C.E., 1997. Recent sediment and organic carbon burial in a shelf sea; the North Sea. Mar. Geol., 144, 131-146.

Dollhopf, M.E., Nealson, K.H., Simon, D.M. and Luther III, G.W. 2000. Kinetics of Fe(III) and Mn(IV) reduction by the black sea strain of *Shewanella putrefaciens* using in situ solid state voltametric Au/Hg electrodes. Mar. Chem., 70, 171-180.

Dos Santos Afonso, M. and Stumm, W. 1992. Reductive dissolution of iron (III) (hydr)oxides by hydrogen sulfide. Langmuir, 8, 1671-1675.

Duinker, J.C., van Eck, G.T.M. and Nolting, R.F. 1974. On the behaviour of copper, zinc, iron and manganese, and evidence for mobilization processes in the Dutch Wadden Sea. Neth. J. Sea Res., 8, 214-239.

Friedl, G., Werhli, B. and A. Manceau. 1997. Solid phases in the cycling of manganese in eutropic lakes: New insights from EXAFS spectroscopy. Geochim. Cosmochim. Acta, 61, 275-290.

Froelich, P.N., Klinkhammer, G.P., Bender, M.L., Luedtke, N.A., Heath, G.R., Cullen, D., Dauphin, P., Hammond, D., Hartman, B., and Maynard, V. 1979. Early oxidation of organic matter in pelagic sediments of the eastern equatorial Atlantic: suboxic diagenesis. Geochim. Cosmochim. Acta, 43, 1075-1090.

Haese, R.R., Wallman, K., Dahmke, A., Kretzmann, U., Müller, P.J. and Schulz, H.D. 1997. Iron species determination to investigate early diagenetic reactivity in marine sediments. Geochim. Cosmochim. Acta, 61, 63-72.

Hem, J.D. and Lind, C.J. 1983. Nonequilibrium models for predicting forms of precipitated manganese oxides. Geochim. Cosmochim. Acta, 47, 2037-2046.

Huettel, M., Ziebis, W., Forster, S., Luther III, G.W., 1998. Advective transport affecting metal and nutrient distributions and interfacial fluxes in permeable sediments. Geochim. Cosmochim.Acta, 62, 613-631.

Kempe, S., Liebezeit, G., Dethlefsen, V., and Harms, U., 1988. Biogeochemistry and distribution of suspended matter in the North Sea and implications to fisheries biology. Syn.. Mitt. Geol.-Paläont. Inst. Univ. Hamburg, SCOPE/UNEP, Sonderband, 65, XI-XXIV.

Koning, E., Brummer, G.-J., van Raaphorst, W., van Bennekom, J., Helder, W. and van Iperen, J. 1997. Settling, dissolution and burial of biogenic silica in the sediments off Somalia (northwestern Indian Ocean). Deep-Sea Res. II, 44, 1341-1360.

Kostka, J.E. and Luther III, G.W. 1994.Partitioning and speciation of solid phase iron in saltmarsh sediments. Geochim. Cosmochim. Acta,58, 1701-1710.

Larsen, O. and Postma, D. 2001.Kinetics of reductive bulk dissolution of lepidocrocite, ferrihydrite, and goethite. Geochim. Cosmochim. Acta,65, 1367-1379.

Luther III, G.W., B. Sundby, B.L. Lewis, P.J. Brendel and N. Silverberg. 1997. Interactions of manganese with the nitrogen cycle: Alternative pathways to dinitrogen. Geochim. Cosmochim. Acta, 61, 4043-4052.

Mandernack, K.W., Post, J. and Tebo, B.M. 1995. Manganese mineral formation by bacterial spores of the marine *Bacillus*, strain SG-1: Evidence for the direct oxidation of Mn (II) to Mn (IV). Geochim. Cosmochim. Acta, 21, 4393-4408.

Murray, J.W., Dillard, J.D., Giovanoli, R., Moers, H. and Stumm, W. 1985. Oxidation of Mn(II): initial mineralogy, oxidation state and ageing. Geochim. Cosmochim. Acta, 49, 463-470.

Myers, C.R. and Nealson, K.N. 1988. Bacterial manganese reduction and growth with manganese oxide as the sole electron acceptor. Science, 240, 1319-1321.

Nelson, Y.M., Lion, L.W., Ghiorse, W.C. and Shuler, M.L. 1999. Production of biogenic Mn oxides by *Leptothrix disophora* SS-1 in a chemically defined growth medium and evaluation of their Pb adsorption characteristics. Appl. Environ. Microbiol., 65, 175-180.

Postma, D. 1993. The reactivity of iron oxides in sediments: a kinetic approach. Geochim. Cosmochim. Acta, 57, 5027-5034.

Postma, D., 1985. Concentration of Mn and separation from Fe in sediments – I. Kinetics and stoichiometry of the reaction between birnessite and dissolved Fe(II) at 10°C. Geochim. Cosmochim. Acta, 49, 1023-1033.

Postma, D., and Jakobsen, R. 1996. Redox zonation: Equilibrium constraints on the Fe(III)/SO_4-reduction interface. Geochim. Cosmochim. Acta, 60, 3169-3175.

Puls, W., and Sündermann, J., 1990. Simulation of suspended sediment dispersion in the North Sea. In: Cheng, R.T. (Ed.), Residual currents and long-term transport, Coastal and estuarine studies, 38, Springer, New York, pp. 35-372.

Ruttenberg, K.C. 1992. Development of a sequential extraction method for different forms of phosphorus in marine sediments. Limnol. Oceanogr., 37, 1460-1482.

Slomp, C.P., Malschaert, J.F.P., Lohse, L., van Raaphorst, W. 1997. Iron and manganese cycling in different sedimentary environments on the North Sea continental margin. Cont. Shelf Res., 17, 1083-1117.

Schenau, S.J. 1999. Cycling of phosphorus and manganese in the Arabian Sea during the late quaternary. Geologica Ultraiectina, 182. Ph.D. thesis. Utrecht University.

Schulzberger, B., D. Suter, C., Schiffert, S. Banwart and W. Stumm. 1989. Dissolution of Fe(III)(hydr)oxides in natural waters; Laboratory assessment on the kinetics controlled by surface coordination. Mar. Chem., 28, 127-144.

Stone, A.T. and Morgan, J.J. 1984. Reduction and dissolution of manganese (III) and (IV) oxides by organics: Survey of the reactivity of organics. Environ. Sci. Technol., 18, 617-624.

Stumm, W. and B. Sulzberger. 1992. The cycling of iron in natural environments: Considerations based on laboratory studies of heterogeneous redox processes. Geochim. Cosmochim. Acta, 56, 3233-3257.

Sündermann, J. 1993. Suspended particulate matter in the North Sea: field observations and modelling. Phil. Trans. Royal Soc., London A, 343, 45-52.

Tarutis Jr, W.J. 1993. On the equivalence of the power and reactive continuum models of organic matter diagenesis. Geochim. Cosmochim. Acta, 57, 1349-1350.

Thamdrup, B., Glud, R.N. and Hansen, J.W. 1994. Manganese oxidation and in situ manganese fluxes from a coastal sediment. Geochim. Cosmochim. Acta, 58, 2563-2570.

Van Cappellen, P. and Wang, Y. 1996. Cycling of iron and manganese in surface sediments: A general theory for the coupled transport and reaction of carbon, oxygen, nitrogen, sulfur, iron and manganese. Am. J. Sci., 296, 197-243.

Van der Zee, C., van Raaphorst, W. and Epping, E. 2001. Adsorbed Mn^{2+} and Mn redox cycling in Iberian continental margin sediments (northeast Atlantic Ocean). J. Mar. Res., 59, 133-166.

Van der Zee, C., van Raaphorst, W., Helder, W. and de Heij, H. 200x. Manganese and iron diagenesis in temporal and permanent depositional areas in the North Sea. Subm.

Van Raaphorst, W., Kloosterhuis, H.T., Berghuis, E.M., Gieles, A.J.M., Malschaert, J.F.P., van Noort, G.J., 1992. Nitrogen cycling in two types of sediments of the southern North Sea (Frisian Front, Broad Fourteens): field data and mesocosm results. Neth. J. Sea Res. 28, 293-316.

Van Raaphorst, W., Malschaert, H., and van Haren, H., 1998. Tidal resuspension and deposition of particulate matter in the Oyster grounds, North Sea. J. Mar. Res., 56, 257-291.

Van Weering, T.C.E., Berger, G.W., Kalf, J. 1987. Recent sediment accumulation in the Skagerrak, northeastern North Sea. Neth. J. Sea Res., 21, 177-189.

CHAPTER FOUR

Adsorbed Mn^{2+} and Mn redox cycling in Iberian continental margin sediments (NE Atlantic Ocean)[3]

ABSTRACT

Although Mn^{2+} sorption has been investigated extensively in the laboratory, the role of Mn^{2+} sorption in natural marine sediments remains speculative. Our objectives were to study (1) the role of Mn^{2+} sorption in the redox cycling of Mn, (2) to quantify Mn cycling and (3) to identify its rate determining factors at the Iberian Margin.

Profiles of pore water Mn^{2+}, adsorbed Mn^{2+} and solid phase Mn were measured together with benthic oxygen fluxes along three transects across the margin from the shelf to the deep-sea as well as in the Nazeré canyon. In the profiles peaks of adsorbed Mn^{2+} were observed in-between those of solid phase Mn and pore water Mn^{2+}. We propose that upon Mn reduction, the produced Mn^{2+} is adsorbed onto adjacent Mn oxide or oxyhydroxide surfaces. Available adsorption-sites diminish and/or saturate as Mn reduction continues, upon which Mn^{2+} is released into the pore water. Mn redox chemistry is controlled by the organic carbon flux to the sediment. A simple steady state model was formulated that includes Mn^{2+} sorption as a combination of an instantaneous reversible equilibrium process and a first-order kinetic reaction. Model derived, depth integrated rates of Mn reduction as well as Mn^{2+} desorption and oxidation rates range between 1 and 35 μmoles m^{-2} d^{-1}. Mn cycling is most intense at moderate carbon fluxes. Moreover, Mn cycling is enhanced at higher deposition fluxes of Mn oxide in the canyon. Budgets based on the model indicate that adsorbed Mn^{2+} is an important redox intermediate between Mn oxide and pore water Mn^{2+} in the reduced sediment layer. Adsorption of Mn^{2+} restrains the efflux of dissolved Mn^{2+} into the water column, by lowering the pore water gradient at stations with a thin oxidation zone. There, adsorbed Mn^{2+} enhances the retention of Mn^{2+} in the sediment column.

INTRODUCTION

Mn can be the most important intermediate oxidant between oxygen and organic carbon in marine sediments (Aller 1990; Canfield *et al.*, 1993; Aller 1994; Thamdrup *et al.*, 1994). Coupled to the oxidation of organic matter is the reduction of a suite of electron acceptors, e.g. oxygen, nitrate, manganese and iron (hydr-) oxides and sulphate (Froelich *et al.*, 1979). Depending on the carbon flux to the sediment,

[3] This chapter by Claar van der Zee, Wim van Raaphorst and Eric Epping has been published in Journal of Marine Research 59, 133-166, 2001.

sedimentation rate and sediment mixing intensity these electron acceptors each contribute to a different extent to the oxidation of organic carbon. At low carbon fluxes, oxygen is the most important electron acceptor (Bender and Heggie, 1984) whereas sulphate reduction is most important at high carbon fluxes (Jørgensen, 1982). The relative contribution of Mn reduction to the oxidation of organic matter is largest at moderate carbon fluxes when oxygen is depleted within a few cm (Aller, 1990). Mn^{2+} is produced upon Mn-oxide reduction, which is either directly coupled to organic carbon oxidation (Myers and Nealson, 1988a) or via the oxidation of reduced solutes like Fe^{2+}, sulphide or organic acids (Myers and Nealson, 1988b; Stone, 1987).

Adsorption of Mn^{2+} is an important step prior to both its oxidation as well as the precipitation of (Ca, Mn)-CO_3 (Franklin and Morse, 1983; Wilson, 1980). Surfaces appear to bind Mn^{2+} in a manner that facilitates the transition state necessary for oxidation (Wilson, 1980). In a classical experiment, Morgan and Stumm (1964) found that the adsorption capacity at pH 7.5 was as much as 0.5 mole Mn^{2+} per mole MnO_2. While many laboratory studies have studied Mn^{2+} sorption (Morgan and Stumm, 1964; Murray, 1975; Wilson, 1980; Franklin and Morse, 1983; Davies and Morgan, 1989; Burdige *et al.*, 1992; Fendorf *et al.*, 1993; Junta and Hochella, 1994; Junta-Rosso et al., 1997), little attention has been paid to the role of Mn^{2+} sorption in natural marine sediments. Van Cappellen and Wang (1996) explicitely included the adsorption reaction of Mn^{2+} as a complexation reaction with hydrated surface sites in their diagenetic model. However, in most diagenetic models adsorption of Mn^{2+} is either neglected (Burdige and Gieskes, 1983; Dhakar and Burdige, 1996; Van Cappellen and Wang, 1995) or instantaneous reversible equilibrium with pore water Mn^{2+} is assumed, using a sorption constant from the literature (Slomp *et al.*, 1997; Aller, 1994). Sorption constants were derived experimentally in a few studies only, e.g. for a Danish coastal sediment (Canfield *et al.*, 1993), for Mn oxides (Burdige *et al.*, 1992), for kaolinite and a mixture of kaolinite with calcite (Burdige and Kepkay, 1983). Canfield *et al.* (1993) noted a pronounced difference in the adsorption capacity of Mn^{2+} onto sediments containing fully oxidised Mn and sediment with Mn oxides having an average oxidation level less than 3.6-3.8. Furthermore, they found that adsorption of Mn^{2+} onto natural sediments was not completely reversible.

In this paper we present data on the vertical distribution of adsorbed Mn^{2+}, pore water Mn^{2+}, and solid phase Mn in sediments from the Iberian continental margin. A simple reaction-diffusion model was formulated in order to estimate depth-integrated rates of Mn reduction, Mn^{2+} desorption and oxidation, as well as to assess the consistency of the distribution of the three Mn phases. In addition, carbon oxidation rates were determined since Mn reduction rates may vary with the amount and degradability of the carbon flux to the sediment. Thus, the following objectives are addressed (1) the role of Mn^{2+} sorption in the Mn redox cycle, (2) quantification of the Mn redox cycle and (3) the identification of its rate determining factors.

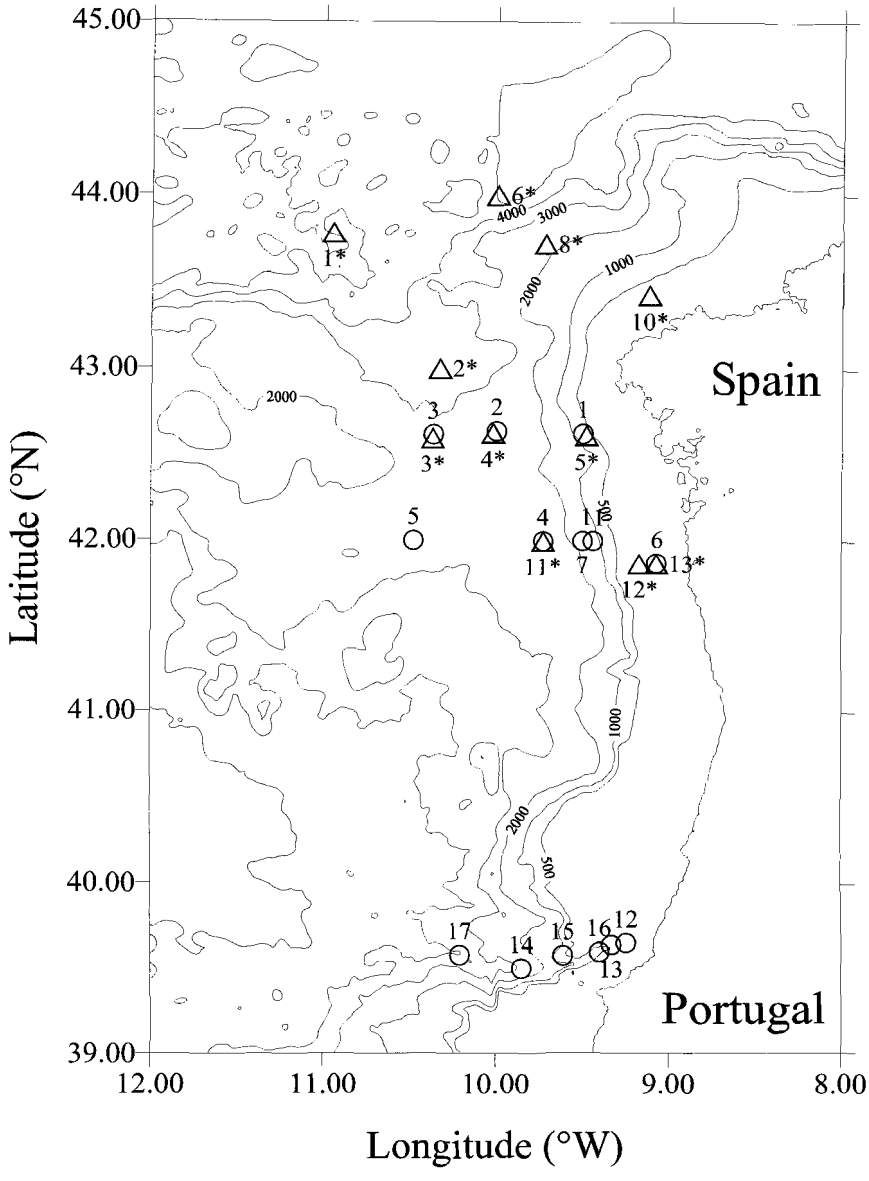

Figure 1. Map of the Iberian Margin indicating positions of sampled stations in 1998 (triangles, numbers with asterisk) and 1999 (circles, numbers without asterisk).

RESEARCH AREA

Our research area comprised the Iberian continental margin in the northeastern Atlantic (Fig.1). The stations were visited during 2 cruises with R.V. *Pelagia* within the Ocean Margin Exchange Project (OMEX II) in August 1998 and May 1999 (Table 1). Sediments are clastic with a minor biogenic component. Sediment transport and accumulation is described in detail by Van Weering *et al.* (2001). Particles are transported from the shelf in benthic nepheloid layers, forming intermediate nepheloid layers at the shelf break. Main deposition occurs within 50 km off shore. Organic carbon contents vary between 0.33 and 4.58 wt% C in the upper sediment layer (Table 1). In general, median grain sizes decrease with increasing distance to the shore, however, some local organic-rich muds are found near the shelf edge. The relative contribution of three grain size fractions to the bulk sediment composition is given in Fig. 2.

Different depositional areas were sampled along three transects from the shelf across the margin to the deep-sea and one transect in the Nazaré canyon. As other submarine canyons (Durrieu de Madron *et al.*, 1999; Monaco *et al.*, 1999; Sanchez-Cabeza *et al.*, 1999) the Nazaré canyon is a preferential transport route for particulate material from the shelf to the deep-sea (Epping *et al.*, subm.; Van Weering *et al.*, 2001). The northern most La Coruña transect is characterised by a gradual decreasing water depth, whereas the slope is steeper at both the Vigo transect north of Vigo, and the main transect south of Vigo. The fourth transect is in the Nazaré canyon further to the south. There, four stations were sampled and an additional two on the adjacent shelf.

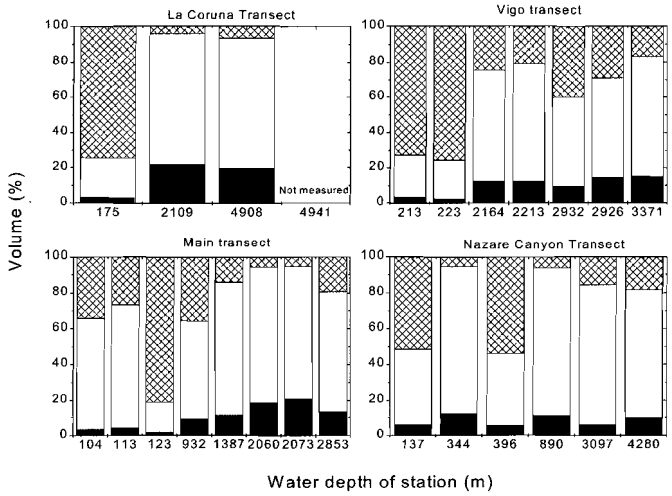

Figure 2. Relative contributions of three grain size fractions to the sediment composition of the upper sediment layer; fraction <2 μm (black), fraction 2-64 μm (white) and the fraction >64 μm (hatched).

Table 1. Name, water depth, geographical position, bottom water (BW) temperature and oxygen concentration and organic carbon content of the visited stations, number 121- stations are visited in August 1998 and number 138- stations are visited in May 1999.

Station	Water depth (m)	Latitude °N	Longitude °W	BW Temp. (°C)	BW O_2 (μM)	Corg* (wt %)
I La Coruña Transect						
121-10	175	43.26	09.07	12.1	225	0.33
121-08	2109	43.43	09.43	3.2	250	1.04
121-06	4908	44.00	10.00	3.1	245	0.72
121-01	4941	43.47	10.57	3.1	245	0.45
II Vigo Transect						
138-01	213	42.38	09.28	12.1	213	0.47
121-05	223	42.38	09.29	12.0	223	0.62
138-02	2164	42.38	10.00	3.4	249	1.35
121-04	2213	42.38	10.01	3.2	250	1.16
138-03	2932	42.37	10.22	2.5	243	1.01
121-03	2926	42.36	10.22	3.1	243	0.87
121-02	3371	43.00	10.20	3.1	245	1.08
III Main Transect						
121-13	104	41.52	09.04	12	235	4.58
138-06	113	41.52	09.04	12.5	210	4.46
121-12	123	41.52	09.10	12.1	230	0.42
138-11	932	42.00	09.26	-	-	1.41
138-07	1387	42.00	09.28	10.3	188	1.99
138-04	2060	42.00	09.44	3.8	247	1.17
121-11	2073	42.00	09.44	3.4	255	1.41
138-05	2853	42.00	10.30	2.6	241	0.88
IV Nazaré Canyon Transect						
138-13	137	39.39	09.20	12.8	209	0.86
138-12	344	39.39	09.15	12.2	206	3.46
138-15	396	39.35	09.37	11.6	200	1.04
138-16	890	39.36	09.24	11.0	189	3.12
138-14	3097	39.31	09.51	2.4	243	3.67
138-17	4280	39.35	10.17	2.1	243	2.56

* Organic carbon content in 0-2.5 mm interval

MATERIAL AND METHODS

Sediment cores were taken with a multi-corer and processed at *in situ* temperature directly upon retrieval. Four sediment cores were sliced simultaneously for pore water collection with a hydraulic core-slicer developed at NIOZ to obtain high spatial resolution at the sediment-water interface. The slicer electronically logs the vertical position of the extruder pistons with an accuracy of < 0.1 mm, relative to the sediment-water interface. The sediment was sectioned in 2.5-mm slices in the upper 10 mm of the sediment, in 5-mm slices from 10 to 30 mm, in 10-mm slices from 30 to 60 mm and in 20-mm slices further down. Slices from corresponding depth intervals were pooled and centrifuged (3000 rpm, 10 min) for pore water extrusion. Depth

intervals were pooled to increase the volume of pore water for analysis of several other pore water constituents required in the OMEX project and might have led to some of the scatter in the profiles. Pore water was filtered (0.45 μm, Acrodisc) and analysed shipboard for nitrate and manganese on a TRAACS-800 auto-analyser. Nitrate was analysed according to Strickland and Parsons (1972). Aliquots for manganese were acidified to pH 2 and analysed according to the method of Brewer and Spencer (1971). After pore water collection the centrifuged sediment was stored frozen (-20 °C) until further analysis for solid phase manganese at the NIOZ laboratory.

Adsorbed Mn^{2+} was determined using a $CuSO_4$ sediment extraction (Bromfield and David, 1976; Lovley and Phillips, 1988). The principle of the extraction method is the exchange of Mn^{2+} by Cu^{2+} (Bromfield and David, 1976). It is assumed that the total dissolved Mn was reduced since 2+ is the dominant valence for dissolved Mn in seawater (Bruland, 1983). To test the optimal incubation time for the $CuSO_4$ extraction, sediment samples were incubated in triplo with 50 mM $CuSO_4$ for 0, 1, 5, 10, 15, 20, 30, 45 and 60 min. The amount of extracted Mn did not further increase upon incubation longer than 20 min (Fig. 3). Thawed sediment from the 1998 cruise was extracted with 50 mM $CuSO_4$ for 20 min in the laboratory. During the 1999 cruise an additional core was sliced and wet sediment was extracted with 50 mM $CuSO_4$ for 20 min directly onboard. The extract was filtered (0.45 μm, Acrodisc), acidified and stored cool (4°C) and in the dark. Corrections were made for the pore water Mn^{2+} in the extract. Freeze-dried and ground sediment was extracted with 1N HCl (24 hrs, 20 °C) for solid phase Mn, which includes reactive Mn-oxides and Mn-carbonates (Thamdrup *et al.*, 1994; Slomp *et al.*, 1997). Mn both in the $CuSO_4$ and the HCl extracts was measured by flame AAS. Porosity was determined from the weight loss of the sediment after drying at 60 °C and assuming a specific weight of the sediment particles of 2.65 g cm^{-3}.

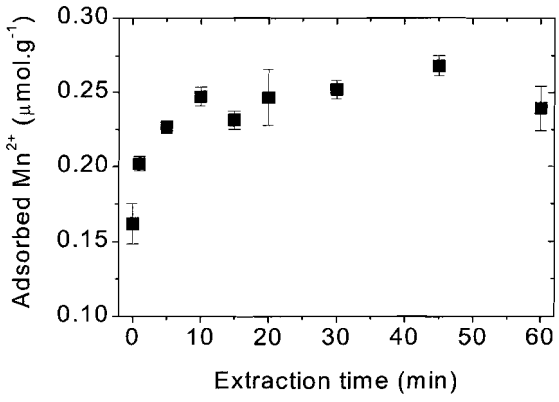

Figure 3. Amount of Mn extracted with 50mM $CuSO_4$ as a function of incubation time. Each data point is the average of three measurements.

Oxygen fluxes were estimated from microprofiles measured *in situ* with Clark-type oxygen microelectrodes mounted on a benthic profiling lander (TROL), or were estimated by modeling the nitrate, ammonium, and sediment organic carbon profile using a numerical, coupled diagenetic model (OMEXDIA) (Soetaert *et al.*, 1996). Further details are described in Epping *et al.* (subm.).

THE MODEL

Description

Early diagenetic models have been developed that couple the diagenesis of Mn to the cycles of C, N, O, P, S and Fe (Rabouille and Gaillard, 1991; Dhakar and Burdige, 1996; Van Cappellen and Wang, 1996; Boudreau et al., 1998). None of these models, however, includes a kinetic sorption reaction for Mn^{2+}. In case instantaneous equilibrium sorption with a depth invariant isotherm dominates, adsorbed and pore water Mn^{2+} have parallel profiles with peaks in the same depth interval (Berner, 1976). Our profiles show that adsorbed Mn^{2+} accumulates at shallower depths in the sediment than dissolved Mn^{2+}, indicating that instantaneous equilibrium sorption was not the only sorption process. Therefore we developed a new, but simpler model than the coupled models mentioned above. This allowed us to reduce the number of variables, limit the uncertainties in data of other elements that could affect the modelling of Mn, and to focus on the role of sorption in the redox cycle of Mn.

Our model is similar to the Mn model of Slomp *et al.* (1997) with additional kinetic sorption. Compared to their model, the uncertainty associated with the kinetic parameters is compensated for by the extra data provided by the adsorbed Mn^{2+} profiles. A listing of all model parameters is given in Table 2. In the model the molecular sediment diffusion coefficient (*Ds*), bioturbation coefficient (*Db*), all reaction rate constants, the instantaneous equilibrium sorption coefficient (K_{eq}) and sediment porosity are assumed to be depth-independent for simplicity sake. Also, the sedimentation rate (ω) is assumed to be constant, which is likely for the deep-sea stations, but for the slope and shelf stations sedimentation is probably more pulsed on a seasonal scale. However, sedimentation rates are not affected by seasonal variation and our profiles do not indicate that pulsed sedimentation had occurred shortly prior to sampling. The model is a one-dimensional steady-state reaction-diffusion model that includes Mn^{2+} sorption as a combination of an instantaneous reversible equilibrium process and a first-order kinetic reaction. The sediment was divided into an oxidised and a reduced layer. The redox boundary at depth L is given by the maximum depth of oxygen penetration if known or the inflection point in the nitrate profile otherwise (Aller, 1994; Slomp *et al.*, 1997).

Table 2. Name, unit and function of model parameters

Name	Unit	Function
Ds	$m^2\ d^{-1}$	Molecular sediment diffusion coefficient
Db	$m^2\ d^{-1}$	Bioturbation coefficient
ω	$m\ d^{-1}$	Sedimentation rate
x	m	Depth in sediment
L	m	Depth of Mn redox boundary
K_{eq}	-	Dimensionless sorption coefficient for equilibrium sorption
C_{eq}	$mol\ m^{-3}$	Pore water equilibrium concentration
ϕ	-	Sediment porosity
ρ	$g\ cm^{-3}$	Average density of the sediment
ϑ	$g\ cm^{-3}$	Conversion factor between pore water and solid or adsorbed phase
C_I	$mol\ m^{-3}$	Pore water Mn^{2+} concentration in the oxidised layer
C_{II}	$mol\ m^{-3}$	Pore water Mn^{2+} concentration in the reduced layer
A_I	$\mu mol\ g^{-1}$	Adsorbed Mn^{2+} concentration in the oxidised layer
A_{II}	$\mu mol\ g^{-1}$	Adsorbed Mn^{2+} concentration in the reduced layer
S_I	$\mu mol\ g^{-1}$	Solid phase Mn concentration in the oxidised layer
S_{II}	$\mu mol\ g^{-1}$	Solid phase Mn concentration in the reduced layer
C_a	$mol\ m^{-3}$	Pore water equilibrium concentration for precipitation
A_{eq}	$\mu mol\ g^{-1}$	Adsorbed Mn^{2+} concentration at which no further reactions occur
S_{eq}	$\mu mol\ g^{-1}$	Solid phase Mn concentration at which no further reactions occur
k_{oxc}	d^{-1}	Dissolved Mn^{2+} oxidation rate constant
k_{oxa}	d^{-1}	Adsorbed Mn^{2+} oxidation rate constant
k_{ads}	d^{-1}	Adsorption rate constant
k_r	d^{-1}	Reduction rate constant
k_{des}	d^{-1}	Desorption rate constant
k_a	d^{-1}	Precipitation rate constant
$J_{Sx=0}$	$\mu mol\ m^{-2}\ d^{-1}$	Flux of solid phase Mn at the sediment-water interface
$J_{Ax=0}$	$\mu mol\ m^{-2}\ d^{-1}$	Flux of adsorbed Mn^{2+} at the sediment-water interface

In the oxidised layer, Mn^{2+} is both oxidised and adsorbed. Oxidation of dissolved and adsorbed Mn^{2+} is described as first-order processes with k_{oxc} and k_{oxa} as the oxidation rate constants, respectively. Kinetic adsorption is described as a first-order process with k_{ads} as the adsorption rate constant. The dimensionless sorption coefficient for equilibrium sorption (K_{eq}) is set at 1 (Slomp *et al.*, 1997) and C_{eq} is the pore water equilibrium concentration. For the conversion between pore water and solid phase Mn or adsorbed Mn^{2+} the factor ϑ (gram of dry sediment per cm^3 of pore water) is used: $\vartheta = \rho\ [(1-\phi)/\phi]$, where ρ is the average density of the sediment (2.65 g cm^{-3}) and ϕ is sediment porosity. Differential equations for dissolved Mn^{2+} (C_I), adsorbed Mn^{2+} (A_I), and solid phase Mn (S_I) in the oxidised layer as a function of depth in the sediment (x) are:

$$[(1+K_{eq})Db + Ds]\frac{\delta^2 C_I}{\delta x^2} - (1+K_{eq})\omega\frac{\delta C_I}{\delta x} - k_{oxc}C_I - k_{ads}(C_I - C_{eq}) = 0 \quad (1)$$

$$Db\frac{\delta^2 A_I}{\delta x^2} - \omega\frac{\delta A_I}{\delta x} - k_{oxa}A_I + \frac{k_{ads}}{\vartheta}(C_I - C_{eq}) = 0 \quad (2)$$

$$Db\frac{\delta^2 S_I}{\delta x^2} - \omega\frac{\delta S_I}{\delta x} + k_{oxa}A_I + \frac{k_{oxc}}{\vartheta}C_I = 0 \quad (3)$$

In the reduced layer, Mn reduction, Mn^{2+} desorption and precipitation occur. Dissolved Mn^{2+} production due to desorption is described as a first-order process with k_{des} as desorption rate constant. Removal of Mn^{2+} due to authigenic mineral formation is described as a first-order process with k_a as the precipitation rate constant. Production of adsorbed Mn^{2+} due to solid phase Mn reduction is described as a first-order process with k_r as the reduction rate constant. The pore water equilibrium concentration for precipitation is C_a. The concentrations for adsorbed Mn^{2+} and solid phase Mn at which no further reactions occur are A_{eq} and S_{eq} respectively. Differential equations for dissolved Mn^{2+} (C_{II}), adsorbed Mn^{2+} (A_{II}), and solid phase Mn (S_{II}) in the reduced layer are:

$$[(1+K_{eq})Db + Ds]\frac{\delta^2 C_{II}}{\delta x^2} - (1+K_{eq})\omega\frac{\delta C_{II}}{\delta x} - k_a(C_{II} - C_a) + \vartheta k_{des}(A_{II} - A_{eq}) = 0 \quad (4)$$

$$Db\frac{\delta^2 A_{II}}{\delta x^2} - \omega\frac{\delta A_{II}}{\delta x} - k_{des}(A_{II} - A_{eq}) + k_r(S_{II} - S_{eq}) = 0 \quad (5)$$

$$Db\frac{\delta^2 S_{II}}{\delta x^2} - \omega\frac{\delta S_{II}}{\delta x} - k_r(S_{II} - S_{eq}) = 0 \quad (6)$$

The 6 differential equations were analytically solved assuming continuity of concentrations and fluxes at the redox boundary and specific conditions at the external boundaries, i.e. the sediment-water interface and at infinite depth. At the sediment-water interface the concentration of dissolved Mn^{2+} equals that in the overlying water (C_0 is set at 0 μM), but the gradient is not necessarily zero. The fluxes of solid phase Mn and adsorbed Mn^{2+} at the sediment-water interface are $J_{Sx=0}$ and $J_{Ax=0}$, respectively. At infinite depth the concentrations of C_{II}, A_{II} and S_{II} converge to C_a, A_{eq} and S_{eq}, respectively, as their gradients and diffusive fluxes diminish. Variance-weighted sums of squares for dissolved and adsorbed Mn^{2+} as well as solid phase Mn were minimised simultaneously, while five parameters (k_{des}, k_r, k_a, $J_{Sx=0}$ and $J_{Ax=0}$) were varied to fit the model to the data using the Excel solver routine.

Parameter values

The values of fixed parameters are given in table 3. The equilibrium concentration of dissolved Mn^{2+} with respect to kinetic adsorption (C_{eq}) is very small and was therefore set at zero. As no literature data on the oxidation rate of adsorbed Mn^{2+} in marine sediments are available, we tuned k_{oxa} values to obtain one suitable value for all stations. The adsorbed Mn gradient close to the redox-boundary cannot be reproduced when k_{oxa} is set lower than 0.001 d^{-1}. On the other hand, when k_{oxa} is increased substantially, the model can not fit the surface maximum unless the flux of adsorbed Mn is unrealistically high which after oxidation would result in an enhanced surface enrichment of solid phase Mn, which is not realistic either. Thus k_{oxa} was set at 0.001 d^{-1} and this value was used at all stations, except for the station at 396 m on the Nazaré canyon transect, where the Mn profiles could only be fit with a slightly higher k_{oxa} (0.003 d^{-1}). The bioturbation coefficients are derived from ^{210}Pb profiles (Van Weering and De Stigter, 1999) and modelled according to Soetaert *et al.* (1996)

(Table 3 and 4). At the stations at 344 and 890 m in the canyon, ^{234}Th derived values were used (Schmidt *et al.*, 2001b). Sedimentation rates are derived from ^{14}C AMS

Table 3. Fixed parameters used in model calculations

Water Depth (m)	(1) k_{oxc} (d^{-1})	(2) k_{oxa} (d^{-1})	(3) k_{ads} (d^{-1})	(4) Db ($m^2 d^{-1}$)	(5) Ds ($m^2 d^{-1}$)	(6) ω (m d^{-1})	(7) L (m)	(8) C_a (μM)	(9) A_{eq} (μmol g^{-1})	(10) S_{eq} (μmol g^{-1})
I La Coruña Transect										
175	1	0.001	0.001	1.95E-7	1.91E-5	9.86E-8	2.5E-3	2.00	0.01	0.38
2109	1	-	-	3.04E-8	2.40E-5	1.48E-7	5.5E-2	3.00	-	1.50
II Vigo Transect										
213	1	0.001	0.001	2.30E-7	2.16E-5	1.37E-7	6.3E-3	0.50	0.01	0.70
223	1	0.001	0.001	2.30E-7	2.04E-5	1.37E-7	1.5E-2	0.10	0.02	0.36
2164	1	0.001	0.001	1.37E-9	2.21E-5	1.67E-7	9.0E-2	3.00	0.14	2.00
2213	1	0.001	0.001	3.29E-9	2.15E-5	1.67E-7	9.0E-2	3.00	0.06	1.00
3371	1	0.001	0.001	1.37E-9	2.00E-5	1.47E-7	1.0E-1	3.00	0.06	2.00
III Main Transect										
104	1	0.001	0.001	4.93E-6	3.50E-5	1.37E-7	3.8E-3	3.35	0.03	1.53
113	1	0.001	0.001	5.48E-7	2.91E-5	1.37E-7	7.5E-3	2.50	0.05	1.75
123	1	-	-	5.48E-7	2.36E-5	1.37E-7	1.5E-2	0.20	-	1.00
932	1	-	-	3.32E-8	2.40E-5	2.74E-7	2.3E-2	3.00	-	1.17
1387	1	0.001	0.001	1.07E-8	2.46E-5	1.37E-6	3.0E-2	4.00	0.17	1.50
2060	1	0.001	0.001	2.19E-9	2.33E-5	2.55E-7	8.0E-2	6.00	0.05	1.00
2073	1	0.001	0.001	2.47E-9	2.33E-5	2.55E-7	9.0E-2	6.00	0.11	2.00
IV Nazaré Canyon Transect										
137	1	0.001	0.001	1.37E-7	2.62E-5	1.37E-6	1.0E-2	1.00	0.02	1.30
396	1	0.003	0.001	1.84E-7	2.43E-5	2.74E-7	2.0E-2	1.00	0.04	1.30
344	1	-	-	1.04 E-	3.38E-5	2.74E-6	7.5E-3	1.00	-	2.80
890	1	0.001	0.001	1.10E-7	2.41E-5	2.74E-6	1.5E-2	4.00	0.15	2.20
3097	1	0.001	0.001	2.74E-7	2.32E-5	2.74E-6	1.3E-2	30.0	0.40	3.30

(1) k_{oxc} is set at 1 d^{-1} (Slomp et al., 1996; Thamdrup *et al.*, 1994) (2) k_{oxa} is set to 0.001 d^{-1} (see text) (3) k_{ads} is set equal to k_{oxa} (4) Db is usually obtained from ^{210}Pb modelling (see text). (5) Ds at 35 PSU and appropriate temperature (Boudreau, 1997) corrected for porosity (Ullman and Aller, 1982) (6) ω is the sedimentation rate (see text). (7) Oxygen penetration depth or nitrate inflection point. (8) Ca is set equal of slightly lower than the deepest Mn^{2+} concentration observed. (9) A_{eq} is set equal or slightly lower than the deepest adsorbed Mn^{2+} concentration observed. (10) S_{eq} is set equal to the deepest solid Mn concentration measured.

calibrated biostratigraphy (Van Weering and De Stigter, 1999; Table 3). There are no data on sedimentation rates for stations at 104 m and 1387 m on the main transect and the shelf stations on the Nazaré canyon transect. The values in table 3 are optimised to fit the model to the data within a reasonable range (0.001-0.05 cm yr^{-1}). The assumed value for the sedimentation rate at the station at 104 m on the main transect has no influence on the model fit, because transport is fully dominated by mixing (Peclet number, $Pe = 10^{-4}$). The sedimentation rate for stations at 344, 890 and 3097 m in the canyon was set on 0.1 cm yr^{-1}, but using a sedimentation rate of 0.01 cm yr^{-1} did not effect any of the integrated Mn reaction rates more than 6%. The Mn model of Slomp *et al.* (1997) was applied to the profiles of solid phase Mn and pore water Mn^{2+} to obtain reduction and oxidation rates for the 2109 m station on the La Coruña transect and the 123 m station on the main transect, since adsorbed Mn^{2+} data were not available for these two stations. This model was also used at the station at 932 m on the main transect, where the adsorbed Mn profile was rather uniform with depth.

Table 4. Bioturbation coefficients

Station Depth (m)	Lower limit *Db* (cm^2 yr^{-1})	Upper limit *Db* (cm^2 yr^{-1})	Used Value *Db* (cm^2 yr^{-1})	How derived
		Vigo Transect		
223	-	3.84	0.84	Empirical relationship #
		Main Transect		
113	0.23	3.1*	2	Empirical relationship #
123	-	5.8	2	Empirical relationship #
		Nazaré Canyon Transect		
137	-	2.8	0.5	Optimised by model fitting
396	0.07	1.24**	0.67	Optimised by model fitting
3097	-	2.9**	1	Optimised by model fitting

Empirical relationship between mixing coefficient and water depth in the OMEX I area at the Goban Spur further to the north on the European continental margin (Soetaert *et al.*, 1996). **Db* values derived from ^{234}Th data (Smidt *et al.*, 2001a), ***Db* values derived from ^{234}Th data (Smidt *et al.*, 2001b). When the sedimentation rate used for the calculation of the *Db* is a lower estimate, then the resulting ^{210}Pb derived *Db* is an upper estimate.

EXPERIMENTAL RESULTS

Profiles of the stations on the *La Coruña transect* are shown in figure 4. At the shallow station the solid phase Mn profile has its maximum at the sediment-water interface, whereas adsorbed Mn has its maximum slightly deeper, i.e. in-between those of solid phase Mn and pore water Mn^{2+}. The concentrations of both solid phase and pore water Mn are highest at the 2109-m station. At the deeper 4908 and 4941-m stations pore water Mn^{2+} concentrations are low. The increase of solid phase Mn with depth at 4908 m suggest a solid phase Mn maximum deeper than 200 mm.

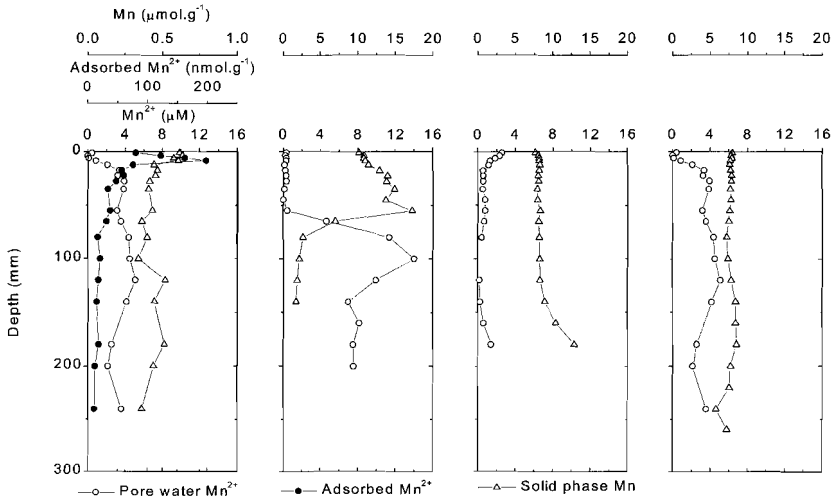

Figure 4. Vertical profiles of pore water Mn^{2+}, adsorbed Mn^{2+} and solid Mn of the stations on the La Coruña transect. Note the different scales for solid Mn at the shallow and the deeper stations.

On the *Vigo transect*, the pairs of stations sampled in August and May at approximately 200, 2200 and 2900 m water depth were almost at the same location (Table 1). The corresponding profiles are not identical, but they do show the same pattern (Fig. 5). At the two shallowest stations concentrations of solid phase Mn are low and the maximum in adsorbed Mn is close to the sediment-water interface. Concentrations of solid phase Mn are one order of magnitude higher at the deeper stations (2164, 2213 and 3371 m).

On the *Main transect* three shallow stations were sampled of which the stations 104 and 113 m are located in a mud patch and show slightly higher concentrations than the other shallow station at 123 m (Fig. 6). The highest concentration of adsorbed Mn^{2+} (note scale) and pore water Mn^{2+} is observed at the 1387-m station.

On the *Nazaré canyon transect* four stations were sampled in the canyon and two stations (137 and 396 m) outside (Fig. 7). The latter two show much lower concentrations of all Mn species than the stations located in the canyon. Remarkably high concentrations of adsorbed Mn^{2+} are found in the canyon stations at 346, 890 and 3097 m, comparable to the 1387 m station on the main transect. Pore water Mn^{2+} concentrations at the 3097-m station reach almost 50 μM, which is much higher than in any of the other profiles. Except for the deepest station, the down-core sequence of maxima is the same as at all stations, i.e. the adsorbed Mn^{2+} maximum is in-between those of solid phase Mn and pore water Mn^{2+}. The deepest canyon station is different from the others, because it consists of alternating layers of Mn poor sand and Mn rich clay with very little adsorbed Mn^{2+}, but high pore water Mn^{2+} concentrations.

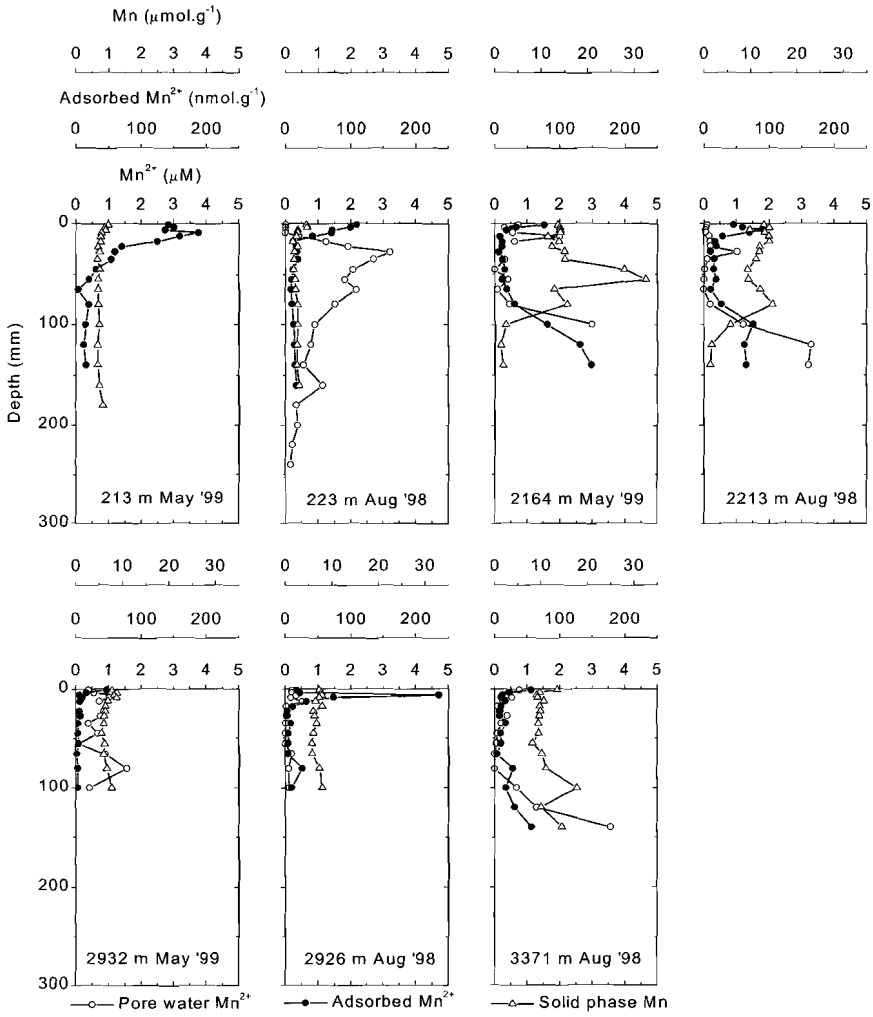

Figure 5. Vertical profiles of pore water Mn^{2+}, adsorbed Mn^{2+} and solid Mn of the stations on the Vigo transect. Note the different scales for solid Mn at the shallow and the deeper stations.

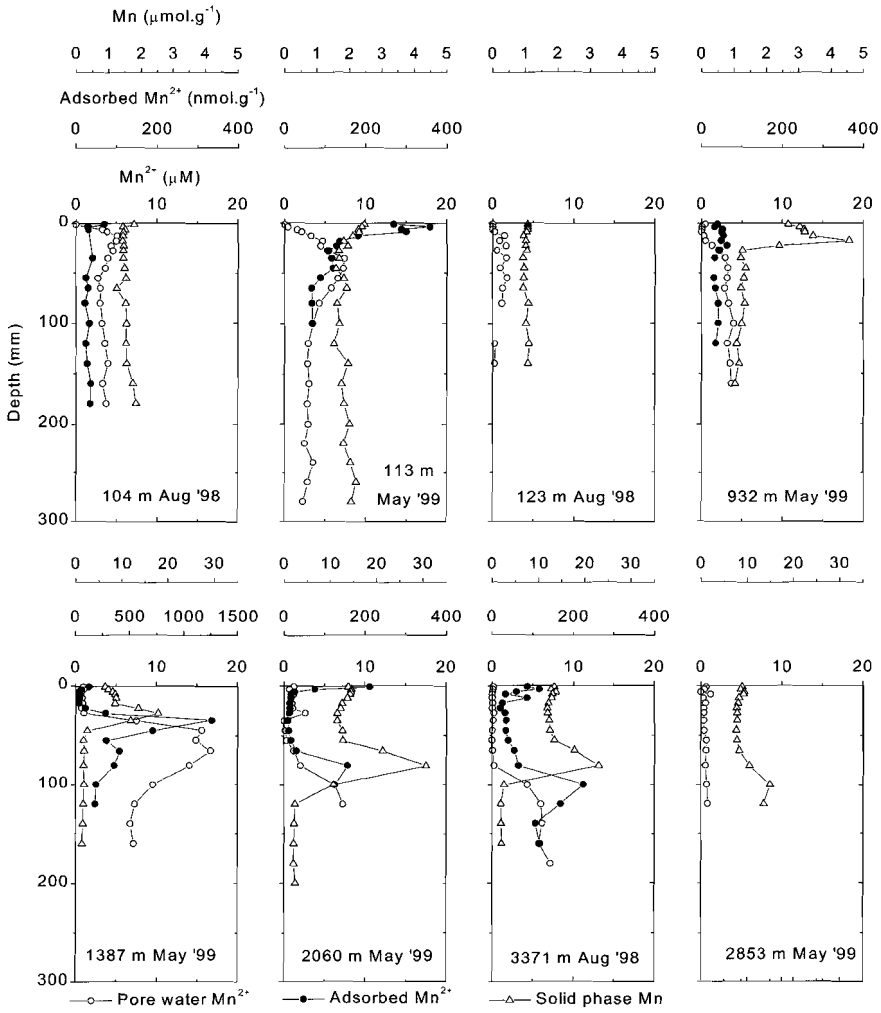

Figure 6. Vertical profiles of pore water Mn^{2+}, adsorbed Mn^{2+} and solid Mn of the stations on the Main transect. Note the different scales for solid Mn at the shallow and the deeper stations.

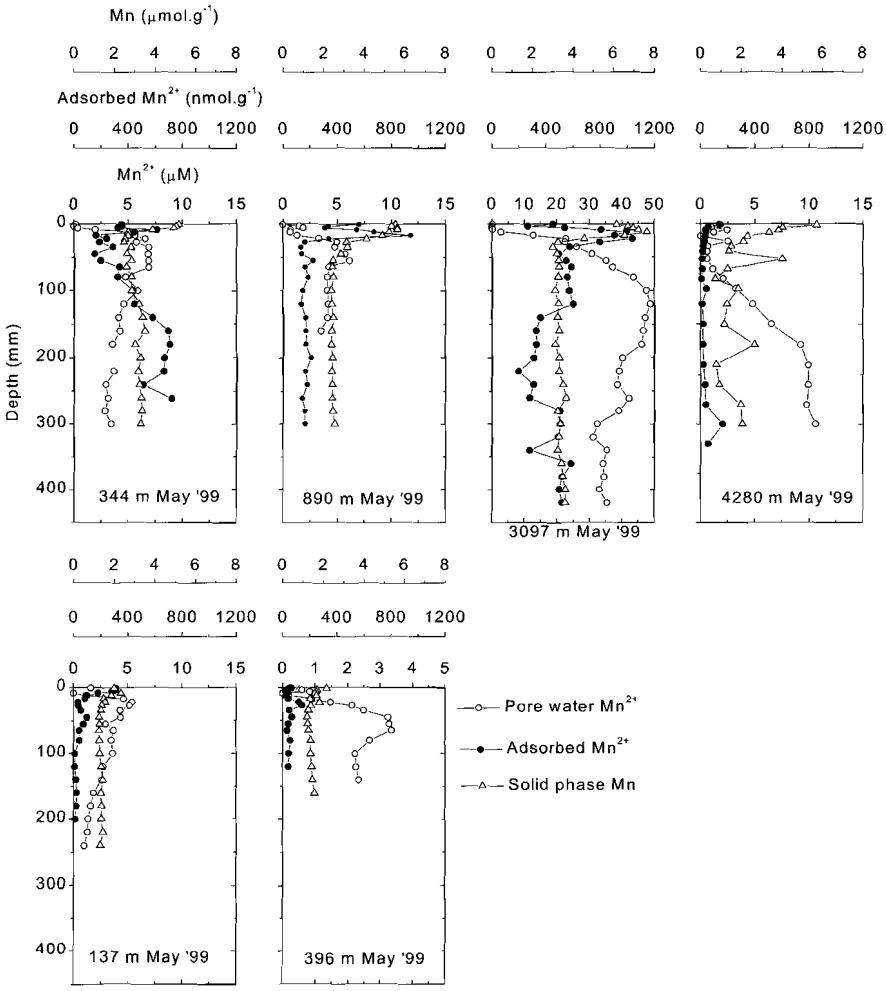

Figure 7. Vertical profiles of pore water Mn^{2+}, adsorbed Mn^{2+} and solid Mn of the stations on the Nazaré Canyon transect. Note the different scale for pore water Mn^{2+} at the 3097-m station.

At the non-canyon transects oxygen fluxes ranged from 2.9 to 10.9 mmol O_2 m^{-2} d^{-1} at depths < 400 m, decreasing to ca 0.6 mmol O_2 m^{-2} d^{-1} at depths exceeding 1000 m (Fig. 8). Applying an oxygen to carbon stoichiometry of 138:106 for aerobic mineralisation, these oxygen fluxes are equivalent to organic carbon mineralisation rates of 9.8 to 37 g C m^{-2} y^{-1} at depths < 400 m and 2 g C m^{-2} y^{-1} at greater water depths (> 1000 m). At the canyon transect, the oxygen fluxes are equivalent to organic carbon mineralisation rates of 13.5, 6.1, and 3.7 g C m^{-2} y^{-1}, respectively. The carbon mineralisation rates for 344 m water depth are well within the range of the other shelf stations, whereas the rates at 3097 and 4280 m water depth exceed the estimates for corresponding water depths along the other transects by a factor of 3 and 2, respectively. More details on carbon cycling will be discussed by Eppinget *al.* (2001)

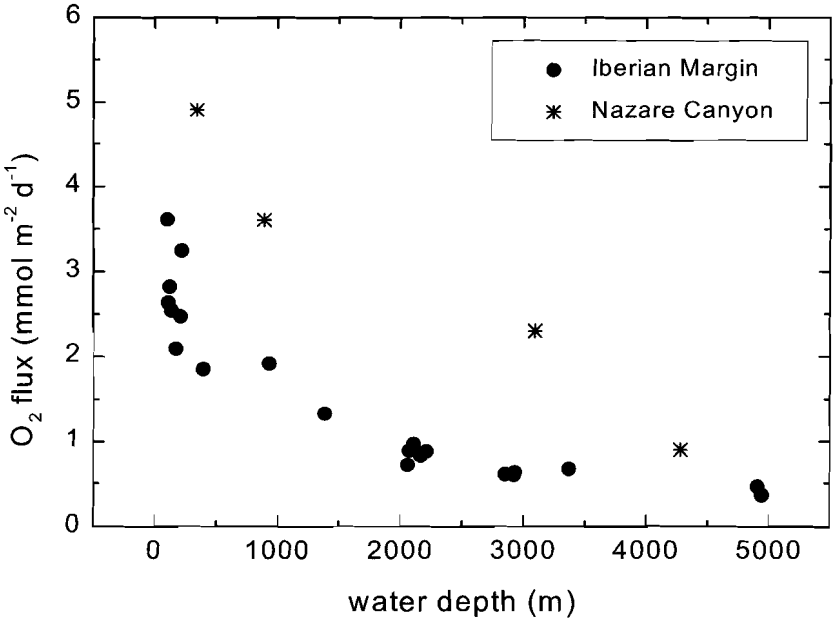

Figure 8. Benthic oxygen fluxes as a function of water depth on the margin (filled circles) and in the canyon (asterisk).

MODEL RESULTS

The model was applied to stations where data of dissolved Mn^{2+}, adsorbed Mn^{2+} and solid phase Mn were available. The profiles of most stations deeper than 3000 m were not modelled because the major redox transitions apparently occurred deeper than our sampling interval. The profiles of the deepest canyon station could not be

modelled due to the alternating layers of Mn-rich clay and Mn-poor sand. The values of the fitted parameters are given in Table 5. The model fits the data reasonably well and the sequence of peaks is well reproduced (Fig.9a-d). A recurring deviation of the model fit from the data is observed in the background concentration of adsorbed Mn^{2+} in the oxic layer. The model fit of the solid phase profile of the station at 2213 m on the Vigo transect (Fig. 9b) is a typical compromise of fitting both the maximum at the redox boundary and the surface enrichment.

The values for the first-order rate constants vary over several orders of magnitude (Table 5) and are comparable to those obtained in a similar way for North Sea sediments (Slomp *et al.*, 1997) and for east equatorial Pacific sediments (Burdige and Gieskes, 1983). According to Slomp et al. (1997), large variation in the first-order rate constants is due to the lumping of a number of processes in one rate constant, which depend on several factors, e.g. the reactivity of the Mn oxide and the type of reductant involved. Burdige and Gieskes (1983) mention differences in surface area and/or mineralogy of the solids, temperature differences, bacterial versus inorganic catalysis and organic matter reactivity to cause differences in rate constants. Sensitivity analyses for the rate constants presented here were conducted by fixing one constant at several values around its optimum and re-fitting the profiles. Fits were least sensitive to the reduction and precipitation rate constants probably because precipitation is not constrained by a (Ca,Mn)-CO_3 profile and desorption is relatively fast. Model fits are more sensitive to the desorption rate constant.

Table 5. Values for k_{des}, k_r, k_a, $J_{Sx=0}$ and $J_{Ax=0}$ obtained by fitting the model to the data.

Water depth (m)	k_{des} (d^{-1})	k_r (d^{-1})	k_a (d^{-1})	$J_{Sx=0}$ ($\mu mol.m^{-2}.d^{-1}$)	$J_{Ax=0}$ ($\mu mol.m^{-2}.d^{-1}$)
I La Coruña Transect					
175	4.33E-4	1.18E-3	1.70E-3	0.95	0.96
2109	-	1.09E-4	1.29E-3	1.05	-
II Vigo Transect					
213	2.29E-3	7.15E-3	1.02E-1	5.81	0.25
223	5.01E-3	1.62E-2	1.20E-2	0.65	0.87
2164	5.44E-2	5.25E-4	5.10E-1	1.51	0.14
2213	2.81E-2	8.47E-5	9.47E-2	0.71	0.22
3371	1.63E-2	1.03E-6	2.68E-3	1.05	0.12
III Main Transect					
104	6.42E-1	3.85E-2	1.19E-1	0.92	15.3
113	2.93E-3	1.42E-3	2.75E-2	5.15	4.32
123	-	4.37E-3	1.83E-2	0.18	-
932	-	3.82E-4	1.98E-2	0.31	-
1387	1.55E-3	2.46E-4	4.67E-3	5.05	0.55
2060	4.23E-3	3.04E-5	5.10E-2	1.43	0.45
2073	1.97E-2	1.68E-3	1.55	1.39	0.37
IV Nazaré Canyon Transect					
137	4.05E-3	6.24E-4	8.56E-3	0.80	4.65
396	2.30E-3	1.10E-2	3.77E-3	0.59	0.59
344	-	4.22E-3	3.55E-4	4.27	-
890	3.95E-3	2.23E-3	2.60E-1	7.52	2.29
3097	2.92E-3	1.18E-3	8.23E-5	11.1	0.20

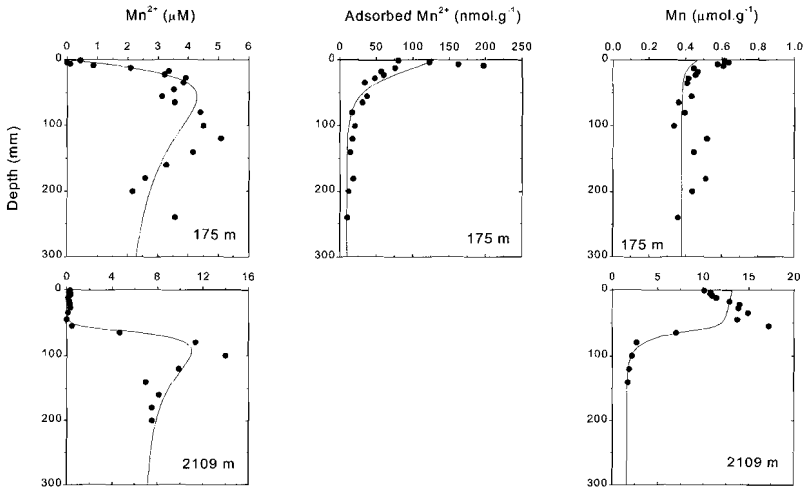

Figure 9a. Model fits (lines) to profiles of pore water Mn^{2+}, adsorbed Mn^{2+} and solid Mn (filled circles) of the stations on the La Coruña transect.

In contrast to the wide range of reaction rate constants is the confined range of the integrated rates of reduction, desorption and oxidation, which were calculated with the model (Table 6), indicating that the overall rates of Mn cycling are not controlled solely by their first order rate constants, but that their combined actions, pool sizes and transport rates are important as well. The Mn reduction rates range between 1 and 35 µmoles m^{-2} d^{-1}, whereas desorption and oxidation rates range from 1 to 30 µmoles m^{-2} d^{-1}. The depth integrated rates of desorption are generally slightly lower than those of reduction. Therefore, only a small amount of adsorbed Mn^{2+} can be found in the deeper part of the profiles. Desorption is more intense than reduction when the redox boundary is very close to the sediment-water interface and the deposition flux of adsorbed Mn^{2+} releases Mn^{2+} into the pore water directly. The Mn oxidation rates are lower than the reduction rates except at the station at 137 m on the Nazaré canyon transect, where the oxidation is slightly faster due to direct oxidation of the deposition flux of adsorbed Mn^{2+}. The rates of reduction, desorption and oxidation at the non-canyon stations show a maximum around 1400 m water depth (Fig. 10). The rates of reduction, desorption and oxidation are relatively high at the 3097-m canyon station compared to stations on the margin at similar water depth. Although the profiles from the deepest canyon station at 4280 m could not be modelled, the reduction and oxidation rate are likely to be lower than at the 3097-m station. The slope of the pore water profile is steeper at the 3097-m station than at the 4280-m station, moreover the pore water concentrations are highest at the 3097-m station. The maximum reduction, desorption and oxidation rates on the Nazaré canyon transect occur at greater water depth than at the other three transects.

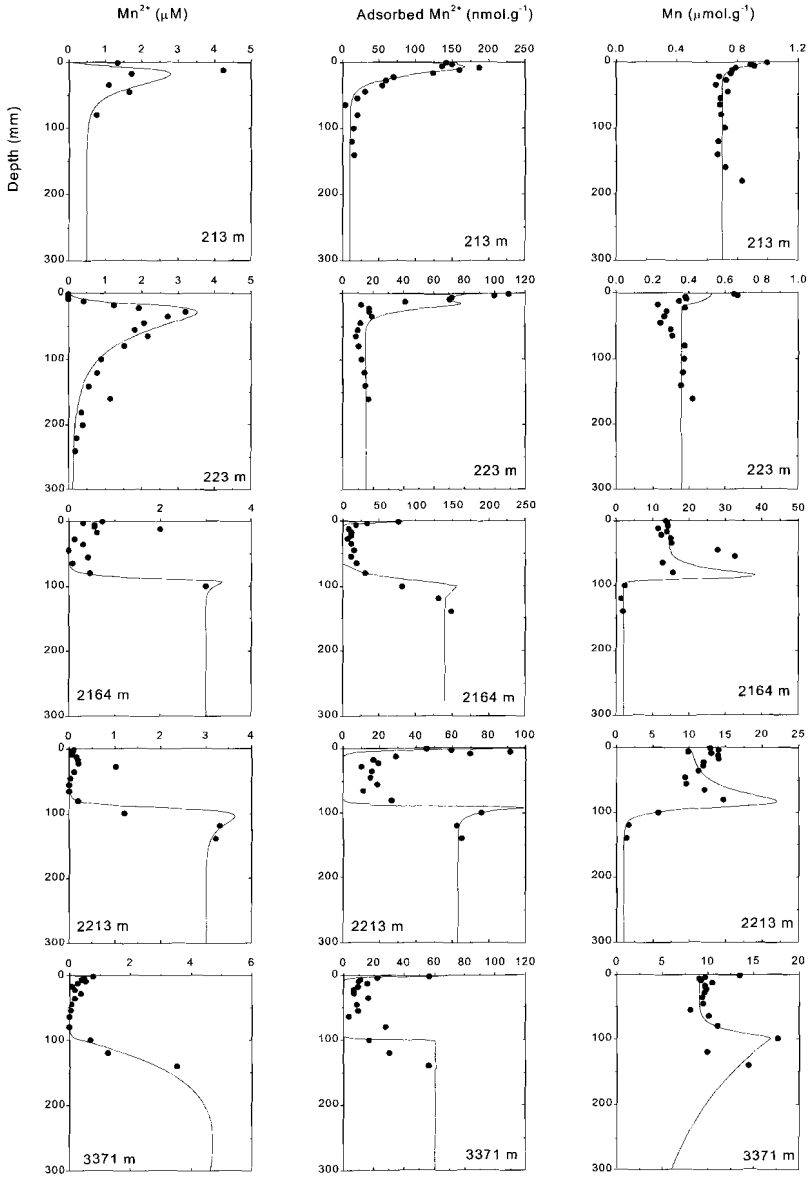

Figure 9b. Model fits (lines) to profiles of pore water Mn^{2+}, adsorbed Mn^{2+} and solid Mn (filled circles) of the stations on the Vigo transect.

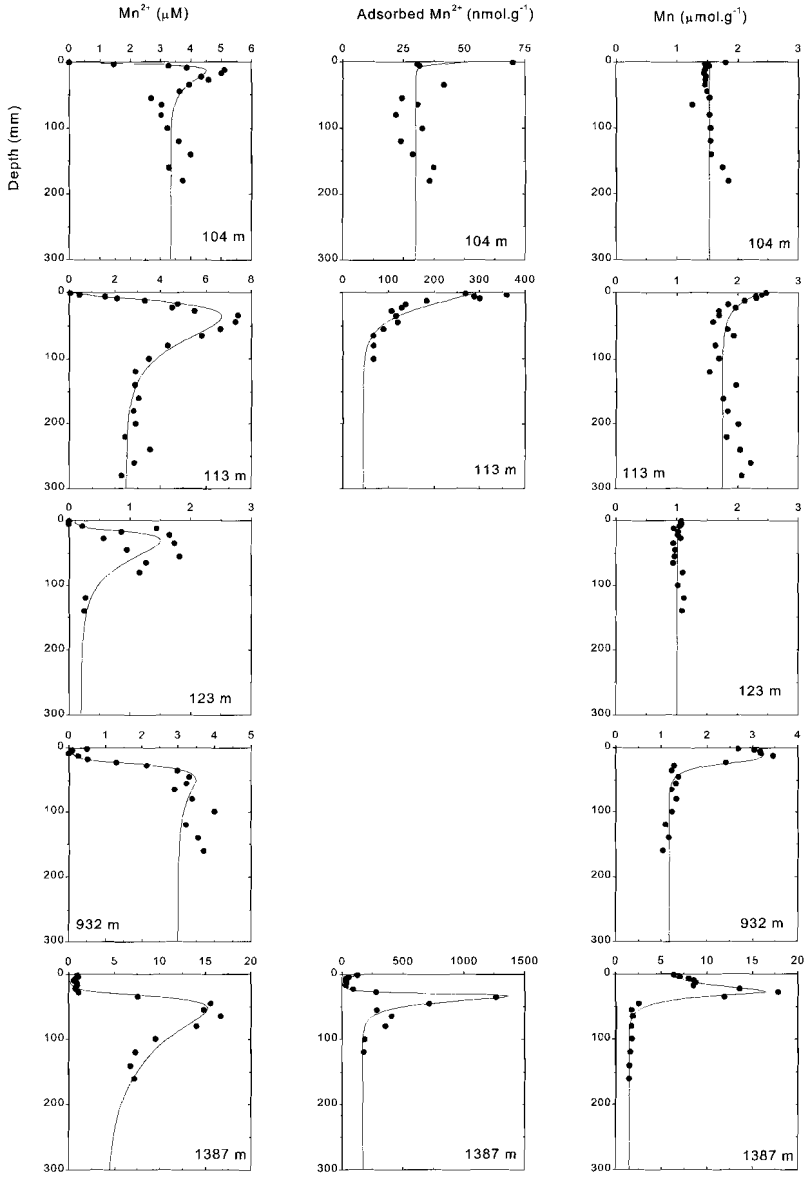

Figure 9c. Model fits (lines) to profiles of pore water Mn^{2+}, adsorbed Mn^{2+} and solid Mn (filled circles) of the stations on the Main transect.

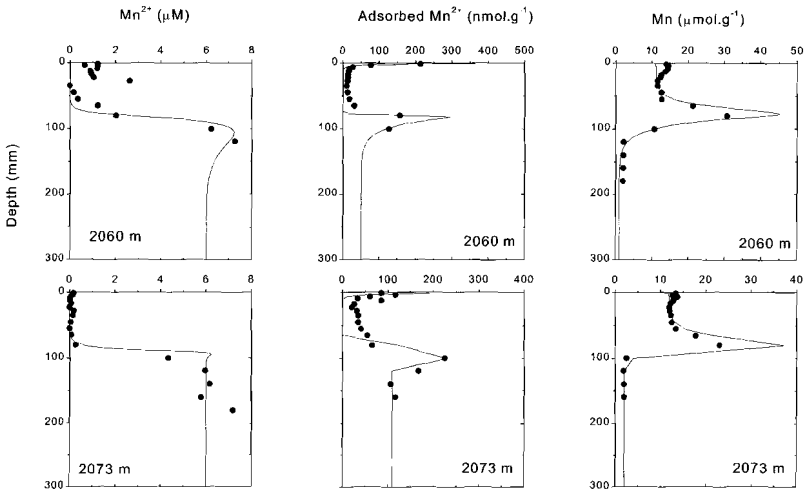

Figure 9c. (continued)

DISCUSSION

Iberian Margin versus other Margins

Manganese is most important as intermediate oxidant in areas with (1) well-oxygenated overlying water, which minimises the loss of Mn^{2+} from the sediment, (2) high bioturbation, which enhances the Mn redox cycle by mixing oxidised and reduced sediment layers, and (3) moderate organic carbon fluxes (Aller, 1994). When relatively large amounts of hydrothermal manganese are supplied to the sea floor in addition to moderate carbon fluxes, Mn cycles driven by bioturbation can account for up to 100% of the organic matter mineralisation as described for the Panama Basin (Aller, 1990).

At the eastern Canadian continental margin bottom waters are well oxygenated and model calculations showed that at a water depth of 230 m 2% of the carbon oxidation could be contributed to Mn reduction, at 525 m16%, whereas at 780 m no Mn^{2+} was detected in the upper 10 cm (Boudreau *et al.*, 1998). In general, however, Mn reduction is a minor mineralisation pathway at continental margins (Archer and Devol, 1992; Reimers *et al.*, 1992; Thamdrup and Canfield, 1996; Lohse *et al.*, 1998). Assuming a stoichiometry of organic C oxidation: Mn reduction of 1:2, the maximum contribution of Mn reduction to the organic matter oxidation is < 2% at the Iberian margin. The reduction rates found in this study are comparable with those of an earlier study in the framework of the OMEX-I programme at the Goban Spur on the N.W. European continental margin (Lohse *et al.*, 1998).

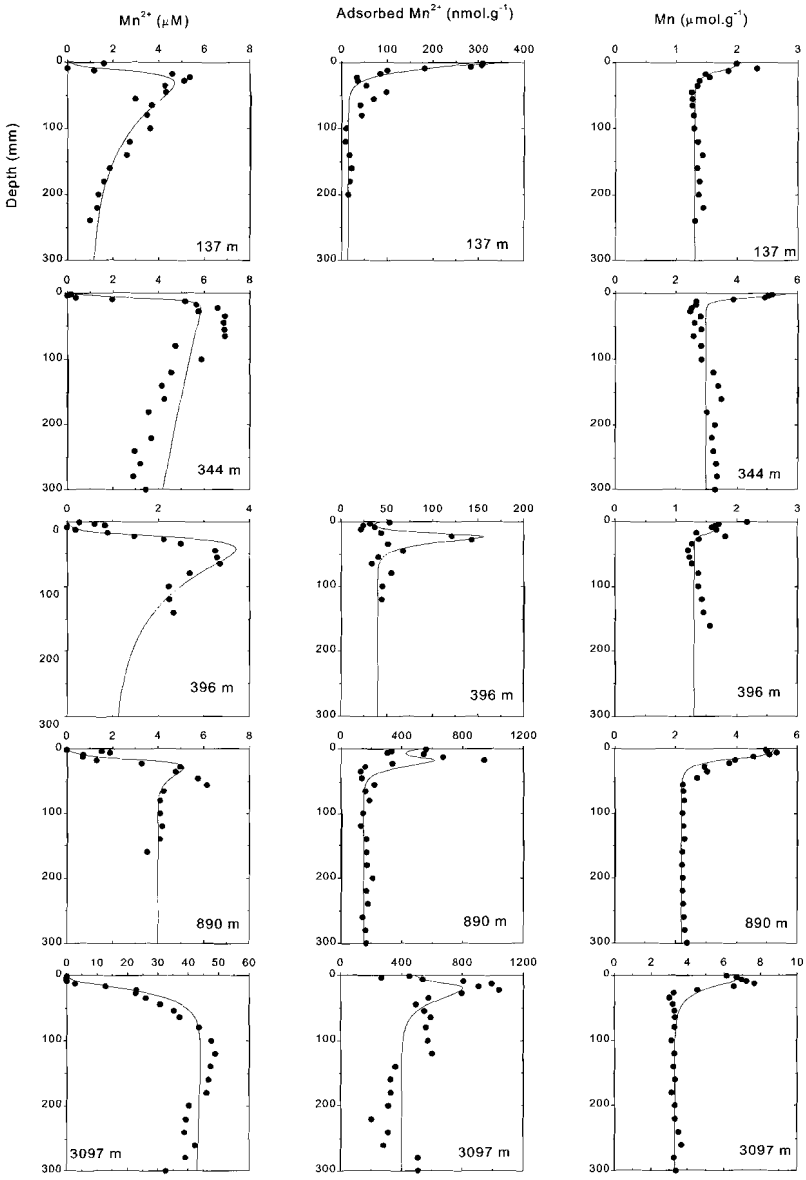

Figure 9d. Model fits (lines) to profiles of pore water Mn^{2+}, adsorbed Mn^{2+} and solid Mn (filled circles) of the stations on the Nazaré Canyon transect.

Table 6. Calculated integrated rates of reduction, desorption, oxidation and precipitation of Mn and the Mn^{2+} flux out of the sediment from values obtained by fitting the model to the data.

Water Depth (m)	Red. Rate ($\mu mol.m^{-2}.d^{-1}$)	Des. Rate ($\mu mol.m^{-2}.d^{-1}$)	Ox. Rate ($\mu mol.m^{-2}.d^{-1}$)	Precip. Rate ($\mu mol.m^{-2}.d^{-1}$)	Mn^{2+} Flux out ($\mu mol.m^{-2}.d^{-1}$)
I La Coruña Transect					
175	1.60	2.11	0.72	0.28	1.56
2109	11.5	-	10.6	0.76	0.37
4908	#	#	#	#	#
4941	#	#	#	#	#
II Vigo Transect					
213	8.72	7.70	3.03	4.25	1.68
223	5.43	4.80	4.84	1.19	0.26
2164	10.8	10.6	9.49	1.41	0
2213	7.24	7.12	6.65	1.13	0
3371	2.05	2.00	1.26	0.93	0
III Main Transect					
104	3.88	19.0	3.17	2.73	13.3
113	11.5	14.0	6.52	5.68	3.57
123	2.46	-	1.81	0.75	0.10
932	4.73	-	4.70	0.27	0.24
1387	25.3	23.3	21.8	3.74	0.09
2060	11.4	11.2	10.1	1.69	0
2073	21.5	20.7	20.4	1.44	0
2853	#	#	#	#	#
IV Nazaré Canyon Transect					
137	5.99	8.07	6.98	1.94	1.70
396	7.91	4.62	7.71	0.64	0.14
344	17.5	-	8.69	0.15	9.64
890	16.9	15.3	12.6	5.47	0.92
3097	34.9	29.4	29.5	0.50	4.27

#Profiles were not modelled because the major redox transitions apparently were positioned deeper than our sampling interval. The rates are assumed to be close to zero.

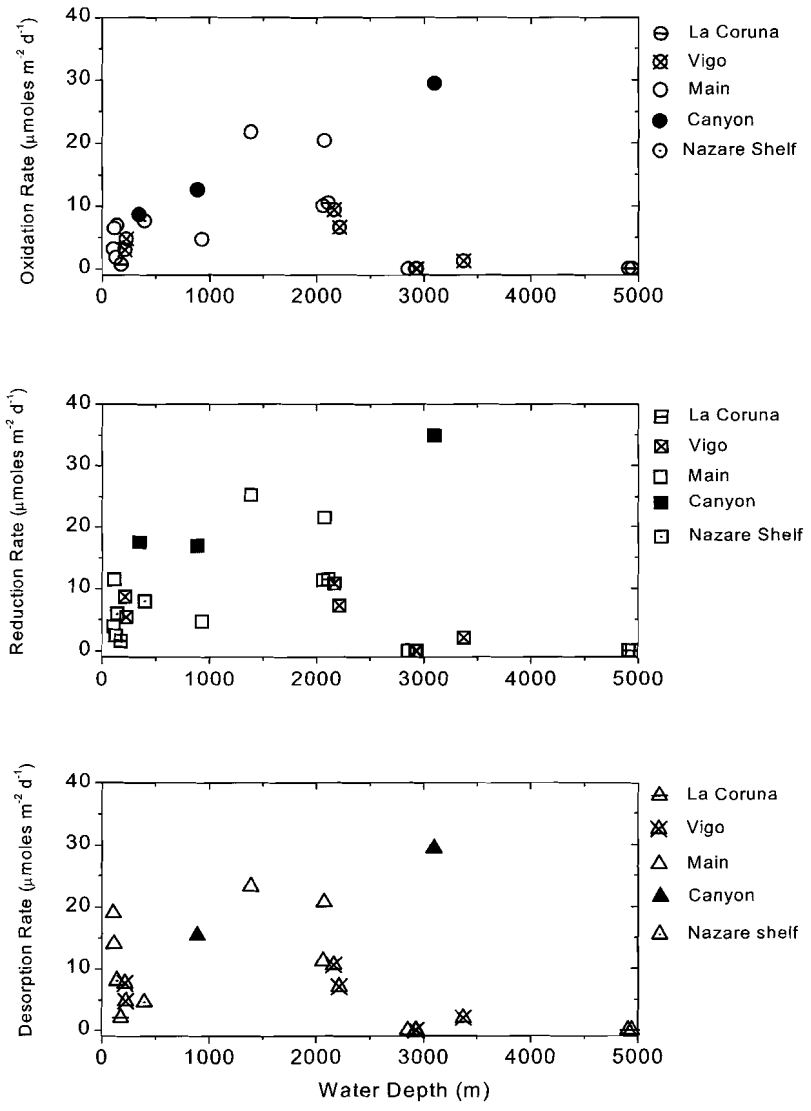

Figure 10. Mn^{2+} oxidation rate, Mn reduction rate and Mn^{2+} desorption rate as a function of water depth.

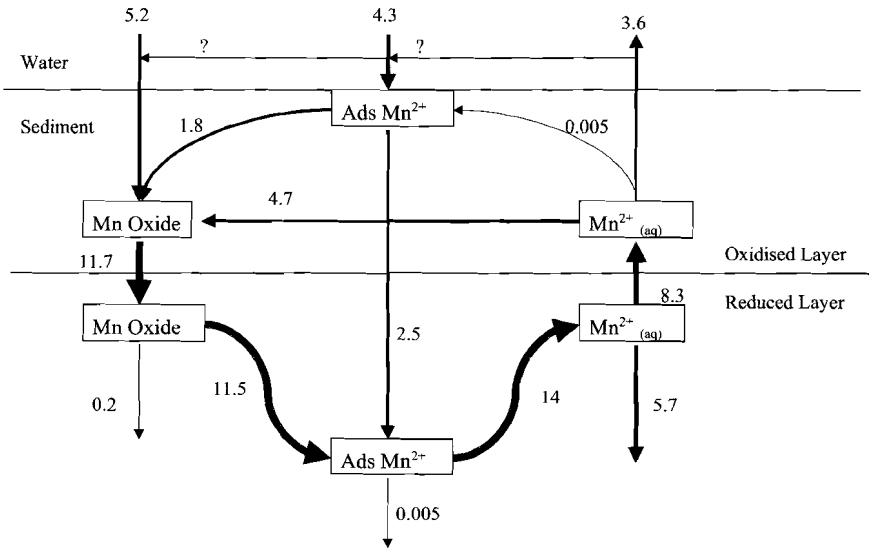

Figure 11. Fluxes of Mn in μmoles m^{-2} d^{-1} as calculated with the model for the 113-m station (main transect).

Canyon versus other Transects

Some stations were sampled both in August 1998 and May 1999, but seasonal fluctuations in the Mn redox chemistry, if present, were not observed. No trend was observed going from north to south on the Iberian margin. However, a large difference in Mn reactivity was found between the stations on the margin and those in the canyon. The highest integrated Mn reaction rates were estimated for the station at 3097 m in the canyon. Reaction rates are higher at the canyon stations compared to those at similar water depth on the margin, indicating a more rapid Mn redox cycling in the canyon. Mass accumulation rates in the canyon are higher than on the shelf with a maximum at the 3097-m station (Van Weering *et al.*, 2001). Along with this higher sedimentation rate is the estimated flux of Mn oxides ($Js_{x=0}$, Table 5) increases with increasing water depth at the canyon transect from 344 to 3097 m, whereas a trend with water depth is less clear at the other transects. Estimated Mn oxide deposition fluxes at the 890 and 3097-m stations in the canyon exceed the Mn oxide fluxes at all other stations. Thus, Mn cycling in the canyon is enhanced at higher input fluxes of Mn oxides.

Rate limiting factors

Budgets were constructed from the model results for the 113-m station (Fig. 11) and the 1387-m station on the main transect (Fig. 12), and for the 3097-m station in the canyon (Fig. 13). The major pathway for redox cycling starts when Mn oxide is mixed and/or advected into the reduced layer. There, adsorbed Mn^{2+} is produced by Mn reduction and subsequently is desorbed and released into the pore water.

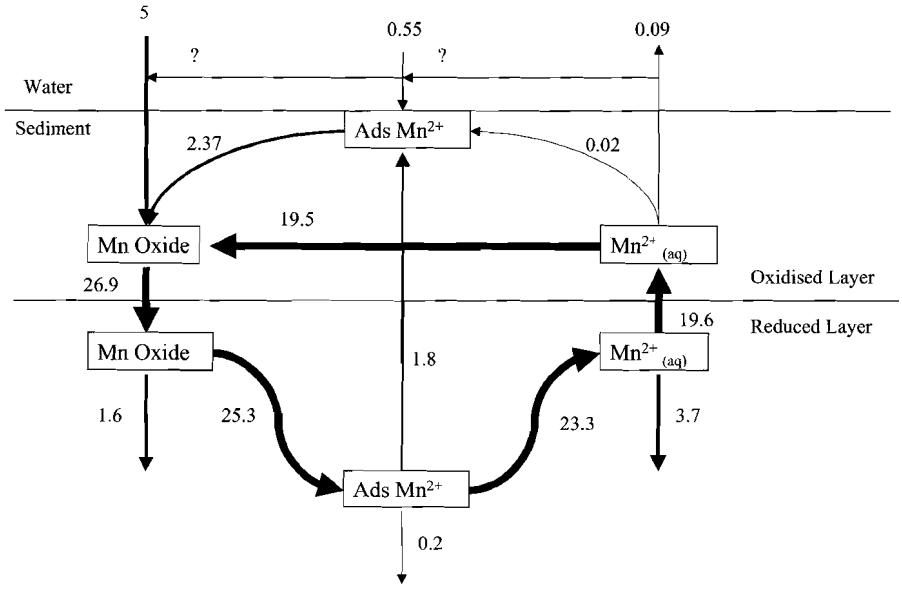

Figure 12. Fluxes of Mn in μmoles m^{-2} d^{-1} as calculated with the model for the 1387-m station (main transect).

The Mn^{2+} diffuses upward into the oxidised layer and is oxidised. When the oxidised layer is relatively thin some Mn^{2+} can escape from the sediment as is shown for the 113-m station (Fig. 11) and the canyon station (Fig. 13). Mn^{2+} in the water column may adsorb or oxidise onto sinking particles, indicated by the arrow with question mark in the budgets (Fig. 11-13) and subsequently re-enter the sediment. The species with the longest turnover time i.e. the rate limiting pools in Mn cycling, are listed in Table 7. In general, at shallow stations (<225 m) and at the 3097-m station in the canyon, the slowest turnover occurs in the oxidation step of adsorbed Mn^{2+}. At the other stations the transport of Mn oxide from the oxidised to the reduced layer is the rate-limiting step for Mn cycling. Thus, the rate limiting factors for Mn redox cycling at the Iberian margin are slow oxidation kinetics and slow mixing.

What controls the Mn redox chemistry?

Klinkhammer (1980) and Burdige and Gieskes (1983) subdivided the sediment column into 4 distinct zones based on the Mn redox chemistry. In our model, the sediment column was divided in an oxidised and a reduced layer with depth L as the Mn redox boundary. However, these layers can be subdivided into two zones each i.e. the oxidised layer consisting of an fully oxidised zone and an oxidising zone, and the reduced layer consisting of a reducing zone and an equilibrium zone. We extended the sediment zonation of Klinkhammer (1980) and Burdige and Gieskes (1983) by including adsorbed Mn^{2+} as indicated in Figure 14. Depending on the depth of the Mn redox boundary in the sediment and the core length, one to four of these zones could

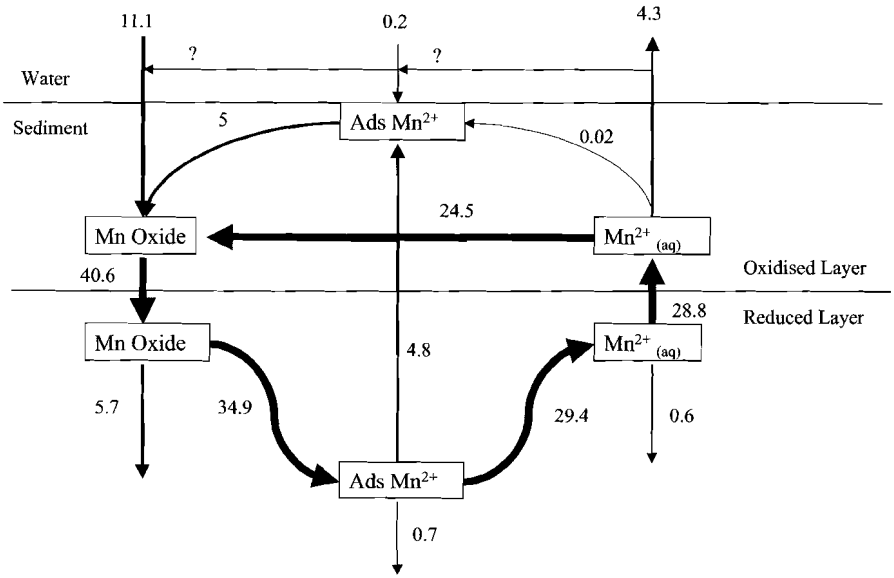

Figure 13. Fluxes of Mn in μmoles m^{-2} d^{-1} as calculated with the model for the 3097-m station (Nazaré transect).

be identified within the sampled interval. Based upon their Mn zonation and the concentrations of the three Mn species, all non-canyon stations can be divided into three groups, each category corresponding to a limited water depth range. The first group of shallow stations (100-400 m) is characterised by low concentrations of both solid phase Mn and pore water Mn^{2+}. The solid phase Mn profile has its maximum at the sediment-water interface, whereas the adsorbed Mn has its maximum either at the sediment-water interface or just below. Thus, at the shallow stations only a reducing and an equilibrium zone can be identified, the oxidising zone being too strongly compressed to be sampled adequately. In the second group of stations at intermediate water depth (900-2300 m) all four zones i.e. an oxidised, an oxidising, a reducing and an equilibrium zone can be distinguished. Their solid phase Mn concentrations are one order of magnitude higher than at the shallow stations. Pore water concentrations are similar to or higher than those of the shallow stations, whereas the adsorbed Mn^{2+} concentrations are similar, except at the station at 1387 m (main transect) which has much higher values. In the third group of stations at greater depth (>2300 m), one to two zones were observed i.e. an oxidised and oxidising zone. Pore water Mn^{2+} concentrations are negligible and adsorbed Mn^{2+} is slightly enriched at the sediment surface only. The solid phase Mn concentrations are constant with depth, characteristic of a well oxidised zone, or increase slightly with depth indicating the onset of an oxidising zone deeper down.

In general, sediment mixing is higher at stations with a high carbon flux (Boudreau, 1998), which would increase Mn reaction rates. The stations with high

carbon fluxes (Fig. 8) are the shallow stations and their rate-limiting factor in the Mn cycle is the oxidation of Mn^{2+} (see previous section). The oxygen penetration depths (L, table 3) are shallow and the oxidation kinetics are too slow to prevent a Mn^{2+} efflux across the thin oxic layer (Table 6), resulting in a lowered availability of Mn oxide relative to organic carbon. Mn fluxes at shallow stations at the Iberian margin are limited by Mn oxide regeneration. At stations with low mineralisation rates the oxygen penetration depth is in the order of several cm and deeper. At the depth level where oxygen is depleted in the sediment, the organic matter reaching the Mn reduction zone is aged and probably refractory. Therefore Mn reaction rates at stations at water depths >2300 m at the Iberian margin are limited by the availability of reductants, be they organic or inorganic. Thus, Mn fluxes are highest at stations with moderate organic carbon fluxes, where carbon flux and its degradability control the Mn redox chemistry.

Table 7. Slowest cycling fraction estimated using the model results and the rate limiting process.

Water depth (m)	*Slowest fraction	**In Layer	Rate limiting Process
La Coruña Transect			
175	Ads	red	Desorption
2109	Ox	-	Mixing
4908	-	-	
4941	-	-	
Vigo Transect			
213	Ads	ox	Oxidation
223	Ads	ox	Oxidation
2164	Ox	ox	Mixing
2213	Ox	ox	Mixing
3371	Ox	red	
Main Transect			
104	Ads	ox	Oxidation
113	Ads	ox	Oxidation
123	Ox	-	Mixing
932	Ox	-	Mixing
1387	Ox	ox	Mixing
2060	Ox	ox	Mixing
2073	Ox	ox	Mixing
2853	-	-	
Nazaré Canyon Transect			
137	Ads	ox	Oxidation
396	Ox	ox	Mixing
344	Ox	-	Mixing
890	Ox	ox	Mixing
3097	Ads	ox	Oxidation

*Ads is the adsorbed Mn phase and Ox is the solid phase Mn. The slowest fraction is the fraction with the largest turnover time calculated from the standing stock ($\mu mol\ m^{-2}$) divided by the production rate ($\mu mol\ m^{-2}\ d^{-1}$). ** Ox is the oxidised layer and red is the reduced layer.

The Role of Mn^{2+} Sorption in Mn redox cycling

Adsorbed Mn^{2+} can be an important reaction intermediate in the redox transformations of Mn especially in the reduced layer. Our results show that adsorbed Mn^{2+} has its maximum in-between those of solid phase Mn and pore water Mn^{2+}. Hence, we propose that upon Mn reduction the produced Mn^{2+} is adsorbed at nearby Mn oxide surfaces. Available adsorption-sites on the Mn-oxide are diminished and/or saturated upon continued Mn reduction and Mn^{2+} is released into the pore water deeper in the sediment. When Mn^{2+} diffuses upwards it is either oxidised directly or adsorbed onto Mn oxide surfaces in the oxic layer. Junta & Hochella (1994) showed that oxidation of $Mn^{2+}_{(aq)}$ starts through adsorption along edges (nm scale) on the mineral surfaces, suggesting that the geometric character of the mineral surface is more important than the immediate coordination environment. However, structural data on the Mn oxide birnessite identified a specific sorption site that consisted of three oxygen atoms carrying a double charge (-2) located around a vacancy in the octahedral layer (Drits *et al.*, 1997). Appelo and Postma (1999) formulated a surface complexation model for birnessite based on this doubly charged sorption site, which described experimental data better than monodentate or bidentate complexation models. Friedl *et al.* (1997) identified H^+-birnessite as authigenic Mn oxide in a eutrophic lake and their EXAFS spectra showed large amounts of adsorbed cations at the vacancies of its octahedral layers. Thus, Mn oxides in marine sediments may be important carriers of Mn^{2+} as well, either through sorption at specific vacancies in the crystal lattice or along edges and irregularities on the mineral surface.

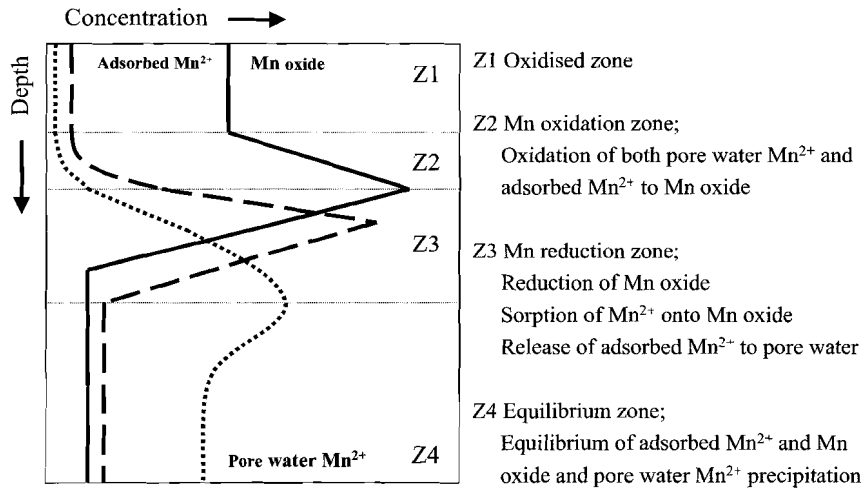

Figure 14. Manganese zonation scheme for pore water Mn^{2+}, adsorbed Mn^{2+} and Mn oxide profiles. Dominant processes in each layer are described.

The enrichment of adsorbed Mn^{2+} at the sediment-water interface suggests that the input of adsorbed Mn^{2+} is associated with recently arrived organic matter. However, adsorbed Mn^{2+} formed in the sediment is likely to be associated with Mn oxides. Small amounts of adsorbed Mn^{2+} associated with Mn oxides persist under oxygenated conditions. This can be explained by the assumption that 2 types of surface species exist, i.e. mono- and bidentate complexes. Davis and Morgan (1989) argue that the Mn^{2+}-bidentate complex is more readily oxidised than the monodentate complex.

Allocation of Mn^{2+} from the pore waters to the solid phase, would in principle result in a reduced pore water gradient of Mn^{2+} at the sediment-water interface and consequently in a lowered efflux of Mn^{2+}. However, this sorptive immobilisation of dissolved Mn^{2+} moving upwards is possible only when adsorption is sufficiently rapid. In our model, the direct oxidation rate constant k_{oxc} is 1000 times k_{ads} implying that oxidation has a far larger impact on the Mn^{2+} gradient in the oxidised layer than adsorption. Kinetic Mn^{2+} sorption lowers, however, the pore water gradient in the Mn reduction zone (Z3 in Fig. 14). At shallow stations, the fully oxidised zone is absent (Z1) and the Mn oxidation zone (Z2) is so strongly compressed that the pore water gradient in the Mn reduction zone (Z3) is decisive for the Mn^{2+} efflux. Thus, kinetic sorption retains the Mn^{2+} efflux at stations with a thin oxidation zone.

CONCLUSIONS

Adsorbed Mn^{2+} is an important reaction intermediate in the redox transformations of Mn especially in the reduced layer between Mn oxide and pore water Mn^{2+}. The implication of an intermediate adsorbed Mn^{2+} phase is a stronger retention of Mn redox cycling in the sediment column at stations with a thin oxidation zone, since adsorbed Mn^{2+} restrains the Mn^{2+} efflux from the pore water to the water column. Adsorbed Mn^{2+} seems to be associated with organic matter upon arrival at the sea floor, whereas the adsorbed Mn^{2+} formed in the sediment is likely to be adsorbed onto Mn oxides. The major pathway for Mn redox cycling starts when Mn oxide is mixed and/or buried below the Mn redox boundary. There, adsorbed Mn^{2+} is formed during Mn oxide reduction. As available sorption sites are diminished and/or saturated, adsorbed Mn^{2+} is desorbed upon continued Mn reduction and released into the pore water. Pore water Mn^{2+} diffuses upward and is oxidised by molecular oxygen to form Mn oxide or is co-precipitated with carbonates.

The non-canyon stations could be divided into three groups based upon their pore water Mn^{2+}, adsorbed Mn^{2+} and solid phase Mn characteristics and this division coincided with water depth i.e. shallow stations (100-400 m), stations at intermediate water depth (900-2300 m) and stations at greater water depth (>2300 m). As the flux of carbon and its degradability decreases with increasing water depth (Epping *et al.*, subm.), this suggests that the carbon flux is the main factor controlling Mn redox cycling. By application of a simple reaction-diffusion model, we have shown that the profiles of solid, adsorbed and pore water Mn are consistent. Mn reaction rates are highest at moderate carbon fluxes and are enhanced by a higher deposition flux of Mn oxide in the canyon. The two important rate-limiting factors for the Mn cycling deduced from turnover times of Mn species are (1) slow oxidation kinetics at the

shallow stations (< 225 m) and the 3097-m canyon station and (2) slow mixing of Mn oxides at the other stations.

Acknowledgements The authors would like to thank the captain and crew of R.V. Pelagia for providing safe cruises and a pleasant working environment. Shipboard nutrient analyses were performed by Karel Bakker, Jan van Ooijen and Evaline van Weerlee (NIOZ, department of Marine Chemistry and Geology). Grain size data were kindly provided by Wim Boer, Henko de Stigter and Tjeerd van Weering. The investigations were carried out in the framework of the Sedimentary Manganese and Iron cycLEs project (SMILE). C.v.d.Z. was supported through a grant to W.v.R. by the Research Council for Earth and Life Science (ALW) with financial aid from the Netherlands Organisation for Scientific Research (NWO) (no. 750.297.01). We thank Willem Helder for critically reading the manuscript. E. E. was supported through a grant to W.H. by the European Community EC-MAST OMEX-II project (MAS3-CT96-0056). This is publication no. 3487 of the Netherlands Institute for Sea Research.

REFERENCES

Aller, R.C. 1990. Bioturbation and manganese cycling in hemipelagic sediments. Phil. Trans. Royal Soc. Londen, A331, 51-68.

Aller, R.C. 1994. The sedimentary Mn cycle in Long Island Sound: Its role as intermediate oxidant and the influence of bioturbation, O_2, and C_{org} flux on diagenetic reaction balances. J. Mar. Res., 52, 259-295.

Appelo, C. A. J. and D. Postma. 1999. A consistent model for surface complexation on birnessite (-MnO2) and its application to a column experiment. Geochim. Cosmochim. Acta, 63, 3039-3048.

Archer, D. and A. Devol. 1992. Benthic oxygen fluxes on the Washington shelf and slope: A comparison of in situ microelectrode and chamber flux measurements. Limnol. Oceanogr., 37, 614-629.

Bender, M. L. and D. T. Heggie. 1984. Fate of organic carbon reaching the deep-sea floor: a status report. Geochim. et Cosmochim. Acta, 48, 977-986.

Berner, R.A. 1976. Inclusion of adsorption in the modelling of early diagenesis. Earth Plan. Sci. Lett. 29, 333-340.

Boudreau, B. P. 1997. Diagenetic models and their implementation, Springer Verlag, Heidelberg, 414 pp.

Boudreau, B. P. 1998. The mean mixed depth of sediments: the wherefor and why? Limnol. Oceanogr., 43, 524-526.

Boudreau, B. P., A. Mucci, B. Sundby, G. W. Luther and N. Silverberg. 1998. Comparative diagenesis at three sites on the Canadian continental margin. J. Mar. Res., 56, 1259-1284.

Brewer, P. G. and D. W. Spencer. 1971. Colorimetric determination of manganese in anoxic waters. Limnol. Oceanogr., 16, 107-110.

Bromfield, S. M., and D. J. David. 1976. Sorption and oxidation of manganous ions and the reduction of manganese oxide by cell suspensions of a manganese oxidizing bacterium. Soil Biol. Biochem., 8, 37-43.

Bruland, K.W. 1983. Trace elements in sea-water, *in* Chemical oceanography, J.P. Riley and R. Chester, eds., Academic Press, London, 157-220.

Burdige, D. J. and J. M. Gieskes. 1983. A pore water/ solid phase diagenetic model for manganese in marine sediments. Am. J. Sci., 283, 29-47.

Burdige, D. J. and P. E. Kepkay. 1983. Determination of bacterial oxidation rates in sediments using an *in-situ* dialysis technique, I. Laboratory studies. Geochim. Cosmochim. Acta, 47, 1907-1916.

Burdige, D. J., S. P. Dhakar and K. H. Nealson. 1992. Effects of manganese oxide mineralogy on microbial and chemical manganese reduction. Geomicrobiol. J., 10, 27-48.

Canfield, D. E., B. Thamdrup, and J. W. Hansen. 1993. The anaerobic degradation of organic matter in Danish coastal sediments: Iron reduction, manganese reduction, and sulphate reduction. Geochim. Cosmochim. Acta, 57, 3867-3883.

Davies, S. H. R. and J. J. Morgan. 1989. Manganese(II) oxidation kinetics on metal oxide surfaces. J. Colloid Interface Sci., 129, 63-77.

Dhakar, S. P. and D. J. Burdige. 1996. A coupled non-linear, steady state model for early diagenetic processes in pelagic sediments. Am. J. Sci., 296, 296-330.

Drits, V. A., E. Silvester, A. I. Gorshkov and A. Manceau. 1997. Structure of synthetic monoclinic Na-rich birnessite and hexagonal birnessite: I. Results from X-ray diffraction and selected area electron diffraction. Am. Mineral., 82, 946-961.

Durrieu de Madron, X., P. Castaing, F. Nyffeler and T. Courp. 1999. Slope transport of suspended particulate matter on the Aquitanain margin of the Bay of Biscay. Deep-Sea Res. II, 46, 2003-2027.

Epping, E. H. G. and W. Helder. 1997. Oxygen budgets calculated from in situ oxygen microprofiles for Northern Adriatic sediments. Cont. Shelf Res., 17, 1737-1764.

Epping, E., C. Van der Zee, K. Soetaert, W. Helder. 2001. On the mineralisation and burial of organic carbon in sediments of the Iberian Margin and Nazaré Canyon (NE Atlantic). Progr. Oceanogr. Accepted.

Fendorf, S. E., D. L. Sparks, J. A. Franz and D. M Camaioni. 1993. Electron paramagnetic resonance stopped-flow kinetic study of manganese(II) sorption-desorption on birnessite. Soil Sci. Soc. Am. J., 57, 57-62.

Franklin, M. L. and J. W. Morse. 1983. The interaction of manganese(II) with the surface of calcite in dilute solutions and seawater. Mar. Chem., 12, 241-254.

Friedl, G., B. Werhli and A. Manceau. 1997. Solid phases in the cycling of manganese in eutrophic lakes: New insights from EXAFS spectroscopy. Geochim. Cosmochim. Acta, 61, 275-290.

Froelich, P. N., G. P. Klinkhammer, M. L. Bender, N. A Luedtke, G. R. Heath, D. Cullen, P. Dauphin, D. Hammond, B. Hartman and V. Maynard. 1979. Early oxidation of organic matter in pelagic sediments of the eastern equatorial Atlantic: suboxic diagenesis. Geochim. Cosmochim. Acta, 43, 1075-1090.

Jørgensen, B. B. 1982. Mineralisation of organic matter in the sea bed – the role of sulphate reduction. Nature, 296, 643-645.

Junta, J. L. and M. F. Hochella Jr. 1994. Manganese(II) oxidation at mineral surfaces: A microscopic and spectroscopic study. Geochim. Cosmochim. Acta, 58, 4985-4999.

Junta-Rosso, J. L., M. F. Hochella Jr. and J. D. Rimstidt. 1997. Linking microscopic and macroscopic data for heterogeneous reactions illustrated by the oxidation of manganese(II) at mineral surfaces. Geochim. Cosmochim. Acta, 61, 149-159.

Klinkhammer, G.P. 1980. Early diagenesis in sediments from the eastern equatorial Pacific, II. Pore water metal results. Earth Plan. Sci. Lett., 49, 81-101.

Lohse, L., W. Helder, E. H. G. Epping and W. Balzer. 1998. Recycling of organic matter along a shelf-slope transect across the N.W. European Continental Margin (Goban Spur). Progr. Oceanogr., 42, 77-110.

Lovley, D. R. and E. J. P. Phillips. 1988. Manganese inhibition of microbial iron reduction in anaerobic sediments. Geomicrobiol. J., 6, 145-155.

Monaco, A. X. Durrieu de Madron, O. Radakovitch, S. Heussner and J. Carbonne. 1999. Origin and variability of downward biogeochemical fluxes on the Rhone continental margin (NW Mediterranean). Deep-Sea Res. I, 46, 1483-1511.

Morgan, J. J. and W. Stumm. 1964. Colloid-chemical properties of manganese dioxide. J. Colloid Sci., 19, 347-359.

Morse, J. W. and G. W. Luther III. 1999. Chemical influences on trace metal-sulphide interactions in anoxic sediments. Geochim. Cosmochim. Acta,*63*, 3373-3378.

Murray, J. W. 1975 The interaction of metal ion at the manganese dioxide-solution interface. Geochim. Cosmochim. Acta, 39, 505-519.

Myers, C. R and K. H. Nealson. 1988a. Bacterial manganese reduction and growth with manganese oxide as the sole electron acceptor. Science, 240, 1319-1321.

Myers— and — 1988b. Microbial reduction of manganese oxides: Interaction with iron and sulfur. Geochim. Cosmochim. Acta, 52, 2727-2732.

Reimers, C. E., R. A. Jahnke and D. C. McCorkle. 1992. Carbon fluxes and burial rates over the continental slope and rise off central California with implications for the global carbon cycle. Global Biogeochem. Cycles, 6, 199-224.

Sanchez-Cabeza, J. A., P. Masqué, I. Ani-Ragolta, J. Merino, M. Frignani, F. Alvisi, A. Palanques and P. Puig. 1999. Sediment accumulation rates in the southern Barcelona continental margin (NW Mediterranean Sea) derived from 210Pb and 137Cs chronology. Progr. Oceanogr., 44, 313-332.

Schmidt, S., T. C. E. Van Weering and H. C. De Stigter. 2001a. Enhanced short-term deposition within the Nazaré Canyon, North-East Atlantic. Mar. Geol., 173, 55-67.

Schmidt. S., T. C. E. Van Weering, J-L. Reyss and P. Van Beek. 2001b. Very recent deposition and reworking at the sea-water interface over the Iberian Margin: seasonal and spatial trends. Progr. Oceanogr. (in press).

Slomp, C. P., J. F. P. Malschaert, L. Lohse and W. Van Raaphorst. 1997. Iron and manganese cycling in different sedimentary environments on the North Sea continental margin. Cont. Shelf Res., 17, 1083-1117.

Soetaert, K., P.M.J. Herman, and J.J. Middelburg. 1996. A model of early diagenetic processes from the shelf to abyssal depths. Geochim. Cosmochim. Acta,*60*, 1019-1040.

Soetaert, K., P. M. J. Herman, J. J. Middelburg, C. Heip, H. C. De Stigter, T. C. E. Van Weering, E. Epping and W. Helder. 1996. Modelling ^{210}Pb-derived mixing activity in ocean margin sediments: Diffusive versus nonlocal mixing. J. Mar. Res., 54, 1207-1227.

Stone, A. T. 1987. Microbial metabolites and the reductive dissolution of manganese oxides: Oxalate and pyruvate. Geochim. Cosmochim. Acta, 51, 919-925.

Strickland, J. D. and T. R. Parsons. 1972. A practical handbook of seawater analysis. Vol. 167, 2nd ed., Bulletin of the Fisheries Board of Canada.

Thamdrup, B. and D. E. Canfield. 1996. Pathways of carbon oxidation in continental margin sediments off central Chile. Limnol. Oceanogr., 41, 1629-1650.

Thamdrup, B., R. N. Glud and J. W. Hansen. 1994. Manganese oxidation and in situ manganese fluxes from a coastal sediment. Geochim. Cosmochim. Acta, 58, 2563-2570.

Ullman, W. J. and R. C. Aller. 1982. Diffusion coefficients in nearshore marine sediments. Limnol. Oceanogr., 27, 552-556.

Van Cappellen, P. and Y. Wang. 1995. Metal cycling in surface sediments: modelling the interplay of transport and reaction, *in* Metal Contaminated Aquatic Sediments, H. E. Allen, ed., Ann Arbor Press, 21-64.

Van Cappellen, P. and Y. Wang. 1996. Cycling of iron and manganese in surface sediments: a general theory for the coupled transport and reaction of carbon, oxygen, nitrogen, sulfur, iron and manganese. Am. J. Sci., 296, 197-243.

Van Weering, T. C. E. and H. C. De Stigter. 1999. Recent transport and accumulation on the western Iberian Margin. OMEX II-Phase II, Second Annual Science Report, 83-92.

Van Weering, T.C.E., H.C. De Stigter, W. Boer and H. De Haas. 2001. Recent sediment transport and accumulation at the western Iberian margin. Progr. Oceanogr., Accepted.

Wilson, D. E. 1980. Surface and complexation effects on the rate of Mn(II) oxidation in natural waters. Geochim. Cosmochim. Acta, 44, 1311-1317.

APPENDIX

Solutions to differential equations

$$C_I = B1Exp(e1x) + B2Exp(e2x) +$$

$$C_{II} = IExp(e10x) + \iota HExp(e8x) + \upsilon GExp(e6x) + C_a$$

$$A_I = J1Exp(e3x) + J2Exp(e4x) - \lambda B1Exp(e1x) - \mu B2Exp(e2x) + \frac{k_{ads}}{\vartheta.k_{oxa}}\left\{\frac{k_{ads}.C_{eq}}{k_{ads}+k_{oxc}} - C_{eq}\right\}$$

$$A_{II} = HExp(e8x) + \rho GExp(e6x) + A_{eq}$$

$$S_I = F1Exp(\omega.x/Db) - J1Exp(e3x) - J2Exp(e4x) + \gamma B1Exp(e1x) + \varepsilon B2Exp(e2x) + F2$$

$$S_{II} = GExp(e6x) + S_{eq}$$

$$e1 = \frac{\omega(1+K_{eq}) + \sqrt{(\omega(1+K_{eq}))^2 + 4[(1+K_{eq})Db + Ds](k_{oxc} + k_{ads})}}{2[(1+K_{eq})Db + Ds]}$$

$$e2 = \frac{\omega(1+K_{eq}) - \sqrt{(\omega(1+K_{eq}))^2 + 4[(1+K_{eq})Db + Ds](k_{oxc} + k_{ads})}}{2[(1+K_{eq})Db + Ds]}$$

$$e3 = \frac{\omega + \sqrt{\omega^2 + 4Dbk_{oxa}}}{2Db}$$

$$e4 = \frac{\omega - \sqrt{\omega^2 + 4Dbk_{oxa}}}{2Db}$$

$$e6 = \frac{\omega - \sqrt{\omega^2 + 4Dbk_{r}}}{2Db}$$

$$e8 = \frac{\omega - \sqrt{\omega^2 + 4Dbk_{des}}}{2Db}$$

$$e10 = \frac{\omega - \sqrt{\omega^2 + 4Dbk_{a}}}{2Db}$$

$$\iota = \frac{-\vartheta.k_{des}}{[(1+K_{eq})Db + Ds](e8)^2 - (1+K_{eq})\omega.e8 - k_a}$$

$$\upsilon = \frac{-\vartheta.k_{des}\rho}{[(1+K_{eq})Db + Ds](e6)^2 - (1+K_{eq})\omega.e6 - k_a}$$

$$\lambda = \frac{k_{ads}}{\vartheta(Db(e1)^2 - \omega.e1 - k_{oxa})}$$

$$\mu = \frac{k_{ads}}{\vartheta(Db(e2)^2 - \omega.e2 - k_{oxa})}$$

$$\rho = \frac{-k_r}{(k_r - k_{des})}$$

$$\gamma = \frac{k_{oxa}.\lambda - \frac{k_{oxc}}{\vartheta}}{Db(e1)^2 - \omega.e1}$$

$$\varepsilon = \frac{k_{oxa}.\mu - \frac{k_{oxc}}{\vartheta}}{Db(e2)^2 - \omega.e2}$$

The integration constants (B1, B2, J1, J2, F1, F2, I, H and G) were solved with the following boundary conditions:

When $x = 0$; $C_I = C_0$, $J_{Ax=0} = -\vartheta\phi(DbA_I' - \omega A_I)$, and $J_{Sx=0} = -\vartheta\phi(DbS_I' - \omega S_I)$,

When $x = L$; $C_I = C_{II}$, $A_I = A_{II}$, and $S_I = S_{II}$,

$$[(1+K_{eq})Db+Ds]C_I' - (1+K_{eq})\omega C_I = [(1+K_{eq})Db+Ds]C_{II}' - (1+K_{eq})\omega C_{II},$$

$$DbA_I' - \omega A_I = DbA_{II}' - \omega A_{II} \text{ and } DbS_I' - \omega S_I = DbS_{II}' - \omega S_{II},$$

When $x = \infty$; $C_{II} = C_a$, $A_{II} = A_{eq}$ and $S_{II} = S_{eq}$

Instantaneous reversible sorption: $[A] = \frac{K_{eq}}{\vartheta}[C]$

CHAPTER FIVE

Adsorbed Fe^{2+} and Fe Redox Cycling in Iberian Continental Margin Sediments (North East Atlantic)[4]

ABSTRACT

In this paper, data are presented on the vertical distribution of loosely adsorbed Fe^{2+}, pore water Fe^{2+} and solid phase Fe in sediments along four across-slope transects including the Nazaré canyon at the Iberian margin. Our objectives were (1) to investigate the role of Fe^{2+} sorption in the Fe redox cycle, (2) to quantify Fe redox cycling and (3) to determine its rate limiting factors. Pore water Fe^{2+} and loosely adsorbed Fe^{2+} concentrations increased simultaneously until a maximum was reached, upon which the pore water Fe^{2+} concentration rapidly declined and the adsorbed Fe^{2+} concentration either slowly diminished or remained unchanged. We propose that loosely adsorbed Fe^{2+} acts as a buffer for pore water Fe^{2+} and its transformation into authigenic ferrous minerals. Upon Fe reduction, Fe^{2+} is released into the pore water. Dissolved Fe^{2+} either directly precipitates or adsorbs onto the sediment matrix. Through sorption, authigenic ferrous mineral formation is delayed and Fe^{2+} is transported deeper into the sediment. There, loosely adsorbed Fe^{2+} can act as a deep source for authigenic ferrous mineral formation. A simple steady-state model was formulated that includes Fe^{2+} sorption as a first-order kinetic reaction to estimate Fe reaction rates. Fe oxidation and reduction rates were most intense at the shelf, where organic carbon mineralization rates are high, and decreased with water depth. In the canyon, where deposition fluxes were high, Fe reaction rates increased with water depth until a maximum at 3097 m and decreased again at 4280 m. Turnover times estimated for pore water Fe^{2+}, loosely adsorbed Fe^{2+} and solid phase Fe both in the oxidised and reduced layer indicated that sediment mixing was the most important rate limiting factor for Fe cycling at the Iberian margin. The contribution of Fe reduction to organic matter mineralization was 5% at the 104-m and 113-m station on the main transect and 6% at the 3097-m station in the canyon, at the other stations Fe reduction contributed less than 4% to the mineralization.

INTRODUCTION

Fe reduction may be coupled to the bacterial oxidation of organic matter (Lovley and Phillips, 1988) or to the oxidation of reduced solutes such as sulphides (Rickard,

[4] This chapter by Claar van der Zee, Wim van Raaphorst and Willem Helder has been submitted to Journal of Marine Research.

1995). Fe^{2+} released into the pore water upon solid phase Fe^{3+} reduction, may either adsorb onto the sediment matrix, precipitate as authigenic ferrous minerals or oxidise upon diffusive transport into the oxidised layer. Adsorbed Fe^{2+} may also be transported into the oxidised layer through sediment mixing and subsequently re-oxidise and precipitate as Fe oxyhydroxide.

In contrast to sorption of other metals, little is known about adsorbed Fe^{2+}. Fe oxyhydroxides are known to be important substrates for trace metal sorption in aquatic systems (Tessier *et al.*, 1996). As the commonly applied determination of adsorbed trace metals on Fe oxyhydroxides involves their reductive dissolution, it is not suitable for the determination of adsorbed Fe^{2+} (Tessier *et al.*, 1979; Tessier *et al.*, 1996). Zhang *et al.* (1995) applied the technique of diffusion gradients in thin films (DGT) to measure *in situ* fluxes of metals. Depending on the metal involved and application time, the DGT technique can be used to measure pore water concentrations (diffusive flux is dominant) or to calculate fluxes from solid phase to solution. In the case of Fe^{2+}, partial re-supply from the solid phase to the solution was observed in Lake Esthwaite Water (UK), suggesting that sorption processes controlled pore water concentrations (Zhang *et al.*, 1995).

In most diagenetic models, Fe^{2+} sorption is neglected (Aller, 1980; Dhakar and Burdige, 1996) or described as an instantaneous equilibrium process with pore water Fe^{2+} (Slomp *et al.*, 1997). In the multi-component reactive transport model STEADYSED, Fe^{2+} sorption is included as a surface-controlled equilibrium process and adsorbed Fe^{2+} profiles are simulated assuming Mn oxides, Fe oxyhydroxides, minerals and organic material as the substrate surfaces controlling Fe^{2+} sorption (Van Cappellen and Wang 1996; Wang and Van Cappellen, 1996). Simulations with this model showed the importance of adsorption-desorption of Fe^{2+} in the Fe redox cycling and the impact on pore water alkalinity and pH (Wang and Van Cappellen, 1996). Van Cappellen and Wang (1996) simulated a profile of adsorbed Fe^{2+} and emphasise the importance of heterogeneous oxidation, i.e. oxidation with surface-bound Fe^{2+} as reactant instead of pore water Fe^{2+}. Field data including profiles of adsorbed Fe^{2+} to confirm the modelling results are, however, lacking, so far.

We measured the vertical distribution of loosely adsorbed Fe^{2+}, dissolved Fe^{2+} and solid phase Fe in sediments from the Iberian continental margin. A simple steady state model was formulated in order to estimate the depth-integrated rates of Fe reduction and oxidation. Our first objective was to study the role of Fe^{2+} sorption in the redox cycling of Fe in natural marine sediments. Furthermore, we wanted to quantify Fe redox cycling and determine its rate limiting factors at the Iberian continental margin. First, we will discuss the role of loosely adsorbed Fe^{2+} in the Fe cycle, possible substrates for Fe^{2+} sorption and the rate-limiting factor for Fe cycling estimated from the model results. Then, we will compare the canyon results with the rest of the Iberian margin and the Iberian margin with the rest of the world. Finally, differences are discussed between the Mn cycle and the Fe cycle at the Iberian margin.

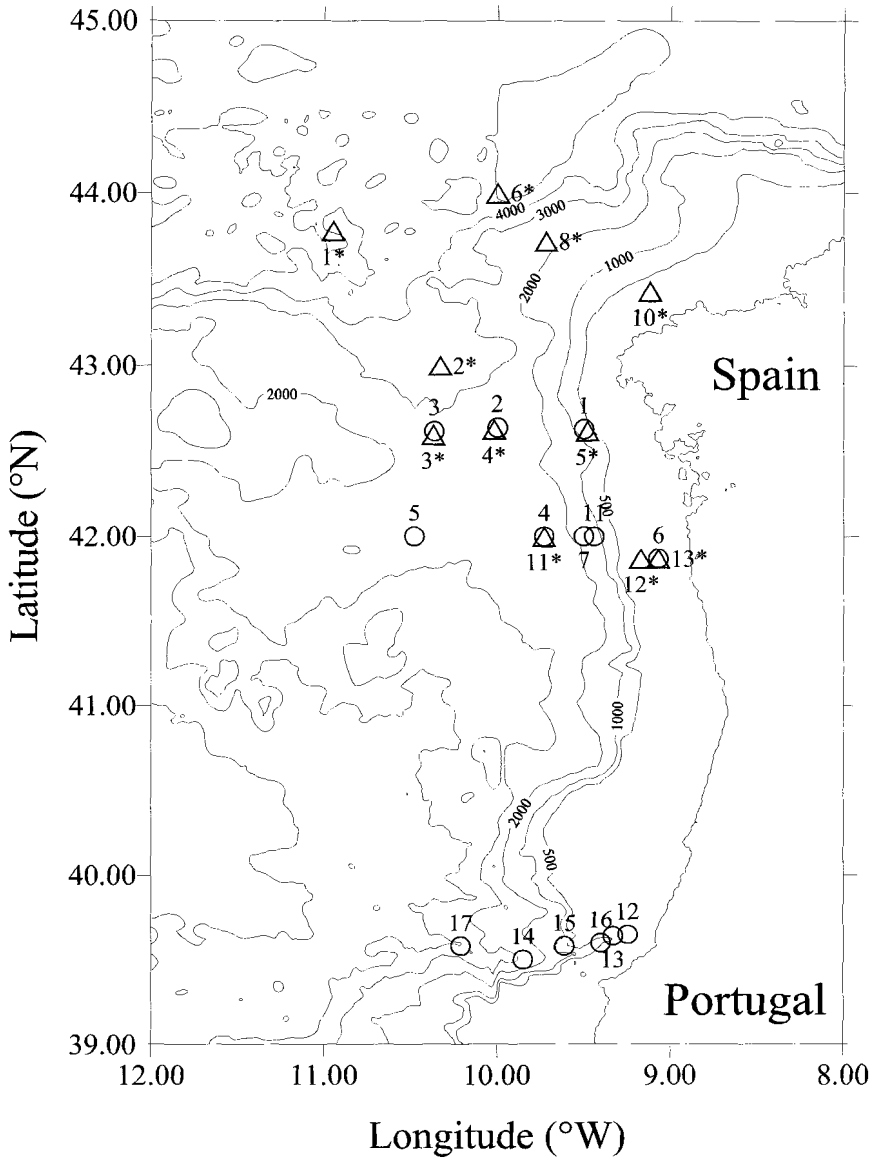

Figure 1. Map of the Iberian Margin indicating positions of sampled stations in 1998 (triangles, numbers with asterisk) and 1999 (circles, numbers without asterisk).

RESEARCH AREA

Our research area comprised the Iberian continental margin in the northeastern Atlantic (Fig.1). Stations were located at different depositional areas, on four transects across the margin including one in the Nazaré canyon, and were sampled during 2 cruises within the Ocean Margin Exchange Project (OMEX-II) in August 1998 and May 1999. Characteristics of the visited stations are listed in Table 1. Organic carbon contents range from 0.33 to 4.58 wt% C. The northern most La Coruña transect is characterised by a gradual decreasing water depth, whereas the slope is steeper at both the Vigo transect, north of Vigo, and the main transect situated south of Vigo. As canyons are important conduits for particle transport from the shelf directly to the deep-sea (Durieu de Madron *et al.*, 1999; Monaco *et al.*, 1999; Sanchez-Cabeza *et al.*, 1999), we selected an additional transect in the Nazaré canyon further to the south (Schmidt *et al.*, 2001), where four stations were sampled inside the canyon and an additional two on the adjacent shelf. Details on carbon cycling at the Iberian Margin are discussed in Epping *et al.* (2001). Benthic oxygen fluxes on the shelf range from 2 to 3.6 mmol O_2 m^{-2} d^{-1} exponentially decreasing to 0.6 mmol O_2 m^{-2} d^{-1} at 3000-m water depth at the non-canyon transects. In the canyon the benthic oxygen fluxes decrease from 4.9 at 344-m water depth to 2.3 at 3097 m and 0.9 mmol O_2 m^{-2} d^{-1} at 4280 m.

MATERIALS AND METHODS

Sediment handling

Sediment cores were taken with a multi-corer and processed directly at *in situ* temperature. Four sediment cores were sliced simultaneously for pore water collection with a hydraulic core-slicer developed at NIOZ (Van der Zee *et al.*, 2001) to obtain high spatial resolution at the sediment-water interface. The sediment was sectioned in 2.5-mm slices in the upper 10 mm of the sediment, in 5-mm slices from 10 to 30 mm, in 10-mm slices from 30 to 60 mm and in 20-mm slices further down. The sediment slices were pooled and centrifuged (3000 rpm, 10 min) for pore water extrusion. Pore water was filtered (0.45 μm) and analysed for nitrate and iron shipboard on a TRAACS-800 auto-analyser. Nitrate was analysed according to the method of Strickland and Parsons (1972). Aliquots for iron were acidified to pH 2 and analysed according to the method of Stookey (1970). After pore water collection the sliced sediment was stored frozen (-20 °C) until further analysis for solid phase iron at the NIOZ laboratory. Freeze-dried and ground sediment was extracted with 1N HCl (24 hrs, 20 °C) for reactive solid phase Fe (Canfield, 1988; Slomp *et al.*, 1997). Fe was measured in 1N HCl (solid phase Fe) and Ferrozine (adsorbed Fe^{2+}; see below) extracts by flame AAS. Porosity was determined from the weight loss of the sediment after drying at 60 °C assuming a sediment dry density of 2.65 g cm^{-3}. Sediment cores were not sectioned entirely anoxic and therefore small oxidation artefacts may have affected the pore water profiles of iron. The estimated Fe reduction rates are consequently minimum estimates.

Table 1. Name, water depth, geographical position, bottom water (BW) temperature and oxygen concentration and organic carbon content of the visited stations, number 121- stations are visited in August 1998 and number 138- stations are visited in May 1999.

Station	Water depth (m)	Latitude °N	Longitude °W	BW Temp (°C)	BW O_2 (μM)	Corg* (wt %)
I La Coruña Transect						
121-10	175	43.26	09.07	12.1	225	0.33
121-08	2109	43.43	09.43	3.2	250	1.04
121-06	4908	44.00	10.00	3.1	245	0.72
121-01	4941	43.47	10.57	3.1	245	0.45
II Vigo Transect						
138-01	213	42.38	09.28	12.1	213	0.47
121-05	223	42.38	09.29	12.0	223	0.62
138-02	2164	42.38	10.00	3.4	249	1.35
121-04	2213	42.38	10.01	3.2	250	1.16
138-03	2932	42.37	10.22	2.5	243	1.01
121-03	2926	42.36	10.22	3.1	243	0.87
121-02	3371	43.00	10.20	3.1	245	1.08
III Main Transect						
121-13	104	41.52	09.04	12	235	4.58
138-06	113	41.52	09.04	12.5	210	4.46
121-12	123	41.52	09.10	12.1	230	0.42
138-11	932	42.00	09.26	-	-	1.41
138-07	1387	42.00	09.28	10.3	188	1.99
138-04	2060	42.00	09.44	3.8	247	1.17
121-11	2073	42.00	09.44	3.4	255	1.41
138-05	2853	42.00	10.30	2.6	241	0.88
IV Nazaré Canyon Transect						
138-13	137	39.39	09.20	12.8	209	0.86
138-12	344	39.39	09.15	12.2	206	3.46
138-15	396	39.35	09.37	11.6	200	1.04
138-16	890	39.36	09.24	11.0	189	3.12
138-14	3097	39.31	09.51	2.4	243	3.67
138-17	4280	39.35	10.17	2.1	243	2.56

* Organic carbon content in 0-2.5 mm interval

Adsorbed Fe^{2+}

The Fe reduction assay that extracts Fe^{2+} produced during Fe reduction in marine sediments was applied to determine adsorbed Fe^{2+} (Sørensen, 1982; Stookey, 1970). Thawed wet sediment from the 1998 cruise was extracted with 1 g/L Ferrozine in 50mM HEPES (pH 7.0) for 5 min in the laboratory. On the 1999 cruise an additional core was sliced and fresh wet sediment was extracted with 1 g/L Ferrozine in 50mM HEPES (pH 7) for 5 min. The extract was filtered (0.45 μm), acidified and stored at 4 °C. Corrections were made for the pore water Fe^{2+} in the extract. Tugel *et al* (1986) extended this technique with the addition of 1N HCl for 15 s before adding the buffered ferrozine solution to release Fe^{2+} associated with acid-soluble material like FeS. Lovley and Phillips (1986) applied the procedure as developed by Sørensen (1982) with and without first extracting the samples with 0.5N HCl and concluded that the hydrochloric acid extraction method was superior to ferrozine extraction in

extracting solid Fe^{2+} forms, including FeS, produced during Fe reduction. We applied the technique without the HCl addition to extract adsorbed Fe^{2+} while minimizing the dissolution of other authigenic Fe^{2+} phases (e.g. iron monosulphide, iron carbonate, magnetite, green rusts and iron bound in clay minerals) produced upon Fe reduction.

Triplicate samples of iron monosulphide (FeS, Aldrich 34,316-1, 99.9%), magnetite (Fe_3O_4, Alfa Aeser 012374, 97%) and siderite (natural $FeCO_3$, collection of S.J. van der Gaast) were extracted with the buffered ferrozine solution (1gr/L ferrozine in 50mM HEPES pH 7.0). After 5 min. less than 1% Fe was leached from the iron monosulphide, magnetite and siderite. The extraction procedure was not tested on green rusts or reduced iron bound in clay minerals. It is highly unlikely, however, that buffered ferrozine (pH 7.0) could extract substantial amounts of structural Fe^{2+} from the clay mineral lattice within 5 min. Three kinds of mineral dissolution can be distinguished, i.e. proton-, ligand- and reductant-promoted dissolution (Sulzberger *et al.,* 1989). Both ferrozine and oxalate operate as ligands. Oxalate liberates less than 3% of the total iron from clay minerals, whereas solutions of 1N HCl and dithionite-acetate-citrate (pH 4.8) can leach up to 32% of the total Fe from chlorite, nontronite and biotite (Canfield, 1988; Kostka and Luther, 1994). Natural green rusts in marine sediments have not been positively identified yet (Hansen *et al.,* 1994). Green rust has been detected, however, as corrosion product of cast iron pipes (Stampfl, 1969), in an ochre sludge (Koch and Mørup, 1991) and in a reductomorphic soil (Trolard *et al.*, 1997). The buffered ferrozine solution may extract some iron from green rusts if present.

Batch adsorption experiments were conducted with sediment of the 344-m station at the Nazaré Canyon Transect in N_2-purged seawater buffered with 50mM HEPES pH 7.8. Canfield *et al.* (1993) reported difficulties to control the pH satisfactory in their Fe adsorption experiments, therefore the seawater was buffered with HEPES (*cf.* Burdige and Kepkay, 1983). Single additions of Fe^{2+} were made using a particle concentration in the experiments of ~15 g L^{-1}. Solutions were left to equilibrate for 30 minutes, which was found to be the optimum time in separate experiments. Dissolved Fe^{2+} was measured in the supernatant and adsorbed Fe^{2+} was determined with the Ferrozine extraction in the sediment. Control experiments both without sediment and without Fe^{2+} addition were performed. The observed isotherm (Fig. 2) could be described with the Freundlich equation with the amount of adsorbed $Fe^{2+} = K_F \times [Fe^{2+}]^{1/n}$. The Freundlich constant, K_F, is 0.60 dm^3 g^{-1} and the Freundlich exponent, n, is 2.72. The concentrations used in the adsorption experiment span the same range as found in the sediment. Mass balance calculations indicated that the buffered Ferrozine reagents recovered 35% of the added Fe^{2+}, using longer equilibration times than 30 min resulted in a lower recovery while control experiments without sediment did not loose their Fe^{2+}. This suggests that the Fe^{2+} reacted with substances in the sediment in this time. Alternatively, the Fe^{2+} may become more strongly bound to the sediment matrix. Therefore, we will refer to the buffered ferrozine-extractable Fe^{2+} as loosely adsorbed Fe^{2+}.

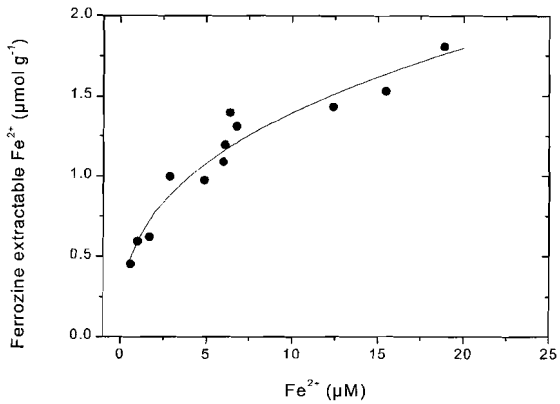

Figure 2. Isotherm data from the adsorption experiment (dots) fit with the Freundlich equation (line).

MODEL

Early diagenetic models have been developed that couple the diagenesis of Fe to the cycles of C, N, O, S and Mn (e.g. Dhakar and Burdige, 1996; Van Cappellen and Wang, 1996). Sorption as used here concerns the exchange of ions between the dissolved phase and the surface of the solid phase, whereas precipitation is the separation of a substance in solid form from a solution. When the rate of adsorption and desorption is fast relative to transport processes, then they can be viewed as equilibrium sorption (Berner, 1976). Conversely, when sorption is slow compared to transport, the kinetic approach is more appropriate. Equilibrium sorption of dissolved Fe^{2+} (Berner, 1976; Schink and Guinasso, 1978) with a linear sorption coefficient *Ks* (*Ks* is 1; Slomp *et al.*, 1997) and the amount of adsorbed Fe^{2+} = *Ks* x [Fe^{2+}] could account only for a few percent of the measured loosely adsorbed Fe^{2+} in the sediment. Moreover, equilibrium sorption could not reproduce the adsorbed Fe^{2+} depth distributions and there is no *a priori* reason to assume linear sorption of Fe^{2+}. Since kinetic sorption has been proven successful in describing adsorbed Mn^{2+} distributions (Van der Zee *et al.*, 2001), we developed a simple one-dimensional steady-state reaction-diffusion model that includes Fe^{2+} sorption as a first-order kinetic process. This allowed us to reduce the number of variables compared to coupled models, limit the uncertainties in data of other elements that could affect the modelling of Fe, and to better focus on sorption and the Fe redox cycle. A list of model parameters is given in Table 2. The molecular sediment diffusion coefficient (*Ds* in m^2 d^{-1}), mixing coefficient (*Db* in m^2 d^{-1}), all reaction rate constants (*k* in d^{-1}), sediment porosity (ϕ in m^3 m^{-3}) and the sedimentation rate (ω in m d^{-1}) are assumed to be depth-independent. Irrigation is not included, as no data are available on this process. The sediment was divided into an oxidised and a reduced layer. The depth of the redox boundary (L) is

given by the depth where the nitrate concentration is <5 μM (limiting nitrate concentration between 1-10 μM; Van Cappellen and Wang, 1995).

Table 2. Name, unit and function of model parameters

Name	Unit	Function
		Molecular sediment diffusion coefficient
Db	$m^2\ d^{-1}$	Bioturbation coefficient
ω	$m\ d^{-1}$	Sedimentation rate
x	m	Depth in sediment
L	m	Depth of Fe redox boundary
ϕ	-	Sediment porosity
ρ	$g\ cm^{-3}$	Average density of the sediment
ϑ	$g\ cm^{-3}$	Conversion factor between pore water and solid or loosely adsorbed phase
C_I	$mol\ m^{-3}$	Pore water Fe^{2+} concentration in the oxidised layer
C_{II}	$mol\ m^{-3}$	Pore water Fe^{2+} concentration in the reduced layer
A_I	$\mu mol\ g^{-1}$	Loosely adsorbed Fe^{2+} concentration in the oxidised layer
A_{II}	$\mu mol\ g^{-1}$	Loosely adsorbed Fe^{2+} concentration in the reduced layer
S_I	$\mu mol\ g^{-1}$	Solid phase Fe concentration in the oxidised layer
S_{II}	$\mu mol\ g^{-1}$	Solid phase Fe concentration in the reduced layer
C_a	$mol\ m^{-3}$	Pore water equilibrium concentration for precipitation
A_{eq}	$\mu mol\ g^{-1}$	Loosely adsorbed Fe^{2+} concentration at which no further reactions occur
S_{eq}	$\mu mol\ g^{-1}$	Solid phase Fe concentration at which no further reactions occur
k_{oxc}	d^{-1}	Dissolved Fe^{2+} oxidation rate constant
k_{oxa}	d^{-1}	Adsorbed Fe^{2+} oxidation rate constant
k_r	d^{-1}	Reduction rate constant
k_s	d^{-1}	Adsorption rate constant
k_a	d^{-1}	Dissolved Fe^{2+} precipitation rate constant
k_p	d^{-1}	Adsorbed Fe^{2+} precipitation rate constant
$J_{Ax=0}$	$\mu mol\ m^{-2}\ d^{-1}$	Flux of loosely adsorbed Fe^{2+} at the sediment-water interface
$J_{Sx=0}$	$\mu mol\ m^{-2}\ d^{-1}$	Flux of solid phase Fe at the sediment-water interface

In the oxidised layer, oxidation of both dissolved and loosely adsorbed Fe^{2+} takes place, described as first-order processes with k_{oxc} and k_{oxa} as the oxidation rate constants, respectively. Pore water Fe^{2+} concentrations (C_I and C_{II}) have units in mol m^{-3}, loosely adsorbed Fe^{2+} (A_I and A_{II}) and solid phase Fe (S_I and S_{II}) concentrations are in $\mu mol\ g^{-1}$. For the conversion between pore water and solid phase Fe or adsorbed Fe^{2+} the factor ϑ (gram of dry sediment per cm^3 of pore water) is used: $\vartheta = \rho\ [(1-\phi)/\phi]$, where ρ is the average dry density of the sediment (2.65 g cm^{-3}). Differential equations for dissolved Fe^{2+} (C_I), loosely adsorbed Fe^{2+} (A_I), and solid phase Fe (S_I) in the oxidised layer as a function of depth in the sediment (x) are:

$$[Db + Ds]\frac{\partial^2 C_I}{\partial x^2} - \omega\frac{\partial C_I}{\partial x} - k_{oxc}C_I = 0 \quad (1)$$

$$Db\frac{\partial^2 A_I}{\partial x^2} - \omega\frac{\partial A_I}{\partial x} - k_{oxa}A_I = 0 \quad (2)$$

$$Db\frac{\partial^2 S_I}{\partial x^2} - \omega\frac{\partial S_I}{\partial x} + k_{oxa}A_I + \frac{k_{oxc}}{\vartheta}C_I = 0 \quad (3)$$

In the reduced layer, Fe reduction, Fe^{2+} sorption and precipitation occur. Production of dissolved Fe^{2+} due to solid phase Fe reduction is described as a first-order process with k_r as the reduction rate constant. Removal of dissolved and loosely adsorbed Fe^{2+} due to authigenic mineral formation is described as a first-order process with k_a and k_p as the precipitation rate constants, respectively. The "precipitation" of adsorbed Fe^{2+} describes Fe^{2+} desorption and its subsequent precipitation in authigenic ferrous minerals. The pore water and loosely adsorbed Fe^{2+} equilibrium concentrations for precipitation are C_a and A_{eq}, respectively. Sorption of dissolved Fe^{2+} is described as a first-order process with k_s as the sorption rate constant. The solid phase Fe concentration at which no further reaction occurs is S_{eq}. Differential equations for dissolved Fe^{2+} (C_{II}), loosely adsorbed Fe^{2+} (A_{II}) and solid phase Fe (S_{II}) in the reduced layer are:

$$[Db + Ds]\frac{\partial^2 C_{II}}{\partial x^2} - \omega\frac{\partial C_{II}}{\partial x} - k_s C_{II} + k_r\vartheta(S_{II} - S_{eq}) - k_a(C_{II} - C_a) = 0 \quad (4)$$

$$Db\frac{\partial^2 A_{II}}{\partial x^2} - \omega\frac{\partial A_{II}}{\partial x} + k_s\frac{C_{II}}{\vartheta} - k_p(A_{II} - A_{eq}) = 0 \quad (5)$$

$$Db\frac{\partial^2 S_{II}}{\partial x^2} - \omega\frac{\partial S_{II}}{\partial x} - k_r(S_{II} - S_{eq}) = 0 \quad (6)$$

The 6 differential equations were analytically solved assuming continuity of concentrations (C_I=C_{II}, A_I=A_{II} and S_I=S_{II}) and fluxes at the redox boundary and specific conditions at the external boundaries, i.e. the sediment-water interface and at infinite depth (see Appendix). At the sediment-water interface the concentration of dissolved Fe^{2+} equals that in the overlying water (C_0 is set at 0 μM), the flux of solid phase Fe is $J_{Sx=0}$ (μmol m^{-2} d^{-1}) and the flux of loosely adsorbed Fe^{2+} ($J_{Ax=0}$) is zero. At infinite depth the concentrations of C_{II}, A_{II} and S_{II} converge to C_a, A_{eq} and S_{eq}, respectively, as their fluxes diminish. Variance-weighted sums of squares (Slomp *et al.*, 1997) for dissolved and loosely adsorbed Fe^{2+} and solid phase Fe were minimised simultaneously, while five parameters (k_r, k_s, k_a, k_p and $J_{Sx=0}$) were varied to fit the model to the data using the Excel™ solver routine.

The values of fixed parameters are given in Table 3. As no literature data on the oxidation rate of loosely adsorbed Fe^{2+} in marine sediments were available, we assumed the rate constant for loosely adsorbed Fe^{2+} oxidation to be equal to the rate constant for dissolved Fe^{2+} oxidation. For the 2109-m station on the La Coruña transect and the 123-m station on the main transect for which loosely adsorbed Fe^{2+} data were not available, the more simple Fe model of Slomp *et al.* (1997), which does not contain loosely adsorbed Fe^{2+}, was applied to the profiles of solid phase Fe and pore water Fe^{2+} to assess Fe reduction and oxidation rates.

Table 3. Fixed parameters used in model calculations

Water Depth (m)	(1) k_{oxc} (d^{-1})	(2) k_{oxa} (d^{-1})	(3) Db ($m^2 d^{-1}$)	(4) Ds ($m^2 d^{-1}$)	(5) ω ($m d^{-1}$)	(6) L (m)	(7) C_a (μM)	(8) A_{eq} (μmol g^{-1})	(9) S_{eq} (μmol g^{-1})
I La Coruña Transect									
175	10	10	1.95E-7	1.61E-5	9.86E-8	0.04	1	0.39	240
2109	10	-	3.04E-8	2.50E-5	1.48E-7	0.075	5	-	90
II Vigo Transect									
223	10	10	2.30E-7	1.70E-5	1.37E-7	0.01	0.1	0.1	122
III Main Transect									
104	10	10	5.48E-7	2.11E-5	1.37E-7	0.0015	6	0.3	150
113	10	10	5.48E-7	2.35E-5	1.37E-7	0.015	2	0.9	195
123	10	-	5.48E-7	2.35E-5	1.37E-7	0.01	2	-	140
932	10	10	3.32E-8	1.97E-5	2.74E-7	0.03	17	0.25	107
1387	10	10	1.07E-8	2.10E-5	2.74E-7	0.03	10	0.8	130
2060	10	10	2.19E-9	2.02E-5	2.55E-7	0.095	2	0.2	59
2073	10	10	2.47E-9	2.02E-5	2.55E-7	0.095	1.5	0.2	130
IV Nazaré Canyon Transect									
137	10	10	1.37E-7	2.11E-5	1.37E-6	0.025	4	0.2	316
396	10	10	1.84E-7	2.01E-5	2.74E-7	0.03	1	0.8	121
344	10	10	1.04E-7	2.80E-5	2.74E-6	0.01	1.5	3.3	242
890	10	10	1.10E-7	2.77E-5	2.74E-6	0.0275	22	4.17	208
3097	10	10	2.74E-7	1.91E-5	2.74E-6	0.0225	100	3.4	207
4280	10	10	6.58E-8	1.20E-5	2.74E-7	0.055	20	0.2	120

(1) k_{oxc} is set at 10 d^{-1} (Slomp et al., 1997) (2) k_{oxa} is set to 10 d^{-1} (see text) (3) Db is the mixing coefficient taken from Van der Zee *et al.*, 2001), except the Db of the 104-m station, which is set equal to the Db of the 113-m station. (4) Ds at 35 PSU, appropriate temperature and corrected for tortuosity (Boudreau, 1997) (5) ω is the sedimentation rate taken from Van der Zee *et al.*, 2001, except the 1387-m station on the main transect (0.01 instead of 0.05 cm yr^{-1}). (6) Nitrate < 5 μM depth (7) Ca is set equal or slightly lower than the deepest Fe^{2+} concentration observed. (8) A_{eq} is set equal or slightly lower than the deepest loosely adsorbed Fe^{2+} concentration observed. (9) S_{eq} is set equal to the deepest solid Fe concentration measured.

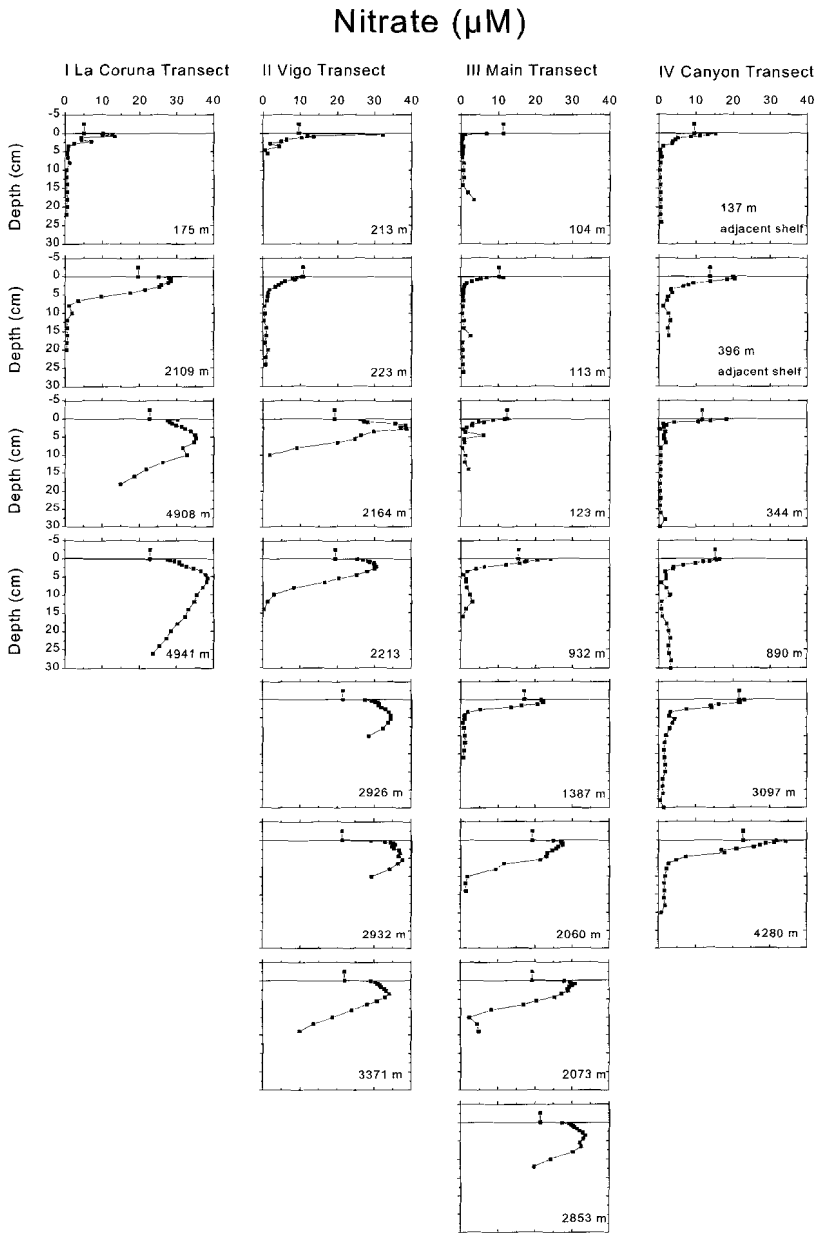

Figure 3. Vertical profiles of pore water nitrate concentrations.

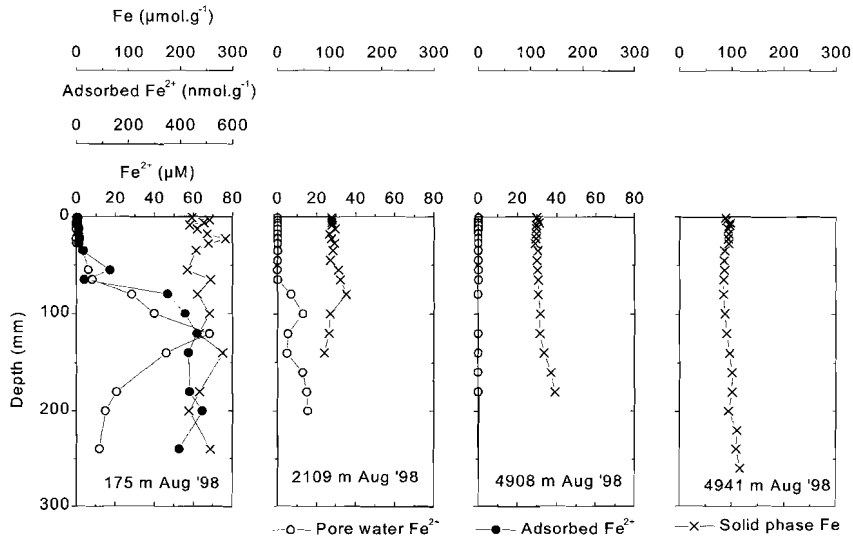

Figure 4. Vertical profiles of pore water Fe^{2+}, loosely adsorbed Fe^{2+} and solid phase Fe of the stations at the La Coruña transect.

EXPERIMENTAL RESULTS

At low concentrations of nitrate (< 5µM), Fe^{2+} may start to accumulate in the pore water. Therefore, nitrate profiles are suitable to describe the relevant Fe redox conditions in the sediment. The maximum nitrate concentration as well as the depth in the sediment where nitrate is depleted increases with water depth. At the *La Coruña transect*, the shallow 175-m station is rapidly depleted in nitrate (Fig. 3). At the two deepest stations, the nitrate concentration is higher than 10 µM throughout the sampled interval and therefore Fe reduction is not expected to occur. Nitrate is depleted around 5 cm depth in the sediment at the two shallow stations on the *Vigo transect*, indicating that Fe reduction may occur. The two stations around 2200 m show the depletion of nitrate at the bottom of the sampled interval, therefore Fe reduction is expected to start just below that interval. The nitrate concentration at the three deepest stations is too high throughout the sampled interval for Fe reduction to occur. At the *main transect*, the shallow stations are rapidly depleted in nitrate. At the two stations around 2000-m water depth, low nitrate concentrations at the bottom of the sampled intervals suggest it to be close to the Fe redox boundary. At the *canyon transect*, the same trend can be observed, i.e. the nitrate concentration and the depth where nitrate is depleted both increase with water depth, however, nitrate is more rapidly depleted in the canyon stations compared to stations at the same water depth on the margin.

Fe profiles of the stations on the *La Coruña transect* are given in Fig. 4. At the shallow station pore water and loosely adsorbed Fe^{2+} increase simultaneously until the pore water maximum is reached at 120 mm depth, after which the loosely adsorbed Fe^{2+} concentration remains constant but the pore water Fe^{2+} concentration decreases. The initial increase in both the pore water and the loosely adsorbed Fe^{2+} concentration suggests equilibrium between the two Fe^{2+} phases. The deeper profile, however, suggest precipitation of dissolved Fe^{2+} that is not accompanied by desorption of Fe^{2+}. The pore water Fe^{2+} concentrations as well as the solid Fe content decrease going down slope.

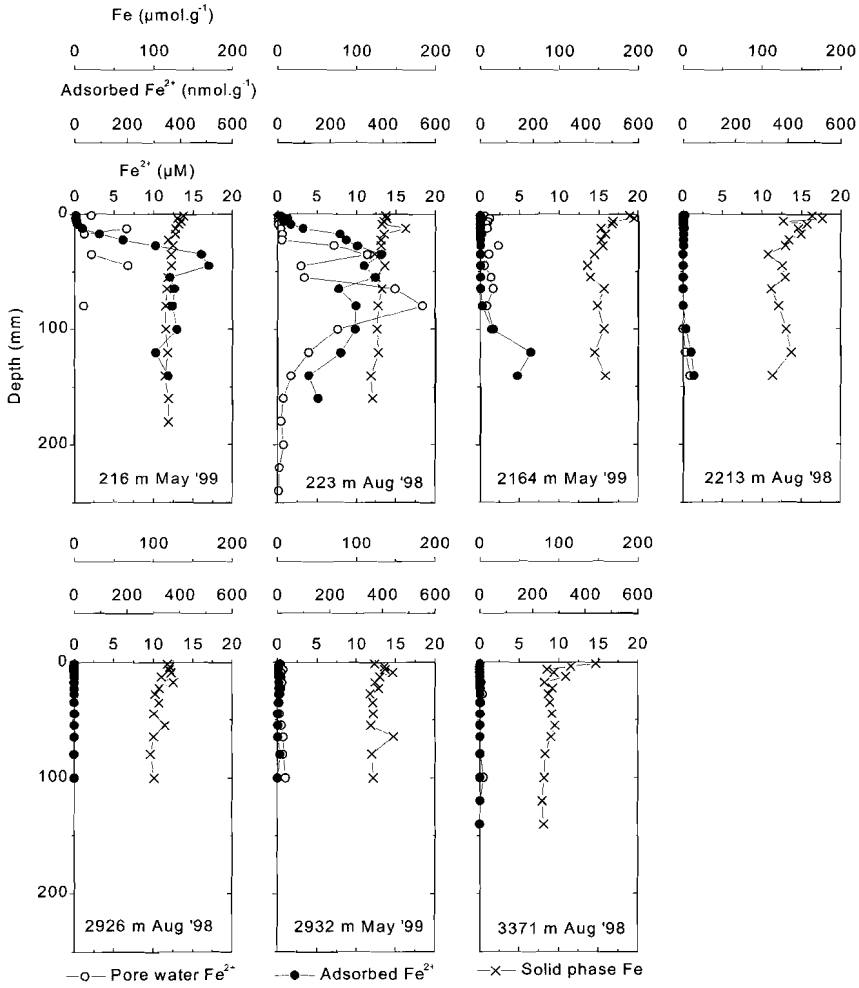

Figure 5. Vertical profiles of pore water Fe^{2+}, loosely adsorbed Fe^{2+} and solid phase Fe of the stations at the Vigo transect.

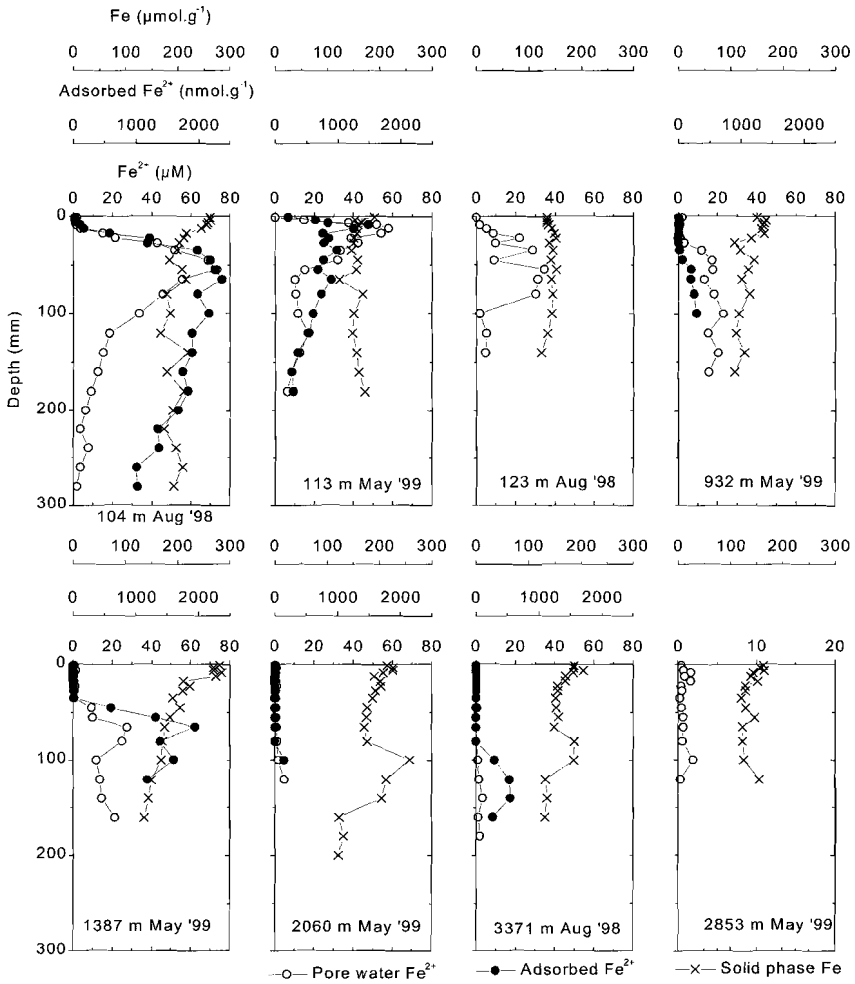

Figure 6. Vertical profiles of pore water Fe^{2+}, loosely adsorbed Fe^{2+} and solid phase Fe of the stations at the Main transect.

At the two shallowest stations on the *Vigo transect* (Fig. 5), both loosely adsorbed and dissolved Fe^{2+} concentrations decrease below 5-8 cm depth, albeit that pore water Fe^{2+} diminishes most rapidly. The relevant redox boundary is too deep at the other stations of this transect to show this phenomenon. There, we can only observe the maximum values of loosely adsorbed and dissolved Fe^{2+} decrease with increasing depth on the slope. Pore water as well as loosely adsorbed Fe^{2+} concentrations generally decrease from shallow to deeper stations on the *main transect* with a relatively high loosely adsorbed Fe^{2+} concentration at the 1387-m station (Fig. 6). At

all stations pore water and loosely adsorbed Fe^{2+} increase simultaneously until their maxima are reached, after which both decrease again or remain constant. The 104-m station clearly illustrates the initial equilibrium between pore water and loosely adsorbed Fe^{2+} and the change in behaviour as pore water Fe^{2+} precipitates deeper than 55-mm depth. The concentrations of loosely adsorbed Fe^{2+} are much higher at the stations at 104, 113 and 1387 m on this transect than at stations on the previously discussed transects. At2060 and 2073 m, the profiles show a clear solid phase Fe peak at 100 mm and 80 mm, respectively.

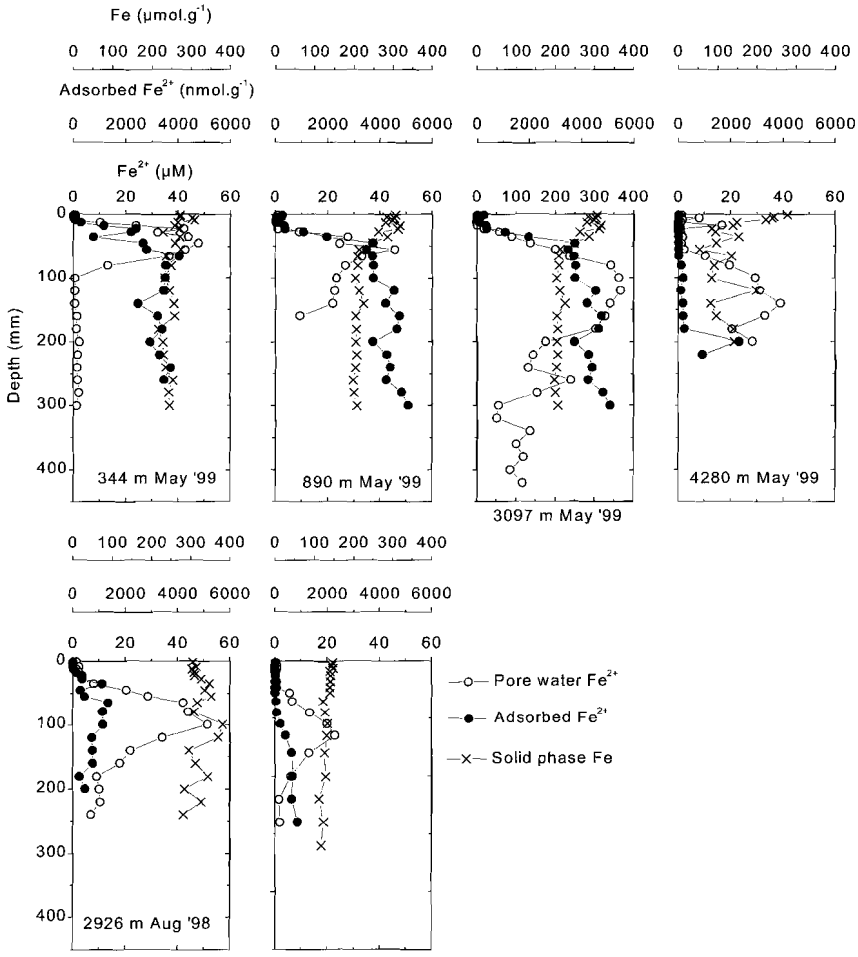

Figure 7. Vertical profiles of pore water Fe^{2+}, loosely adsorbed Fe^{2+} and solid phase Fe of the stations at the Nazaré canyon transect.

Four stations are located in the canyon on the *Nazaré canyon transect*, whereas both the 137- and the 396-m station are situated on the adjacent shelf (Fig. 7). Again, simultaneous increase of pore water and loosely adsorbed Fe^{2+} is observed and suggests initial equilibrium in the Fe reduction layer, after which pore water Fe^{2+} is removed due to precipitation, but the loosely adsorbed Fe^{2+} concentration remains constant. Pore water Fe^{2+} concentrations at the stations in the canyon are comparable to stations at shallow water depth on the other transects, except at the canyon station at 3097 m where it is an order of magnitude higher. Loosely adsorbed Fe^{2+} concentrations are high at the 346-, 890- and 3097-m stations. The solid phase Fe profiles are strongly enriched at the sediment-water interface at the stations in the canyon.

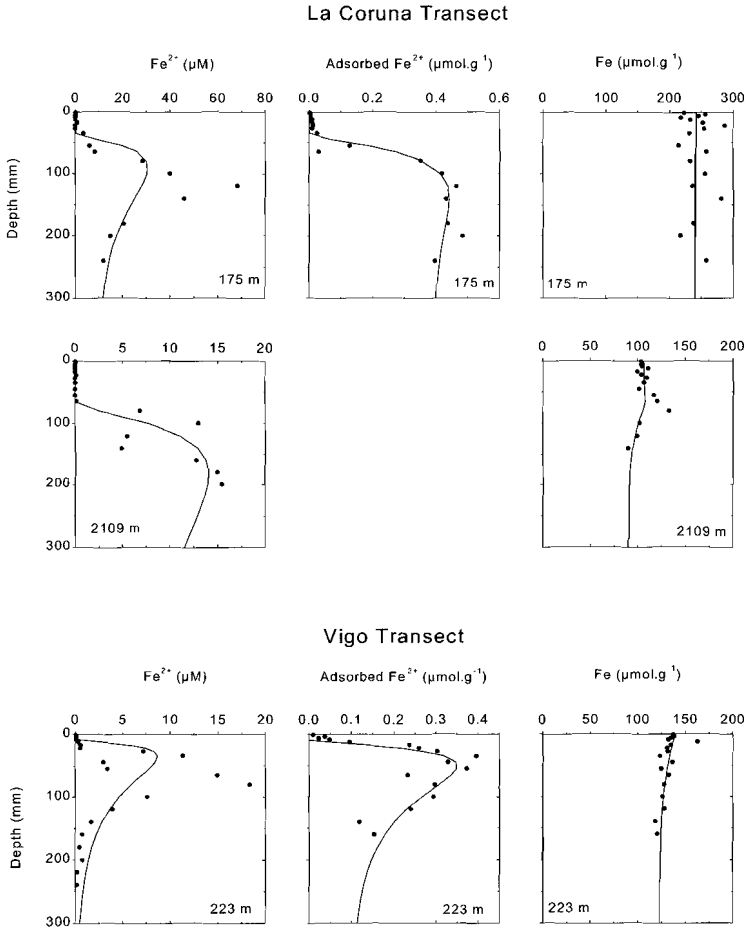

Figure 8a. Model fits (lines) to profiles of pore water Fe^{2+}, loosely adsorbed Fe^{2+} and solid phase Fe (filled circles) of the stations at the La Coruña and Vigo transect.

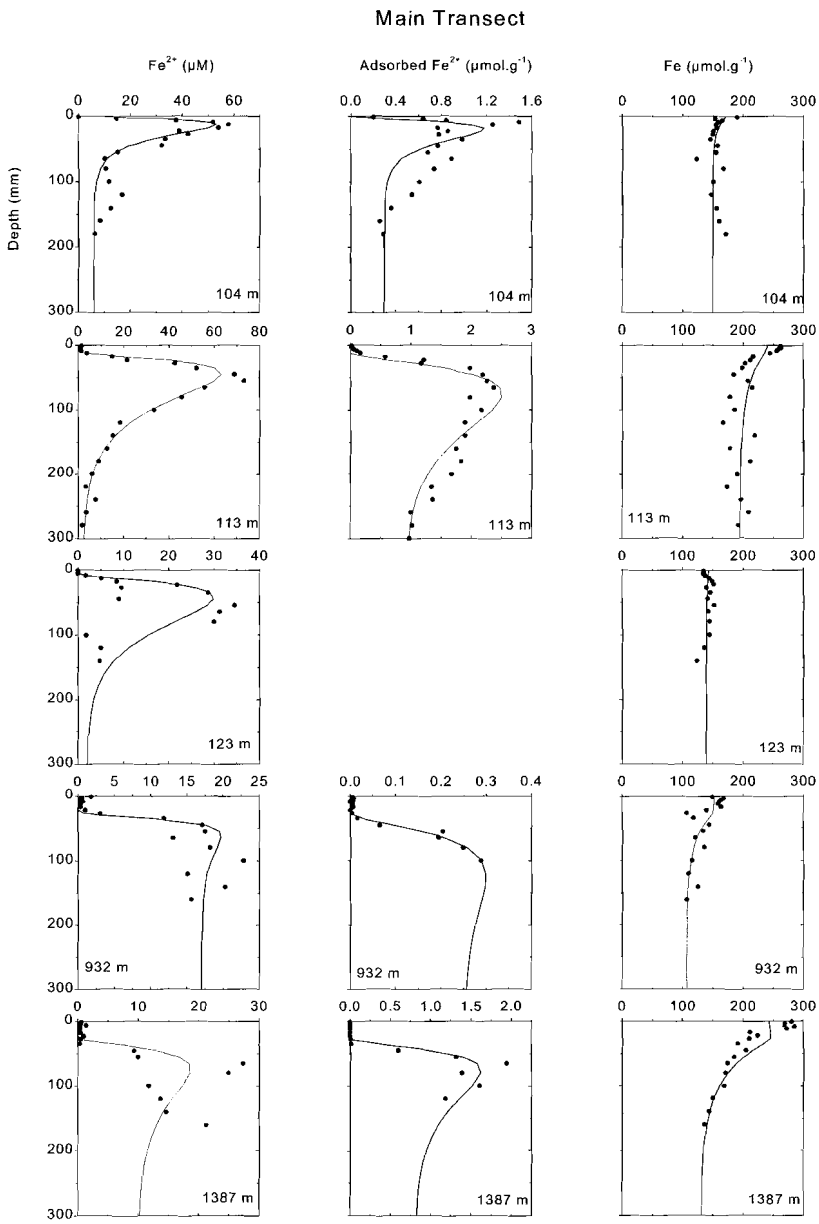

Figure 8b. Model fits (lines) to profiles of pore water Fe^{2+}, loosely adsorbed Fe^{2+} and solid phase Fe (filled circles) of the stations at the Main transect.

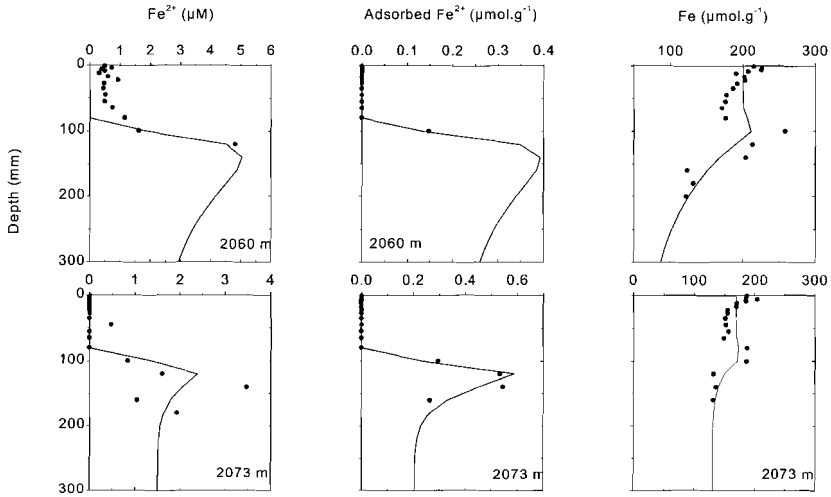

Figure 8b continued.

MODEL RESULTS

The model was applied to stations where dissolved Fe^{2+} accumulated in the pore water. Model fits to the data are given for the *La Coruña* and *Vigo transect* (Fig. 8a), the *main transect* (Fig. 8b) and the *Nazaré canyon transect* (Fig. 8c). The model fits the data reasonably well. The model can describe only one Fe^{2+} pore water maximum per profile, however, at several stations double peaks occur. Moreover, the pore water Fe^{2+} maxima are underestimated by the model. Both problems are illustrated by the model fit of the profiles of the 223-m station on the Vigo transect. The underestimated pore water maximum is probably due to a more abrupt decline in pore water Fe^{2+} than the model can simulate leading to a model fit in-between the high values of the maximum and the low values deeper in the sediment, e.g. the 344-m station at the Nazaré canyon transect. The model fit of the deepest station in the canyon is not very good, especially for the solid phase, because the sediment consists of alternating layers of clay and sand containing different amounts of Fe. The 1N HCl solution likely extracts some of the ferrous solid phase Fe (Wallmann *et al.*, 1993). However, the model treats it as Fe(III) resulting is an underestimation of the Fe(III) concentration gradient and consequently the Fe reduction rate.

The values of the fitted first order rate constants vary several orders of magnitude due to the lumping of a number of factors into one parameter, e.g. Fe oxyhydroxide reactivity, type of reductant, organic matter reactivity, microbial activity and temperature (Table 4; Burdige and Gieskes, 1983; Slomp *et al.*, 1997; Dollhopf *et al.*, 2000). However, the ranges for all first order rate constants as well as the estimated Fe deposition fluxes ($J_{Sx=0}$) are similar to those estimated for the North Sea (Slomp *et al.*,

1997). The values for the first order rate constants are comparable to those obtained for Mn cycling at the Iberian margin, whereas the estimated Fe deposition fluxes are higher than those for Mn (Van der Zee *et al.*, 2001). Integrated rates of reaction can be calculated from the model results (Table 5). At the non-canyon stations, depth-integrated reduction and oxidation rates are highest and most variable at stations shallower than 400 m (Fig. 9). Here, depth-integrated rates of reduction and oxidation decrease with increasing water depth and are close to zero deeper than ~ 2200 m. At the 344-m station in the head of the canyon, depth-integrated rates of Fe reduction and oxidation are similar to other shallow water stations, but higher than at the 396-m station on the adjacent shelf. In the canyon, integrated rates of Fe oxidation and reduction increase with water depth until a maximum at the 3097-m station is reached. At the 4280-m station in the canyon the rates are lower again, although relatively high as compared with deep stations outside the canyon.

Table 4. Values for k_r, k_s, k_a, k_p and $J_{Sx=0}$ obtained by fitting the model to the data

Water Depth (m)	k_r (d^{-1})	k_{ads} (d^{-1})	k_a (d^{-1})	k_p (d^{-1})	$J_{Sx=0}$ ($\mu mol.m^{-2}.d^{-1}$)
I La Coruña Transect					
175	2.0E-4	3.5E-3	0	2.6E-4	34
2109	1.51E-5	-	5.88E-4	-	10
II Vigo Transect					
223	3.8E-5	1.2E-1	0	1.2E-3	71
III Main Transect					
104	1.4E-3	4.4E-1	0	1.1E-2	481
113	2.1E-4	3.2E-2	4.3E-2	4.2E-4	254
123	5.7E-4	-	2.4E-2	-	56
932	2.9E-5	2.6E-3	2.0E-1	1.5E-5	40
1387	8.7E-6	3.9E-2	1.9E-11	3.6E-4	50
2060	2.3E-6	1.0E-2	5.3E-2	1.8E-4	34
2073	1.3E-5	2.0E-1	0	5.2E-4	29
IV Nazaré Canyon Transect					
137	7.7E-5	5.7E-3	0	8.0E-5	57
396	1.3E-4	4.6E-3	8.4E-2	5.3E-7	97
344	4.0E-4	4.2E-3	3.5E-2	1.0E-5	446
890	2.8E-4	1.7E-2	2.0E-1	1.0E-9	122
3097	8.0E-5	1.4E-3	6.3E-3	8.1E-4	566
4280	3.5E-6	9.8E-4	1.3E-2	8.1E-7	63

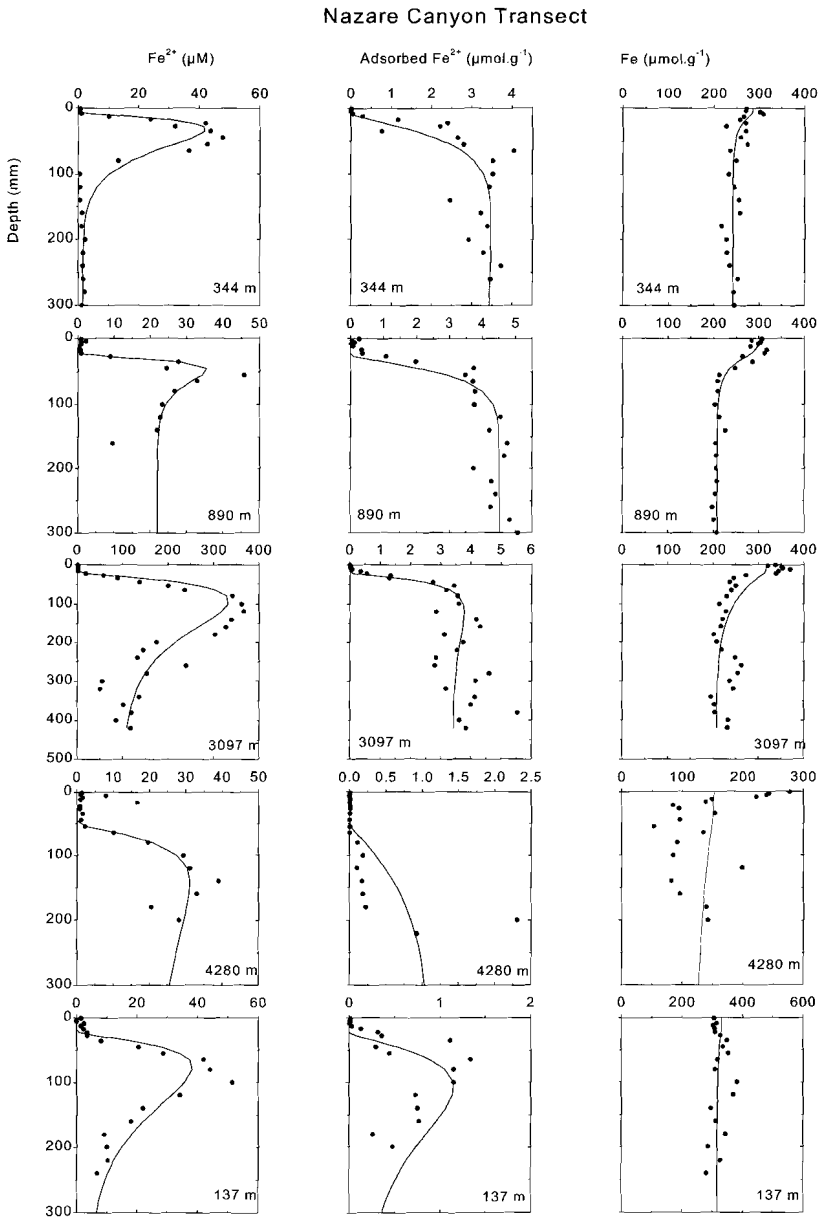

Figure 8c. Model fits (lines) to profiles of pore water Fe^{2+}, loosely adsorbed Fe^{2+} and solid phase Fe (filled circles) of the stations at the Nazaré Canyon transect.

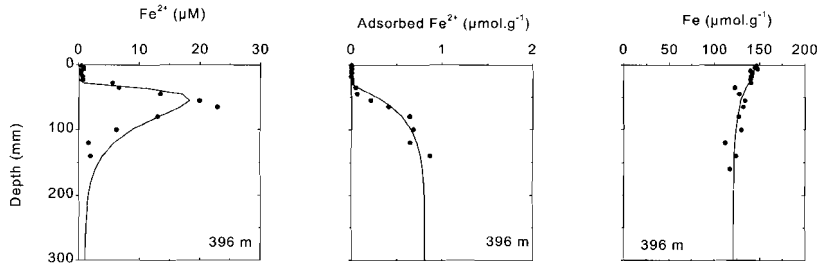

Figure 8c continued

Table 5. Calculated integrated rates of reduction, sorption, oxidation, precipitation and burial of Fe from the model results.

Water Depth (m)	Reduction ($\mu mol.m^{-2}.d^{-1}$)	Sorption ($\mu mol.m^{-2}.d^{-1}$)	Oxidation ($\mu mol.m^{-2}.d^{-1}$)		Precipitation ($\mu mol.m^{-2}.d^{-1}$)		Burial Fe ($\mu mol.m^{-2}.d^{-1}$)
			$Fe^{2+}_{(aq)}$	$Fe^{2+}_{(ads)}$	$Fe^{2+}_{(aq)}$	$Fe^{2+}_{(ads)}$	
La Coruña Transect							
175	17	4	12	4	0	0	34
2109	8	-	7.4	-	0.3	-	10
4908	#	#	#	#	#	#	#
4941	#	#	#	#	#	#	#
Vigo Transect							
213	-	-	-	-	-	-	-
223	63	56	8	7	0	49	23
2164	#	#	#	#	#	#	#
2213	#	#	#	#	#	#	#
2926	#	#	#	#	#	#	#
2932	#	#	#	#	#	#	#
3371	#	#	#	#	#	#	#
Main Transect							
104	599	454	53	87	0	368	21
113	364	117	89	45	158	72	23
123	65	-	34	-	31	-	24
932	41	0.2	27	0.1	14	0	26
1387	41	24	18	1	0	23	27
2060	29	4	5	0	20	4	10
2073	11	7	5	0	0	7	22
2853	#	#	#	#	#	#	#
Nazaré Canyon Transect							
137	42	17	25	4	0	13	44
396	87	3	23	3	61	0	36
344	177	9	96	4	72	0	369
890	198	7	99	7	91	0	30
3097	426	41	191	30	194	5	361
4280	25	1	7	0	17	1	45

Most likely zero, not able to determine

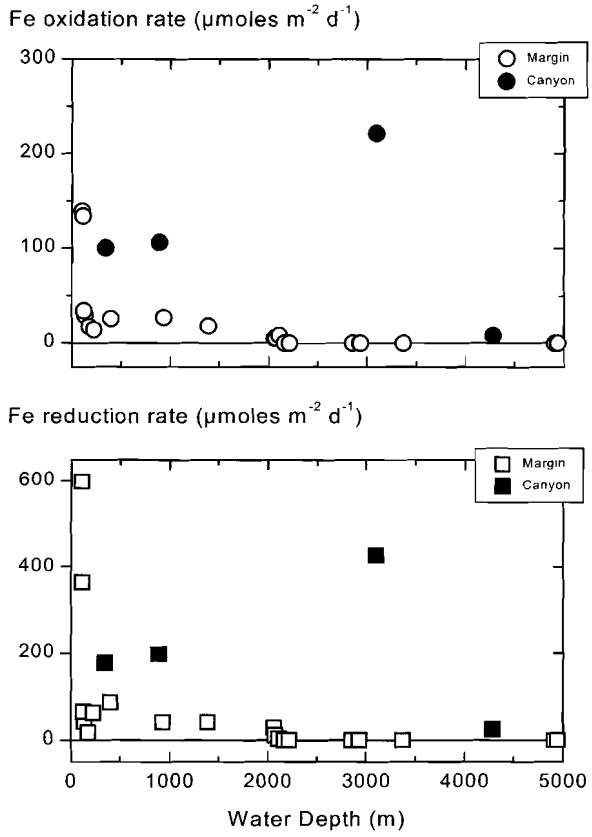

Figure 9. Fe^{2+} oxidation rate (circles) and Fe reduction rate (squares) as a function of water depth on the margin (open symbols) and in the canyon (filled symbols).

DISCUSSION

Role of loosely adsorbed Fe^{2+} in Fe cycling

Our data show a strong coupling between pore water Fe^{2+} and loosely adsorbed Fe^{2+} in the upper sediment layers, confirming the DGT data of Zhang*et al.* (1995) and suggesting an initial equilibrium between the two phases. However, deeper down where the pore water Fe^{2+} concentration decreases due to precipitation, loosely adsorbed Fe^{2+} does not seem to be in equilibrium with pore water Fe^{2+}. The decrease in adsorbed Fe^{2+} concentrations is always accompanied by a decline in pore water Fe^{2+} concentration, i.e. desorption is always accompanied by Fe^{2+} precipitation. In the model, the precipitation of loosely adsorbed Fe^{2+} describes Fe^{2+} desorption plus its

subsequent precipitation. Loosely adsorbed Fe^{2+} can be released into the pore water and immediately precipitate as authigenic ferrous phases, then dissolved Fe^{2+} does not accumulate. The sum of the dissolved and the loosely adsorbed Fe^{2+} precipitation rate is assumed to equal the authigenic ferrous mineral formation rate. When precipitation of pore water Fe^{2+} is zero (Table 5), this indicates that all dissolved Fe^{2+} is adsorbed. Deeper down, however, Fe^{2+} is released again from the loosely adsorbed phase into the pore water and instead of accumulating there it is immediately precipitated. When precipitation of loosely adsorbed Fe^{2+} is zero (Table 5), this indicates that Fe^{2+} is transported into the sediment below our sampled interval, without transforming into authigenic ferrous minerals. We propose that loosely adsorbed Fe^{2+} acts as a buffer for reduced Fe in the anoxic layer. Close to the redox boundary, upon Fe reduction, Fe^{2+} is released into the pore water and subsequently adsorbed. Pore water Fe^{2+} can diffuse up into the oxic layer, whereas loosely adsorbed Fe^{2+} can be mixed up into the oxic layer and both will be re-oxidised. Dissolved Fe^{2+} is transported faster due to molecular diffusion than loosely adsorbed Fe^{2+}, which is transported by diffusive mixing. The difference in transport rate even increases during downward transport over longer distances. Although the mixing coefficient (*Db*) is kept constant with depth in our model, the mixing intensity is likely to decrease with depth in the sediment and therefore transport of loosely adsorbed Fe^{2+} is even slower. Pore water Fe^{2+} concentrations can decline very rapidly, leading to a sharply defined zone of authigenic ferrous mineral formation. Through Fe^{2+} sorption, the authigenic ferrous mineral formation is partly delayed. However, the loosely adsorbed Fe^{2+} is transported deeper into the sediment, where it can act as a deep source for authigenic ferrous mineral formation, increasing the thickness of the authigenic ferrous mineral formation zone. Thamdrup *et al.* (1994) measured profiles of non-S-bound Fe^{2+} that was involved in FeS formation, since its concentration decreased with increasing FeS content. Their non-S-bound Fe^{2+} is distributed like their pore water Fe^{2+} and our adsorbed Fe profiles. On the Chilean slope, non-S-bound Fe^{2+} was the largest Fe^{2+} pool measured in the solid phase, exceeding pyrite 5-fold (Thamdrup and Canfield, 1996). Canfield *et al.* (1993) also report a large non-S-bound Fe^{2+} pool in North Sea sediments, representing more than 50% of the Fe^{2+} in the solid phase and suggest it could be bound in Fe carbonates or adsorbed onto sediment particles. Wang and Van Cappellen (1996) used these data in their STEADYSED model and attributed non-S-bound Fe^{2+} largely to adsorbed Fe^{2+} and a minor fraction to siderite ($FeCO_3$). Their estimates showed that the main oxidation pathway is heterogeneous, i.e. via oxygenation of adsorbed Fe^{2+}. Also, laboratory studies showed enhanced oxygenation rates when Fe^{2+} is adsorbed to particle surfaces (Stumm and Sulzberger, 1992). Although, it is very likely that adsorbed Fe^{2+} will be rapidly oxidised, it is not possible to extract information about the preferred oxidation pathway from our data.

Substrates for Fe^{2+} sorption

Both microbial and abiotic Fe oxide reduction are surface-controlled processes (Nevin and Lovley, 2000; Stumm and Sulzberger, 1992). Adsorbed or precipitated Fe^{2+} on the surface of goethite was found to limit the rate and extent of dissimilatory Fe reduction by bacteria (Roden *et al.*, 1996, 1999). Urrutia *et al.* (1999) argued that Fe reduction is enhanced by aqueous or solid phase compounds, which prevent or delay Fe^{2+} sorption onto the Fe oxide or the Fe reducing bacterial cells. Aluminium oxides and layered silicates were suggested as alternate sinks for Fe^{2+} in the sediment,

because goethite was reduced more readily when aluminium oxide was placed in a dialysis bag in their experimental setting, due to sorption of Fe^{2+} to the Al oxide (Urrutia *et al.*, 1999). Higher contents of loosely adsorbed Fe^{2+} do not correspond with lower Fe reduction rates at the Iberian margin. However, stations with loosely adsorbed Fe^{2+} contents higher than 1 μmol g^{-1} also have a relatively high C_{org} content (Table 1). Thus, Fe^{2+} might sorb onto Fe minerals and organic material, without inhibiting Fe reduction. We conclude that loosely adsorbed Fe^{2+} is probably associated with organic matter, Al oxides and layered silicates.

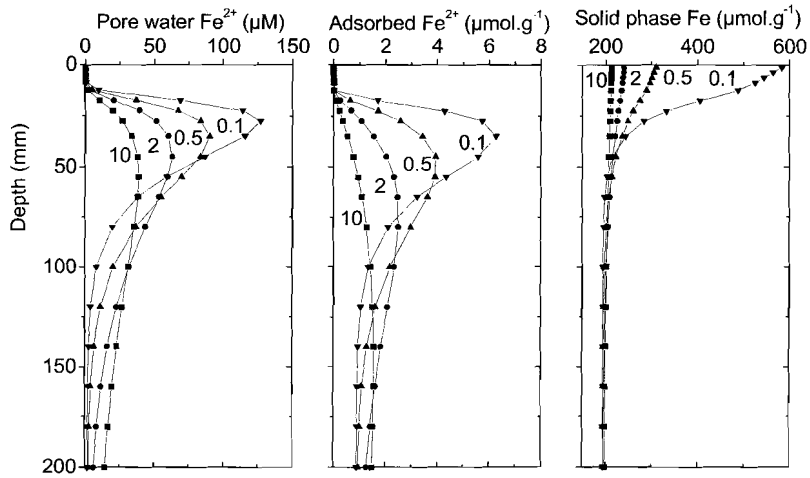

Figure 10. Effect of varying the mixing coefficient on the pore water Fe^{2+}, loosely adsorbed Fe^{2+} and solid phase Fe profiles of the 113-m station at the main transect.

The rate controlling factor for Fe cycling

The organic carbon mineralisation rates are highest at the shelf (see Research Area). Fe reaction rates are highest at the shelf as well, decreasing with increasing water depth at the non-canyon stations. Turnover times were estimated from the standing stock divided by the production rate for the pore water Fe^{2+}, loosely adsorbed Fe^{2+} and solid phase Fe in both the oxidised and the reduced layer. The highest turnover time was found for solid phase Fe in the oxidised layer for all stations, except for the 2060-m station on the main transect, where the solid phase Fe in the reduced layer has a slightly higher turnover time. Pore water and loosely adsorbed Fe^{2+} had turnover times 2-6 orders of magnitude smaller. We conclude that the rate-limiting step is the transfer of solid phase Fe^{3+} in the oxidised to the reduced layer. Thus, solid phase mixing limits Fe cycling at the Iberian margin. Sediment mixing is necessary to bring Fe oxyhydroxides into the reduced layer and to stimulate anoxic organic carbon mineralization by burial of reactive organic matter (Aller, 1986). Dhakar and Burdige (1996) simulated the effect of increasing bioturbation on their model determined depth-integrated rates of oxic and sub-oxic (nitrate, manganese and iron) organic carbon mineralization rates and showed that the sub-oxic

respiration increased while the total carbon mineralization remains constant with increasing *Db*. The effect of changing the mixing coefficient (*Db*) on the Fe profiles of the 113-m station on the main transect, while other parameters from Table 3 and 4 were kept constant, is shown in Fig. 10. Pore water Fe^{2+}, loosely adsorbed Fe^{2+} and solid phase Fe profiles show increasing maxima with a decreasing value for Db. Thus, mixing smoothes the profiles as expected. To assess the influence of sediment mixing on the homogeneous and heterogeneous oxidation rate as well as on the reduction rate, the Fe profiles of the 113-m station on the main transect were fitted with various *Db* values (Fig. 11), while keeping the other input parameters constant (Table 3). Enhanced mixing increases both the oxidation and the reduction rate, showing the importance of sediment mixing in Fe cycling. Moreover, heterogeneous oxidation becomes more important with enhanced sediment mixing. These values are probably underestimates for the heterogeneous contribution to the oxidation, because the same oxidation rate constant (k_{ox} is 10 d^{-1}) is used for both the pore water and the loosely adsorbed Fe^{2+}, whereas heterogeneous oxidation is likely to be the more rapid pathway (Stumm and Sulzberger, 1992).

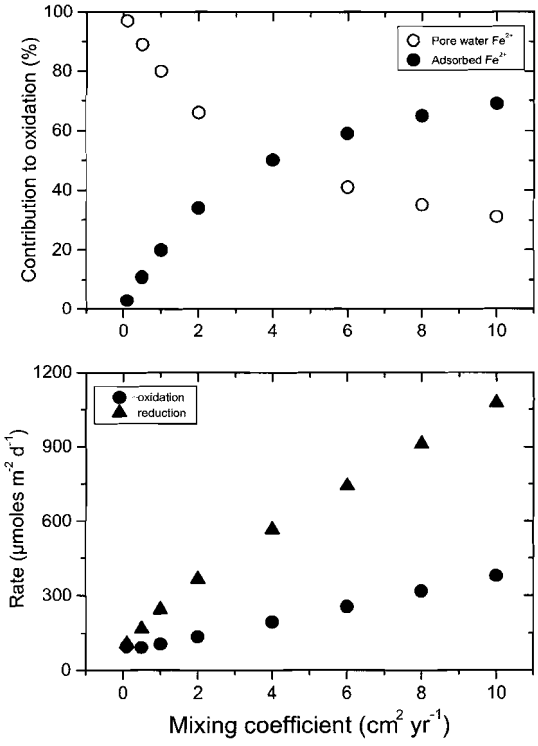

Figure 11. Effect of varying the mixing coefficient on pore water Fe^{2+} and loosely adsorbed Fe^{2+} oxidation rates and Fe reduction rates of the 113-m station at the main transect.

Canyon vs. Margin – The influence of the bulk sediment accumulation rate

The three transects over the margin show the same decreasing trend in Fe oxidation and reduction rates with water depth, whereas the rates in the Nazaré canyon transect slightly increase with depth until 3097 m. The organic carbon mineralization rates decrease with water depth both in the canyon as well as outside the canyon. At the 344-m station in the head of the canyon, the organic carbon mineralization rate and the Fe reduction rate are well within the range found for the shelf stations. However, while the organic carbon mineralization rate is a factor three higher at the 3097-m canyon station, the Fe reduction rate is orders of magnitude higher than at similar water depth outside the canyon. The Fe deposition fluxes obtained from the model fits (Table 4) show enhanced Fe deposition at the 344-, 890- and 3097-m stations in the canyon compared to stations on the margin at similar water depth. The Nazaré canyon focuses sediment and transports it from the shelf directly to the deep sea (Smith *et al.*, 2001). The bulk sediment accumulation rate in the canyon is largest at 3097 m, and one order of magnitude higher than on the shelf (Van Weering *et al.*, 2001), the mineralization rate, however, is lower at 3097 m compared to the shelf. Thus, the high bulk sediment accumulation rate is likely the driving force for the Fe reduction at the 3097-m canyon station.

Iberian Margin vs. the World – the troubles of estimating Fe reduction rates

Thamdrup and Canfield (1996) argued that a substantial contribution of Fe reduction in the organic matter oxidation could be widespread on continental margins, because O_2 and NO_3^- penetration into shelf and slope sediments is only a few mm's to cm's (Reimers *et al.*, 1992; Brandes and Devol, 1995). Estimated contributions of Fe reduction to the mineralisation using bag incubations are up to 29% on the Chilean continental margin (Thamdrup and Canfield, 1996), 25% in a high-Arctic fjord in Greenland (Rysgaard *et al.*, 1998) and up to 51% in the Skagerrak (Canfield et al., 1993). However, bag incubations tend to stimulate and therefore overestimate anoxic processes, due to the depletion of O_2 and NO_3^- during incubation (Thamdrup and Canfield, 1996). Estimates from pore water profile modelling indicated that Fe reduction is less important (<2%) at the Canadian and central Californian continental margins (Boudreau *et al.*, 1998; Reimers *et al.*, 1992), and <4% at the North Sea continental margin, with the exception of the Skagerrak ~20% (Slomp *et al.*, 1997). Pore water profile-derived estimates are likely too low, because an unknown amount of Fe^{2+} is adsorbed to the solid phase (Canfield *et al.*, 1993). Therefore, we choose to estimate Fe reduction rates from pore water Fe^{2+}, loosely adsorbed Fe^{2+} and solid phase Fe profile modelling. Assuming 1:4 stoichiometry for the C_{org} oxidation : Fe reduction rate, the Fe contribution is 5% at the 104-m and 113-m stations on the main transect and 6% the 3097-m station in the canyon, at the other stations Fe reduction contributes less than 4% to mineralization. Other solid phase ferrous compounds, which have higher concentrations than adsorbed Fe^{2+}, are important for Fe cycling as well (e.g. Canfield *et al.*, 1993; Thamdrup *et al.*, 1994; Thamdrup and Canfield, 1996). Estimates of Fe reduction rates can be further improved by including all ferrous phases in diagenetic models. Upon mixing into the oxic layer, the ferrous phases are re-oxidized, supplying Fe(III) for Fe reduction and their recycling rate will be enhanced with sediment mixing in the same way as for the adsorbed Fe^{2+} described here. Reactive soluble Fe(III) complexed to organic ligands has been identified as an

important oxidant in anoxic pore waters of salt marshes and a 31 m deep station on the New Jersey shelf (Luther *et al.*, 1992; Luther *et al*, 1996; Taillefert *et al.*, 2000). The Fe(III) remains in solution due to dissolved humic matter derived from plants (Luther *et al.*, 1996). Would organically complexed Fe(III) be a significant Fe phase in open marine settings, such as our sites, they may contribute to the Fe redox cycling as well.

Manganese vs. Iron

Fe reaction rates are highest on the shelf, decreasing with increasing water depth, whereas the Mn reaction rates are highest halfway on the slope (Van der Zee *et al.*, 2001). Our previous results on Mn modelling showed that Mn cycling at shallow stations (<225 m) is limited by slow oxidation kinetics (k_{ox} is 1 d^{-1}). Fe^{2+}, however, is more rapidly oxidised (k_{ox} is 10 d^{-1}) than Mn^{2+}, thus, is more intense cycled at the shelf than Mn. At the stations >225 m, the rate limiting factor for Mn cycling is the same as the rate limiting factor for Fe, i.e. sediment mixing. Deposition fluxes of Fe are larger than those of Mn. Thus, in addition to the faster oxidation kinetics of Fe, the supply of metal oxide from the water column is larger. Both factors enhance the Fe oxyhydroxide content in the oxic layer as compared to Mn oxide and thus comparatively more Fe oxyhydroxides are transported into the anoxic layer. Therefore, Fe reduction is faster than Mn reduction at the Iberian Margin.

The role of adsorbed Mn^{2+} in Mn cycling is very different from the role of loosely adsorbed Fe^{2+} in Fe cycling. Adsorbed Mn^{2+} is concentrated near the Mn redox boundary, whereas loosely adsorbed Fe^{2+} concentrations are highest below the Fe redox boundary. Adsorbed Mn^{2+} is an intermediate between Mn oxide and pore water Mn^{2+} and enhances the retention of Mn^{2+} in the sediment. Loosely adsorbed Fe^{2+}, however, is not an intermediate between Fe oxyhydroxides and pore water Fe^{2+} in the anoxic layer, but most likely a deep source for authigenic ferrous mineral formation via desorption to pore water Fe^{2+}. Loosely adsorbed Fe^{2+} is faster oxidised than adsorbed Mn^{2+}, it is absent in the oxic layer, whereas small amounts of adsorbed Mn^{2+} are present, indicating that loosely adsorbed Fe^{2+} might also be important in the Fe oxidation.

CONCLUSIONS

Loosely adsorbed Fe^{2+} is proposed to be a buffer in the transformation of pore water Fe^{2+} to authigenic ferrous minerals. Close to the redox boundary, Fe^{2+} is released into the pore water upon Fe reduction, and subsequently either adsorbed onto the sediment matrix and/or precipitated to form authigenic ferrous minerals. Deeper down in the sediment, the loosely adsorbed Fe^{2+} is released again, however, dissolved Fe^{2+} does not accumulate, but is immediately precipitated. Thus, loosely adsorbed Fe^{2+} acts as a deep source for authigenic ferrous mineral formation. The substrate for Fe^{2+} sorption is likely to be organic material, aluminium oxides and layered silicates. Fe oxidation and reduction rates decreased with water depth at the non-canyon stations. At the shelf organic carbon mineralization rates are highest and drive the Fe cycle. In the canyon, the high deposition fluxes drive the Fe cycle. The highest contributions of Fe reduction to the overall organic matter oxidation are 5% at the

104-m and 113-m stations on the main transect and 6% at the 3097-m deposition station in the canyon. The rate-limiting factor for Fe cycling, as deduced from the turnover times, is sediment mixing. Model simulations showed that heterogeneous oxidation becomes relatively more important with increased sediment mixing.

Acknowledgements The authors wish to thank the captain and crew of R.V. Pelagia for providing safe cruises and a pleasant working environment. Shipboard nitrate and iron analyses were performed by Karel Bakker, Jan van Ooijen and Evaline van Weerlee (NIOZ, department of Marine Chemistry and Geology). We thank Eric Epping for very kindly providing the nitrate data. Two anonymous referees are thanked for their comments, which greatly helped us to improve the manuscript. The investigations were carried out in the framework of the Sedimentary Manganese and Iron cycLEs (SMILE) program that was supported by the Research Council for Earth and Life Science (ALW) with financial aid from the Netherlands Organisation for Scientific Research (NWO) (no. 750.297.01). W.H. was supported through a grant by the European community EC-MAST OMEX-II project (MAS3-CT96-0056). This is publication no. 3517 of the Royal Netherlands Institute for Sea Research.

REFERENCES

Aller, R. C. 1980. Diagenetic processes near the sediment-water interface of Long Island Sound II. Fe and Mn. Adv. Geophys., 22, 351-415.

Aller, R. C., J. E. Mackin and R. T. Cox, Jr. 1986. Diagenesis of Fe and S in Amazon inner shelf muds: apparent dominance of Fe reduction and implications for the genesis of ironstones. Cont. Shelf Res., 6, 263-289.

Berner, R. A. 1976. Inclusion of adsorption in the modelling of early diagenesis. Earth Plan. Sci. Lett., *29*, 333-340.

Boudreau, B.P., A. Mucci, B. Sundby, G.W. Luther and N. Silverberg. 1998. Comparative diagenesis at three sites on the Canadian continental margin. J. Mar. Res., 56, 1259-1284.

Brandes, J. A., and A. H. Devol. 1995. Simultaneous nitrate and oxygen respiration in coastal sediments: Evidence for discrete diagenesis. J. Mar. Res., 53, 771-797.

Burdige, D.J. and J.M. Gieskes. 1983. A pore water / solid phase diagenetic model for manganese in marine sediments. Am. J. Sci., 283, 29-47.

Burdige, D.J. and P.E. Kepkay. 1983. Determination of bacterial manganese oxidation rates in sediments using a in-situ dialysis technique, I. Laboratory studies. Geochim. Cosmochim. Acta, 47, 1907-1916.

Canfield, D. E. 1988. Dissertation. Sulfate reduction and the diagenesis of iron in anoxic marine sediments. Yale University.

Canfield, D. E., B. Thamdrup and J. W. Hansen. 1993. The anaerobic degradation of organic matter in Danish coastal sediments: Iron reduction, manganese reduction and sulfate reduction. Geochim. Cosmochim. Acta, 57, 3867-3883.

Dhakar, S. P. and D. J. Burdige. 1996. A coupled non-linear, steady state model for early diagenetic processes in pelagic sediments. Am. J. Sci., 296, 296-330.

Dollhopf, M.E., K.H. Nealson, D.M. Simon, and G.W. Luther III. 2000. Kinetics of Fe(III) and Mn(IV) reduction by the black sea strain of *Shewanella putrefaciens* using in situ solid state voltametric Au/Hg electrodes. Mar. Chem., 70, 171-180.

Durieu de Madron, X., P. Castaing, F. Nyffeler and T. Courp. 1999. Slope transport of suspended particulate matter on the Aquitanain margin of the Bay of Biscay. Deep-Sea Res. II, 46, 2003-2027.

Epping, E., C. Van der Zee, K. Soetaert and W. Helder. 2002. On the mineralisation and burial of organic carbon in sediments of the Iberian margin and Nazaré Canyon (NE Atlantic). Progr. Oceanogr. Accepted.

Hansen, H.C.B., O.K. Borggaard, and J. Sørensen. 1994. Evaluation of the free energy of formation of Fe(II)-Fe(III) hydroxide-sulphate (green rust) and its reduction of nitrite. Geochim. Cosmochim. Acta, 58, 2599-2608.

Koch, C.B. and S. Mørup. 1991. Identification of GR in an ochre sludge. Clay Mineral., 26, 577-582.

Kostka., J.E. and G.W. Luther III. 1994. Partitioning and speciation of solid phase iron in saltmarsh sediments. Geochim. Cosmochim. Acta, 58, 1701-1710.

Lovley, D.R. and E.J.P. Phillips. 1986. Organic matter mineralization with reduction of ferric iron in anaerobic sediments. Appl. Environ. Microbiol., 51, 683-689.

Lovley, D. R. and E. J. P. Phillips. 1988. Novel mode of microbial energy metabolism: Organic carbon oxidation coupled to the dissimilatory reduction of iron and manganese. Appl. Environ. Microbiol., 54, 1472-1480.

Luther III, G.W., J.E. Kostka, T.M. Church, B. Sulzberger and W. Stumm. 1992. Seasonal iron cycling in the salt-marsh sedimentary environment: the importance of ligand complexes with Fe(II) and Fe(III) in the dissolution of Fe(III) minerals and pyrite, respectively. Mar. Chem., 40, 81-103

Luther III, G.W., P.A. Shellenbarger, and P.J. Brendel. 1996. Dissolved organic Fe(III) and Fe(II) complexes in salt marsh porewaters. Geochim. Cosmochim. Acta, 60, 951-960.

Monaco, A., X. Durrieu de Mardon, O. Radakovitch, S. Heussner and J. Carbonne. 1999. Orgin and variability of downward biogeochemical fluxes on the Rhone continental margin (NW Mediterranean). Deep-Sea Res. I. 46, 1483-1511.

Nevin, K. P. and D. R. Lovley. 2000. Lack of production of electron-shuttling compounds or solubilization of Fe(III) during reduction of insoluble Fe(III) oxide by *Geobacter metallireducens*. Appl. Environ. Microbiol., 66, 2248-2251.

Reimers, C. E., R.A. Jahnke and D.C. McCorkle. 1992. Carbon fluxes and burial rates over the continental slope and rise off central California with implications for the global carbon cycle. Global Biogeochem. Cycles, 6, 199-224.

Rickard, D. 1995. Kinetics of FeS precipitation: Part 1. Competing reaction mechanisms. Geochim. Cosmochim. Acta, 59, 4367-4379.

Roden, E. E. and J. M. Zachara. 1996. Microbial reduction of crystalline iron(III) oxides: Influence of oxide surface area and potential for cell growth. Environ. Sci. Technol., 30, 1618-1628.

Roden, E. E. and M. M. Urrutia. 1999. Ferrous iron removal promotes microbial reduction of crystalline iron (III) oxides. Environ. Sci. Technol., 33 1847-1853.

Rysgaard, S., B. Thamdrup, N. Risgaard-Petersen, H. Fossing, P. Berg, P. B. Christensen and T. Dalsgaard. 1998. Seasonal carbon and nutrient mineralisation in a high-Arctic coastal marine sediment, Young Sound, Northeast Greenland. Mar. Ecol. Progr. Ser., 175, 261-276.

Sanchez-Cabeza, J.A., P. Masqué, I. Ani-Ragolta, J. Merino, M. Frignani, F. Alvisi, A. Palanques and P. Puig. 1999. Sediment accumulation rates in the southern

Barcelona continental margin (NW Mediterranean Sea) derived from 210Pb and 137Cs chronology. Progr. Oceanogr., 44, 213-332.

Schink, D.R. and N.L. Guinasso. 1978. Redistribution of dissolved and adsorbed materials in abyssal marine sediments undergoing biological stirring. Am. J. Sci., 278, 687-702.

Schmidt, S., T. C. E. Van Weering, H. C. De Stigter. 2001. Enhanced short-term deposition within the Nazaré Canyon, North-East Atlantic. Mar. Geol., 173, 55-67.

Schulzberger, B., D. Suter, C . Schiffert, S. Banwart and W. Stumm. 1989. Dissolution of Fe(III)(hydr)oxides in natural waters; Laboratory assessment on the kinetics controlled by surface coordination. Mar. Chem. 28, 127-144.

Slomp, C. P., J. F. P. Malschaert, L. Lohse and W. Van Raaphorst. 1997. Iron and manganese cycling in different sedimentary environments on the North Sea continental margin. Cont. Shelf Res., 17, 1083-1117.

Sørensen, J. 1982. Reduction of ferric iron in anaerobic, marine sediment and interaction with reduction of nitrate and sulfate. Appl. Environ. Microbiol. 43, 319-324

Stampfl, P.P. 1969. Ein basisches Eisen-II-III-karbonate. Rost. Corros. Sci., 9, 185-187.

Stookey, L. L. 1970. A new spectrophotometric reagent for iron. Anal. Chem., 42, 779-781.

Stumm, W. and B. Sulzberger. 1992. The cycling of iron in natural environments: Considerations based on laboratory studies of heterogeneous redox processes. Geochim. Cosmochim. Acta, 56, 3233-3257.

Taillefert, M., A.B. Bono and G.W. Luther III. 2000. Reactivity of freshly formed Fe(III) in synthetic solutions and (pore) waters: voltametric evidence of an aging process. Environ. Sci. Technol., 34, 2169-2177.

Thamdrup, B., H. Fossing and B. B. Jørgensen. 1994. Manganese, iron, and sulfur cycling in a coastal marine sediment, Aarhus Bay, Denmark. Geochim. Cosmochim. Acta, 58, 5115-5129.

Thamdrup, B. and D. E. Canfield. 1996. Pathways of carbon oxidation in continental margin sediments off central Chile. Limnol. Oceanogr., 41, 1629-1650.

Tessier, A., P. G. C. Campbell and M. Bisson. 1979. Sequential extraction procedure for the speciation of particulate trace metals. Anal. Chem.,*51*, 844-851.

Tessier, A., D. Fortin, N. Belzile, R. R. DeVitre and G. G. Leppard. 1996. Metal sorption to diagenetic iron and manganese oxyhydroxides and associated organic matter: Narrowing the gap between field and laboratory measurements. Geochim. Cosmochim. Acta, 60, 387-404.

Trolard, F., J.-M.R. Génin, M Abdelmoula, G. Boerrié, b. Humbert and A. Herbillon. 1997. Identification of a green rust mineral in a reductomorphic soil by Mössbauer and Raman spectroscopies. Geochim. Cosmochim. Acta, 61, 1107-1111.

Tügel, J.B., M.E. Hines and G.E. Jones. 1986. Microbial iron reduction by enrichment cultures isolated from estuarine sediments. Appl. Environ. Microbiol. 52, 1167-1172.

Urrutia, M. M., E. E. Roden and J. M. Zachara. 1999. Influence of aqueous and solid-phase Fe(II) complexants on microbial reduction of crystalline iron (III) oxides. Environ. Sci. Technol., 33, 4022-4028.

Van Cappellen, P. and Y. Wang. 1995. Metal cycling in surface sediments: Modeling the interplay between transport and reaction, *in* Metal contaminated aquatic sediments, H. E. Allen, eds., Ann Arbor Press, 21-64.

Van Cappellen, P. and Y. Wang. 1996. Cycling of iron and manganese in surface sediments: a general theory for the coupled transport and reaction of carbon, oxygen, nitrogen, sulfur, iron, and manganese. Am. J. Sci., 296, 197-243.

Van der Zee, C., W. van Raaphorst, E. Epping. 2001. Adsorbed Mn^{2+} and Mn redox cycling in Iberian continental margin sediments (North East Atlantic). J. Mar. Res. 59: 133-166.

Van Weering, T.C.E., H.C. De Stigter, W. Boer and H. De Haas. 2002. Recent sediment transport and accumulation at the western Iberian margin. Progr. Oceanogr., accepted.

Wallmann, K., K. Hennies, I. Konig, W. Petersen, and H-D. Knauth. 1993. New procedure for determining reactive Fe(III) and Fe(II) minerals in sediments. Limnol. Oceanogr., 38, 1803-1812.

Wang, Y. and P. Van Cappellen. 1996. A multicomponent reactive transport model of early diagenesis: Application to redox cycling in coastal marine sediments. Geochim. Cosmochim. Acta, 60, 2993-3014.

Zhang, H., W. Davison, S. Miller and W. Tych. 1995. In situ high resolution measurements of fluxes of Ni, Cu, Fe and Mn and concentrations of Zn and Cd in porewaters by DGT. Geochim. Cosmochim. Acta, 59, 4181-4192.

APPENDIX

Solutions to differential equations

$$C_I = B1Exp(e1x) + B2Exp(e2x)$$

$$A_I = F1Exp(e3x) + F2Exp(e4x)$$

$$S_I = G1 + G2.Exp(\frac{\omega.x}{Db}) + \alpha.B1.Exp(e1.x) + \beta.B2.Exp(e2.x) - F1.Exp(e3.x) - F2.Exp(e4.x)$$

$$C_{II} = J.Exp(e10.x) + \gamma.H.Exp(e6.x) + C_a$$

$$A_{II} = I.Exp(e.8x) + \delta.J.Exp(e10.x) + \varepsilon.H.Exp(e6.x) + A_{eq}$$

$$S_{II} = H.Exp(e6.x) + S_{eq}$$

$$e1 = \frac{\omega + \sqrt{\omega^2 + 4[Db + Ds]k_{oxc}}}{2[Db + Ds]}$$

$$e2 = \frac{\omega - \sqrt{(\omega^2 + 4[Db + Ds]k_{oxc}}}{2[Db + Ds]}$$

$$e3 = \frac{\omega + \sqrt{\omega^2 + 4Dbk_{oxa}}}{2Db}$$

$$e4 = \frac{\omega - \sqrt{\omega^2 + 4Dbk_{oxa}}}{2Db}$$

$$e6 = \frac{\omega - \sqrt{\omega^2 + 4Dbk_r}}{2Db}$$

$$e8 = \frac{\omega - \sqrt{\omega^2 + 4Dbk_p}}{2Db}$$

$$e10 = \frac{\omega - \sqrt{\omega^2 + 4Dbk_a}}{2Db}$$

$$\alpha = \frac{-k_{oxc}}{\theta[Db.e1^2 - \omega.e1]}$$

$$\beta = \frac{-k_{oxc}}{\theta[Db.e2^2 - \omega.e2]}$$

$$\gamma = \frac{k_r.\theta}{[Db + Ds].e6^2 - \omega.e6 - (k_a + k_{ads})}$$

$$\delta = \frac{-k_{ads}}{\theta.(Db.e10^2 - \omega.e10 - k_p)}$$

$$\varepsilon = \frac{-k_{ads}.\gamma}{\theta.(k_r - k_p)}$$

The integration constants (B1, B2, F1, F2, G1, G2, J, H and I) were analytically solved with the following boundary conditions:

When $x = 0$

$$C_I = C_0$$

$$J_{Ax=0} = 0$$

$$J_{Sx=0} = -\phi\theta\ (Db.A_I' - \omega.A_I)$$

When $x = L$

$$C_I = C_{II}$$

$$A_I = A_{II}$$

$$S_I = S_{II}$$

$$[Db+Ds].C_I' - \omega.C_I = [Db+Ds].C_{II}' - \omega.C_{II}$$

$$Db.A_I' - \omega.A_I = Db.A_{II}' - \omega.A_{II}$$

$$Db.S_I'\text{-}\omega.S_I = Db.S_{II}'\text{-}\omega.S_{II}$$

When $x \rightarrow \infty$

$$C_{II} = C_a,$$

$$A_{II} = A_{eq}$$

$$S_{II} = S_{eq}$$

CHAPTER SIX

Authigenic P formation and reactive P burial in sediments of the Nazaré canyon on the Iberian margin (NE Atlantic)[5]

ABSTRACT

Profiles of different forms of sedimentary phosphorus were measured at four sites at the Iberian margin (NE Atlantic), which were chosen on the basis of differences in depositional environment: a shelf site (113 m), a mid-slope station (1387 m) and two stations at the head (396) and base (3097 m) of the Nazaré Canyon. The sediment was sequentially extracted for Fe-bound P, carbonate fluorapatite (CFA) + biogenic P + $CaCO_3$-bound P and detrital Ca-P, and non-sequentially for total P and inorganic P, where the difference between total and inorganic P was assumed to be organic P. Measurements of organic carbon and nitrogen, citrate-dithionite-bicarbonate and citrate-ascorbate-bicarbonate extractable Fe, carbon oxidation rates, Fe reduction rates, phosphate effluxes and sedimentation rates were used to quantify the cycling and burial of phosphorus at each site. CFA formation was observed only in sediments of the Nazaré canyon, where enhanced rates of organic matter decomposition and Fe reduction provided the necessary conditions. The concentrations of reactive P were similar at all sites, but the sediment accumulation rates differed greatly. The high bulk accumulation rate at the base of the canyon results in a reactive P burial rate exceeding those estimated for continental margins including the Iberian margin by an order of magnitude. The estimated P burial efficiency is smallest at the slope station (3-24%), reasonably high (63-86%) at shelf and head of the canyon stations and extremely high (>97%) at the base of the canyon. We propose that local depositories such as those at the base of canyons may be key sites for reactive P burial.

INTRODUCTION

Recycling and removal of phosphorus (P) in the marine environment are important controls on marine productivity, both over geological and shorter time-scales (Holland, 1978; Broecker 1982; Howarth *et al.*, 1995; Van Cappellen and Ingall, 1996). Most removal of P from the water column takes place through sedimentation of organic material on continental margins (Berner, 1982; Froelich *et al.*, 1982). Phosphorus is most effectively sequestered in sediments with oxygenated overlying

[5] This chapter by Claar van der Zee, Caroline P. Slomp and Wim van Raaphorst has been submitted to Marine Geology

bottom waters, via the formation of refractory organic P compounds (Ingall *et al.*, 1990) and through binding to Fe oxides (Krom and Berner, 1981; Slomp *et al.*, 1996b; Ingall and Jahnke, 1997). Phosphate is released into the pore water both upon organic matter degradation and reduction of Fe oxides loaded with P. In the reduced part of the sediment, phosphate release can lead to supersaturation of the pore waters with respect to authigenic P minerals and, consequently, carbonate fluorapatite (CFA) precipitates (Ingall and Van Cappellen, 1990; Ruttenberg and Berner, 1993; Ingall and Jahnke, 1997). The formation of CFA may occur at the expense of either organic P or Fe-bound P (Ruttenberg and Berner, 1993; Lucotte *et al.*, 1994). Slomp *et al.* (1996a) proposed a mechanism for early diagenetic CFA formation in which Fe-bound-P acts as an intermediate between organic P and CFA at the Goban Spur continental margin (NE Atlantic).

Recently, Filippelli (1997) showed that ranges of sedimentary P concentrations are comparable between continental margins and the deep sea environment. However, P accumulation rates are higher on the margin due to much higher sedimentation rates (Ruttenberg, 1993). Very high P concentrations are found in areas on the continental margin, where significant phosphogenesis takes place, but these phosphorite deposits do not represent significant sinks in the marine P cycle due to very low sedimentation rates (Filipelli, 1997). Authigenic carbonate fluorapatite (CFA), a major sedimentary P sink, is not restricted to active coastal upwelling areas, thus 'normal' continental margin sediments are a significant sink for reactive P in the ocean (Ruttenberg, 1993; Filipelli, 1997). Continental shelves and slopes can function as traps for both terrestrial and marine particulate material, whereas submarine canyons incising the continental margin can act as preferential conduits for particulate material from the shelf to the deep sea (Carson *et al.*, 1986; Gardner, 1989; Granata *et al.*, 1999). The hydrodynamic conditions, size and morphology of the canyon, and its location relative to continental sources have great impact on its potential for organic matter accumulation (Buscail and Germain, 1997; Etcheber *et al.*, 1999). Sedimentation rates found in some canyons, particularly near the mouth, are much higher than those found on open slopes (Carpenter *et al.*, 1982; Cremer *et al.*, 1999). Thus, P burial is potentially important in sediments of the shelf and slope as well as in high deposition areas of canyons and their fans.

The present study on P cycling was carried out within the framework of the Ocean Margin EXchange project (OMEX-II) at the Iberian continental margin. Other studies on elemental cycling at the Iberian margin have focused on carbon and nitrogen (Epping *et al.*, 2002), manganese (Van der Zee *et al.*, 2001), iron (Van der Zee *et al*, submitted) and silica (Koning *et al.*, in prep.). The Iberian shelf is relatively narrow and interspersed with numerous canyons, amongst which is a large submarine canyon in the south of the margin, the Nazaré Canyon. This canyon represents an active locus for sediment focusing and deposition on the Iberian Margin (Schmidt *et al.*, 2001; Van Weering *et al.*, 2002). Enhanced organic matter deposition fluxes like those found in the Nazaré Canyon (Epping *et al*, 2002) also imply an enhanced P flux to the sediment since organic matter is the most important carrier of P to the sediment (Froelich *et al.*, 1982; Berner *et al.*, 1993). In this study, P cycling and burial are investigated in sediments of (1) a depositional area on the shelf, (2) a slope site, (3) a sandy area at the head of the Nazaré Canyon and, (4) a depositional area at the base of the Canyon. The objectives were (1) to make a comparison between P cycling at the

depositional shelf and canyon stations and the sandy shelf and slope site and (2) to study the potential of the canyon as sink for reactive P. A modified version of the SEDEX scheme (Ruttenberg, 1992) was applied to our sediments. First, we address the organic matter deposited at these contrasting sites using C/N and C/P ratios. Second, the inorganic P geochemistry is discussed, i.e. P interactions with Fe cycling and apatite precipitation. Finally, we conclude with a discussion onphosphorus burial in these different continental margin environments.

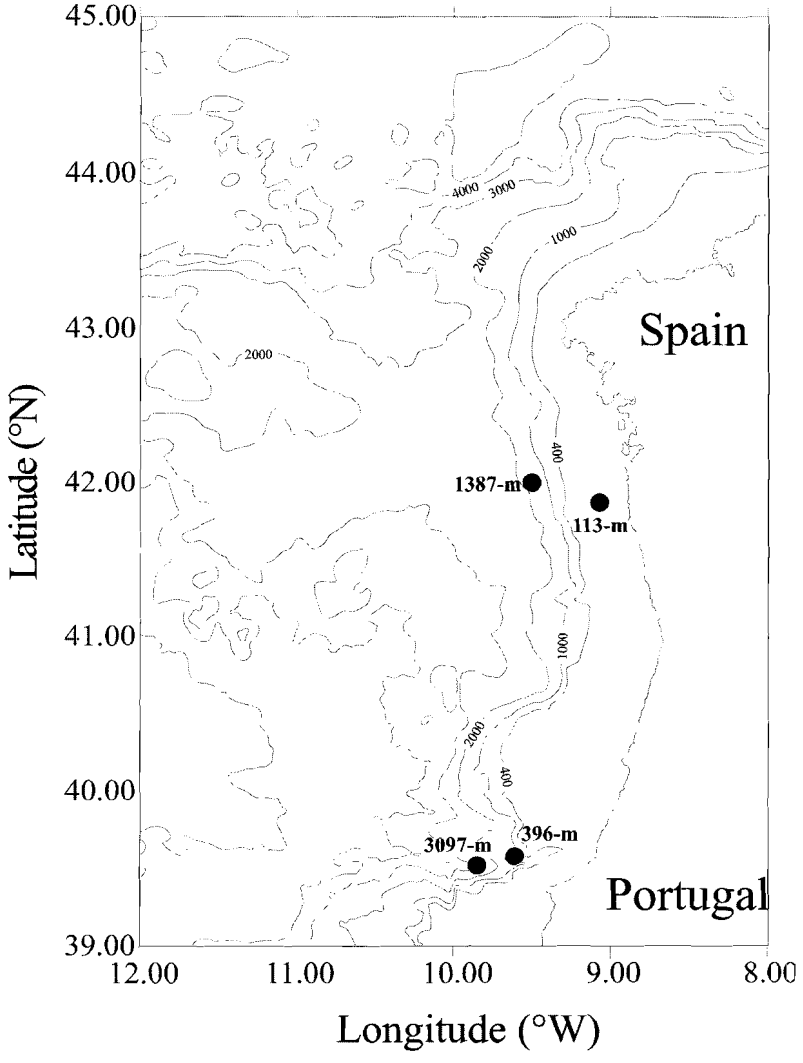

Figure 1. Map of the Iberian Margin indicating the positions of the stations and the water depth.

STUDY AREA

Our research area comprises the Iberian Margin in the NE Atlantic (Fig. 1). The Iberian shelf is relatively narrow (200-m isobath situated at 15-30 km off shore). Seasonal upwelling invokes temporal high primary productivity and benthic carbon deposition. The carbon oxidation rates are relatively low compared to other upwelling areas, e.g. the Chilean margin, however (Epping *et al.*, 2002). Sediment transport and accumulation in this region are described by Van Weering *et al.* (2002). Organic carbon oxidation rates in the sediment decrease with water depth, from ~11 on the shelf to ~2 g C m^{-2} y^{-1} at 5 km depth on the open slope (i.e. non-canyon sites). In the Nazaré canyon sediment is focussed, leading to sedimentation rates exceeding those of the adjacent shelf (Van Weering *et al.*, 2002). The Nazaré canyon is quantitatively important in concentrating organic matter, resulting in carbon oxidation rates three times higher at the 3097-m canyon base compared to sites at similar water depth outside of the canyon (Epping *et al.*, 2002). Four of the Iberian Margin stations that were sampled during the PE138 cruise with RV Pelagia in May 1999 were selected for this study. The two northern stations are (1) a 113-m station located in a depositional area on the shelf and (2) a mid-slope station at 1387-m water depth. The two southern stations are (1) a 396-m station located near the head of the Nazaré canyon and (2) a 3097-m station situated in the depositional area at the basis of the Nazaré canyon.

Table 1. Name of stations, geographical location, water depth, bottom water oxygen concentration, bottom water temperature (BWT), median grain size (MGS) of the upper 2.5 mm (Van Weering *et al.*, 2001), carbon oxidation rate (Epping *et al.*, 2001) and Fe reduction rate (Van der Zee *et al.*, subm.) of the sampled stations.

Name	Lat.	Long.	Depth (m)	BW O_2 (μM)	BW T (°C)	MGS (μm)	C ox (mmol m^{-2} d^{-1})	Fe red. (mmol m^{-2} d^{-1})
138-06	41.52	09.04	113	210	12.5	37.8	2.02	0.36
138-07	42.00	09.28	1387	188	10.3	15.1	1.02	0.04
138-15	39.35	09.37	396	200	11.6	69.4	1.42	0.09
138-14	39.31	09.51	3097	243	2.4	22.7	1.77	0.43

MATERIALS AND METHODS

Sediment cores were taken with a multi-corer equipped with polycarbonate liners and processed at *in situ* temperature directly upon retrieval. Four sediment cores were sliced simultaneously with a hydraulic core slicer developed at NIOZ. The sediment was sectioned in 2.5-mm slices in the upper cm of the sediment, 5-mm slicesfrom 10-30 mm, 10-mm slices from 30-60 mm and 20-mm slices further down core. Slices from corresponding depth intervals were pooled and centrifuged (5000 g, 10 min) for separation of the interstitial water from the solid phase. The centrifuged sediment was stored frozen (-20°C) until further analysis for solid phase constituents at the NIOZ laboratory.

Freeze-dried and ground sediment (Teflon or agate mortar and pestle) was extracted for solid phase P according to Ruttenberg (1992) as modified by Slomp *et al.* (1996a). The sediment is sequentially extracted for Fe-bound P, CFA + biogenic P + $CaCO_3$-bound P, and detrital Ca-P. Fe-bound P was extracted as citrate-dithionite bicarbonate extractable P (CDB, pH = 7.3, 8 hrs, 20 °C) and the sediment residue was washed once with 1M $MgCl_2$ (pH = 8, 30 min, 20 °C). CFA, biogenic P and $CaCO_3$-bound P were subsequently extracted with 1M Na-Acetate buffer (pH = 4, 6 hrs, 20 °C) and the sediment was washed again with 1M $MgCl_2$ (pH 8, 30 min, 20 °C). The rinses with $MgCl_2$ are necessary to reverse secondary adsorption. Finally the sediment residue was extracted with 1M HCl (24 hrs, 20 °C), which dissolves the detrital Ca-P. Organic P was determined as the difference between total P (total destruction, see below) and inorganic P (1M HCl, 24 hrs, 20 °C). Differences between the sum of the inorganic phases in the sequential procedure and the inorganic P extracted with IM HCl are due to propagation of the analytical errors. Therefore, we used the inorganic P values obtained by the single extraction instead of adding three values each with their own associated error. Analytical precision for the P extractions was better than 16% for Fe-bound P, 6% for authigenic P, 10% for detrital P, 3% for inorganic P and 2% for total P. Aliquots of the freeze-dried and ground sediment were additionally extracted with citrate-ascorbate-bicarbonate (CAB) solution for poorly crystalline Fe according to the method of Kostka and Luther (1994).

The P and Fe concentrations in the CDB extraction were determined using ICP-OES (Spectro Analytical Instruments). CDB extractable Fe is assumed to consist of Fe from Fe oxides, although it may also extract some Fe from clay minerals and Fe sulphides (Slomp *et al.*, 1996b). All other P analyses were performed on a Hitachi U-1100 spectrophotometer using the method of Strickland and Parsons (1972). Total P and Fe were determined after total destruction of the sediment with a mixture of HF, HNO_3 and $HClO_4$ and final solution of the residue in 1M HCl using ICP-OES (Perkin Elmer Optima 3000). The Fe concentrations in the CAB extracts were measured on a Hitachi U-1100 spectrophotometer using the method of Stookey (1970). Total carbon and nitrogen and organic carbon were measured on a Carlo-Erba 1500 elemental analyser (Verardo *et al.*, 1990). $CaCO_3$ was determined as the difference between total and organic carbon. Total nitrogen is assumed to represent organic nitrogen (Lohse *et al.*, 2000).

RESULTS

General sediment characteristics

The organic carbon contents are high (~4 wt%) in the 0-1 cm interval at the 113-m shelf and 3097-m canyon-base depositional stations, whereas the $CaCO_3$ contents are low (~5-10 wt%) (Fig. 2). The $CaCO_3$ content is relatively high, ~20 to 30 wt%, at the 1387-m mid-slope station and at the 396-m site at the head of the canyon, whereas their organic carbon contents are lower, ~2 wt% and ~0.6 wt% in the 0-1 cm interval, respectively. CAB-extractable Fe profiles show clear (sub-)surface enrichments of Fe oxides formed upon re-oxidation of mobilised Fe^{2+} diffusing upward into the oxic layer. The concentration of CAB-extractable Fe is always lower than that extracted with CDB, suggesting a considerable contribution of relatively crystalline Fe oxides

in the sediment. CDB-extractable Fe is a small percentage of the total Fe because the major fraction of Fe is bound in clay minerals (Raiswell and Canfield, 1998). Only at the 1387-m station is an enrichment in CDB-extractable Fe observed at the Fe redox boundary. The total and CDB-Fe contents are lower at the 396-m and 1387-m stations than at the depositional sites (113-m and 3097-m).

Solid phase P profiles

Organic P varies only slightly with depth in the sediment at all locations, except at the 1387-m station where it decreases below ~65 mm depth (Fig. 3). Inorganic and total P decrease somewhat with depth at the 113-m and 396-m shelf stations. Subsurface maxima of inorganic and total P are observed at the 1387-m and 3097-m station and the Fe-bound P profiles show the same trend. At the shelf stations, Fe-bound P is relatively depth invariant. Authigenic P profiles show some variation with depth at the shelf and slope stations. At the 3097-m station, it could be presently forming as indicated by the increase with depth. The lack of an increase in authigenic P with depth at the other stations does not necessarily preclude ongoing precipitation, since this could occur at the sediment-water interface or be masked by bioturbation. Both are probably not important at these stations because the pore water phosphate concentrations and gradients are rather low (E. Epping, pers. com.) and do not indicate supersaturation of the pore waters with respect to authigenic P minerals and consequent CFA precipitation. The authigenic P profiles are also presented on a carbonate free basis to assess whether changes in the $CaCO_3$ flux can explain trends in the authigenic P profile, which is not the case. Detrital P is constant with depth at the 1387-m station, whereas it declines at the other three stations.

DISCUSSION

Organic material

Organic C/N and C/P atomic ratios are used to characterise the organic material in the sediment (Fig. 4). The C_{org}/N ratios are constant with depth at the two organic-poor stations (396-m and 1387-m), whereas they slightly decrease with depth at the organic-rich stations (113-m and 3097-m). At the 113-m station, the C_{org} content drops in the first 3 cm from 4.5 to 1.5 wt. % and because the N content does not decrease similarly, the C_{org}/N ratio declines as well. The C_{org}/N signature of the sediment is probably caused by the terrestrial component in the organic matter at this depositional shelf station. Microscopic observations have revealed that remains of vascular plants are present in the sediment of the 113-m station. The C_{org}/N ratios of the other stations (1387-m, 396-m and 3097-m) suggest an oceanic source of organic material.

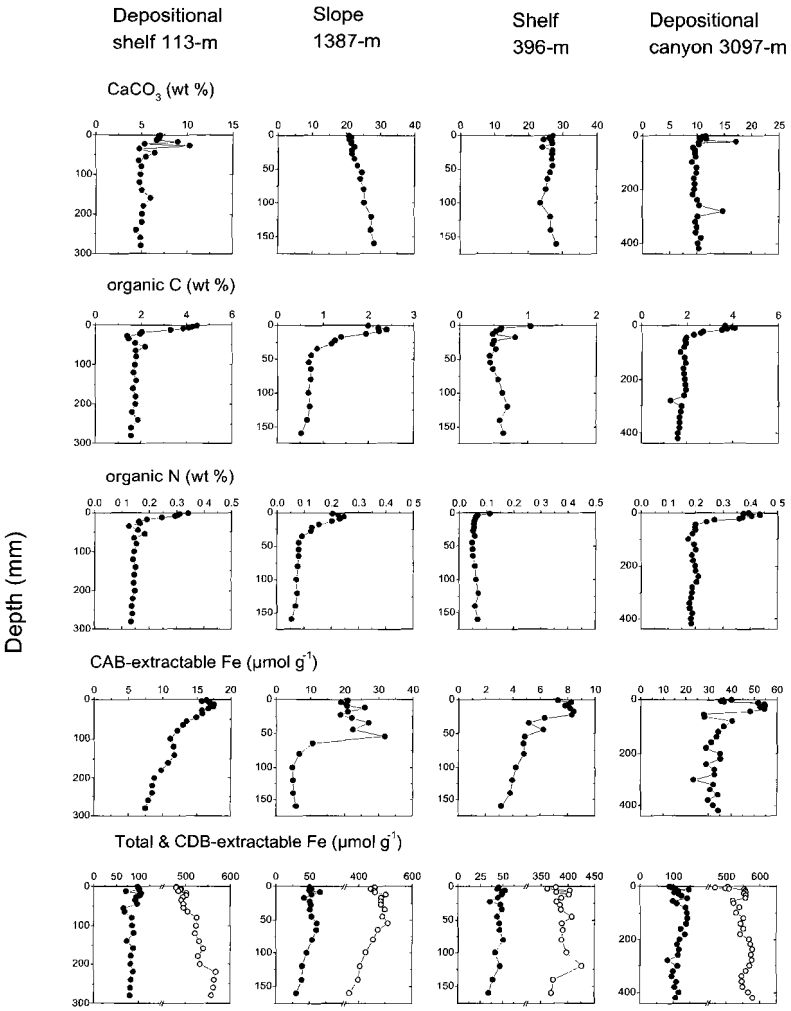

Figure 2. Vertical profiles of calcium carbonate, organic carbon and nitrogen, CAB-extractable Fe, total (solid circles) and CDB-extractable (open circles) iron. Organic carbon and nitrogen contents are high at the 113-m and 3097-m stations. Carbonate contents are relatively high at the 396-m and 1387-m station. Fe enrichments at the redox boundary are most pronounced in the CAB-extractable fraction.

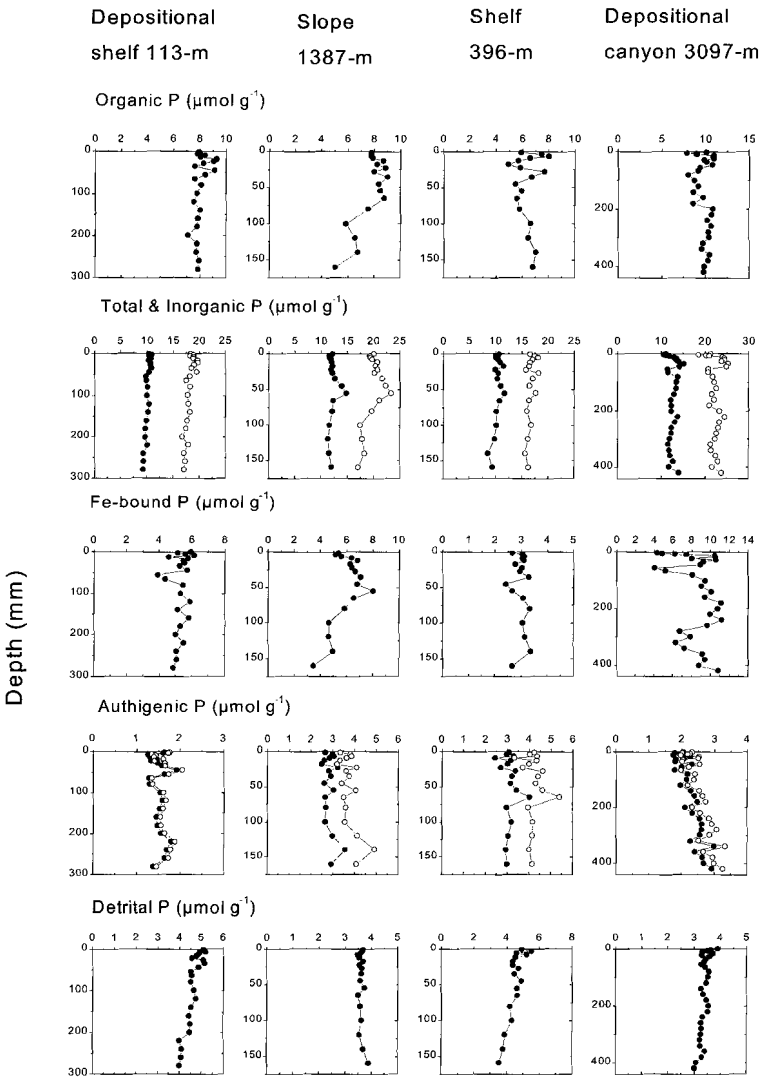

Figure 3. Vertical profiles of organic P, total (open circles) and inorganic (solid circles) P, iron bound P, authigenic P (open circles are concentrations on carbonate-free basis), and detrital P. Organic P was calculated as the difference between total P and inorganic P (1M HCl-extractable P). Organic P declines strongly with depth, at the 1387-m slope station only. The authigenic P fraction is the sum of carbonate fluorapatite, biogenic P and $CaCO_3$-bound-P. Authigenic P increases with depth at the 3097-m canyon station, whereas it does not show a distinct trend with depth at the other stations.

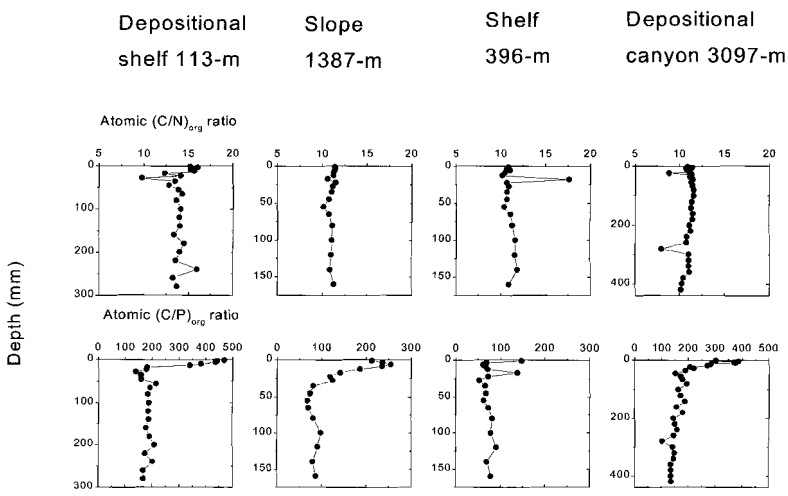

Figure 4. Vertical profiles of organic carbon to nitrogen atomic ratios, and organic carbon to organic phosphorus atomic ratios. The atomic $(C/N)_{org}$ ratios are constant with depth (1387-m and 396-m sites) or decrease slightly (113-m and 3097-m sites), whereas the atomic $(C/P)_{org}$ ratios strongly decrease with depth, except at the 396-m site.

The organic C/P profiles reflect the C_{org} trend with depth due to small variations in P_{org} with depth compared to C_{org}. Fresh marine planktonic organic matter has an average C/P ratio of about 106 (Redfield *et al.*, 1963). The 113-m, 1387-m and 3097-m stations have higher organic C/P ratios at the sediment-water interface and decreasing values at depth suggesting that the organic matter arriving at the sediment-water interface is not fresh marine detritus. The microscopic observations and the C_{org}/N profile of the 113-m station indicated the presence of vascular plant material. As terrestrial plants can have C/P ratios as high as 800 (Simpson, 1977) to 2050 (Likens *et al.*, 1981), this explains the high C/P ratio at the sediment-water interface of the 113-m station. The higher C/P ratios at the sediment-water interface of the 1387-m and 3097-m stations can be explained by preferential P regeneration under oxic decomposition in the water column during the ~200 and ~300 days prior to deposition at these stations, respectively (Epping *et al.*, 2002). The lack of a decrease in organic P content with depth does not preclude changes in the nature of the organic P compounds with depth. The decreasing organic C/P ratio with depth in the sediment at the 1387-m and 3097-m stations can be caused by the formation of refractory material enriched in P, such as aminophosphonic acids (Ingall and Van Cappellen, 1990; Kittredge and Roberts, 1969). *In situ* synthesised bacterial biomass with a low C/P ratio might contribute to the decrease in the oxic layer of the sediment as well (Vadstein et al., 1988). At the 396-m station, the low organic C/P ratio is rather constant with depth, which may indicate that P is not preferentially degraded or enriched in refractory material in the sediment. Thus, the decrease in C/P ratio with

depth in the sediment can be explained by the presence of relatively labile organic matter deprived of P in the upper part of the sediment caused by preferential P degradation in the water column. Upon the degradation of organic matter, the relatively labile organic carbon is respired and the little P that is liberated is immediately re-incorporated in organic compounds. This has also been reported to occur during the oxidation of organic matter in sapropels (Slomp et al., 2002). The system is probably P limited as suggested by the high C/P ratios supporting the re-incorporation hypothesis. As a consequence, organic P is efficiently retained in the sediment column.

Ingall and Van Cappellen (1990) argued that the sedimentation rate is the master variable of the burial ratio of organic carbon over organic phosphorus (C/P_{∞}) in a non-linear fashion. Low residual organic C/P_{∞} ratios (<200) are typical for areas with sedimentation rates either < 0.002 cm yr^{-1} or > 1 cm yr^{-1}, whereas higher ratios, up to 600, are found in areas with intermediate sedimentation rates. Our shallowest stations have intermediate sedimentation rates (0.06 and 0.09 cm yr^{-1}), but nevertheless low residual C/P_{∞} ratios. This suggests that the organic P is of a relatively more refractory nature than organic C. The organic C/P_{∞} ratios of the canyon (1.45 cm yr^{-1}) and slope station (~0.001-0.01 cm yr^{-1}) are consistent with the model of Ingall and Van Cappellen (1990). The 396-m and 1387-m stations have lower C/P_{∞} ratios (75-90) and the 113-m and 3097-m stations have relatively higher C/P_{∞} ratios (140-160). All stations fall within the range of low residual C/P ratios. Thus, the P_{org} content that is buried is relatively high compared to the C_{org} content.

Inorganic P geochemistry

Fe oxides have a high affinity for phosphate (Berner 1973; Slomp *et al.*, 1996b) and consequently, Fe oxides present in the oxic layer of the sediment can act as a trap for upward diffusing phosphate (Krom and Berner, 1980; Sundby et al., 1992; Slomp *et al.*, 1996a). When Fe oxides are reduced in the anoxic sediment layer the adsorbed phosphate is liberated, in addition to the P released during organic matter degradation (Krom and Berner, 1981). The Fe-bound P profiles do not show evidence of phosphorus enrichment due to Fe re-oxidation, except at the slope station. The Fe/P ratios for Iberian margin sediments extracted with CDB range between 6 and 25 (Fig. 5). Jensen and Thamdrup (1993) reported Fe/P ratios of 6 to 8 for Aarhus Bay sediments, 10-16 for Kattegat sediments and a ratio of 17 for a station in the Skagerrak. An Fe/P ratio of 14 has been reported for suspended particles in the St Lawrence estuary (Lucotte and d'Anglejan, 1988). Higher Fe/P ratios of 20-26 are reported for the North Atlantic and the Labrador Sea (De Lange, 1986; Lucotte et al., 1994). The high Fe/P ratio may indicate that the Fe oxides extracted with CDB have a higher proportion of relatively crystalline phases in those samples, because crystalline Fe phases bind less P while poorly crystalline Fe oxides have a higher P sorption capacity due to their larger surface areas (Borggaard, 1983). Poorly crystalline akageneite and ferrihydrite, identified by differential XRD, proved to be the Fe phases that play a dominant role in P binding in North Sea sediments (Slomp et al., 1996b). Ascorbate is a milder reductant than dithionite and only extracts poorly crystalline Fe oxides (Kostka and Luther, 1994) that have a lower P sorption capacity. The CAB-extractable Fe concentration is only between ~10-50% of the CDB-extractable Fe at our stations, which also indicates that a considerable amount of Fe in the sediment is

of a more crystalline nature. Anschutz et al. (1998) extracted similar amounts of P, but not of Fe, with CDB and CAB from marine sediments, suggesting that P was only associated with poorly crystalline Fe. The Fe/P ratio was smaller and less variable using the CAB-Fe and P instead of the CDB-Fe and P (Anschutz et al., 1998). Fe-bound P has been suggested to represent a permanent sink of reactive P on continental margins (Ruttenberg and Berner, 1993; Jensen and Thamdrup, 1993; Slomp et al., 1996b). CDB-extractable Fe and Fe-bound P persist in the anoxic layer of the sediment, suggesting that Fe-bound P is at least a temporary sink on the Iberian margin.

The authigenic P fraction is the sum of CFA, biogenic-P, such as fish debris, and $CaCO_3$-bound-P. When expressed on a carbonate free basis the trend with depth remains unchanged, indicating that changes in the $CaCO_3$ flux can not explain the apparent increase of authigenic P with depth. It is possible that a larger contribution of biogenic-P causes this increase, but there is no reason to assume that more fish debris is present deeper in the sediment as it is more prone to dissolution than authigenic apatite (Shenau *et al.,* 2000). Although we can not exclude the possibility that non-steady state conditions are causing the authigenic P fraction to increase with depth, there is no indication for non-steady state from other solid phase data, including organic carbon (Epping *et al.,* 2002), manganese (Van der Zee *et al.,* 2001) and natural radionuclides (Schmidt *et al.,* 2001). We conclude that, most likely, CFA is forming in the sediment of the 3097-m station at the base of the canyon. The other solid phase P fractions do not show a mirror image of the authigenic P, making a single particular source of P unlikely. The authigenic P formation could be fuelled by a combination of sources and because the increase is only moderate over the sampled interval, no clear decreases in the other P fractions are observed. CFA formation in marine sediments is important because it is a permanent sink of reactive P, whereas organic P and Fe-bound P can still be released after burial. The two prerequisites for authigenic P formation are high enough concentrations of phosphate for precipitation and nucleation sites (Van Cappellen and Berner, 1988). The required intense subsurface production of phosphate may not be produced solely by the decomposition of organic matter, but additional sources may be needed, e.g. dissolution of inorganic fish hard parts (Van Cappellen and Berner, 1988; Schenau *et al.*, 2000) or release from Fe oxides (Slomp *et al.*, 1996a). Phosphate release due to the reductive dissolution of Fe oxides is potentially most important at stations with higher Fe reduction rates, e.g. at the 113-m and 3097-m station (Table 1). Incidentally, these stations also have the highest C oxidation rates. At the 3097-m station, both ammonia and dissolved Fe reach high concentrations (up to ~1100 μM and 360 μM, respectively) and are produced relatively deep in the sediment (Epping *et al.*, 2002; Van der Zee *et al.*, subm.). Thus, both organic matter degradation and Fe reduction rates are high and take place relatively deep in the sediment thereby providing the necessary conditions for the build up of phosphate concentrations which are sufficiently high for authigenic P formation.

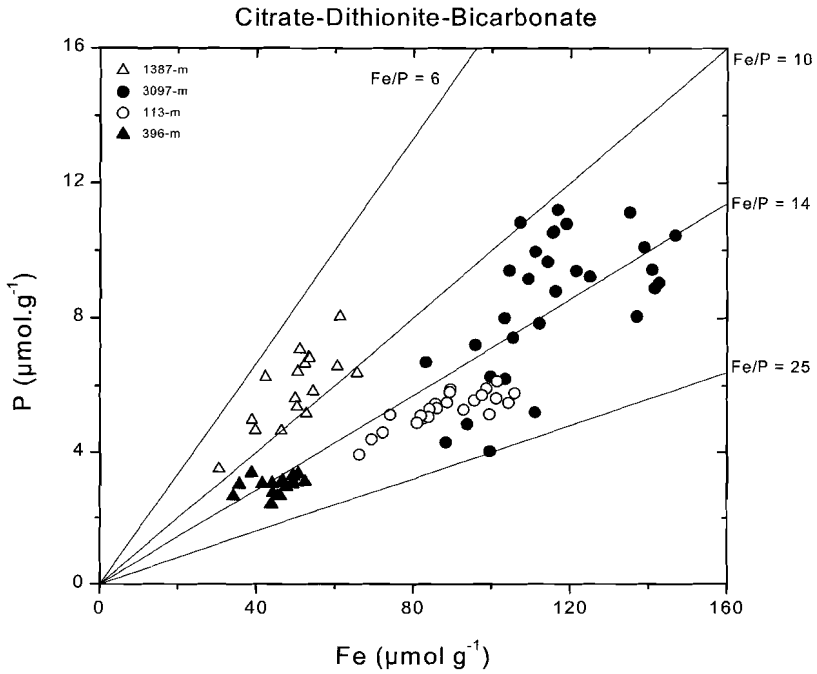

Figure 5. Citrate-dithionite-bicarbonate buffer extractable phosphorus versus iron in sediments of the 113-m (open circles), 1387-m (open triangles), 396-m (solid triangle) and 3097-m (solid circles) stations. The higher Fe/P ratios suggest that the CDB-extractable Fe oxides have a higher proportion of crystalline phases in those samples, which bind less phosphate per atom of Fe.

Phosphorus burial

The relative contributions of the P fractions to the pool of total P in our sediments (Table 2) differ greatly with those of deep-sea sediments of the equatorial Pacific investigated by Filippelli and Delaney (1996). They reported on P cycling at 7 equatorial Pacific sites (2520 - 3861-m water depth), where authigenic P is the dominant P-bearing component (61-86%), followed by Fe-bound P (7-17%), organic P (3-12%), adsorbed P (2-9%), and detrital P (0-1%). The composition of the sedimentary P at the Iberian margin resembles more the sediments of the FOAM and Mississippi Delta sites studied by Ruttenberg and Berner (1993). The percentages of Fe-bound P and detrital P at the Iberian margin are very similar to those of the Mississippi Delta, whereas the percentage organic P is higher in our sediments and that of authigenic P lower than at the FOAM and Mississippi Delta sites (Ruttenberg and Berner, 1993).

Table 2. Water depth of station, Bulk sediment accumulation rate (Van Weering *et al*, 2002), Total P content, Total P burial rate, Percentage of Fe-bound P, authigenic P, organic P and detrital P to total P.

Depth (m)	Bulk SAR (g m^{-2} yr^{-1})	Total P (μmol g^{-1})	P burial (mmol m^{-2} yr^{-1})	Fe-bound P (%)	Auth. P (%)	Org. P %	Detr. P %
113	809	17.2	13.9	29	9	46	23
1387	~10-100	17.1	~0.2-1.7	24	19	33	21
396	634	16.2	10.3	19	19	44	23
3097	9623	22.3	215	39	11	44	15

P concentrations of the two deepest sampled intervals are averaged, except for the 3097-m station, where it is an averaged value over the 5-43 cm interval. Bulk SAR is not determined at the 1387-m station. The trend of the bulk SAR with water depth results in an estimate of between 10 to 100 g m^{-2} yr^{-1} (Van Weering *et al.*, 2001). Sums of percentages are 107% (113-m), 98% (1387-m), 104% (396-m) and 109% (3097-m).

Long-term sinks of reactive P may involve organic P, Fe-bound P and authigenic P (Berner *et al.*, 1993; Ruttenberg and Berner, 1993; Ingall *et al.*, 1990; Slomp *et al.*, 1996a). For the calculation of P budgets the burial of reactive P should be considered, because this fraction is potentially bio-available P, in contrast to detrital P (Ruttenberg, 1993). Filipelli (1997) compiled data from several margins and estimated that the total P accumulation rates for continental margins range between 0.9 and 80 mmol P m^{-2} yr^{-1}. Total P burial rates of between 1.6 and 16 mmol P m^{-2} yr^{-1} are reported for the deep troughs of the Gulf of St-Lawrence (Louchouarn *et al.*, 1997). These are maximum values for reactive P, with the actual value being perhaps up to 50% lower, because continental margin sediments can have detrital P contents of 15% to over 40% of the total (Ruttenberg, 1993; Filipelli, 1997). Based on estimated P burial rates using the bulk sediment accumulation rate (Van Weering *et al.*, 2002) and the solid phase P concentrations (Table 2), our values for the Iberian shelf and slope are well within the range for continental margin sediments. The canyon P accumulation rate, however, exceeds that estimate and is an order of magnitude higher. Differences in phosphorus burial rates are primarily caused by differences in the bulk sediment accumulation rate at our sites, just as they are in other environments (Filippelli, 1997). The P burial efficiency, calculated from (burial rate/ (burial rate + efflux))*100%, is smallest at the slope station, reasonably high at both shelf stations and extremely high at the canyon station (Table 3). Ingall and Jahnke (1994) showed evidence for enhanced P regeneration in sediments overlain by oxygen depleted waters. Total P burial efficiencies of sediments overlain by oxygenated waters of ~13-55% were reported for the margins of North Carolina and California (Ingall and Jahnke, 1994). Reactive P burial efficiencies of ~46-74% were estimated in sediments from the Arabian Sea, excluding those sediments located in the oxygen minimum zone (Bottom water oxygen concentration <2 μM) (Schenau, 1999). Thus, the burial efficiency calculated for the canyon station is very high. The P burial efficiency increases with increasing bulk sediment accumulation rate. Similarly, the sedimentation rate was found to be the master variable for the organic carbon burial efficiency (Epping *et al.*, 2001). The suggested factors controlling organic carbon preservation are sorptive preservation, oxygen exposure time or otherwise. The P burial efficiencies (Table 3) are much higher than the organic C burial efficiencies

(0.6 to 48%), which can be due to efficient re-incorporation of released phosphate by the phosphorus limited benthic community and to sorption onto Fe oxides in the oxic layer.

Table 3. Burial efficiency

Depth (m)	Total P burial (mmol m^{-2} d^{-1})	Diff. HPO_4^{2-} efflux (mmol m^{-2} d^{-1})	Burial Efficiency (%)	In situ HPO_4^{2-} efflux (mmol m^{-2} d^{-1})	Burial Efficiency (%)
113	0.038	0.023	63	0.006 ± 0.001	86
1387	~0.001-0.005	0.019	3-20	0.015 ± 0.008	4-24
396	0.028	0.015	65	-	-
3097	0.589	0.015	97	-0.012 ± 0.032	97-100

Diffusive phosphate efflux is calculated with Fick's first law from the concentration gradient between the first sediment interval and the overlying water. The diffusion coefficient is corrected for temperature and tortuosity (Boudreau, 1997). E. Epping kindly provided the in situ phosphate efflux (n=3) obtained during in situ experiments with the benthic lander, TROL (Epping *et al*, 2001). The TROL was not deployed at the 396-m station.

Epping *et al.* (2002) found a large discrepancy between estimated organic carbon delivery and total organic carbon deposition on the shelf. In the absence of off shore depocenters, this suggests that canyons are quantitatively important in focusing and burying shelf derived organic matter (Epping *et al.*, 2002). The impact on the global P budget is difficult to assess from only one site in the canyon. Deeper than 5 m in a piston core retrieved from the same canyon site, the sediment becomes more sandy/silty indicating a different sedimentation regime. Thus, there were apparently ~333 years of relative quiet conditions after the last great canyon flushing event (H. de Stigter, pers.comm.). The present study demonstrates the potential of canyons to act as a sink for reactive P phases.

CONCLUSIONS

The Iberian shelf stations represent contrasting depositional environments, but their P burial rates are very similar. The total P burial rate is smallest on the slope. The depositional site at the base of the Nazaré canyon is the only station where ongoing forming of authigenic carbonate fluorapatite is suggested to occur, presumably because organic matter decomposition and Fe reduction occur relatively deep in the sediment of this station. The high organic matter deposition flux in the canyon stimulates both organic matter degradation and Fe reduction rates resulting in the necessary build up of phosphate in the pore water. We propose that local deposition areas such as occur at the lower part of canyons may be key sites for reactive P burial in the global ocean.

Acknowledgements The authors thank the captain, crew and scientific party of R.V. Pelagia for their help during the cruises. Grain size data were kindly provided by Wim Boer, Henko de Stigter and Tjeerd van Weering (NIOZ, department of Marine Chemistry and Geology). The investigations were carried out in the framework of the Sedimentary Manganese and Iron cycLEs project (SMILE). C.v.d.Z. was supported through a grant to W.v.R. by the Research

Council for Earth and Life Science (ALW) with financial aid from the Netherlands Organisation for Scientific Research (NWO) (no. 750.297.01). C.P.S was supported through the European Union Marine Science and Technology Programme, contract no. MAS3-CT97-0137, and by a fellowship of the Royal Academy of Arts and Sciences. The helpful comments from Dr Ingall, Dr Filipelli and Dr Emeis greatly improved this paper. This is publication no. 3593 of the Royal Netherlands Institute for Sea Research.

REFERENCES

Anschutz, P., S. Zhong, B. Sundby, A. Mucci and C. Gobeil. 1998. Burial efficiency of phosphorus and the geochemistry of iron in continental margin sediments. Limnol. Oceanogr. 43, 53-64.

Berner, R.A. 1973. Phosphate removal from seawater by adsorption on volcanogenic ferric oxides. Earth Planetary Sci. Lett. 18, 77-86.

Berner, R.A. 1982. Burial of organic carbon and pyrite sulfur in the modern oceans: Its geochemical and environmental significance. Am. J. Sci., 282, 451-473.

Berner, R.A., K.C. Ruttenberg, E.D. Ingall and J.-L. Rao. 1993. The nature of phosphorus burial in modern marine sediments, In: R.Wollast, F.T. Mackenzie and L. Chou, eds. Interactions of C, N, P, and S Biogeochemical cycles and Global Change, Springer-Verlag, NATO ASI Series Vol. 14, 521 p.

Borggaard, O.K. 1983. Effect of surface area and mineralogy of iron oxides on their surface charge and anion-adsorption properties. Clays Clay Miner. 31, 230-232.

Boudreau, B.P., 1997. Diagenetic models and their implementation, Springer Verlag, Heidelberg, pp. 414.

Broecker, W.S. 1982. Ocean chemistry during glacial time. Geochim. Cosmochim. Acta 46, 1689-1705.

Buscail, R. and C. Germain. 1997. Present-day organic matter sedimentation on the NW Mediterranean margin: Importance of off-shelf export. Limnol. Oceanogr. 42, 217-229.

Canfield, D.E., B. Thamdrup and J.W. Hansen. 1993. The anaerobic degradation of organic matter in Danish coastal sediments: iron reduction, manganese reduction and sulphate reduction. Geochim. Cosmochim. Acta, 57, 3867-3883.

Carpenter, R., M.L. Peterson, and J.T. Bennett. 1982. 210Pb derived sediment accumulation and mixing rates for the Washington continental slope. Marine Geology 48: 135-164.

Carson, B., E. T. Baker, B.M. Hickey, C.A. Nittrouer, D.J. DeMaster, K.W. Thorbjarnarson, and G.W. Snyder. 1986. Modern sediment dispersal and accumulation in Quinault submarine canyon – A summary. Mar. Geol., 71, 1-13.

Colman, A.S., and H.D. Holland. 2000. The global diagenetic flux of phosphorus from marine sediments to the oceans: Redox sensitivity and the control of atmospheric oxygen levels. In: SEPM Special Publication 66, Marine Authigenesis: From Microbial to Global (eds. C. Glenn, L. Prevot-Lucas, and J. Lucas), p 53-76.

Cremer, M., Weber, O., Jounneau, J.-M., 1999. Sedimentology of box cores from the Cap-Ferret Canyon area (Bay of Biscay). Deep-sea Res. II 46, 2221-2247.

De Lange, G.J. 1986. Early diagenetic reactions in interbedded pelagic and turbiditic sediments in the Nares Abyssal Plain (western North Atlantic): Consequences for

the composition of sediment and interstitial water. Geochim. Cosmochim. Acta 50, 2543-2564.

Epping, E., C. van der Zee, K. Soetaert and W. Helder. 2002. On the oxidation and burial of organic carbon in sediments of the Iberian margin and Nazaré canyon (NE Atlantic). Progr. Oceanogr., Accepted.

Filippelli, G.M. and Delaney, 1996. Phosphorus geochemistry of equatorial Pacific sediments. Geochim. Cosmochim. Acta, 60, 1479-1495.

Filippelli, G.M. 1997. Controls on phosphorus concentration and accumulation in oceanic sediments. Mar Geol., 139, 231-240.

Froelich, P.N., M.L. Bender, N.A. Luedtke, G.R. Heath and T. DeVries. 1982. The marine phosphorus cycle. Am. J. Sci. 282, 474-511.

Gardner, W.D., 1989. Baltimore Canyon as a modern conduit of sediment to the deep sea. Deep-sea Res. 36, 323-358.

Granata, T.C., B. Vidondo, C.M. Duarte, M.P. Satta and M. Garcia. 1999. Hydrodynamics and particle transport associated with a submarine canyon off Blanes (Spain), NW Mediterranean Sea. Continental Shelf Research 19, 1249-1263.

Holland, H.D. 1978. The chemistry of atmosphere and oceans. Wiley Interscience, NY.

Howarth, R.W., H.S. Jensen, R. Marino and H. Postma. 1995. Transport to and processes of phosphorus in near-shore and oceanic waters. In H.Tiesen (ed) Phosphorus in the global environment, Wiley NY, SCOPE 54, 323-346.

Ingall, E.D. and R. Jahnke. 1994. Evidence for enhanced phosphorus regeneration from sediments overlain by oxygen depleted waters. Geochim. Cosmochim. Acta 58, 2571-2575.

Ingall, E.D., and R. Jahnke. 1997. Influence of water-column anoxia on the elemental fractionation of carbon and phosphorus during sediment diagenesis. Mar. Geol. 139, 219-229.

Ingall, E.D., P.A. Schroeder and R.A. Berner. 1990. The nature of organic phosphorus in marine sediments: New insights from 31P-NMR. Geochim. Cosmochim. Acta 54, 2617-2620.

Ingall, E.D. and P. Van Cappellen. 1990. Relation between sedimentation rate and burial of organic phosphorus and organic carbon in marine sediments. Geochim. Cosmochim. Acta 54, 373-386.

Jensen, H.S. and B. Thamdrup. 1993. Iron-bound phosphorus in marine sediments as measured by bicarbonate-dithionite extraction. Hydrobiologica, 253, 47-59.

Kittredge, J.S. and Roberts, E. 1969. A carbon –phosphorus bond in nature. Science 164, 37-42.

Kostka., J.E. and G.W. Luther III. 1994. Partitioning and speciation of solid phase iron in saltmarsh sediments. Geochim. Cosmochim. Acta 58, 1701-1710.

Krom, M. D. and R.A. Berner. 1980. Adsorption of phosphate in anoxic marine sediments. Limnol. Oceanogr. 25, 797-806.

Krom, M. D. and R.A. Berner. 1981. The diagenesis of phosphorus in a nearshore marine sediment. Geochim. Cosmochim. Acta, 45, 207-216.

Likens, G.E., F.H. Bormann, and N.M. Johnson. 1981. Interaction between major biogeochemical cycles in terrestrial ecosystems. In, Some perspectives of the

major biogeochemical cycles SCOPE 17 (ed. G.E. Likens), p 93-112. John Wiley and Sons.

Lohse, L., Kloosterhuis, R.T., De Stigter, H.C., Helder, W., Van Raaphorst, W., and T.C.E. Van Weering. 2000. Carbonate removal by acidification causes loss of nitrogenous compounds in continental margin sediments. Mar. Chem. 69, 193-201.

Louchouarn, P., Lucotte, M., Duchemin, E., de Vernal, A., 1997. Early diagenetic processes in recent sediments of the Gulf of St-Lawrence: phosphorus, carbon and iron burial rates. Mar. Geol. 139, 181-200.

Lucotte, M. and B. d'Anglejan. 1988. Processes controlling phosphate adsorption by iron hydroxides in estuaries. Chem. Geol. 67, 75-83.

Lucotte, M., A. Mucci, C. Hillaire-Marcel and S. Tran. 1994. Early diagenetic processes in deep Labrador Sea sediments: reactive and nonreactive iron and phosphorus. Can. J. Earth Sci., 31, 14-27.

Raiswell, R. and Canfield, D.E., 1998. Sources of iron for pyrite formation in marine sediments. Am. J. Sci. 298, 219-245.

Redfield, A.C., B.H. Ketchum and F.A. Richard. 1963. The influence of organisms on the composition of sea water. In, The Sea (ed. M.N. Hill), vol.2, pp. 26-87. John Wiley and Sons.

Ruttenberg, K.C. 1992. Development of a sequential extraction method for different forms of phosphorus in marine sediments. Limnol. Oceanogr., 37, 1460-1482.

Ruttenberg, K.C. 1993. Reassessment of the oceanic residence time of phosphorus. Chem. Geol. 107, 405-409.

Ruttenberg, K.C. and R.A. Berner. 1993. Authigenic apatite formation and burial in sediments from non-upwelling, continental margin environments. Geochim. Cosmochim. Acta, 57, 991-1007.

Schenau, S.J. 1999.Cycling of phosphorus and manganese in the Arabian Sea during the late quaternary. Geologica Utraiectina 182, PhD thesis, Utrecht University.

Schenau, S.J., C.P. Slomp and G.J. De Lange. 2000. Phosphogenesis and active phosphorite formation in sediments from the Arabian Sea Oxygen Minimum Zone. Mar. Geol. 169, 1-20.

Schmidt. S., de Stigter, H.C. and van Weering, T.C.E., 2001. Enhanced short-term sediment deposition within the Nazaré Canyon, North-East Atlantic. Mar. Geol. 173, 55-67.

Simpson, H.J. 1977. Man and the global nitrogen cycle. In, Global chemical cycles and their alterations by man (ed. W. Stumm), p 253-274. Abakon-Verlagsgesellschaft.

Slomp, C.P., E.H.G. Epping, W. Helder and W. van Raaphorst. 1996a. A key role for iron-bound phosphorus in authigenic apatite formation in North Atlantic continental platform sediments. J. Mar. Res., 54, 1179-1205.

Slomp, C.P., S.J. van der Gaast and W. van Raaphorst. 1996b. Phosphorus binding by poorly crystalline iron oxides in North Sea sediments. Mar. Chem., 52, 55-73.

Slomp, C.P., J. Thomson, and G.J. de Lange. 2002. Enhanced regeneration of phosphorus during formation of the most recent eastern Mediterranean sapropel (S1). Geochim. Cosmochim. Acta, in press.

Stookey, L.L. 1970. Ferrozine – A new spectrophotometric reagent for iron. Analytical chemistry, 42, 779-781.

Sundby, B., C. Gobeil, N. Silverberg, A. Mucci. 1992. The phosphorus cycle in coastal marine sediments. Limnol. Oceanogr. 37, 1129-1145.

Vadstein, O., A. Jensen, Y. Olsen and H. Reinertsen. 1988. Growth and phosphorus status of limnetic phytoplankton and bacteria. Limnol. Oceanogr., 33, 489-503.

Van Cappellen, P. and R.A. Berner. 1988. A mathematical model for the early diagenesis of phosphorus and fluorine in marine sediments: apatite precipitation. Am. J. Sci. 288, 289-333.

Van Cappellen, P. and E.D. Ingall. 1996. Redox stabilisation of the atmosphere and oceans by phosphorus-limited marine productivity. Science 271, 493-496.

Van der Zee, C., W. van Raaphorst and E. Epping. 2001. Adsorbed Mn^{2+} and Mn redox cycling in Iberian continental margin sediments (North East Atlantic Ocean). J. Mar. Res. 59, 133-166.

Van der Zee, C., W. van Raaphorst and W. Helder. Adsorbed Fe^{2+} and Fe redox cycling in Iberian continental margin sediments (North East Atlantic Ocean). Submitted.

Van Weering, T.C.E., H.C. de Stigter, W. Boer and H. de Haas. 2002. Recent sediment transport and accumulation at the western Iberian margin. Progress in Oceanography. Accepted.

Verardo, D.J., P.N. Froelich and A. McIntyre. 1990. Determination of organic carbon and nitrogen in sediments using the Carlo-Erba Na-1500 analyser. Deep Sea Research, 37, 157-165.

SUMMARY

The highly dynamic cycles of iron (Fe) and manganese (Mn) in marine sediments are coupled to the biogeochemical cycles of carbon, oxygen, sulphur, nitrogen, phosphorus and several trace elements. Aim of this thesis was to study manganese and iron cycling in different depositional environments going from the shelf across the slope to the abyssal plain. Another aim was to study the recycling and burial of phosphorus (P) in sediments of the European continental shelf.

Mn and Fe reduction are the most important organic matter degradation pathways that depend on solid phase oxidants. Consequently, transport processes involving the solid phase, including intermittent perturbations, are decisive for Mn and Fe cycling. Mn and Fe diagenesis is stimulated in dynamic temporal deposition areas due to burial of reactive Mn- and Fe-oxides and organic material below the depth of oxygen penetration, thereby providing the prerequisites for suboxic diagenesis. These "disturbed" sediments, that occupy a major part of shelf seas, are important, yet often overlooked areas for suboxic diagenesis. In the temporal depositional areas at the Frisian Front and the German Bight in the North Sea, sediment profiles of solid phase Mn and Fe were transient, although the pore water profiles appeared at steady state. Association of the Mn- and Fe-oxides with organic matter that is preferentially reworked by biota was one reason of non-steady state depth distributions. The second reason was the hydrodynamic regime at these shallow sites which affected the vertical layering of particle size distribution and thus of the Mn and Fe associated with small grain sizes.

The intrinsic reactivity of natural Mn-oxide assemblages was assessed by application of a reactive continuum model to the reductive dissolution of Mn-oxides in ascorbic acid. North Sea sediments from three sites characterised by different intensities of sediment reworking were investigated. The reactivity of the Mn-oxide assemblages during reductive dissolution in ascorbic acid varied by up to ~9 orders of magnitude. The largest heterogeneity in Mn oxide reactivity in oxidised North Sea sediments was found at the site experiencing most intense sediment reworking, the German Bight, while the most homogeneous Mn oxide assemblage was found at the least intense reworked site, the Skagerrak. Due to sediment mixing, Mn^{2+} ions experience a variable chemical environment resulting in different oxidation products and thus, a large heterogeneity. The perturbations that mix the sediments of the Frisian Front and German Bight result in a layering of the sediment. Therefore these perturbations increase the sedimentary heterogeneity instead of homogenising the sediments. The rather homogeneous assemblage of Mn-oxides in the reduced sediment samples suggests that some recalcitrant Mn-oxides may escape direct reduction in the sediment. Considering the broad spectrum of Mn-oxide reactivities, extensive overlap of the Mn reduction zone with that of Fe is expected.

The roles that adsorbed Mn^{2+} and Fe^{2+} play in their redox cycles are very different (Fig. 1). Adsorbed Mn^{2+} is an important reaction intermediate in the reduced layer between Mn oxide and pore water Mn^{2+}. When Mn oxide is mixed and/or buried below the Mn redox boundary, it is reduced and the produced Mn^{2+} is adsorbed onto remaining adjacent Mn oxide surfaces. Upon continued Mn oxide reduction, the available sorption sites are diminished and/or saturated. Then, adsorbed Mn^{2+} is

desorbed and released into the pore water. Pore water Mn^{2+} diffuses upward and is oxidised by molecular oxygen to form Mn oxide or downward where it is co-precipitated with carbonates. Adsorbed Mn^{2+} seems to be associated with organic matter upon arrival at the sea floor, whereas the adsorbed Mn^{2+} formed in the sediment is likely to be adsorbed onto Mn oxides. The implication of an intermediate adsorbed Mn^{2+} phase is a stronger retention of Mn redox cycling in the sediment column at stations with a thin oxidation zone, since adsorbed Mn^{2+} limits the Mn^{2+} efflux from the pore water to the water column.

Adsorbed Fe^{2+} does not function as intermediate, but rather as a buffer for pore water Fe^{2+} and its transformation into authigenic ferrous minerals. Below the Fe redox boundary, Fe^{2+} is released into the pore water upon Fe reduction, and subsequently adsorbed onto the sediment matrix and/or precipitated to form authigenic ferrous minerals. Deeper down in the sediment, the adsorbed Fe^{2+} is released again, after which the dissolved Fe^{2+} is precipitated immediately. Through sorption, authigenic ferrous mineral formation is delayed and Fe^{2+} is transported deeper into the sediment. There, adsorbed Fe^{2+} acts as a deep source for authigenic ferrous mineral formation. The substrate for Fe^{2+} sorption is likely to be organic material, aluminium oxides and layered silicates.

Fe oxidation and reduction rates decreased with water depth at non-canyon stations of the Iberian margin. At the shelf, organic carbon mineralisation rates are highest and drive the Fe cycle. Mn oxidation and reduction rates are highest halfway on the continental slope at moderate carbon fluxes. The high deposition fluxes in the Nazaré Canyon off the Portuguese coast enhance Fe and Mn reaction rates. Mn cycling at the shelf is limited by slow oxidation kinetics. Fe^{2+} is more rapidly oxidised than Mn^{2+} and consequently Fe oxidation and reduction rates are higher at the shelf. At the other stations of the Iberian margin, the rate limiting factor for both Mn and Fe cycling is sediment mixing, i.e. the transport of Mn and Fe oxides into the reduced sediment layer.

Canyons may be key sites for reactive P burial. Enhanced organic matter decomposition and Fe reduction provide the conditions necessary for authigenic carbonate fluorapatite (CFA) formation in the depositional area of the Nazaré Canyon. CFA formation was not observed in sediments of the adjacent shelf and slope. Phosphorus cycling and burial in sediments of the Iberian Margin were assessed at four sites, which were chosen on the basis of their deposition-characteristics, two contrasting shelf sites, a slope and a canyon station. The concentrations of reactive P were similar at all sites, in contrast to the sediment accumulation rates. The high bulk accumulation rate at the canyon site results in a reactive P burial rate exceeding those estimated for continental margins including the Iberian margin by an order of magnitude. Continental margins may contribute even more to the global P burial budget, when canyon sediments are included in the budget calculations.

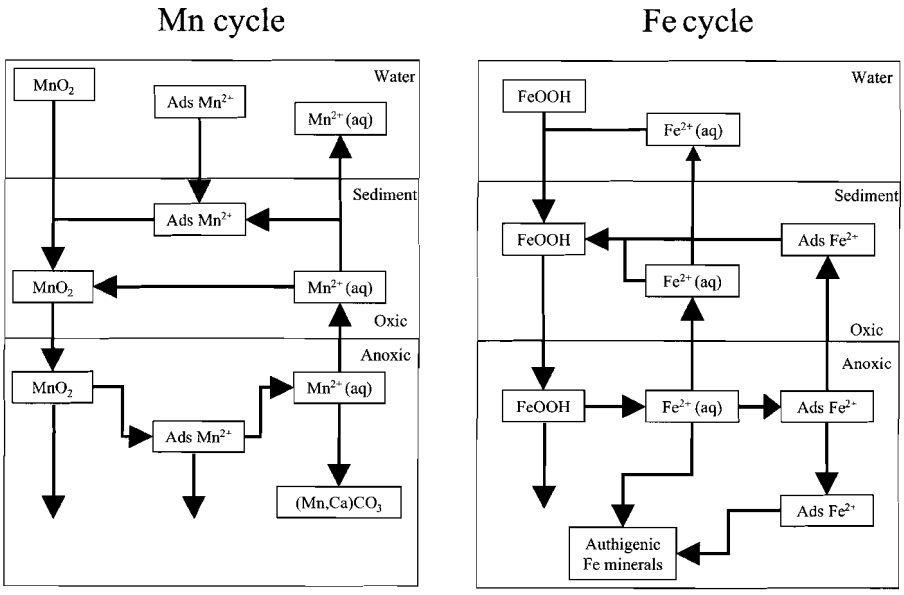

Figure 1. Schematic representation of the roles of adsorbed Mn^{2+} and Fe^{2+} in their redox cycles.

SAMENVATTING

De zeer dynamische kringlopen van ijzer (Fe) en mangaan (Mn) in de zeebodem zijn gekoppeld aan die van koolstof, zuurstof, zwavel, stikstof, fosfor en verscheidene spoor-elementen. In de zeebodem breken bacteriën het organisch materiaal af door het te oxideren met behulp van zuurstof, totdat dat geheel verbruikt is en vervolgens met nitraat, dan met mangaanoxide, ijzeroxide en tenslotte met sulfaat. Dit proefschrift beschrijft de resultaten van een studie naar de reductie van mangaan en ijzer in verschillende depositiegebieden, van het continentaal plat over de helling naar de diepzee. Ook wordt de kringloop en vastlegging van fosfor (P) in sedimenten van het Europese continentale plat en de helling naar de diepzee beschreven. Het bodemsediment bestaat uit klei en zandkorrels, de vaste fase, en het water wat daartussen zit, het poriewater. Mangaanoxiden en ijzeroxiden zijn aan de vaste fase gebonden, terwijl gereduceerd Mn en Fe opgelost is in het poriewater. Vanuit het zeewater diffundeert zuurstof het sediment in, waar het wordt verbruikt bij de oxidatie van organisch materiaal en andere gereduceerde stoffen totdat het op een bepaalde diepte zuurstofloos (anoxisch) wordt. Mangaanoxiden (Mn^{4+}) en ijzeroxiden (Fe^{3+})

zijn stabiel in het zuurstofrijke (oxische) deel van het sediment. De oxiden worden gereduceerd tot opgelost Mn^{2+} en Fe^{2+} in het zuurstofloze gedeelte van het sediment, waar de opgeloste gereduceerde vormen van mangaan en ijzer stabiel zijn. Het opgeloste Mn en Fe kan naar boven diffunderen en daar opnieuw geoxideerd worden, waardoor een kringloop ontstaat. De kringlopen van fosfor en ijzer zijn aan elkaar gekoppeld doordat fosfaat (PO_4^{3-}) adsorbeert aan ijzeroxiden. Als deze worden gereduceerd komt behalve het Fe^{2+} ook het fosfaat vrij in het poriewater.

De invloed van verstoringen in het sediment op de Mn- en Fe-kringlopen

De reductie van mangaan en ijzer zijn de belangrijkste routes voor de afbraak van organisch materiaal die afhangen van aan de vaste fase gebonden oxidanten. Transportprocessen die de verdeling van de vaste fase beïvloeden, waaronder onregelmatige verstoringen, zijn daarom erg belangrijk voor de kringlopen van mangaan en ijzer. Mangaanreductie en ijzerreductie in dynamische tijdelijke depositiegebieden worden gestimuleerd doordat reactieve mangaan- en ijzeroxiden samen met organisch materiaal op onregelmatige wijze worden begraven in het diepere anoxische deel van het sediment. Op die manier worden de juiste omstandigheden geschapen voor de reductie van mangaan en ijzer. Deze verstoorde sedimenten beslaan een groot deel van ondiepe randzeeën als de Noordzee en zijn belangrijke, maar nog weinig bestudeerde gebieden voor de reductie van Mn en Fe. In de tijdelijke depositiegebieden in de Noordzee nabij het Friese Front en in de Duitse Bocht zijn de sedimentprofielen van het aan de vast fase gebonden Mn en Fe vergankelijk, ook al lijken de poriewaterprofielen in "steady state" te zijn. Een mogelijke oorzaak is de verbinding van de Mn- en Fe-oxiden met organisch materiaal, dat selectief in het sediment wordt omgewerkt door organismen. Een andere oorzaak is het hydrodynamische regime op deze ondiepe stations, waardoor de verticale gelaagdheid in korrelgrootte verstoord wordt en daarmee het Mn en Fe die vooral gebonden zijn aan de kleinere korrels.

Reactiviteit van mangaanoxiden

Om de reactiviteit van natuurlijke mangaanoxiden in verschillende sedimenten te bepalen, werd hun reductieve oplossnelheid in ascorbinezuur bepaald. In sedimenten komen verschillende mangaanoxiden voor, de meest reactieve daarvan lossen het snelste op in ascorbinezuur en de minder reactieve mangaanoxiden langzamer, waardoor de reactiviteit van een mangaanoxiden mengsel modelmatig kan worden beschreven als een reactief continuum. De grootste verschillen in reactiviteiten binnen een Mn-oxiden mengsel in zuurstofrijke Noordzee sedimenten werd gevonden bij de locatie waar het sediment het meest intens omgewerkt was, terwijl het meest homogene Mn-oxiden mengsel werd gevonden op de locatie waar de omwerking van het sediment het minst intens was. Mn^{2+} ionen ondergaan verschillende chemische omgevingen tijdens het omwerken van het sediment. Dit leidt tot verschillende oxidatieproducten en daarom tot een grote heterogeniteit in de reactiviteit van het mengsel. De onregelmatige verstoringen in de sedimenten nabij het Friese Front en in de Duitse Bocht veroorzaken een gelaagdheid in het sediment en stimuleren daardoor de heterogeniteit van de mangaanoxiden. Van het meest heterogene mengsel van mangaanoxiden neemt de reactiviteit tijdens reductieve oplossing in ascorbinezuur met maar liefst 9 ordegrootten af. De daarentegen vrij homogene mengsels van

mangaanoxiden in het gereduceerde deel van het sediment geven aan dat de sommige mangaanoxiden ontsnappen aan reductie en worden begraven in het sediment. Door het brede spectrum aan reactiviteiten van Mn-oxiden bestaat er een grote overlap van de Mn reductiezone met die van Fe oxiden.

De rol van geadsorbeerd Mn^{2+} en Fe^{2+} in mariene sedimenten

De functies die geadsorbeerd Mn^{2+} en Fe^{2+} vervullen in hun kringlopen zijn erg verschillend (Fig. 1). Geadsorbeerd Mn^{2+} is een belangrijk intermediair voor de reductie van Mn-oxide en Mn^{2+} dat oplost in het poriewater in de gereduceerde laag. Mn-oxide wordt gereduceerd wanneer het wordt gemengd of begraven onder de Mn(II-IV) redox grens en de gevormde Mn^{2+} ionen adsorberen aan het aangrenzende Mn-oxide oppervlak. Als de reductie van Mn-oxide doorgaat neemt het aantal beschikbare adsorptie plaatsen af en raakt het oxide oppervlak verzadigd. Vervolgens komt het geadsorbeerd Mn^{2+} vrij in het porie water. Opgelost Mn^{2+} diffundeert naar boven waar het wordt geoxideerd door moleculair zuurstof tot Mn-oxide of het diffundeert naar beneden en kan daar neer slaan als mangaancarbonaat. Geadsorbeerd Mn^{2+} lijkt gebonden te zijn aan organisch materiaal wanneer het aankomt op de zeebodem, terwijl het Mn^{2+} dat in het sediment wordt gevormd zeer waarschijnlijk adsorbeert aan Mn-oxiden. Het gevolg van geadsorbeerde Mn^{2+} als intermediaire fase is een sterkere retentie van de Mn kringloop in sedimenten met een dunne oxidatie zone, omdat geadsorbeerd Mn^{2+} de Mn^{2+} efflux vanuit het poriewater naar de waterkolom vermindert.

Geadsorbeerd Fe^{2+} fungeert niet als intermediair, maar als een buffer voor opgelost Fe^{2+} in het poriewater dat uit de oplossing verdwijnt door de nieuwvorming van Fe(II)mineralen. Tijdens de reductie van Fe-oxiden komt Fe^{2+} vrij in het poriewater. Een deel daarvan diffundeert naar boven waar het oxideert tot ijzeroxiden met mangaanoxiden, nitraat of moleculair zuurstof. Een ander deel adsorbeert direct aan de sediment matrix of diffundeert naar beneden waar het precipiteert als een Fe(II)mineraal. Dieper in het sediment komt het geadsorbeerde Fe^{2+} weer vrij in het poriewater, waarna het opgeloste Fe^{2+} onmiddelijk neerslaat als Fe(II)mineraal. Door sorptie wordt de nieuwvorming van ijzermineralen dus vertraagd en wordt Fe^{2+} dieper in het sediment getransporteerd. Substraten voor sorptie van Fe^{2+} zijn waarschijnlijk organisch materiaal, aluminiumoxiden en gelaagde silicaten.

Processnelheden in de kringlopen van mangaan en ijzer

Diepte-geintegreerde processnelheden, zoals oxidatie-, reductie-, precipitatie- en sorptiesnelheden voor mangaan en ijzer in het sediment, werden geschat voor een serie locaties voor de Portugese en de noord-Spaanse kust met behulp van diagenetische modellen. De snelheden van ijzeroxidatie en ijzerreductie nemen af met de water diepte bij de niet-canyon stations van het Iberisch continentaal plat en de helling. Organisch koolstof wordt op het continentaal plat met een hoge snelheid geoxideerd en deze snelheid nam af in sedimenten op grotere water diepte over de continentale helling naar de diepzee. De hoge oxidatiesnelheid van organisch materiaal drijft de Fe kringloop aan. Snelheden van mangaanoxidatie en mangaanreductie zijn het hoogst halverwege de continentale helling. De hoge depositiefluxen van sediment in de Nazaré Canyon bij de Portugese kust verhogen de Mn en Fe processnelheden. De kringloop van Mn wordt gelimiteerd door de langzame

oxidatie op het continentaal plat. Fe^{2+} wordt sneller geoxideerd dan Mn^{2+} en daarom zijn de reductie- en oxidatiesnelheden van Fe hoger op het continentaal plat. De intensiteit waarmee het sediment omgewerkt wordt is de snelheidsbepalende factor in de kringloop van Mn en Fe elders op het Iberische plat en op de helling, omdat dit het transport van Mn en Fe oxiden van de oxische naar de anoxische laag bepaalt.

De vastlegging van fosfor in het sediment.

Fosfor en stikstof zijn essentiële voedingsstoffen voor algen, die soms limiterend zijn. Omdat sommige algen stikstof kunnen vastleggen wordt algemeen aangenomen dat fosfor het beperkende bestanddeel is voor algengroei op de langere termijn. Het is daarom van belang te weten hoeveel fosfor wordt begraven in de zeebodem en dus niet meer biologisch beschikbaar is. In het depositiegebied van de Nazaré Canyon veroorzaken de verhoogde oxidatiesnelheden van organisch materiaal en reductiesnelheden van ijzer de nieuwvorming van carbonaat-fluorapatiet (CFA). Als fosfor eenmaal vast is gelegd als CFA dan is het permanent uit de fosfor kringloop verdwenen. CFA-vorming is niet waargenomen in sedimenten van het aangrenzende continentale plat en helling. De concentratie van fosfor in het sediment was overal vergelijkbaar, dit in tegenstelling tot de accumulatiesnelheden van het sediment. De hoge accumulatiesnelheid in de canyon resulteerde in een begravingssnelheid van fosfor die een orde groter is dan in andere continentale randen inclusief het Iberisch continentaal plat en de helling. Als de bijdrage van canyon sedimenten mee zou worden genomen in de berekeningen van de mondiale begraving van fosfor op continentale hellingen, dan zou hun rol nog groter kunnen blijken dan reeds aangenomen.

Dankwoord

Tot slot wil ik iedereen bedanken die op het NIOZ, aan boord van de Pelagia of waar dan ook heeft bijgedragen aan het tot een goed einde brengen van de hele proefschrift-toestand.

Met name wil ik Wim van Raaphorst bedanken omdat hij mij de mogelijkheid heeft gegeven dit onderzoek te verrichten, voor zijn goede adviezen en het feit dat hij altijd even tijd had. Philippe van Cappellen, hartelijk dank voor het promoten. Erica, je bent geweldig: dank voor alle regelneef-promotie-dingen!

Curriculum Vitae

Clara van der Zee werd geboren op 19 juni 1974 te Amstelveen. Na het behalen van haar atheneum diploma in 1992 aan het Keizer Karel College te Amstelveen, begon zij aan de studie Scheikunde aan de Universiteit van Amsterdam (UvA). Zij verrichtte 2 doctoraal onderzoeken, één op het gebied van ecologische microbiologie (UvA) en één in de mariene geochemie (Koninklijk Nederlands Instituut voor Onderzoek der Zee, NIOZ). In augustus 1997 studeerde zij af bij de vakgroep Microbiologie van de faculteit Scheikunde. Aansluitend werd zij door de Nederlandse organisatie voor Wetenschappelijk Onderzoek (NWO) bij het NIOZ te Texel aangesteld als Onderzoeker in Opleiding bij de afdeling Mariene Chemie en Geologie. Daar verrichtte zij het in dit proefschrift beschreven geochemische onderzoek aan mariene sedimenten. Sinds oktober 2001 werkt zij als post-doc bij de Department of Physics van de University of Ottawa, Canada, aan het project Lake Sediment Structure and Evolution (LSSE).

Zodoende dus